The structure and properties of SiC-modified carbon fibre reinforced carbon composites

Pardini, Luiz Claudio

Award date:
1994

Awarding institution:
University of Bath

THE STRUCTURE & PROPERTIES OF SiC-MODIFIED CARBON FIBRE REINFORCED CARBON COMPOSITES

submitted by Luiz Claudio Pardini

for the degree of PhD of the University of Bath

1994

ProQuest LLC
789 East Eisenhower Parkway
P.O. Box 1346
Ann Arbor, MI 48106-1346

ACKNOWLEDGEMENTS

The work described in this thesis was carried out in the School of Materials Science of the University of Bath, between March 1991 and February 1994. Financial support from the Conselho Nacional de Desenvolvimento Científico e Tecnológico - CNPq - Brasil is gratefully acknowledged.

I am sincerely grateful to Professor Brian McEnaney, my supervisor at Bath, for his help throughout this work, guidance and constant encouragement.

My appreciation goes to the technical staff at the University of Bath for their invaluable services.

My thanks to Borden-UK for providing the phenolic resin used in this work; and my thanks also to INPE-Brasil and Inasmet-Spain for carrying out the mercury porosimetry and dynamic mechanical analysis, respectively.

My thanks to Centro Técnico Aeroespacial - Brasil for providing the opportunity to study for the PhD degree.

My thanks to Miss A. Kawamoto to her help during this work.

DEDICATION

This thesis is dedicated to my parents, Bruno and Ivone,

and my family for their support.

"There is nothing more difficult to take in hand, more perilous to conduct, or more uncertain in its success than to take the lead in the introduction of a new order of things, because the innovator has for enemies all those who have done well under the old condition, and lukewarm defenders in those who may do well under the new."

Niccolo Machiavelli,
IL PRINCIPE (1513)

ABSTRACT

This thesis reports a three-part study of the influence of sol-gel derived SiC upon the microstructure and flexural properties of carbon fibre reinforced carbon composites (CFRC). ***First.*** Application of SiC coatings to two woven CFRC (KKarb and Sigri) produces a thicker external coating on the less porous KKarb composite, resulting in a significant increase in flexural modulus. Pore penetration by SiC occurred in the Sigri material leading to an increase in flexural strength; in both cases application of SiC made the failure mode more brittle. ***Second.*** Unidirectional CFRC composites were made from a resin carbon matrix with ex-PAN carbon fibres which were either treated, sized (TS composites) or untreated, unsized (UU composites); hybrid composites were also made consisting of alternating laminae containing TS and UU fibres. *Heat treatment to 1100°C.* The TS composites failed in a brittle manner, whereas failure of the UU composites was dominated by fibre bundle sliding. A synergistic increase in flexural strength was found for the hybrid composite. *Heat treatment to 2500°C.* For the TS composite there was a large increase in flexural strength and a tougher failure mode. For the UU composite there was a reduction in flexural strength with no change in the failure mode; for both composites the changes were related to stress graphitisation of the matrix. The flexural strength and modulus of the hybrid composite lay between those of the other composites. ***Third.*** Unidirectional carbon fibre composites with hybrid matrices containing resin carbon and SiC were made by: (i) incorporation of the SiC sol gel precursor between prepreg laminae, and (ii) external brush application of the sol gel to the unmodified composite. Incorporation of SiC, in the interlaminar region in method (i), and mainly by pore penetration in method (ii), both significantly improved flexural properties of the CFRC, but resulted in more brittle behaviour. Acoustic emission monitoring proved to be a valuable tool for studying failure of the composites. The most effective system for oxidation control of the composites up to 1200°C in air was a coating of SiC with a borate glass.

CONTENTS

CHAPTER TWO

EXPERIMENTAL METHODS

CHAPTER THREE

COMMERCIAL CFRC COMPOSITES RESULTS AND DISCUSSION

CHAPTER FOUR

UNIDIRECTIONAL CFRC COMPOSITES RESULTS AND DISCUSSIONS

CHAPTER FIVE

MODIFIED UNIDIRECTIONAL C-SIC COMPOSITES RESULTS AND DISCUSSIONS

CHAPTER SIX

SUMMARISING DISCUSSIONS AND CONCLUSIONS

INTRODUCTION

High temperature technology is of major importance in many types of industry, such as primary metal and non-metal production, materials processing, chemical engineering, transportation, power generation and aerospace technology. Materials for high temperature applications must be able to operate in environments with a wide spectrum of mechanical loadings and chemical conditions (Meetham - 1991, Weisshaus - 1990a). Operating temperatures in various applications are compared in Figure I, to demonstrate the extreme conditions to which these materials are subjected (Meetham - 1991).

Carbon and graphite have been used in high temperature applications that require mechanical strength at high temperature, thermal shock resistance and low density. They are unique materials in that some mechanical properties improve with increasing temperature, partly as a result of stress relief and microcrack closure which occur with thermal expansion as the material is heated back to its formation temperature (Thomas - 1986). A major disadvantage of carbon materials is their low resistance to oxidation in air at temperatures > 450°C and the modest mechanical properties of conventional polygranular graphites (<40 MPa with grain).

The need for stronger and tougher carbon material was met by the advent of carbon fibre reinforced carbon (CFRC) in the beginning of the sixties (Meetham - 1991, Chlopek - 1991, Zaldivar - 1991b). Unidirectional CFRC composites have been made with tensile strength up to 800 MPa.

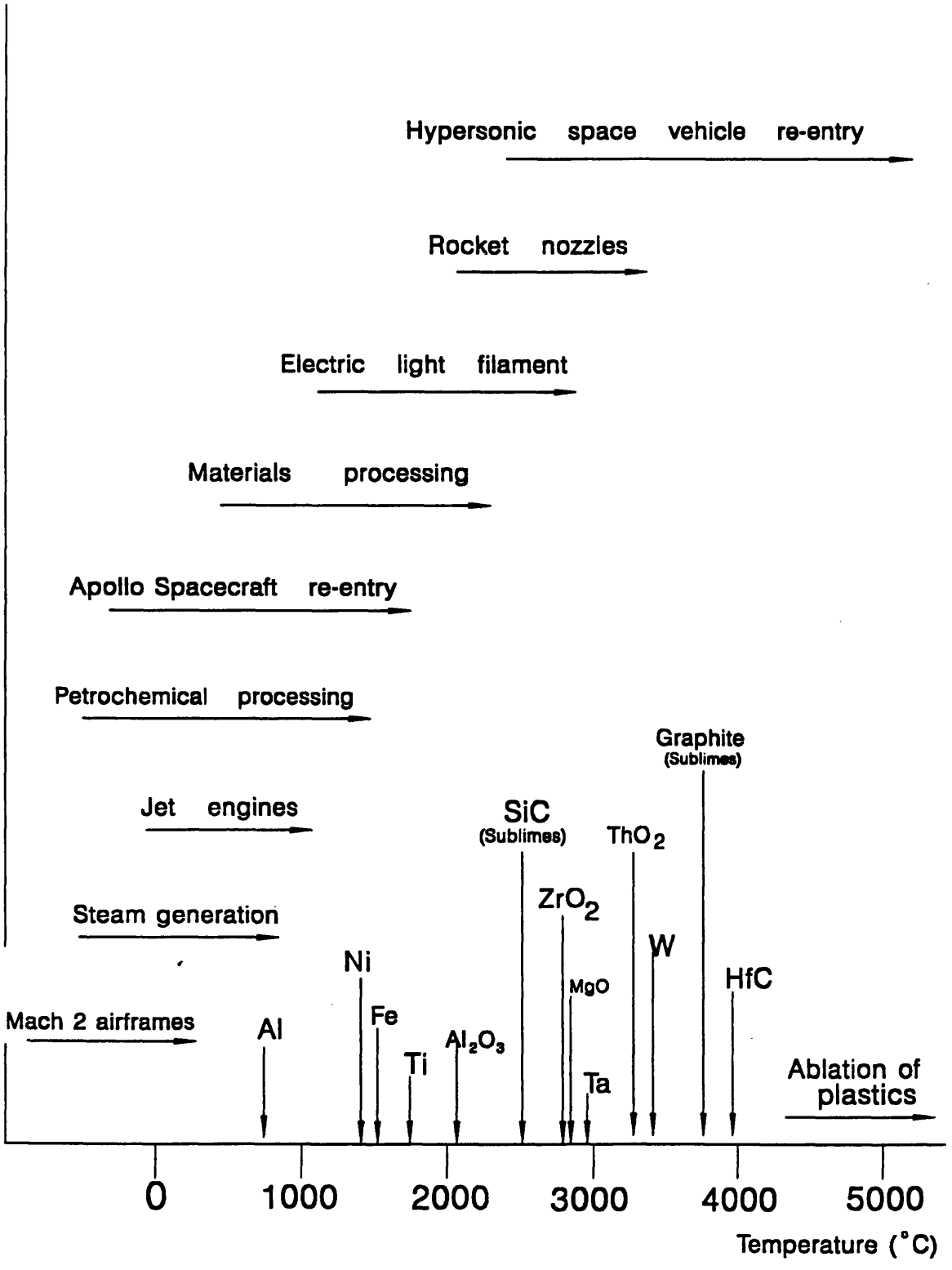

Figure I - Operating temperatures of high temperature materials (Meetham - 1991).

The ability of CFRC to retain their mechanical properties at higher temperatures, than any other material, has resulted in their exploitation as structural materials in space vehicle heat shields, rocket nozzles and aircraft brakes. However, the full potential of these materials has yet to be realised due to very high fabrication costs and poor oxidation resistance. Carbon fibre reinforced carbons exhibit thermal stability as a solid, high resistance against thermal shock due to high thermal conductivity, low thermal expansion behaviour, high strength and stiffness and chemical inertness to many substances, however they start to oxidise at temperatures as low as 500°C. A strong research effort has been applied to get less costly fabrication methods and to improve oxidation resistance, using internal additives and external coatings enabling these materials to be used for a longer time at higher temperatures (Rummler - 1983, Castro - 1991). Mainly because of the thermal expansion anisotropy of most carbonaceous materials, satisfactory coatings have proved very difficult to develop, in spite of intense effort during the past 20 years or more. There are two technical methods of oxidation protection for carbon materials. One is to coat the surface of carbon materials by refractory materials. The other is to fabricate carbon materials with an internal inhibitor, such as SiC.

The development of CFRC composites modified by internal additives and/or external coatings is therefore a subject of great technical importance for the further development of CFRC. The material which is most widely used both as a component of external coatings and as an internal additive is SiC. The incorporation of ceramic additives such as SiC into CFRC effectively converts them to hybrid materials whose mechanical and other properties will differ significantly from those of the original CFRC. Despite the extensive amount of work on coatings and additives to improve oxidation resistance of CFRC composites, there has been very little work on the effects

of these additives on mechanical properties. It is this subject which forms the basis of the work proposed in this thesis.

Thus, the overall aim of this work is to study the mechanical properties, microstructure and oxidation behaviour of CFRC composites modified by SiC obtained by a sol-gel technique. Both commercial and laboratory-manufactured CFRC were used. The structure of this thesis is as follows. In Chapter One, the literature on CFRC is reviewed from raw materials to oxidation protection systems; Chapter Two describes the experimental methods, the materials that were utilised, the manufacturing methods of the sol-gel system, the manufacturing methods of the uni-directional CFRC and C-SiC composites and the techniques to characterise them; Chapter Three details the results and discussions achieved on commercial CFRC composites; the same is done in Chapter Four and Chapter Five but in relation to the uni-directional CFRC composites and on uni-directional C-SiC composites, respectively. Chapter Six presents the summarising discussions, conclusions and proposals for future works.

CHAPTER ONE
REVIEW OF THE LITERATURE

This chapter is intended to review Carbon Fibre Reinforced Carbon (CFRC) composites. The review concerns the background information on CFRC composites from fabrication (Section 1.1), processing (Section 1.2), structure and morphology (Section 1.3), and mechanical properties (Section 1.4) to oxidation protection (Section 1.5).

1.1 - Fabrication of CFRC composites

1.1.1 - Introduction

Carbon fibre reinforced carbon composites (CFRC composites) originated probably in the late fifties, and their exact origin as a new material has not been recorded in the literature (Schmidt - 1972). It is most likely that they are the result of an accidental laboratory discovery arising from research on fibre reinforced ablative plastics, where it was found that the plastic matrix retained its binder function after carbonisation. The materials have desirable properties of monolithic graphites, such as thermal shock resistance and retention of mechanical properties at high temperatures in non oxidising environments, and in addition, the high strength of fibre reinforced composites (Schmidt - 1962, Schmidt - 1972).

One can define CRFC as a specialised engineering material composed of a carbonaceous or graphitic matrix, which is reinforced with a carbon or graphitic reinforcement material (Schmidt - 1972, Lewis - 1989, Fitzer - 1987). Their strength and stiffness are dominated by fibres and some representative values of tensile strength for different arrangement of fibres in the composite architecture are in Table 1.1 (Thomas - 1986).

Under normal conditions of temperature and pressure carbon has no liquid phase and it usually is deposited from vapour or by carbonisation of organic materials, like polymer resins or pitches (Jortner - 1986, Savage - 1988).

The technology of CFRC is similar to conventional graphite technology. Like in graphite technology, many of the properties and characteristics of CFRC can be tailored over wide ranges through variation in materials composition, construction features, and processing (Schmidt - 1972, McAllister - 1983). Their fabrication technology involves a complicated multi-stage process, with successive cycles of impregnation and heat treatments until a desired density is attained (Weisshaus - 1990a, 1990b).

CFRC	Tensile Strength (MPa) Direction		
	X	Y	Z
unidirectional (UD) fibres in x-direction	770	25	25
bidirectional (2D) fibres in x-y plane	330	330	25
orthogonal weave (3D) bundle size ratios, x:y:z=2:2:3	175	175	250

Table 1.1 - Effect of fibre bundle orientation on the tensile strength of CFRC (Thomas - 1986)

In graphite fabrication technology solid filler particles of coke, called primary carbon, are combined with a binder, which then acts as precursor for the secondary carbon formed during the baking process, *i.e.*, the carbonisation treatment. Therefore, the resulting *all carbon* material has two different phases, the primary carbon as *filler carbon* and the secondary

carbon as *binder carbon*. Carbon fibres are used as primary carbon instead of filler grains in the manufacture of CFRC (Fitzer - 1987).

There is not a universal or common process to obtain a final CFRC structure. Different types of fibres, different arrangements of reinforcement, precursors matrices, additives and processes are used (Sato - 1989). Thus, a very wide range of CFRC is possible by varying the fibre orientation and manufacturing method.

1.1.2 - Reinforcements for CFRC composites

Carbon fibres, whether from PAN, rayon or pitch precursors, are widely used to fabricate CFRC. The choice of fibre is based on the required properties and design of the final product. The final mechanical properties of the CFRC are influenced not only by the carbon fibre precursor but also by the chemical surface activity of the carbon fibres used, *i.e.*, the surface chemical groups present, or even the surface roughness of the fibre. Fibre surface treatments are proprietary processes and their main purpose is to increase the surface activity of the fibre to enhance the bonding with the precursor matrix. They are generally based on oxidative treatments under gas phase, liquid phase, electrochemical means or even by plasma etching (Kowbel - 1990, Donnet - 1990).

1.1.3 - Skeletal Preform for CFRC composites

The skeletal preform can be made in a wide variety of forms, from one-directional (UD) to n-directional (2D, 3D, etc) using unidirectional tows, tapes, or woven cloth. The preforms are described by yarn type, number of

yarns per site, spacing between adjacent sites, volume fraction of yarn in each direction, shape and nature of the preform, weave geometry and preform density as can be seen in Figure 1.1 (McAllister - 1987; Ko - 1989). Mechanical properties of the composite can be readily tailored to meet the property requirements of the final product by correct selection of the preform design (Rummler - 1983, Lachman - 1978, Gebhardt - 1976, Manocha - 1988a).

The use of a balanced filament pattern can also provide a means of reducing carbonisation stresses due to anisotropic shrinkage and shear sensitivity of the CFRC (Stoller - 1969, Huettner - 1990). Stresses and microstructural defects can also be introduced by thermo-cycling procedures due to the overall anisotropy of CFRC with emphasis on the coefficient of thermal expansion (CTE).

Two-directional (2D) fabrics are a useful form of interwoven yarns for CFRC and are characterised by the spacing between adjacent yarns, bundle size, percent of yarn in each direction, yarn packing efficiency and the complexity of the interwoven pattern. Although numerous modifications can be made to fabric weave geometry, the inherent strength of the fabric structure lies in a two-dimensional plane bounded by the thickness of the fabric (McAllister - 1983). Although CFRC composites with unidirectional orientations of fibres have no importance for technical applications, many basic investigations had been performed using them as models (Huettner - 1990).

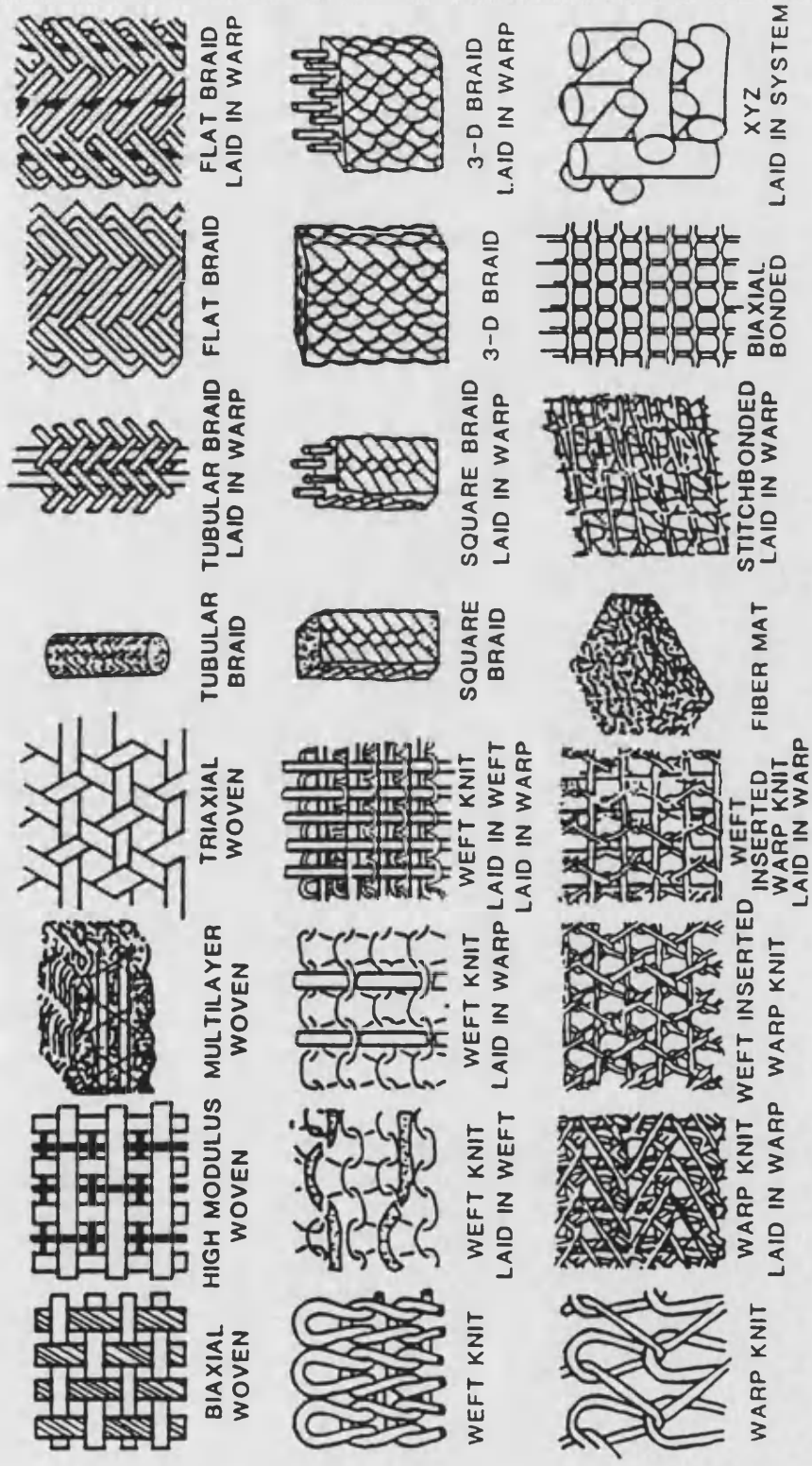

FIGURE 1.1 - Linear, planar and three-dimensional fibrous structures (Ko - 1989).

Three-directional (3D) preform structures having principally an orthogonal array of fibre bundles have been used to achieve higher isotropy of mechanical and thermal properties of CRFC. During the heat treatment process the 3D fibre arrangement reduces the problems of shrinkage of the matrix and thermal strain allowing the CFRC to be submitted to multiple thermal cycling (McAllister - 1983, McAllister - 1972, Rolincik - 1987, Lurie - 1970). As a consequence, the interlaminar shear properties of 3D CFRC will depend on the yarn density across a particular shear plane. Nowadays the designs of 3D preforms or other multidirectional weaves are aimed to improve the off-axis properties and to minimise the empty spaces that occur at filament cross-over locations (Rolincik 1987).

1.1.4 - Precursor matrices for CFRC composites

The matrices for CFRC are derived from various carbon sources and are obtained by different methods: liquid and gas phase impregnation. Gas phase impregnation (Chemical vapour deposition/infiltration) is discussed in section 1.2.1. In the liquid impregnation routes matrix precursors can be divided in two general categories :

1) aromatic (or similar) ring structured thermosetting resins, such as phenolics, polyfurfuryl alcohol, epoxides, polyimides, polyarylacetylene, furans, polybenzimidazole, and

2) pitches derived from coal tar and petroleum residues.

Due to the weight loss and change of density during carbonisation, a severe shrinkage of the precursors occurs inducing crack formation. High carbon yields reduce the shrinkage and specially the shrinkage stresses (Huettner - 1990).

When pyrolysed, thermosetting resins form a glassy, isotropic carbon with carbon yield in the range of 50-60% by weight and experimental data indicate that yields are not increased so much by the application of pressure during carbonisation. Although the conversion to carbon is low it represents a conversion efficiency around 95% of the carbon actually available. Under normal conditions they do not graphitise up to 3000°C. Shrinkage stresses induced during heat treatment can lead to a graphitic matrix structure around the fibre (Burger - 1975; Hishiyama - 1974; Zimmer - 1983).

The most common polymer matrix used to obtain a carbon char in CFRC is phenolic resin because of its easy availability and low price. They also maintain their technical importance as matrix precursor at least for the fixation of the fibre array (Fitzer - 1981, Fitzer - 1980). Phenolic resins are products of the reaction of a phenol or substituted phenol with an aldehyde, especially formaldehyde. They are classified as: novolac resins and resole resins. Phenolic novolacs are processed with a formaldehyde-phenol molar ratio between 0.5 and 0.8. Phenolic resoles are processed with a ratio of formaldehyde to phenol of 1.2:1 to 3.0:1. The different structural relationships of phenolic resins, resol or novolak, formaldehyde ratio, and cross-link density, have only a moderate effect on carbon yield (Knop - 1985). In that particular, Schmidt (1972) pointed out that the variables that influence the char yields are the carbon/hydrogen/oxygen ratio, cross-link density, presence of foreign elements like chlorine, degree of aromaticity and symmetry, and ability to undergo cyclisation and ring fusion during carbonisation.

In order to reduce and control the cross-sectional shrinkage of CFRC it is a common procedure to add fine-grained filler or extender to the matrix precursor (Fitzer - 1981, Yasuda - 1988). An extremely fine filler powder (2-3 μm) is required to penetrate the small spaces between the fibre

monofilaments. The linear shrinkage of an uncured phenolic resin is reduced from 20 to 5%, if 50 wt% graphite is added. Such filler addition is most effective if untreated fibres are used for reinforcement in the carbonised composite because the graphite powder releases stress concentration at crack tips, and crack branching easily occurs (Yasuda - 1988).

Recent studies on matrices for CFRC have considered polyarylacetylene (PAA) and polybenzimidazole (PBI) (Zaldivar - 1991b, Sandor - 1990, Economy -1992). These polymers are claimed to be useful for the design of one-step fabrication process for CFRC, as PAA and PBI carbonised at 700°C to give a carbon yield of 95% and 78% respectively. Moreover PAA graphitizes using carborane ($C_2B_{10}H_{12}$) as a graphitisation catalyst. Heat treatment at 2400°C of a PAA/carborane(5%) sample shows evidence of graphitisation by decrease of the interlayer spacing (d_{002}) to 0.3358 nm, closely approaching that of graphite (0.3354 nm) (Zaldivar - 1991a, 1991b, 1991c).

The use of pitches as matrix precursors in CFRC is an extension of the technology used in the graphite processing industry. Pitch precursors are an oligomeric mixture of polynuclear aromatic hydrocarbons which are thermoplastic in nature. The most important characteristics of pitches when chosen as matrix precursor for CFRC processing are the graphitic carbon microstructure, high density (≈2 g/cm^3), high carbon yields at atmospheric pressure (≈50% wt%), and under pressure (≈100 MPa - 90 wt%).

As represented schematically by the curves in Figure 1.2 these materials soften first at T_S, about 400°C, then viscosity shows a strong minimum at T_{Vmin} determined by DTA and plasticity measurements (Oberlin - 1984). At this stage they undergo various changes including volatilisation of low molecular weight compounds, polymerisation, cleavage

and rearrangement of molecular structure. Single mesophase spheres nucleate at the temperature for which viscosity is a minimum (T_{vmin}), then grow, coalesce and finally form a material which is still plastic, called bulk mesophase, at T_{LMO} (LMO - Local Molecular Orientation). This stage preceeds the semi-coke stage when the material solidifies (at T_R).

At the semi-coke stage, the viscoelastic solid suddenly becomes a brittle solid. At higher temperatures as the material progressively graphitizes, and increasing number of layer pairs align in the AB sequence and reach the 0.3354 nm interlayer spacing of graphite, as can be seen in Figure 1.3. The higher the pressure the more coarse and isotropic will be the microstructure. This is thought to be due to the suppression of gas formation and escape during the carbonisation reaction (Savage - 1988).

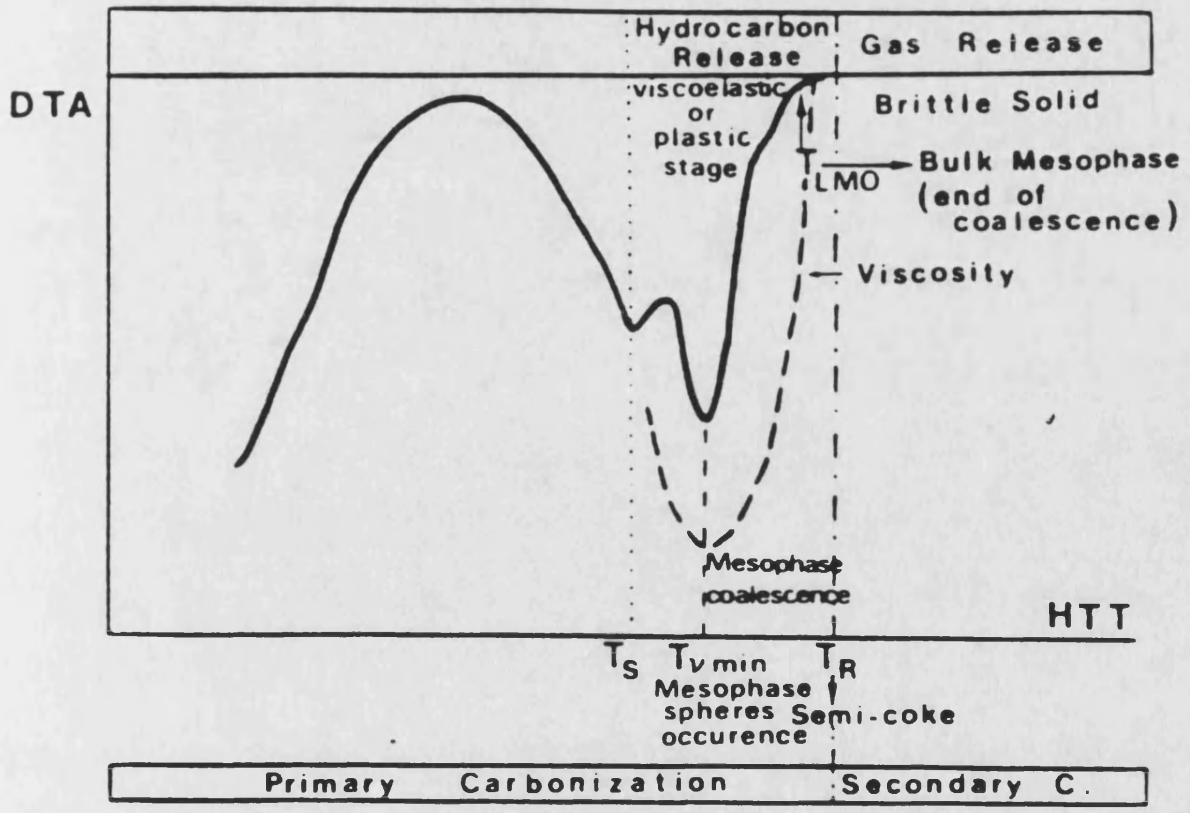

FIGURE 1.2 - Schematic sketch of the carbonisation of a graphitising carbon. T_S is the softening temperature, T_{vmin} the temperature of the minimum viscosity (mesophase spheres nucleation), T_R the resolidification temperature, T_{LMO} the temperature of bulk mesophase formation (end of coalescence and hardening). The solid line corresponds to the DTA, the dashed line corresponds to the viscosity (Oberlin - 1984).

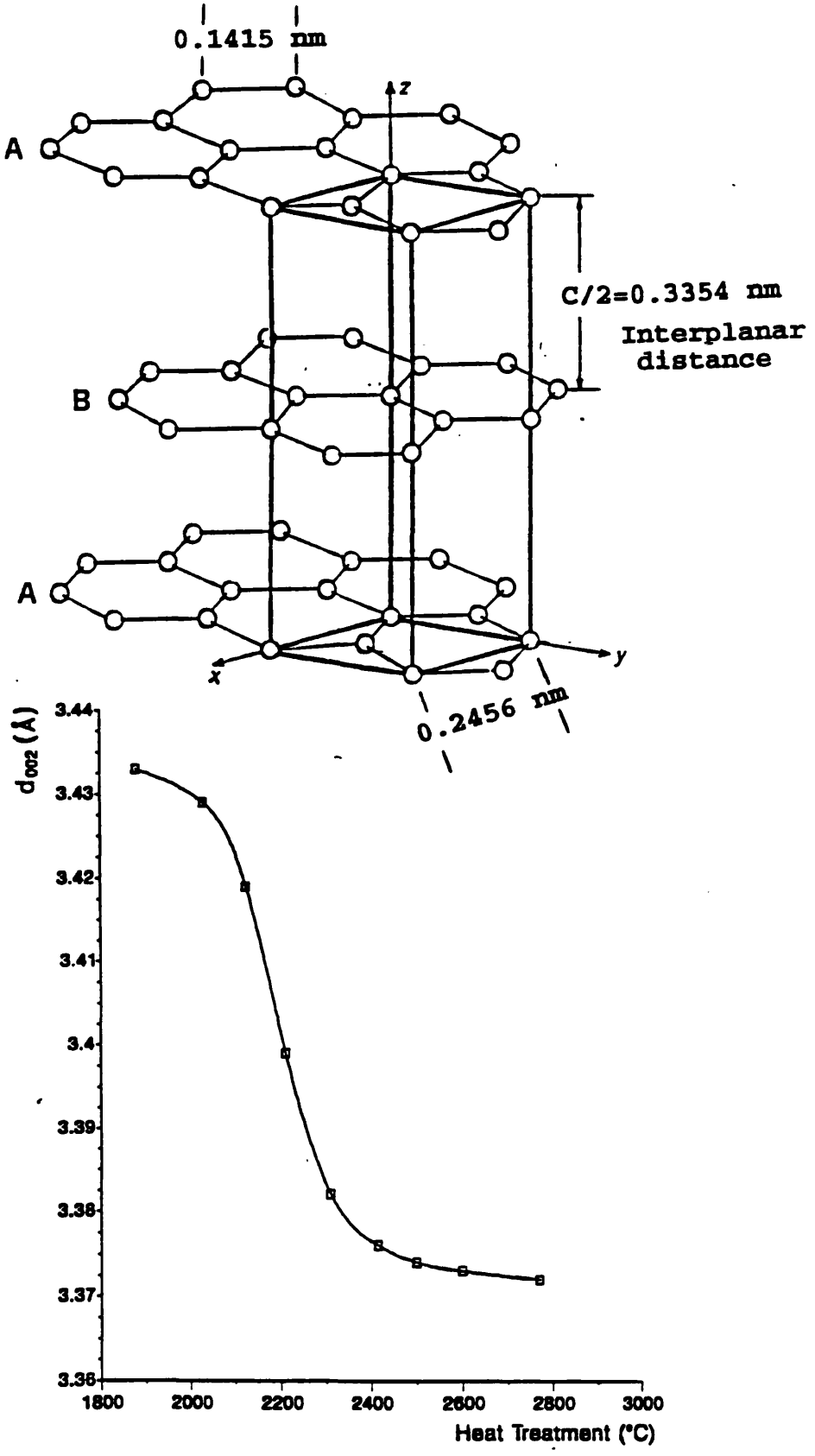

FIGURE 1.3 - Graphite structure and X-ray measurements of d_{002} of the graphitisation of a coal tar pitch carbon (Oberlin - 1984)

1.2 - Processing of CFRC composites

A schematic simplified flowchart of the fabrication of the CFRC in Figure 1.4 shows the complexity involved in the fabrication of this material. The fabrication of CFRC nowadays is a costly and time consuming process. This fact is partially due to the multiple repetition of the densification step necessary to minimise pore content and increase the density (Schmidt - 1972). The densification of the composite involves filling the interstices between the carbon fibres by basically two processes to obtain a monolithic CFRC : Gas Phase Impregnation (Chemical Vapour Deposition/Infiltration), Autoclave Liquid Impregnation and Hot Isostatic Pressing (Stoller -1969, Schmidt - 1972, Gray - 1990, Chard - 1976, Kotlensky - 1973).

The liquid impregnation procedure is similar to those of conventional fibre-reinforced resin laminating techniques. Both Liquid Impregnation and Gas Phase Impregnation (CVD/CVI) can be matched at any step of the manufacturing process tailoring the component to a specific application (Schmidt - 1972, Buckley - 1988). The choice of a process route depends upon many factors amongst which are shape, dimensions, physical, mechanical and environmental requirements, number required, availability of the equipment (Thomas - 1986).

A general rule of thumb employed by manufacturers is that the gas phase route is adequate for thin walled parts (up to a few centimetres) and the liquid method is preferable for thick parts and components requiring a high density where high pressure pitch impregnation is used (Savage - 1988). These two processes will be discussed in the next sections.

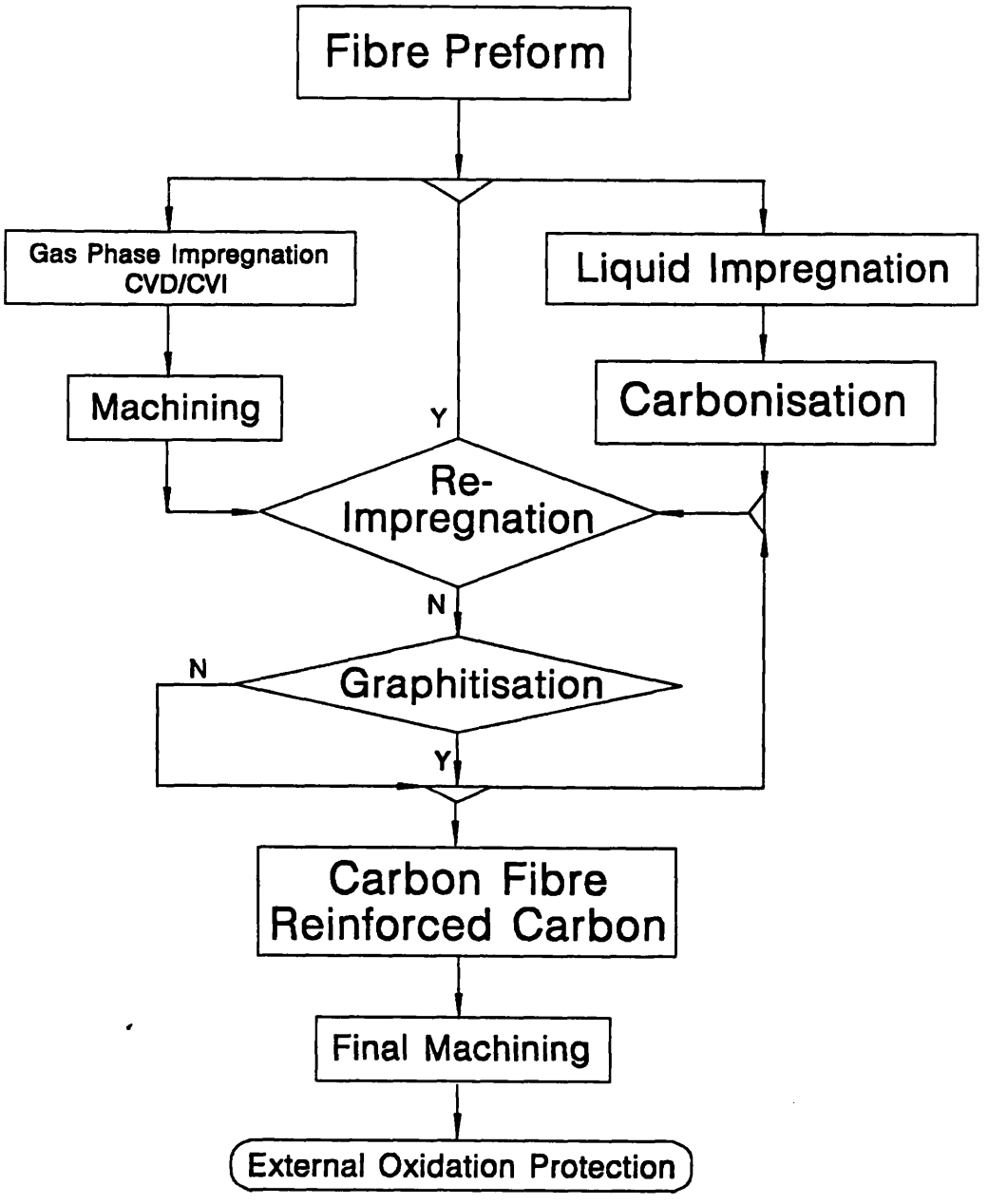

FIGURE 1.4 - Simplified flowchart of the production technology of carbon fibre reinforced carbon.

1.2.1 - Gas Phase Impregnation (CVD/CVI)

Chemical Vapour Deposition (CVD) is defined as the deposition of solid material from the vapour phase, brought about by a thermally induced chemical reaction. The CVD process where deposition occurs on an atomic scale gives very coherent deposits of controlled composition and extremely low permeability (Bashford - 1992, Dacic - 1981, Kotlensky - 1973). When the vapour phase is a carbon-bearing material the resulting product is *pyrolytic carbon*. Although in this work CVD is concerned only with carbon deposition the technology is applicable to diffusion coatings, overlay coatings, free standing monolithic components and infiltrated composites.

The different characteristics of the gas phase impregnation deposits (*i.e.* composition, thickness, smoothness, structure) are related to experimental parameters such as temperature, pressure, gas flow rate, dilution of the reactants in an inert gas carrier, method of heating the substrate (HF, flame, plasma, electric arc) and to the general configuration of the apparatus. The conditions of processing can vary, depending upon the component thickness, degree of densification and structure required. Typical gas phase process may require several cycles, taking several hundred hours and maybe months with a residual porosity of up to 10 to 20%. Between cycles it is usually necessary to machine the composite to remove excess pyrocarbon deposit, which may seal the outside surface. One of the major problems of the gas phase process is that of densifying the inner layers of a component as fully as the outer layers (Thomas - 1986). The efficient determination of the optimum experimental parameters and the degree to which they must be controlled in order to prepare reproducible products requires a detailed understanding of each system. It is also necessary to know the chemistry of the system, the equilibrium thermodynamic yields, the possible chemical kinetic rate-limiting mechanisms and mass transport

processes (Duret - 1986).

An essential requirement of the CVD process is the availability of suitable vapour sources, the selection of which is important, both in terms of process costs and deposition temperature. Selection can markedly influence the morphology of the coatings which are invariably formed by columnar grain growth (Bashford - 1992).

The coatings achieved within porous, eg fibrous substrates, to produce densified composites are referred to as Chemical Vapour Infiltration (CVI) (Bashford - 1992). As in all heterogeneous gas-solid reactions, the temperature dependence of the chemical reaction is many times higher than that of the transport steps, and the control of the overall reaction rate by diffusion must be avoided. So, low temperatures will promote reaction rate control of the heterogeneous deposition, although this condition will take a lengthy impregnation time (Fitzer - 1987).

There are basically three CVD techniques that can be employed for infiltrating pyrocarbon into a porous substrate and they are defined according to the decomposition temperature and the method of introduction of the gas, that are schematically illustrated in Figure 1.5 (Schmidt - 1972, Buckley - 1988, Diefendorf - 1987, Gebhardt - 1976, Kotlensky - 1973).

The processing difficulties associated with maintaining the thermal and pressure gradient methods means that they are generally only employed to densify single artefacts whereas the isothermal technique can be used on multiple workpieces. In the isothermal method, Figure 1.5A, a carbon containing gas is passed over and through a porous heated preform which is radiantly heated by an electrical resistance furnace or induction coil at about 980°C to 1500°C and carbon is deposited within the open pores under a pressure of 7 kPa to 1000 kPa. The isothermal technique produces deposits

of high density, high modulus, highly graphitisable and which are quite pure. In this technique there is a tendency for preferential deposition on the exterior surfaces of the sample, resulting in the formation of a crust, requiring machining and multiple infiltration cycles. The structure consists of turbostratic crystallites of 15-35 nm apparent diameter and 10-25 nm apparent thickness, with the basal planes oriented approximately parallel to the substrate surface (Warren - 1972).

When a carbon matrix is deposited from propane it gives a microstructure that can be isotropic, rough laminar and columnar depending on the pressure, temperature and percentage of the hydrocarbon in the gas, as can be seen by the diagram on Figure 1.6 (Oh - 1988, Kimura - 1981). During the infiltration process the pyrolytic carbon matrix will deposit as a sheath around each fibre, with the basal planes (AB direction) aligned parallel to the long axes of the fibre (Granoff - 1973). As a general rule there is a decrease in the strength with increasing deposition temperature due to the change in the microstructure from laminar to granular. Thus the CVI process has to be carried out at a low temperature and pressure in order to obtain the desired rough laminar microstructure (Kowbel - 1989).

In the pressure differential method, Figure 1.5B, a differential pressure is established across the thickness of an isothermally heated porous preform. The carbon containing gas is forced to flow through the porous substrate that results in a uniform deposit.

In the thermal gradient technique (differential temperature), Figure 1.5C, the part to be impregnated is supported by an inductively-heated mandrel at atmospheric pressure. The inside surface of the substrate will therefore be the hottest. Surface crusting is eliminated because the decomposition rate is greater on the hotter fibres close to the mandrel, whereas the cooler outer fibres receive little or no deposit.

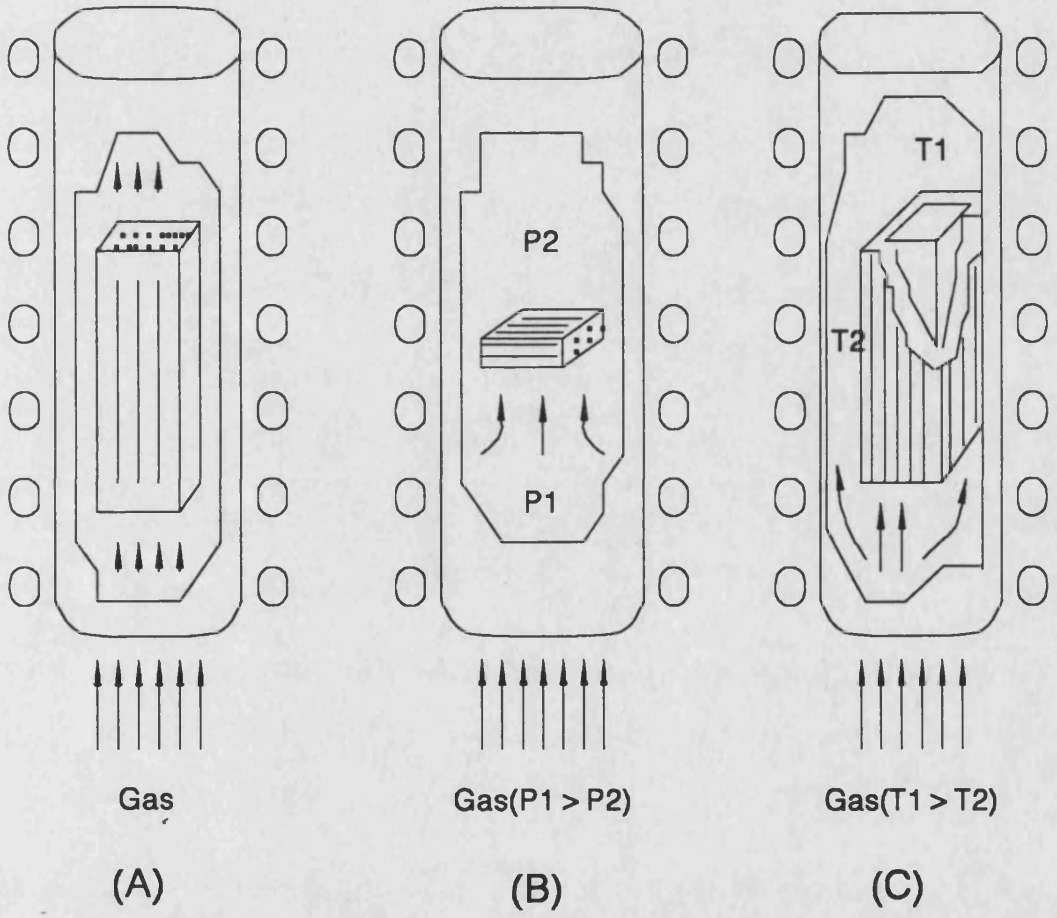

FIGURE 1.5 - Gas phase impregnation processes. 5A - isothermal, 5B - pressure differential, 5C - thermal gradient (Kotlensky - 1973).

The outer surface temperature of the low density substrate is kept below the threshold pyrolysis temperature of the carbon-bearing gas or at a temperature where the deposition rate at the surface is below the deposition rate of carbon in the pores, thereby minimising the deposition of a surface coating and leading to shorter infiltration times required to reach a desired density. Under working conditions the carbon is first deposited on the inside surface and, in a continuous process, progresses radially through the substrate as the impregnated substrate itself becomes inductively heated (Savage - 1988). The limitations of this particular process is low reproducibility, nonuniform deposition within the part and inability to process multiple parts at one time (Buckley - 1988).

The type, rate and efficiency of pyrocarbon infiltration is highly dependent upon the following conditions:

a) carbon composition and flow rate of the gas,

b) presence of a carrier gas,

c) pyrolysis conditions including temperature and pressure, and

d) architectural structure of the preform.

The kinetic of infiltration is determined by open pore volume and not by the surface area on which the deposition of carbon takes place. Therefore it follows that infiltration is controlled by reactions occurring in the volume of the open pores, rather than on their walls (Marinkovic - 1985). The mechanical properties are found to increase more rapidly with apparent density when the fibre content is higher, which is explained by the smaller average interfibre distance, leading to the creation of more bridges between fibres per introduced quantity of CVD carbon (Marinkovic - 1985).

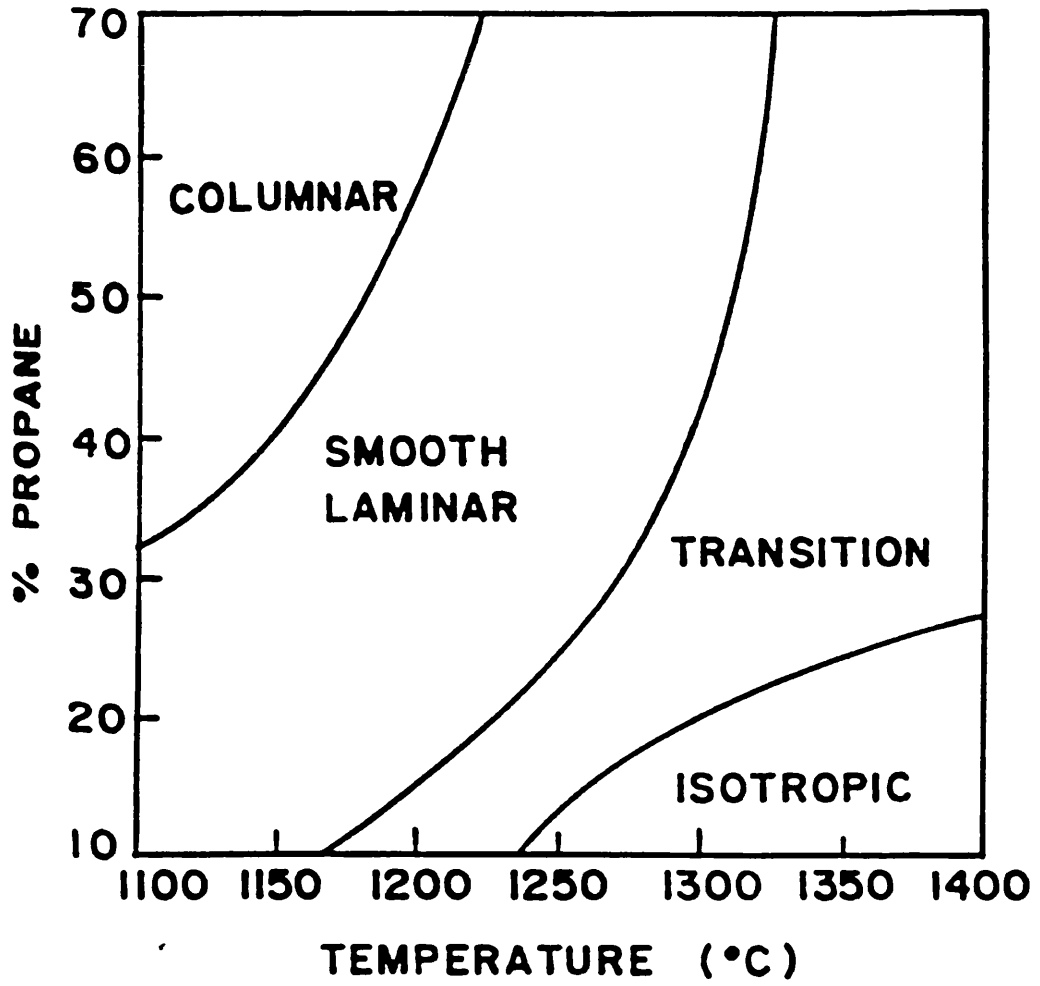

FIGURE 1.6 - Effect of deposition conditions on microstructure of pyrolytic carbon matrix deposited from propane (Oh - 1988).

To increase the versatility of CVD, there are other options for initiating a reaction other than heat alone, these are energised routes using, for example, lasers, microwaves and plasmas (Bashford - 1992).

1.2.2 - Liquid Impregnation of CFRC composites

The liquid impregnation can be made either in an autoclave or in a hot isostatic press (Fitzer - 1986, Chard - 1976). The initial impregnation of the preform is generally done to stabilise it. The characteristics that must be considered in the selection of a matrix precursor are viscosity, carbon yield, matrix microstructure and matrix crystal structure (Fitzer - 1987). During the impregnation process, good wetting is essential for filling the fine pores and the residue of the impregnation liquid should shrink away from the pore surfaces in order to open new pore entrances, and inhibit pore blocking (Fitzer - 1987, Gray - 1990). Carbonisation under pressure can be used to improve the compatibility of blend components and it has a strong influence on the porosity of the resultant carbon (Forrest - 1983).

Hot Isostatic Pressing (HIP) is a well known process in powder metallurgy and can also be used to obtain CFRC. In this case, the preform and the organic matrix are sealed in a can and placed in the HIP unit. The temperature is raised at a programmed rate and the pressure is increased and maintained at the level required. The sealed container acts like a *rubber bag* and it aids the pressure transference to the work piece. As the organic matrix begins to carbonise the high isostatic pressure will maintain the more volatile fractions in a condensed phase (Gray - 1990).

When reheating impregnated materials under atmospheric pressure a relative large back-flow of organic matrix, of molten pitch or resin occurs,

which is called *exudation*. For pitches, after heating up to 800°C, only 30% weight of the initially introduced pitch remain as coke in the porosity (Guajioty - 1990). The gas flow out during the heating up on the samples is the main driving force of the exudation process.

A theoretical limit of pitch densification efficiency is estimated to be about 55%, although at atmospheric pressure densification results in efficiencies of only 15% to 20%. Hot isostatic pressing processing to 100 MPa results in densification efficiencies of about 35% in the early cycles and in a fifth cycle to almost 50%. This increase in efficiency, *i.e.*, the higher density/lower porosity in later cycles, is believed to be due to the greater surface area-to-volume ratio of carbon matrix and the greater tortuosity of the pore structure (Rellick - 1990). Greater surface area promotes gas-cracking reactions that increase carbon yield, and greater tortuosity serves to reduce pitch expulsion resulting from gas evolution during pyrolysis (Rellick-1990).

1.2.3 - Heat Treatment of CFRC composites

After curing the composite and/or impregnation of the CFRC, the *green* component is pyrolysed in a schedule known as carbonisation, which results in the formation of residual carbon (Schmidt - 1972, Chlopek - 1991). The carbonisation process is exceedingly complex and known to involve a wide variety of concurrent and sequential chemical reactions and the heating rates depend on the size and the shape of the composite (Lewis - 1990).

The carbonisation can be performed at atmospheric pressure or under pressures ranging from 6 to 100 MPa, although above 70 MPa the

increase in carbon yield becomes almost negligible. Pressure, applied during the period while the precursor is liquid, influences total bubble volume; at low pressures the gas volume is sufficient to expel liquid from the skeleton, leading to a reduction in effective carbon yield. High-pressure carbonisation improves yield by suppressing outflow, as well as by improving chemical efficiency (Jortner - 1989). Results from Dillon (1990) indicate that there is a rapid decrease in the total surface area with increasing carbonisation pressure.

Slow carbonisation cycles are required to minimise the effects of gas evolution from the carbonising impregnant (McAllister - 1987, Burns - 1976). In general, the heating rates and final heat treatment temperatures are the most important process parameters. As a general rule the shrinkage increases with increasing heating rate. Low heating rates during conversion improve the final strength properties; an intermediate graphitisation between other carbonisation steps improves the Young's modulus and results in high bulk densities (Fitzer - 1981, Fitzer - 1986, Schmidt - 1972).

Differential thermogravimetric analysis (DTA) and dilatometry are the techniques that give a suitable idea of how a carbonisation heat cycle can be performed. With DTA analysis one can identify the exothermic/endothermic reactions and weight loss inflection points. With dilatometry the temperature range where the linear shrinkage is greatest can be identified. This information can be used to derive a heating schedule which avoids large shrinkage stresses leading to cracks and possible damage of the fibres. A general carbonisation heat cycle based on DTA for some thermosetting resins was suggested by Perry (1974): starting from room temperature to 280°C at 30°C/h, from 280°C to 450°C at 10°C/h , and from 450°C to 800°C at 40°C/h. The main shrinkage interval for phenolics corresponds to the weight loss interval (≈400°C) and the final linear

shrinkage of 20% at 1000°C is characteristic (Burger - 1975).

Thermogravimetric curves of the pyrolysis of phenolic resins obtained by Jenkins (1976) at different rates of temperature rise (from 0.1 to 2.0°C/min), showed that all curves are superimposable if weight loss is plotted against temperature. This can be interpreted as an indication that at any given temperature the chemical process of pyrolysis moves to completion so rapidly that the chemical kinetics have no effect on the weight-loss curves.

The thermal degradation of phenolics is conveniently divided into three stages, indicated by weight loss and volume change. In the first stage up to 300°C, the polymer remains virtually intact. The quantity of gaseous components released during this stage is relatively small (1-2%) and consists mainly of water and unreacted monomers, phenol and formaldehyde, which were entrapped during cure. The second stage begins with the start of the decomposition at 300°C, and from this temperature until 600°C, where the reaction rate reaches a maximum, mainly gaseous components are emitted. In this stage gases described earlier are released and during this degradation stage random chain scission occurs, but shrinkage is relatively low.

The third stage above 600°C, gaseous products such as CO_2, CH_4, H_2O, benzene, toluene, phenol, cresols and xylenes are liberated. There is always a thermo-oxidative process taking place regardless of whether the pyrolysis reaction occurs in an oxidative or inert atmosphere. The high oxygen content of phenolic resins is the reason for this (Knop - 1985, Bradshaw - 1978).

Gas analysis and mass spectrometry data concerning the carbonisation of cured bulk samples of resol type phenol formaldehyde resin

showed that the evolution of water is significant between 150°C and 700°C, stabilising at this temperature with 12% water evolution per unit weight of sample, Figure 1.7 (Lausevic - 1986). Regarding Figure 1.7, the rate of hydrogen evolution occurs in two overlapping reactions with a deflection at about 550°C with a maximum at 700°C. The maximum of the first reaction leading to hydrogen evolution coincides with the maximum rate of CH_4 and CO formation. The maximum rate of CO_2 evolution is shifted towards higher temperatures, Figure 1.8. Above 600°C condensation of aromatic ribbon molecules starts followed by large evolution of hydrogen (Jenkins - 1976). As in the bulk samples diffusion is hindered, it results in a high vapour and capillary pressure of water which can react with the surrounding polymer structure, releasing H_2.

A co-carbonisation process is also possible in a composite when made with oxidised PAN fibres in a phenolic resin matrix (Markovic - 1980). The experiment showed that the fibres would shrink away from the carbon matrix possibly reducing internal strains leading to breakage of the fibres. The chemical reactions between the oxidised PAN fibres and the phenolic matrix starts at 300°C and the most important changes were produced at 600-700°C, when the fibre and matrix coalesce into a almost uniform mass. The obtained product had relatively high density and low narrow porosity although it was not suitable for structural use

Pitch-based carbons and graphites are unique among structural materials in forming their microstructures by liquid crystal mechanisms (White - 1989). Upon pyrolysis aromatic polymerisation carries most of it through a mesophase (liquid crystalline) state, in which the graphitisability of the coke is established by parallel alignment of the large aromatic molecules.

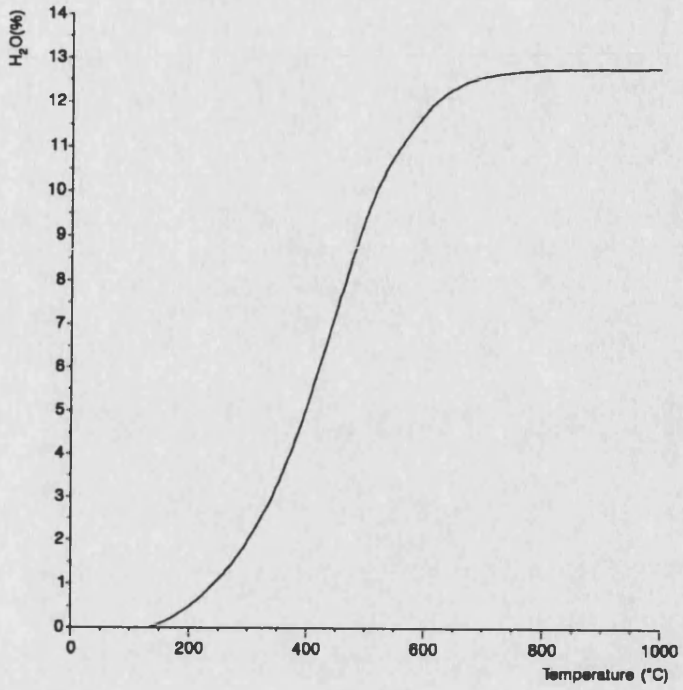

FIGURE 1.7 - Water evolution per unit weight of bulk cured phenolic resin as a function of temperature (Lausevic - 1986).

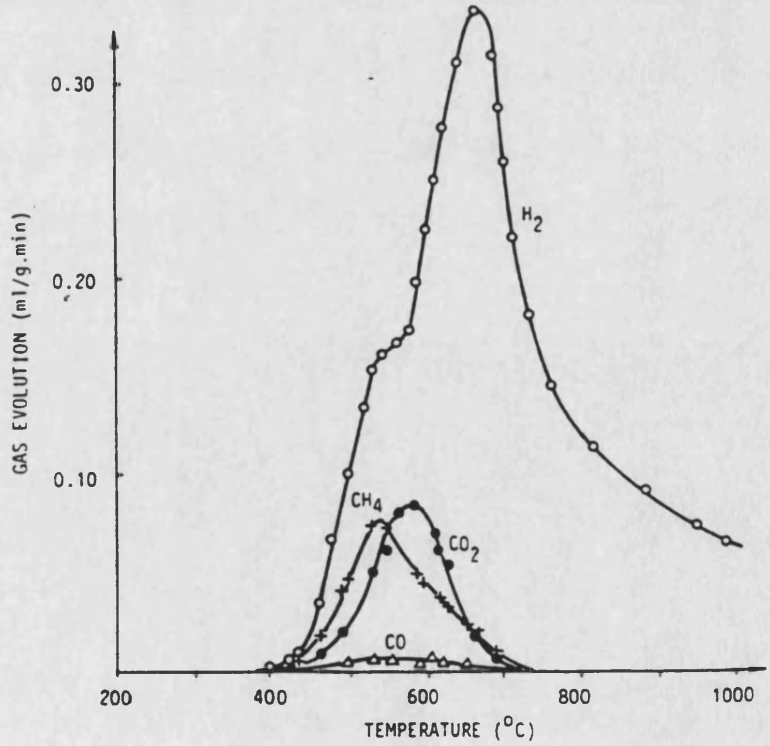

FIGURE 1.8 - Rate of gas evolution for bulk cured phenolic resin as a function of temperature (Lausevic 1986).

When there is a lack of reinforcement in a given direction, as in 2D preforms, some composites are vulnerable to bloating during pyrolysis. Trying to avoid this problem White (1989) carried out an oxidation process at 222°C on a pitch impregnated 2D preform and then carbonised it up to 1100°C. The author claimed that the oxidation step offered the advantages of prevention of mesophase softening and bloating in carbonisation, preservation of the matrix microstructure established while the mesophase was fluid or deformable, increased carbon yield and elimination of the need for high-pressure autoclaves in composite processing.

The graphitisation process for CFRC is an optional step and depends on the required operational conditions of the component. The most significant trend is believed to be the reduction of elastic modulus and the increased strain-to-failure of materials in the graphitised condition (Stoller - 1969). The degree of graphitisation is characterised by the interlayer spacing (d_{002}) and crystallite height (L_c). Experimental results indicate that the duration of graphitisation, either long or short, had a minor effect on the final extent of graphitisation and structure, although compression strength tends to be reduced with longer processes (Weisshaus -1990, Weisshaus - 1991). As a general rule graphitisation cycles are often interspersed with re-impregnation or CVD cycles in order to achieve higher densities (Thomas-1986).

1.2.4 - Dimensional changes during carbonisation of CFRC composites

Manocha (1988b) studied pyrolysis of unidirectional composites made with four types of high modulus PAN based carbon fibres having different surface characteristics. The fibres used were nonsurface treated

and unsized, nonsurface treated and sized, surface treated and unsized and surface treated and sized, with a polyfurfuryl alcohol resin as matrix precursor. The results showed that dimensional changes taking place in direction parallel to the fibres are controlled by the longitudinal thermal expansion of the carbon fibres. The matrix shrinks due to thermal degradation of polymer chains in the temperature range 350-600°C and coalescence of C-C chains in the temperature range 600-800°C.

The thermal expansion of carbon fibres is very small, and these composites exhibit very little dimensional changes in the direction parallel to them. However, in a direction perpendicular to the fibres (width as well as thickness direction), appreciable dimensional changes are observed. The composites and the unreinforced polymer exhibit expansion up to about 200°C due to the reversible physical phenomenon of thermal expansion in solids. On further heat treatment, a decrease in the rate of expansion was observed and in the temperature range 300-450°C, they started to exhibit shrinkage. In composites made with carbon fibres, shrinkage starts at 350°C while in those made with non surface treated carbon fibres it starts at around 420°C. However, in all composites the maximum shrinkage takes place in the temperature range 450-650°C. The surface finish, either a coating of PVA or epoxy resin, causes a decreases in the shrinkage of the composites made with surface treated fibres but has the opposite effect on shrinkage or composites made with non surface treated fibres. It was concluded that composites made with non surface treated fibres have a weak physical bonding, weaker than the C-C bonding in the charred matrix, the matrix shrinks away from the fibres with little displacement of the fibres, and these composites exhibit low carbonisation shrinkage. However, in composites made with surface treated fibres, the fibre/matrix bonding is quite strong and during pyrolysis the matrix does not leave the fibres, rather it shrinks onto them, resulting in a large carbonisation shrinkage.

1.3 - Structure and morphology of CFRC composites

1.3.1 - Introduction

It is difficult to categorise CFRC composites because of the wide variation possible in the fabrication process and type of materials employed to make them (Davis - 1976). Their structure depends on a number of factors such as the available raw materials and includes voids, interfaces of several different types and morphologies.

A representative minimechanical microstructure of a 3D CRFC composite is shown in Figure 1.9 (Jortner - 1986). The building blocks of the 3D CFRC composite are the fibre bundles (essentially unidirectional composites), the interbundle matrix, and the macroporosity. Shrinkage cracks, thermal-stress cracks and bubble-like pores appear to be unavoidable results of heat treatment, and constitute the main types of macroporosity in these composites.

The matrix microstructure can be intentionally varied by manipulating factors such as fibre spacing, heat-treatment rate and temperature, matrix precursor, and processing pressure (Meyer - 1986, Huettner - 1990, Weisshaus - 1991). If the properties of CRFC are in part determined by the properties of the matrix, then altering the matrix and observing the resulting changes in the composite's thermo-mechanical properties would be important for understanding the behaviour of CRFC (Meyer - 1986, Inagaki - 1990, Jortner - 1986).

1.3.2 - Matrix microstructures

Non-melting polymers such as phenolics and epoxides are precursors

for non-graphitising carbons, the so-called *hard carbons*. They are hard and brittle so that failure occurs catastrophically. Hard carbons also have lower thermal and electrical conductivities and more isotropic structure compared to graphitisable matrices. This behaviour is explained by the strong crosslinkage within the polymer, which results in polyaromatic structures with an isotropic distribution within the residue (Burger - 1975, Jenkins - 1976, Meyer - 1986).

The degree of anisotropy depends on the type of matrix precursor used. The orientation is reduced if matrix precursors, such as pitches, modified with elemental sulphur or cross-linked thermosetting resins which tend to form less graphitisable cokes, are used. Preferred orientation in the matrix, however, is found in all cases. It is now well established that, even with less graphitisable carbons small matrix sheaths surround the fibre surface. This again is a confirmation of the known effect of solid carbon surfaces upon the structure of carbon from non-melting resins, described as the *stress graphitisation effect* and it is confined usually as a sheath-like structure about 1-3 μm thick adjacent to the fibre (Fitzer - 1981, Zaldivar - 1991c). This phenomenon in *hard carbons* confirms the fact that external stress must be applied at some point in the heat-treatment process to obtain graphitisation. As for example hot-stretching at 2800°C and elongations of nearly 30%, were necessary to increase the modulus of PAN-based carbon fibres from 60 to 90 MPa (Zaldivar - 1991c).

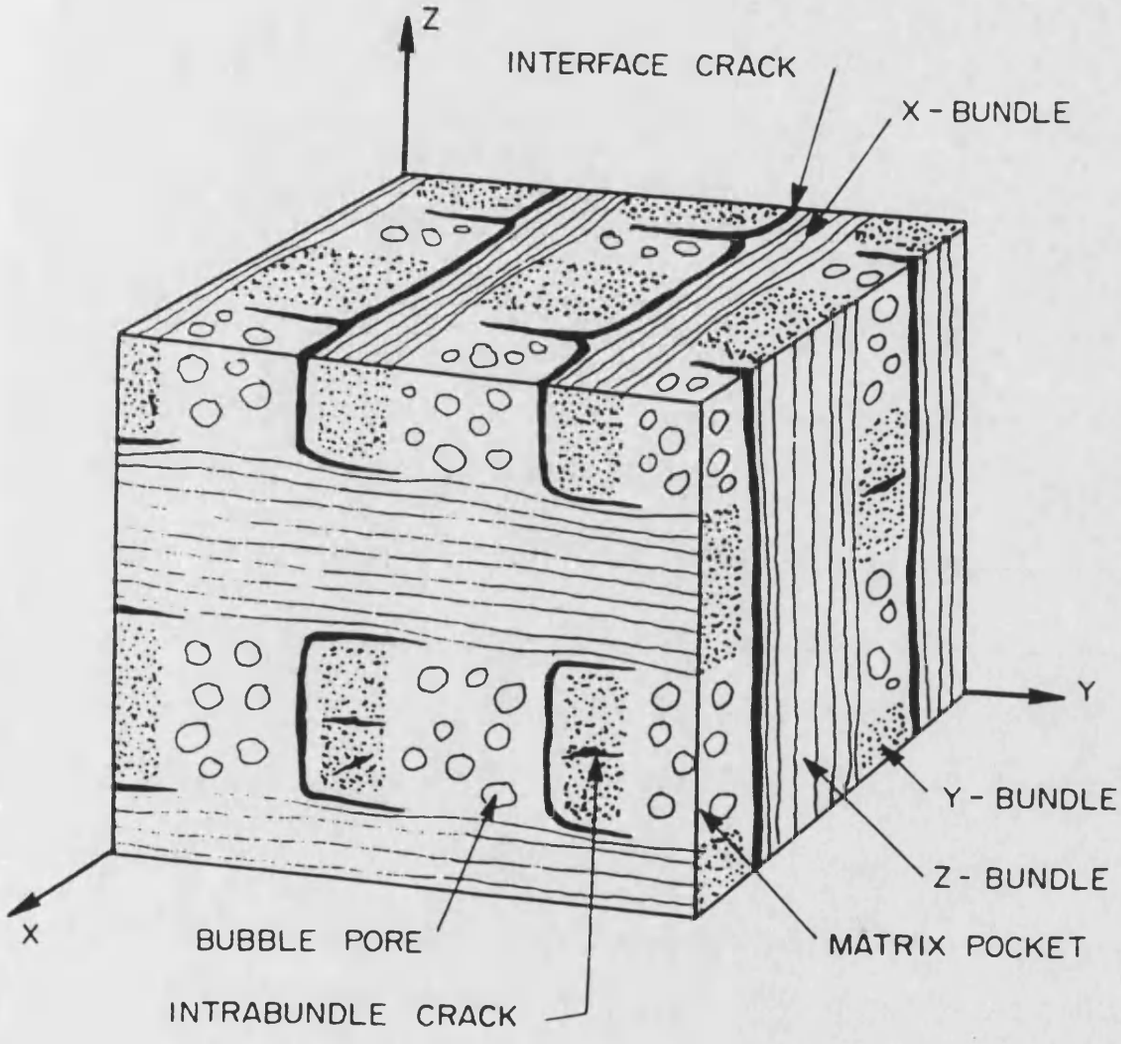

FIGURE 1.9 - Mini-mechanical features of 3D carbon fibre reinforced carbon (Jortner - 1986).

1.3.3 - Resin carbon matrices

The structure of glassy carbons derived from thermosetting resins was defined by Jenkins (1976) and it is widely accepted. Glassy carbons are made up of condensed aromatic ribbon molecules which are oriented randomly and tangled in a complicated manner, as shown in the three-dimensional structural model of Figure 1.10. Transmission electron microscopy of a typical glassy carbon shows that the edges consist of a network arrangement of strings or microfibrils, the thickness of which is about 3 nm. Each string is considered to be a stack of graphite-like ribbon molecules. The microfibrils twist, bend and intertwine. The strong confluences in the network of microfibrils occur where ribbons merge into each other; weak confluences occur where ribbons overlap. The geometry is such that pores are inevitable between the microfibrils. Micropores can be discerned, where the strings form a network structure. The orientation of the microfibrils is clearly random and fracture occurs at the interfibrillar boundary. No *loose ends* are apparent; this explains the characteristic chemical inertness of glassy carbon.

The high resistance to graphitisation of glassy carbon suggests that the configuration of these ribbons is very stable (Jenkins - 1976). But if they are treated to 2400°C or higher a graphitic matrix is formed even with thermoset precursors, a lamellar microstructure appears parallel to the filament surfaces (Huettner - 1990). The broad amorphous 001 peaks observed after carbonising to 1000°C (d_c=0.344 nm, L_c= 6.5 nm) changed on graphitising to sharper complex double peaks, which indicated the presence of more highly ordered structures (d_c=0.338 nm, L_c=35 nm) (Thomas - 1978). These structural changes were found to be anisotropic, *i.e.* the graphitic nature of the 001 diffraction peaks observed normal to the fibres was not observed when viewed parallel to the fibres. This led to the idea that the

matrix was undergoing graphitisation with orientation of basal planes parallel to the fibres, leading to the stress-induced graphitisation which occurred at the fibre-matrix interface, the fibre and matrix being consumed in the formation of a graphitic sheath with basal planes (Thomas - 1978a, Meyer - 1986, Manocha - 1988c).

1.3.4 - Pitch carbon matrices

Pitches are mesogenic, indicating the importance of the liquid crystalline characteristics of the pitch as far as pitch selection is concerned. The resulting matrix morphologies, whether spherular, grain-like or lamellar, may be regarded as *living* morphologies, changing with respect to their location and thermal history. The kinetics of the morphological transformation depend on the size of the structural units, and the smaller the units the faster is transformation. According Weisshaus (1990b) the configuration of the reinforcement, whether unidirectional, bidirectional or tridirectional, affects the developing morphologies due to the interspaces formed and packing density of the fibres. No effects of fibre type and graphitisation duration were observed on the matrix morphology, under conditions used. Microcracks, formed due to thermal induced stresses, are located either at the fibre-lamellar sheath interfaces or between different matrix pocket morphologies. The pitch matrix shows a number of defects in the crystalline structure described as disclinations that are usually formed in the interfilamentary regions. The disclination structure influences the direction of the crack path. No straight, brittle-like cracks can occur, because the crack follows the tortuous disclination shape and energy for crack propagation is therefore consumed.

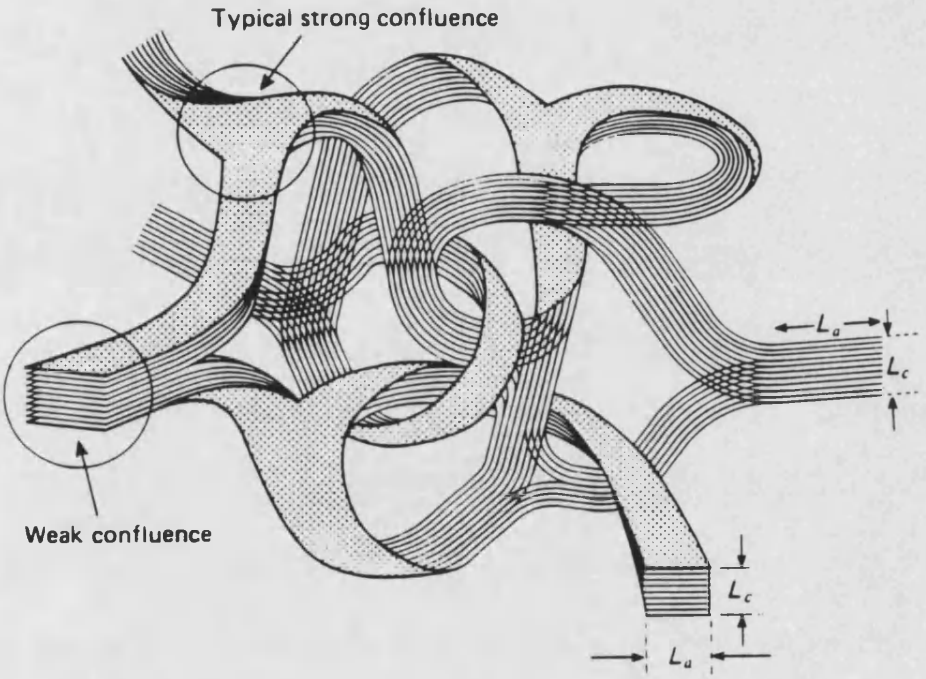

FIGURE 1.10, - Schematic structural model for a glassy carbon (Jenkins - 1976).

Good graphitic order of the matrix carbon reduces toughness, because there is more extensive microcracking in the matrix and the chance for multiple fracturing is the greatest (Huettner - 1990). Crystalline matrices like pitch seem to be not quite as strong as glassy carbons and they have a lower effective modulus. But their increased strain capability ensures that failure is not catastrophic. The energy required for total failure of pitch carbons is greater than for glassy carbons since pitch carbons are more tolerant to defects or stress raisers (Meyer - 1986).

1.3.5 - Carbon matrices derived from resin/pitch blends

It has been reported (Inagaki - 1990) that the carbons with fine mosaic texture (random arrangement of small oriented domains) is the best material as the matrix for these composites because of outstanding resistance to thermal shock and of high mechanical strength. A combination is possible of the graphitic structure of pitch carbons with the higher carbon yield from certain resins by the use of a blend of resin and pitch as matrix precursor in CFRC. However, if pitch and resin do not interact on carbonisation, a two-phase optical texture results in which the isotropic texture of the resin carbon and the anisotropic texture of the pitch carbon occur in sharply defined regions. If the resin and pitch partially interact, these isotropic and anisotropic regions still occur but with a gradation of optical texture across the boundary between them. If they interact completely then a homogeneous anisotropic texture results which is not the same as carbon from the pitch carbonised singly, *i.e.*, the resin modified the optical texture of the pitch carbon. The interaction of pitch and phenolic resin is supposed to be caused by low molecular weight components in the pitch or pyrolysed products from the pitch. They penetrate into phenolic

resin, undergoing pyrolysis, and cause the growth of condensed ring compounds which induce the nucleation of mesophase. So, the interaction between pitch and phenolic resin during pressure carbonisation is caused by low molecular weight components in the pitch or pyrolysed products from the pitch (Inagaki - 1990).

1.3.6 - Cracks and voids in CFRC composites

An important structural feature of the CFRC is that they possess a very low thermal expansion over the range of -150 to 3000°C. Typical plots of the coefficient of thermal expansion for a 2D CFRC composite compared with a fine-grained ATJ graphite and pyrolitic carbon are shown in Figure 1.11 (Huettner - 1990, Meyer - 1986). The thermal expansion of 2D CFRC composites is highly anisotropic but the coefficient of thermal expansion have positive values at temperatures higher than 800°C. The CTE parallel to fibre laminae tends to be fibre dominated having a negative thermal expansion in the range 100-800°C, as graphite itself has a negative thermal expansion coefficient in the (001) plane, while the CTE perpendicular to fibre laminae depends on matrix, fibre and voids.

Significant microcracks and voids in the matrix of the CFRC usually have two causes:

(a) volume changes during heating of the precursor matrix, especially from the shrinkage of carbon matrix, and

(b) stresses due to differences in the coefficient of thermal expansion between fibres and matrix (Pollock - 1990).

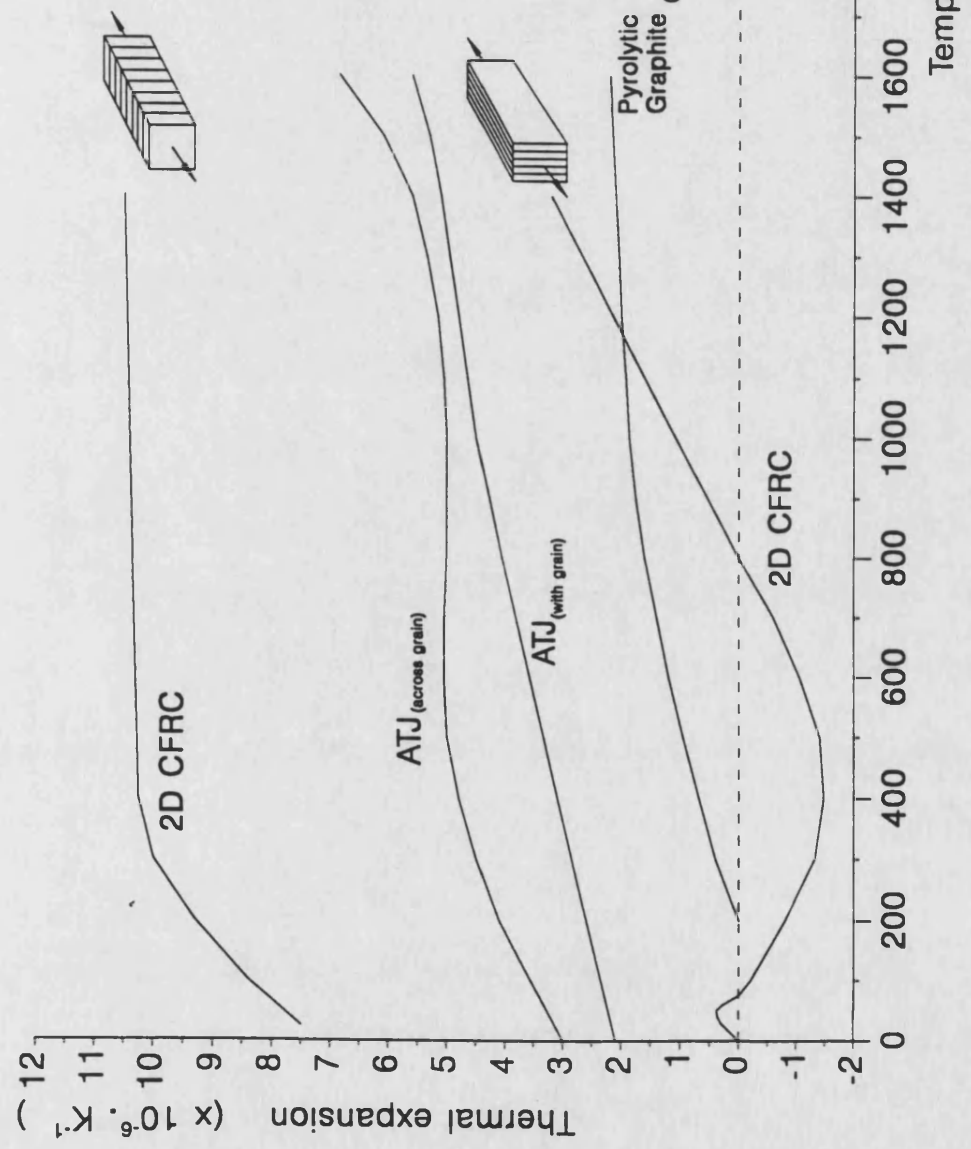

FIGURE 1.11 - Typical plots of the coefficient of thermal expansion of carbon materials. The 2D CFRC is heat-treated at 2500°C (Huettner - 1990).

The interactions between fibre and matrix can be separated into the following categories (Bradshaw - 1978):

1) interactions which occur during prepregging, *e.g.* wetting of individual filaments and filament-roving penetration, and

2) interactions occurring during pyrolysis.

In the latter case pyrolysis may affect:

a) the fibres' properties, *e.g.* degradation in fibre strength resulting from chemical attack of the fibre surface by the gases of pyrolysis:

b) the matrix properties, *e.g.* the formation of pyrolysis cracks due to fibre-matrix differential shrinkage; and

c) the interface properties, *e.g.* the degree of adhesion between fibres and matrix.

Interfaces can occur between fibre and matrix within a fibre bundle; between differently oriented fibre bundles, as in a woven cloth or in a 3D array; between similarly oriented yarns (for example if a bundle is composed of twisted yarns); between layers of reinforcement if in a 2D composite; between fibre bundles and matrix regions; and between matrices derived from different precursor or from separate infiltration/carbonisation cycles. The interfacial regions will be weak because the matrix is weakened by voids and cracks, and because of stress concentrations caused by geometric discontinuities (Jortner - 1986)

The expansion and shrinkage behaviour of the various components in a CFRC during heat treatment causes additional complications in the interactions between the components. Dimensional changes experienced by the fibres and matrix during heating cause stresses that can generate

cracks. During carbonisation by heating, matrices derived from resin or pitch shrink in volume because they are losing mass and because the carbon usually is denser than the precursor. The linear shrinkage is large in comparison to thermal expansions, so the net dimensional change of the new matrix, at temperatures above 600°C or so, is negative. Cracks may be caused also by thermal stresses arising from anisotropy and differences between the thermal expansivities of the bundles and the carbon matrix. The cracks that appear within a fibre bundle are likely to have formed on cooldown (if they are not shrinkage cracks) and cracks at or near interfaces may have formed either on heating or cooling. A multi-directional fibre orientation is able to convert anisotropic shrinkage stresses into more isotropic ones. Generally a 2D CFRC shows an increased shrinkage perpendicular to the fibre laminae and a reduced shrinkage parallel to the fibre laminae. Three-directional CFRC show no bulk shrinkage, but, as mentioned, are characterised by the formation of a continuous intramatrix crack system, Figure 1.9 (Jortner - 1986, Fitzer - 1981, Eitman - 1974).

The type of the fibre used to manufacture the composite is a key factor in the shrinkage of the CFRC. During the carbonisation, the shrinkage with surface treated fibres is larger than that with non-surface-treated ones. When the fibre and matrix bond strongly, the shrinkage of matrix in the direction normal to the fibre in the composite will be blocked. In the case of the composite with surface-treated fibres, shrinkage of the matrix during the carbonisation process is restrained, and the growth of the matrix domains and the crystallite thickness remains small (Huettner - 1990). The explanation for this behaviour is the difference of the coefficient of thermal expansion (CTE) between matrix and fibre (matrix : $2 \rightarrow 6.10^{-6}$/K; fibre longitudinal : -1.10^{-6}/K; fibre transverse : 12.10^{-6}/K), resulting in tensile stresses during heating up (Huettner - 1990, McAllister - 1972).

1.4 - Mechanical properties of CFRC composites

1.4.1 - Introduction

The published information on mechanical properties of CFRC makes any correlation with microstructure difficult because of the variety of fibre reinforcements, different fibre contents of the fabricated components, and the different fabrication parameters and processes. The strength and fracture behaviour of a material are complementary to each other. Fracture of a material depends on the crack initiation as well as crack propagation mechanisms. As in conventional fibre reinforced plastic composites, the overall properties of CFRC are controlled by the properties of the fibres, by the properties of the matrix and the interaction between fibre and matrix (Fitzer - 1987). Typical values of work-of-fracture for CFRC are from one to three orders of magnitude greater than values for graphite single crystals, glassy carbons, and polycrystalline graphites (Zhao - 1985). In addition, strength data for CFRC are generally variable and many data are required before a confident mean can be stated (Thomas - 1978b).

Both components of CFRC composite exhibit brittle failure. The carbon matrix fails in flexure at strains of 0.1 to 0.2% whilst the strain to failure of carbon fibres is around 1%, but they have enhanced mechanical properties compared to graphites, particularly tensile and flexural properties, while compression properties exhibit only minor advantage. As expected, in tensile or flexural loadings, the behaviour is dominated by the fibre (Thomas - 1978a, Weisshaus - 1991). The interlaminar shear strength of the material is largely determined by the properties of the matrix (Downs - 1991). The design and stress analyses of a structure for aerospace applications made from CFRC composites are completely different from those used for conventional carbon fibre reinforced plastics (Stoller - 1969). In CFRC composites large internal stresses are developed which are of

thermomechanical origin. These include those that result from shrinkage of the matrix on carbonisation and those that result from differences in thermal expansion coefficient of the fibre and matrix, and the radial/axial anisotropy of thermal expansion in fibres.

Attempts to evaluate the interlaminar shear strength using methods other than the usual short beam shear test were made by Rahhal (1991). The author compared a modified short beam shear test (MSBS), fabricated by bonding high strength 5HS graphite-epoxy facesheets to a CFRC, with measured interlaminar shear test results from the double notch shear (DNS), direct shear (DS) and standard ASTM short beam shear (SBS). Although the results are in the range of 13.5 MPa, the data scatter for the MSBS is much less than the DNS and DS methods. It was claimed that in his approach for determining shear strength the interlaminar shear stress was isolated and pure shear failure was produced.

Different values are obtained (Oh - 1989) for mechanical properties of CFRC when prepared by CVI using different deposition temperatures and gas concentrations. Deposition of carbon from propane gas into a 2D preform at 1100°C produces a composite which undergoes a nearly catastrophic failure. A stepwise failure behaviour became dominant as deposition temperature increased to 1200°C, 1300°C and 1400°C. Both the strength and modulus decreased with increasing deposition temperature and this could be caused by the reduced bulk density of the composite.

Another way to modify the mechanical properties of a CFRC is by using fine grained graphite powder as a modifier of the microstructure of the precursor matrix which result in a decrease in the shrinkage during carbonisation. It was shown by Yasuda (1988) that additions of 5% of a fine graphite powder in a CFRC made with untreated unsized fibres increase the strength and ductility of a carbonised composite by releasing stress concentration at crack tips.

1.4.2 - Fibre/matrix interface effects

The weakness of fibre-matrix interfaces may be a requirement for a carbonised CFRC. A too strong bond may promote excessive damage to fibres during heat treatment and also may promote brittle behaviour (Jortner - 1986). In CFRC made with high strength surface treated fibres as reinforcement the matrix cannot crack by absorbing fracture energy, because the energy at the tip of the notches or cracks is smaller than the bonding energy between fibre and matrix. The cracks therefore do not stop on the fibre surface but propagate straight thought the composite. So, the strength of these composites is generally small compared to other CFRC, because of the high number of intramatrix cracks perpendicular to the fibre axis. A compromise has to be made between a weak interfacial bond, which improves fracture toughness by debonding and fibre pull-out, and a strong interfacial bonding which leads to a catastrophic failure (Fitzer - 1980, Manocha - 1988b).

In composites with non surface treated fibres, the fibre/matrix bonding is quite weak and crack branching can occur easily at the interface. The matrix crack propagates up to the fibre surface, stops there, delaminates by absorbing fracture energy and propagates further along the fibre/matrix interface. This type of failure has a pseudo-plastic pattern with fibre pull out. Fracture of the composites by this mechanism requires high fracture energy and therefore composites made with non surface treated fibres exhibit generally a high ultimate breaking strength.

Fitzer (1980) has also shown the influence of the fibre surface activity using unidirectional CFRC made with high modulus (HM) and high strength (HS) carbon fibres, with untreated and treated surface. Only CFRC made with untreated high modulus fibres resulted in good mechanical

properties. The CFRC composite with untreated HM fibres yield 60-100% of the fibre strength and exhibited a *pseudoductile non-catastrophic* failure. The CFRC with treated HS fibres yielded 30-60% of the fibre strength, and the fracture behaviour was termed *semicatastrophic*. The CFRC with surface treated HS and HM fibres exhibited less than 30% yield of the fibre strength and their fracture behaviour was of a brittle and catastrophic pattern. The conclusions derived from the work are that to achieve high flexural strength of CFRC good adhesion between the matrix precursor and the fibre surface must be avoided. When the initial strength of such CFRC was low, this strength increased enormously after densification cycles mainly due to a pore filling of the matrix. As the chemical bond is very weak, the final adhesion in the densified CFRC is of a physical nature. Fitzer concluded as well that no densification cycle can compensate nor repair the damage introduced during the first carbonisation.

Similar work was carried out by Manocha (1988b) who monitored the mechanical properties of unidirectional CFRC during various carbonisation steps. Four types of high modulus PAN based carbon fibres were used having different surface characteristics, such as non-surface treated and unsized (UU), non-surface treated and sized (US), surface treated and unsized (SU), and surface treated and sized (TS); a polyfurfuryl alcohol resin was used as matrix precursor. For all composites made with surface treated and non-surface treated fibres flexural strength decreased when the composite was carbonised up to 400°C, and it decreased further when heat treated from 400°C to 600°C. The composites made with surface treated fibres exhibit sharp reductions of 60-70% in strength on further heat treatment in the temperature range 600-800°C. On the other hand, in the same heat treatment temperature range, composites made with non-surface treated fibres exhibit appreciable increases in strength. When using surface

treated and sized fibres the reduction in strength was less. Better results were found using non-surface treated, sized fibres which show a greater increase in strength than those made with unsized fibres.

1.4.3 - Weave pattern effects

Different weave patterns can greatly influence the mechanical properties of CFRC as demonstrated by Manocha (1988a). On densification, the flexural strength and interlaminar shear of the composites made with 8-harness satin fabric increases appreciably by a factor of 7, whereas only marginal improvement is obtained in CFRC made with plain weave fabric. The satin weave construction offers the advantage of floating yarns which contribute more to the strength of the CFRC because of the straight lengths (Lachman - 1978).

The critical points of woven CFRC are the low interlaminar shear strength and out-of-plane strength. No more than 8 to 20 MPa can be achieved and both properties are influenced only by the type of matrix precursor and the final heat treatment of the composite. Failure under mixed loads and also under tensile forces are clearly initiated by shear forces (Huettner - 1990). These problems can be overcome by using 3-D CFRC composites but at the cost of a reduction in mechanical properties and an increase in price (Davis - 1976).

Oh (1989) showed that fracture of 3D CFRC exhibit pseudo-plasticity with strains of up to 5% at room temperature. This atypical fracture behaviour for brittle materials is caused by the continuous crack structure of the matrix whose geometry is dependent on the fibre array. If the mechanical test is made at high temperatures the cracks which originated

from precursor shrinkage and fibre expansion during carbonisation and graphitisation close again, and the stress-strain behaviour of these composites is similar to that of other anisotropic structures. Pseudo-plastic failure was observed in tension tests as well, which is attributed to matrix cracking and filament movement to accommodate the applied load (Fitzer - 1981, Huettner - 1990, Perry - 1976).

1.4.3 - Oxidation inhibitors effect

Incorporation of SiC into the carbon matrix by CVD methods, volume fraction of SiC, $V_{SiC} \approx 0.20$, increases the compression strength, interlaminar shear strength and modulus of elasticity by a factor ranging from 2 to 4.5 times. It has been shown, for $0<V_{SiC}<0.25$, that the properties increase linearly with the volumetric proportion of SiC in the CFRC (Christin - 1980). In a similar experiment, Naslain (1981, 1980) showed that if the carbon matrix is partially replaced by SiC in a bidirectional CFRC, leaving almost no residual open porosity, the compressive strength and Young modulus, parallel to the cloth layers, can be increased by 1.5 to 3 and 2 to 5, respectively. But poor results were obtained by Rossignol (Rossignol - 1987) when using TiC instead of SiC as a modifier. There was an overall decrease in the rupture strain and increase in the brittleness of the material. However, it was concluded that microcracking mechanisms leading to intralayer failure for highly densified composites give the materials an interesting pseudo-plastic behaviour, due to intermittent crack propagation along and across both fibres and fabric layers.

The addition of matrix oxidation inhibitors during the manufacture of CFRC can modify their microstructure and consequently their mechanical properties. Glass forming compounds, such as B_2O_3 and ZrB_2, when added

to a bidirectional CFRC composite reduce drastically the strength and modulus by 10-20% of the original value after heat treatment above 2600°C (Ragan - 1991). The carbonaceous and inhibitor phases probably produce carbides such as B_4C or mixed B_4C/ZrC and a pronounced reduction in mechanical properties was noted.

The infiltration and subsequent pyrolysis of a carbo-silane polymer to CFRC significantly increase its strength. It was reported by Walker (1983) that a CFRC infiltrated with 10%wt of a carbosilane polymer increased the strength by 80%, and an increase of 130% was found when infiltrated with 13%wt of the same polymer.

1.4.4. - Acoustic Emission of CFRC composites

Acoustic emission (AE) has been applied extensively to characterise fracture of fibre reinforced composites and engineering graphites, but very few AE studies have been addressed the fracture of CFRC composites (Yin - 1991, Williams - 1978, Gorman - 1991, Tanamura - 1992). Tanamura (1992) discussed the microcrack propagation on a 3D CFRC composite monitoring the AE events during 3-point bending with different span/depth ratios. The rate of AE events decreased with increasing span/depth ratio and in pure bending mode of failure only a small peak at the failure stress appeared.

When a material is subject to an applied mechanical or thermal stress, discontinuous deformation processes, such as reinforcing fibre breakage, spalling of a coating or any other structural alteration in the solid material, can cause elastic energy to be dissipated as transient elastic stress waves, which spread in all directions from the source due to a rapid release of strain energy. These pulses, typically in the ultrasonic frequency range,

are AE events also known as stress wave emission.

The primary possible AE source mechanisms during mechanical testing of a composite, Figure 1.12, are: (i) fracture of fibre and matrix, (ii) fibre-matrix debonding, (iii) relaxation of fibres if they fracture, and (iv) fibre pullout against friction during composite rupture. Also, in terms of macroscopic sources, AE arises from known (and unknown) structural flaws such as intralaminar and interlaminar cracks, and from stress concentrations (Williams - 1978, Gorman - 1991). The main characteristics of an AE event are the peak amplitude and the number of ringdowns per event as illustrated by the two idealised AE events shown in Figure 1.13. The start and finish of an AE event is determined by the electronic threshold of the AE instrument: the time between the start and finish of an event is the event duration. The start of a new event occurs only after a period of inactivity, *i.e.* a deadtime. The rise-time of an event is the time from the first crossing of threshold to the peak amplitude. Each AE event consists of a number of ringdown counts, each count corresponding to a crossing of the threshold.

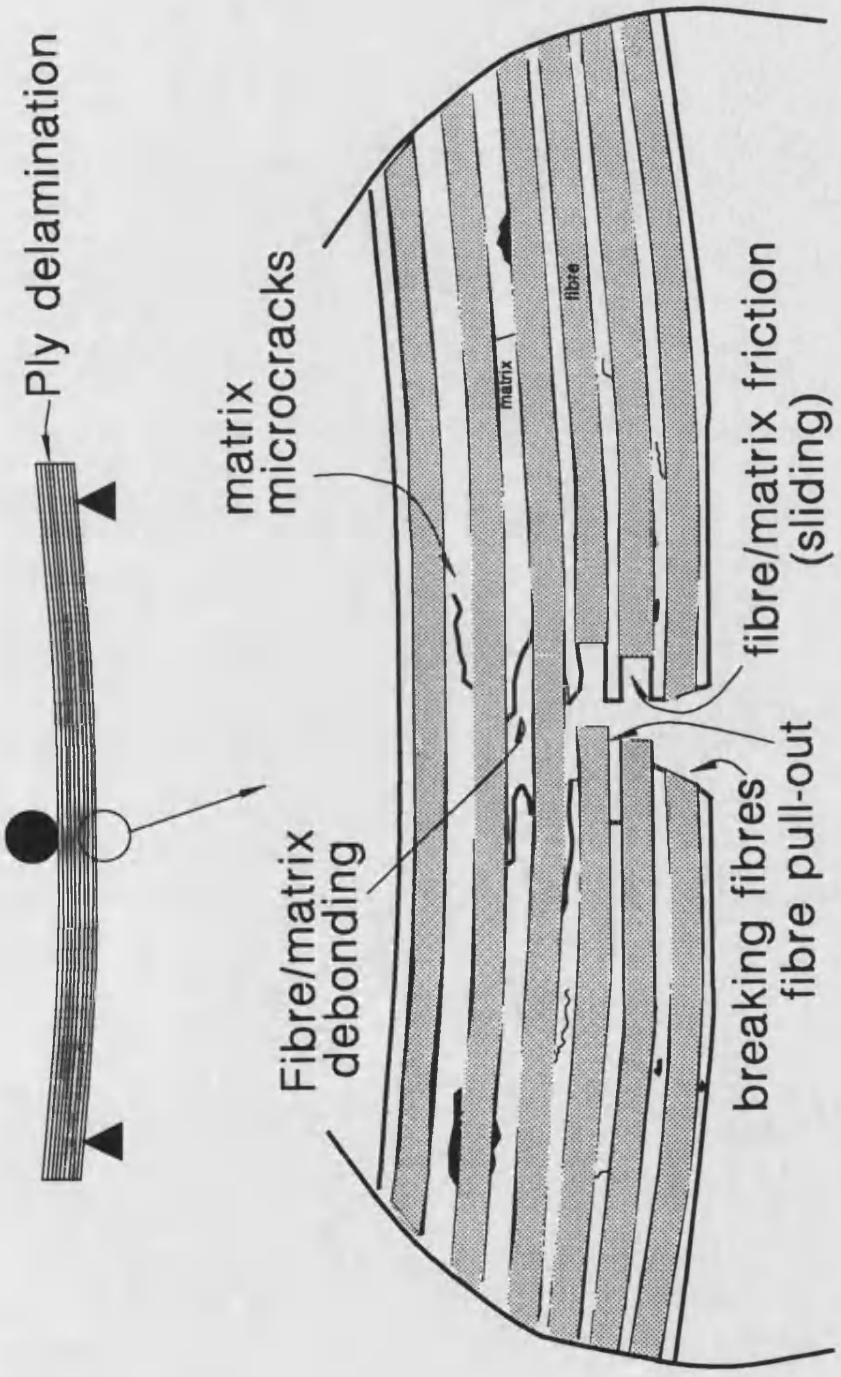

FIGURE 1.12 - Possibly primary acoustic emission sources during bending of a unidirectional CFRC composite.

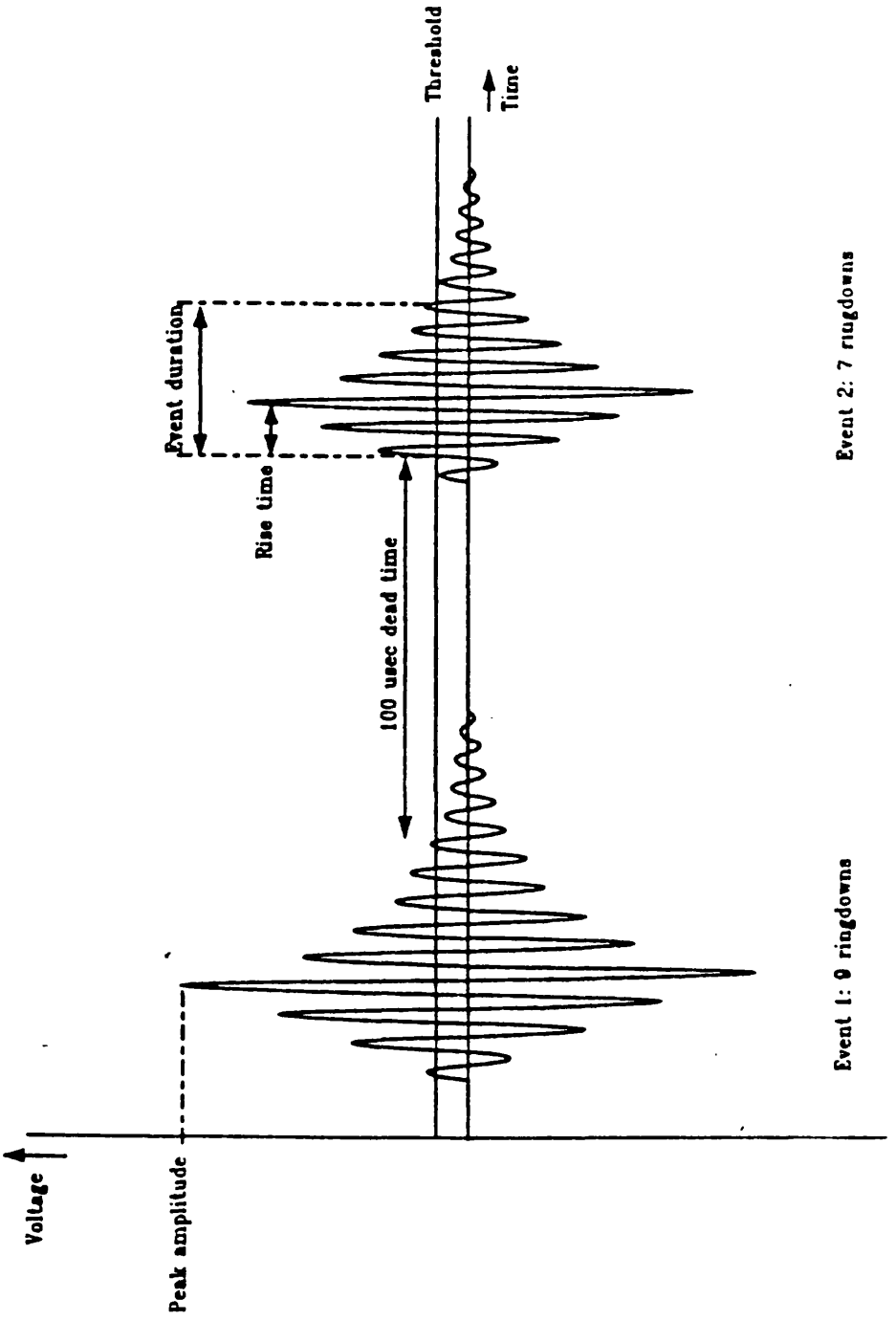

FIGURE 1.13 - Characteristic idealised parameters of two acoustic emission events.

1.5 - Oxidation behaviour of CFRC composites

The most important high-temperature structural applications for CFRC occur in oxidising environments, and clearly the wider use of such materials as high-temperature structural elements requires the development of an effective oxidation protection as the oxidation threshold for carbon materials is about 450°C. Oxidation of CFRC composites has a drastic effect upon mechanical properties. For example, Crocker (1991) found a reduction in flexural modulus of 30% and 14% for a 10% weight loss respectively for KKarb Type A, a bidirectional CFRC composite made with an ex-rayon carbon fibre/pitch carbon matrix, and Sigri CC1501G, a bidirectional CFRC composite made with an ex-PAN carbon fibre/resin matrix.

Work on oxidation protection for CFRC started in the early 1970s with the development of the Shuttle orbiter thermal protection material, although the efforts to protect carbon bodies in general from oxidation span more than a half century (Strife - 1988, Sheehan - 1989). The main use of CFRC will usually be in air and gasification proceeds by the overall reaction:

$$C_{(\text{fibre or matrix})} + O_{2(g)} \rightarrow CO_{(g)}$$

The Gibbs free energy change of the above reaction has a very large negative value over a wide range of temperatures and the reaction always proceeds with a big driving force even at very low O_2 partial pressures.

Considering the graphite single crystal, reaction with air is highly anisotropic with preferential attack at the edges of basal planes, at emerging point and line defects. This reaction anisotropy leads to the concept of active surface area (ASA), *i.e.* the fraction of the total surface area which takes part in gasification. Considering engineering carbons, including CFRC composites, reactivity is also influenced by the presence of catalysts or

impurities.

The development of a reliable oxidation protection is crucial to achieve the full potential of the CFRC by preventing contact with oxygen. This is achieved by coating and sealing CFRC structures with refractory materials which will act as a diffusion barrier to oxygen. The protective effect may result from two different mechanisms. The first one is based on a blockage of the active sites by a deposit which acts then as an inhibitor. The second one relies on a limited transport rate of the gaseous species, oxygen and/or carbon oxides through a oxygen-impermeable barrier layer (McKee - 1991, Ehrburger - 1991, Wu - 1991, Castro - 1991). Generally the first approach is a solution which is only useful at modest temperatures, and the latter is usually the only option available for many very high temperature applications.

Wu (1991) inferred that the lowering of the oxidation rate is a result of reduction in total surface area of the coated sample, and, due to the presence of porosity, the effective surface area over which the reaction can occur is possibly 10 to 100 times higher than the geometric area (Luthra - 1988). Considering the reactivity of CFRC composites, it is influenced by the degree of graphitic character of fibres and matrix carbon

The fibre structure appears to dictate the amount of accessible porosity to corrosive gases in CFRC materials by influencing the development of the associated binder phases. The rate of oxidation increases with temperature and is influenced by the extent of graphitisation, porosity, active sites and impurity level. Crocker (1991) found in the initial stages of gasification of a woven CFRC that there was preferential attack at the fibre/matrix interface, as was also found by McKee (1987). Eventually, the fibres gasify preferentially at the exposed fibre ends, where the basal plane edges are

exposed. The reactivity of the pitch binder carbon depends on the degree of layer plane development during the mesophase transition and the creation of these lamellae. The gasification rates of glassy carbon artifacts are uniform in the different orthogonal directions (Jones - 1986, Goto - 1986, Chang - 1978).

1.5.1 - Mass Transport Effects

A reaction between a porous solid, like carbon, and a gas involves heterogeneous gas-solid reactions. There are three major steps involved in a reaction of this type (Walker - 1959; Lewis - 1966):

(a) transport of gas molecules to the external geometric surface of the solid from the bulk of the gas;

(b) transport of gas molecules from the external surface to reactive sites on the internal surface of pores:

(c) reaction at these sites.

As carbon materials have significant porosity in practical situations, the overall rate of reaction is influenced by in-pore diffusion and by boundary layer diffusion at higher temperatures (Castro - 1992). For oxidation in air, the low-temperature rate-limiting step, below about 600°C, is likely to be the desorption of surface oxide from the carbon network, to give CO and CO_2. At higher temperatures, between 600 and 900°C, the release of the oxidation products, leaving defects in the carbon network, becomes easier (McKee - 1986). The rate is then probably controlled by oxygen diffusion into pores and adsorption at active sites. This lead to a lowering of the activation energy and the rate of gasification is controlled above 900°C by the rate of diffusion of oxygen through the gas phase to the composite surface (McKee - 1986, Gee - 1991).

Evidence for diffusional effects is provided by the variation of reaction rate, or the Arrhenius plots for oxidation with temperature for gas-carbon reactions. The Arrhenius plot shows the apparent activation energy decreasing with increasing temperature, the decrease being attributed to the increasing influence of gaseous diffusion. Ideally, the representation can be divided into three main zones, commonly referred to as zones I, II, and III, as shown in Figure 1.14.

At the lowest temperature zone, Zone I, the overall reaction rate is controlled solely by the chemical reactivity of the solid. The concentration of reactant gas, (C_g), within the pores of the carbon material is everywhere the same as the bulk gas concentration, step (c), and the observed energy of activation E and reaction order n are those pertaining to this reaction. Highly active sites, such as catalysts and structural defects, influence the oxidation rate in this regime and the attack is highly selective of the microstructure. As gas diffusivities are greater than the reaction rates the concentrations of reactant and products are substantially uniform in the pore structure and are equal to the values in the bulk gas. Within Zone a, the concentration of reactant gas at the centre of the carbon will decrease progressively as temperature rises until it eventually falls to zero, representing the transition to Zone II.

As the temperature is increased the rate of reaction increases faster than the diffusivites so that the former approaches the value of the latter. There will be a depletion of reactant molecules along the length of the pores, and a corresponding increase in the concentration of product. Under this condition all gas molecules entering the pores will react and the oxidation moves to an intermediate-temperature zone, zone II. A boundary layer of reaction products, *i.e.* CO and CO_2, is formed, at higher temperatures above 1000°C, on the surface of the specimen, Zone b, and the rate at which oxygen can penetrate this layer determines the oxidation rate in zone III.

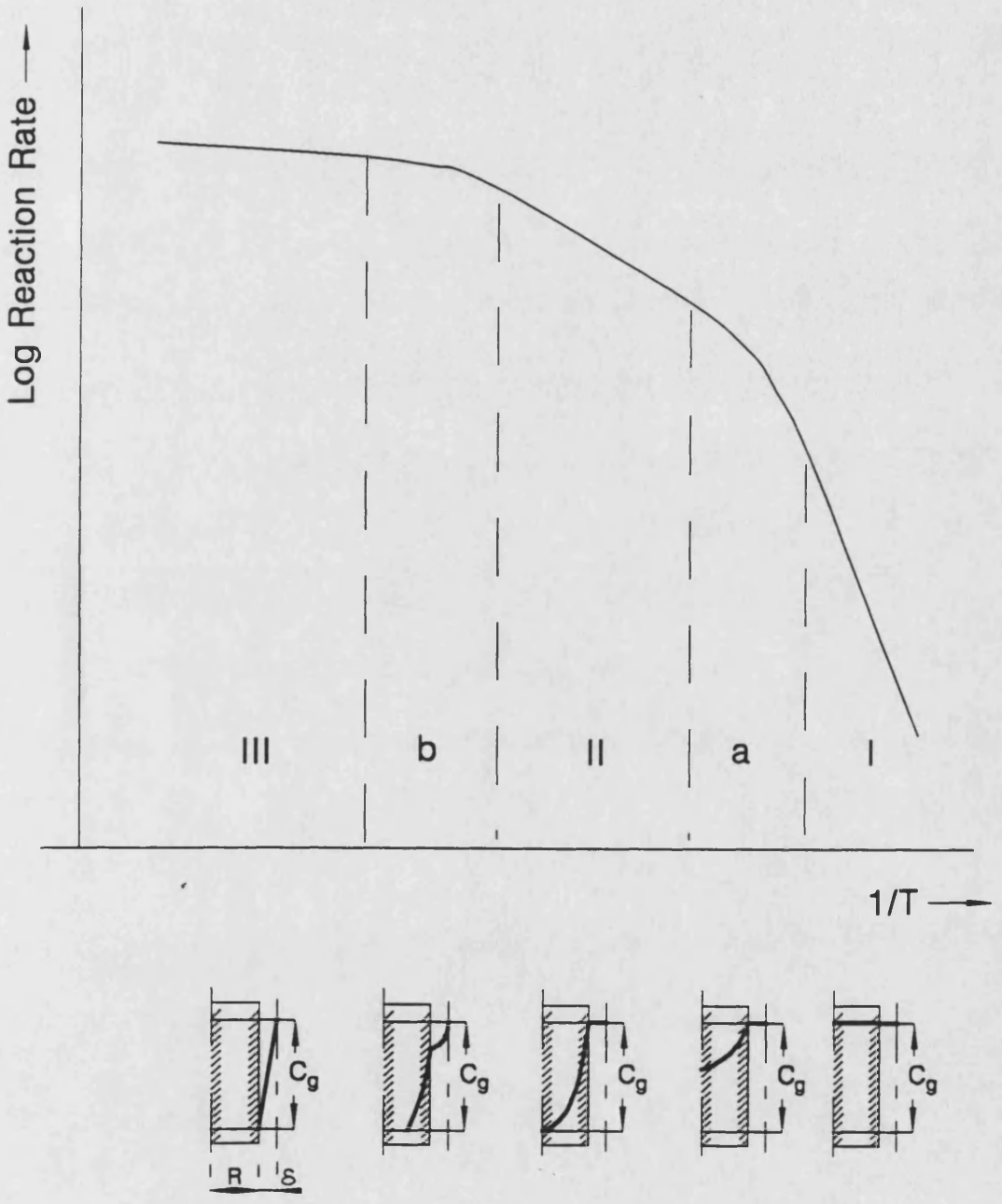

Figure 1.14 - The three zones representing the change of reaction rate of a porous carbon with temperature (Walker - 1959).

So the linear portion of zone II only persists as long as the concentration gradient external to the specimen is small. With increasing temperature the depth to which molecules can penetrate before reacting becomes less and less, and the reaction becomes confined to a thinner and thinner layer adjacent to the external surface. At the same time the concentration gradient external to the surface becomes more and more important until eventually this controls the rate, zone III, where C_g approaches zero. The rate-controlling step is then transport of gas molecules from the bulk of the gas to the surface of the specimen. Attack in this regime is not selective and is confined to surface oxidation.

1.5.2- Internal inhibition of CFRC composites

Carbon materials can be modified internally to improve their oxidation resistance by direct removal and/or deactivation of catalytic impurities, incorporation of oxidation inhibitors, and/or partial substitution of the carbon matrix by a more oxidation resistant one (McKee - 1991, Castro - 1991).

Improvements in the oxidation resistance of CFRC started by dispersing compounds of boron, silicon, phosphorus and refractory metal borides in powder form between the fibre layers or in the impregnating resin. Another method of internal inhibition is to protect the carbon fibres by coating the fibre with borate compounds, such as ammonium borate (McKee - 1986). Carbon fibres which had been treated with this compound, and subsequently heat treated at 500°C in air to promote the formation of a borate glassy coating, showed a very low gasification rate on heating in air, with weight losses of less than 1% when the temperature attained 1000°C. On the other hand, the fibres that were not treated with the borate compound began to

lose weight in air at about 450°C with the gasification rate becoming increasingly fast at higher temperatures. However inhibitor phases added in this way only became effective after appreciable fractions of the carbonaceous material had been gasified (McKee - 1988).

The reaction of the carbon matrix, such as coal-tar pitch pre-heat treated at ≈525°C, and polycarbosilanes, such as polydimethylsilane, to obtain SiC was studied by Kawamura (1992). Using a mixture ratio of 1/0.5/0.5/0.4 respectively for polycarbosilane, pre-heat treated coal tar pitch at 500-550°C, polyvinyl butyral and dibutylphthalate, a dense and uniform C-SiC composite sheet with a bending strength of 200-250 MPa was obtained, when heat treating the compound at 1200°-1300°C. After 5 hours at 500°C the material lost only ≈5% weight, while the pitch carbon lost ≈70%, showing that the compound gives oxidation resistance and improved mechanical strength. Partial substitution of the carbon matrix with SiC and TiC by CVI technique was studied by Christin (1980), Naslain (1980) and Rossignol (1987). Addition of a 20% volume of SiC in the carbon matrix reduced the weight loss in air, at 1500°C, by a factor of 12. TiC did not have the same effectiveness as SiC in reducing the oxidation rate because the TiO_2 film formed from TiC was not an effective barrier as was SiO_2 formed from SiC.

1.5.3 - External protection of CFRC composites

1.5.3.1 - Introduction

The methods used to protect carbon bodies, as well as the oxidation inhibitors applied are very closely related to the operating temperature and the heating and cooling procedures (Castro - 1991). All of the methods for

protecting CFRC composites from oxidation utilise an external ceramic coating as the primary oxygen barrier even if internal oxidation inhibitors are used (Sheehan - 1987, Sheehan - 1989, Strife - 1988, Castro - 1991). The main problem observed in all the external protection methods is related to the very low coefficient of thermal expansion (CTE) exhibited by CFRC composites, Figure 1.11, when compared with the thermal expansion of potential protective coatings, Figure 1.15 (Buckley - 1988, Strife - 1988). Even surface coatings with low CTE still cause significant expansion mismatches with the CFRC base material and tensile cracks develop in the coating on thermal cycling leaving the underlying carbon material susceptible to rapid oxidation. Other factors affecting performance include coating adherence, cracking/spalling, erosion and oxygen permeability (Yoon - 1990).

1.5.3.2 - Primary refractory coatings

The primary coating candidates for oxidation protection at temperatures below 1750°C are silicon-based ceramics, such as SiC and Si_3N_4, because they have the best thermal expansion compatibility, exhibit the lowest oxidation rates of the high temperature ceramics and were not prohibitively expensive (Strife - 1988). The method of inhibiting carbon materials from oxidation using SiC was patented in 1934 by Johnson and the beneficial properties of coating system composed by a layer of SiC have been recognised since that time (Wu - 1991, Castro - 1991). Although coatings of Si_3N_4 have a lower CTE than SiC they have essentially the same temperature limitation as SiC (Strife - 1988, Sheehan - 1987). The temperature limit for use these refractory ceramics in oxidising environments is due to the chemical reaction between the refractory coating

and a silica coating forming volatile SiO, which renders the coating nonprotective. This results in rapid erosion of the refractory coating, as exemplified by the following reaction:

$$SiC + 2SiO_2 \rightarrow 3SiO + CO$$

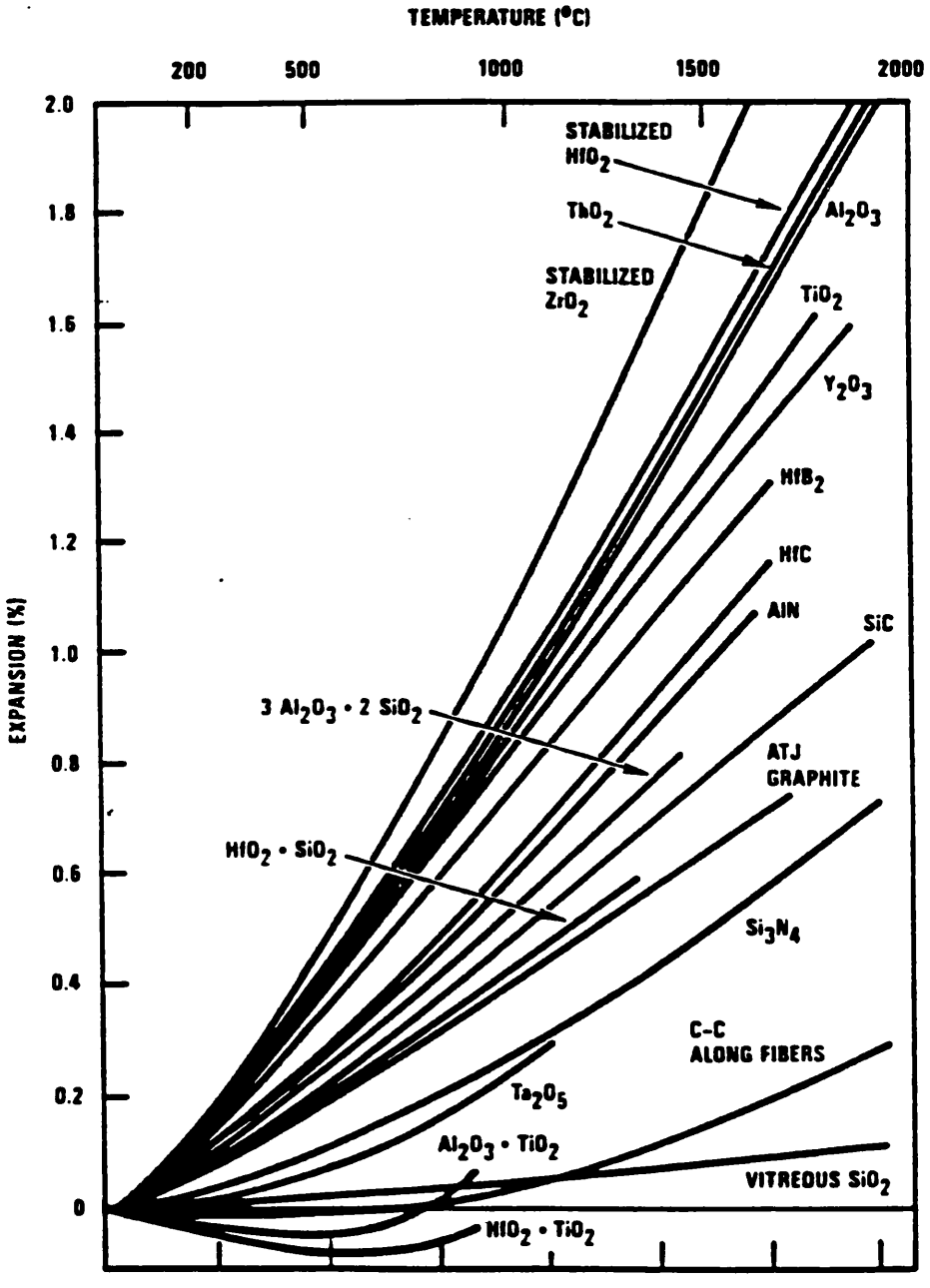

Figure 1.15 - Ceramic thermal expansion characteristics (Strife - 1988).

1.5.3.2.1 - Production of SiC by gas-phase process - CVD

This process is a conventional CVD process, where gases, or vaporised liquids, are reacted at high temperatures, usually in between 1500-1800°C, in either ordinary furnaces or special reactors, to produce SiC (Duret - 1983, Niihara - 1983). The starting materials for gas phase reactions include organosilanes, methane, propane, silicon tetrachloride and dimethyldichlorosilane (Weiss - 1973). They are reacted over a substrate to which the SiC adheres as a result of reactions such as:

$$SiCl_{4(g)} + CH_{4(g)} \rightarrow SiC_{(s)} + 4HCl_{(g)}$$

The different characteristics of the CVD deposits, *i.e.* composition, thickness, smoothness, structure, are related to experimental parameters such as temperature, pressure, gas flow rate, dilution of the reactants in an inert carrier gas, method of heating the substrate, and to the general configuration of the equipment. The efficient determination of the optimum experimental parameters and the degree to which they must be controlled in order to prepare reproducible products requires a detailed understanding of each system. Typical morphological features and textures of a CVD-SiC obtained by Weiss (1973) at various deposition temperatures and different supersaturations of the reactive species in the gas phase, at ≈10 mmHg are shown in Figure 1.16. Pure β-SiC is deposited within the area circumscribed by the broken line. At low temperatures (<1400°C) the deposit contains excess silicon. At high temperatures (>1600°C) excess carbon in the form of soot or pyrolytic graphite deposits. At intermediate regions there is a transition from β-SiC to α-SiC where the latter grows out as hexagonal platelets.

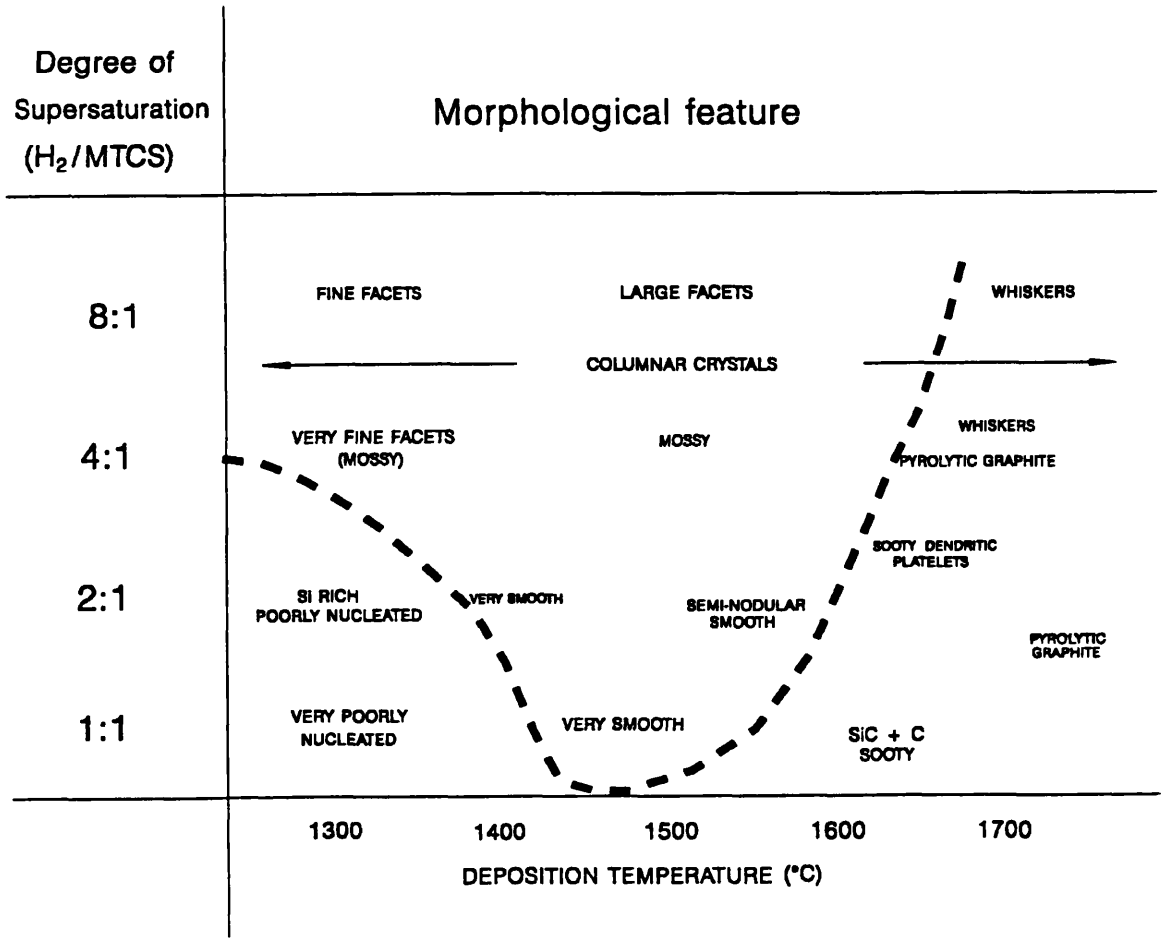

Figure 1.16 - Morphology of last deposited surface as a function of degree of reactant supersaturation and deposition temperatures (Weiss - 1973).

1.5.3.2.2 - Production of SiC by pack cementation process

The pack cementation process has been widely used for nearly 30 years for applying high-temperature protective diffusion coatings to superalloys used in the hot sections of gas turbines (Mevrel - 1986). It consists of immersing the components to be coated in a powder mixture in a sealed or semisealed retort. The entire equipment is placed inside a furnace and heated in a protective atmosphere to a high temperature for a sufficient period for a coating to form. The pack cementation process was used to coat the RCC-3 CFRC composite used for the leading edge of the USA Space Shuttle (Rogers - 1975). The RCC-3 composite is a woven CFRC composite with a resin carbon matrix, reimpregnated and carbonised three times with furfuryl alcohol resin. The pack cementation was carried out placing the RCC-3 in a graphite retort entirely surrounded by a powder mix composed of 10%wt Al_2O_3/60%wt SiC/30%wt Si. A nominal 0.6 mm thick coating was obtained after drying the pack retort at 200°C for 16 hours and firing at 1700°C for ≈3 hours in inert gas atmosphere. The coating is believed to develop in two stages. The first is a liquid controlled phase process in which SiC is formed due to reactions between molten silicon metal and the carbon. The second stage is a vapour transport controlled reaction in which silicon vapours react with the carbon (Rogers - 1975).

The pack cementation technique is relatively simple and can be applied to components of complex shapes and sizes. On the other hand, it is laborious method and heat treatment cycles are rather long.

1.5.2.2.3 - Production of SiC by polymer pyrolysis methods

A comprehensive review on the preparation of polymers containing

elements, such as silicon, carbon and nitrogen, their pyrolysis to produce high temperature ceramics, and the forms and applications of these materials was published by Wynne (1984). Specifically, the process of polymer pyrolysis to obtain SiC involves heating a polycarbosilane precursor to intermediate temperatures (300°C to 400°C) to decompose and evaporate organic components (Wynne - 1984, Wong - 1986, Walker - 1983). When pyrolyzed in a furnace at 300°C to 500°C, volatile organic compounds are driven off leaving a silicon and carbon residue. This residue is then fired at between 1000°C to 1200°C to form β-SiC.

The sol-gel process basically involves suspending the starting materials, usually alkoxides diluted in an appropriate solvent, in a solution from which a gel forms (Wong - 1988, Ulrich - 1988, Castro - 1991). The method uses high purity starting materials and so an uniform material can be obtained. A silica gel containing a carbon source, *e.g.* phenolic resin, is fired at high temperatures (1300°C to 1600°C) to react the two components and form β-SiC (White - 1987). The effectiveness of the method is because no specialised and expensive equipment is required and it is claimed by many authors (Schmidt - 1989, Klein - 1984, Castro - 1991) that it is a reasonable alternative to vapour deposited, vacuum deposited or plasma sprayed coatings, because the costs of raw materials are relatively insignificant and complex shapes can be covered uniformly. The coating obtained by the sol-gel method to protect carbon materials against oxidation is built up in successive SiC layers followed by glassy or glass-ceramic layers on the surface of carbon. Alumina sols were used by Sim (1986) to protected CFRC composites from oxidation. The sol-gel was prepared using aluminium alkoxide and on heating up to 1300°C the coating transformed to α-Al_2O_3. Heating the samples in air at 1000°C the coated samples exhibited a reduction in the weight loss of ≈20% in relation to the same uncoated

samples.

1.5.3.3 - Secondary glassy coatings

Because of the thermal expansion mismatch between the primary refractory coating, *e.g.* SiC, and the carbon substrate, cracking of the coating occurs on thermal cycling. The usual way to minimise the effects of the cracked primary ceramic coating is to use an appropriate glassy material to seal these cracks (Sheehan - 1987, Castro - 1991). These glassy sealants must be chemically compatible with carbon and the primary coating and must have viscosity and wetting characteristics that promote the formation of continuous adherent layers, so providing an effective barrier to inward diffusion of oxygen. In addition, it must have low volatility to prevent excessive erosion in high velocity gas streams (Strife - 1988, Gee - 1991, Sheehan - 1987).

Borate glasses have long been used as a surface coating and internal oxidation inhibitor in early CFRC development, but their use is restricted to temperatures below about 1100°C due to high volatility at high temperatures and moisture sensitivity (Strife - 1988). Another possibility is the use of SiO_2-based glasses that have significant advantages over borate glasses, particularly a lower vapour pressure and lower oxygen permeability. Appropriate modifications must be made, however, to prevent SiO_2 from reacting with carbon and to provide viscosities in the range where flow can occur for effective crack sealing. The stability limit of SiO_2 on SiC is about 1750°C. This suggests that the use of carbide layers is a potential method for achieving the required compatibility of oxide glasses in the range of 1500°-1750°C, and provide enhanced wetting of SiO_2 glasses compared to the glasses on the carbon material itself (Strife - 1988).

The concept of multi-layer refractory coatings was utilised by Castro (1991) using SiO_2-TiO_2 and SiO_2-Al_2O_3-LiO_2 as glassy layers obtained by the sol-gel method. It was claimed that these systems have low permeability to oxygen diffusion, melting point around 500-600°C, when the carbon substrate starts to oxidise, inertness to reaction with carbon, volatilisation temperature above the operating temperature, and coefficient of thermal expansion compatible with the carbon substrate.

Silica and silicate glasses have been widely used as standard shock-resistant materials for a long time because of their ultra-low thermal expansion coefficients, from 0.05 to 0.03×10^{-6} $^oC^{-1}$ in the temperature range of 25 to 800°C (Roy - 1989). The low thermal expansion of vitreous silica is because in the continuous random silica network a change of volume can come only from changes in the silicon-oxygen interatomic distance. But, the Si-O bond is very strong, so that any such changes will be small. The cause of the compositional dependence of the thermal expansion observed in SiO_2-TiO_2 glasses may be because TiO_2 can act as a network-former, by replacing SiO_2 in four-fold coordination sites in the SiO_2 network (Roy - 1989). Besides its low coefficient of thermal expansion, which approaches zero when the TiO_2 concentration is between 6 - 7.4 wt%, this glass also exhibits low permeability to oxygen diffusion that is of fundamental importance for the function of the glassy coating on CFRC composites.

1.5.3.4 - High temperature coatings (T>1750°C)

Oxidation protection systems for CFRC composites above 1750°C involve the use of either noble metal or highly refractory ceramic coatings. These include the platinum group metals iridium, rhodium, ruthenium and some of their intermetallic compounds as primary oxygen barriers. The most

attractive noble metal for carbon protection at very high temperatures is iridium due to its high melting point (2440°C), low oxygen permeability up to 2100°C and its chemical compatibility with carbon up to 2280°C (Sheehan - 1987, Yoon - 1990). Apart of the cost, the disadvantages of iridium coatings are erosion by volatile oxide formation, lack of adherence to carbon, and thermal expansion mismatch with CFRC (McKee - 1990). Long-term protection will require the identification of effective oxygen barriers, chemical compatibility with carbon and thermal expansion mismatch (Sheehan - 1987).

1.6 - Objectives of the work

The literature survey shows clearly that there have been few studies of oxidation protection by sol-gel techniques on CFRC composites and nothing published about the influence of sol-gel coatings on the mechanical properties of these CFRC composites. The first aim of this work will be concentrated on a study of the mechanical properties monitored by acoustic emission, the fracture behaviour and the oxidation resistance of two commercial CFRC composites coated in different ways using the SiC sol-gel system. Glassy coatings will be utilised over the SiC primary refractory layer and the oxidation resistance will be evaluated. The results of this part of the study are presented in Chapter Three.

The second aim of this work will be concentrated on the manufacture of uni-directional CFRC composites using the filament winding technique using carbon fibres with different surface activities and heat treated at different final temperatures. The microstructural features of these models that are important to the mechanical properties, fracture behaviour and oxidation resistance in air will be characterised. The same unidirectional models will be coated with the SiC sol-gel system and similar evaluations of mechanical properties monitored by acoustic emission, fracture behaviour and oxidation resistance will be done. The results of this part of the study are presented in Chapter Four.

The third aim of this work is a natural extension of the ones previously stated, *i.e.* attempts will be made trying to incorporate the SiC sol-gel system in between the prepreg layers of the model unidirectional composite before the moulding stage. Similar procedure will be tried mixing the precursor phenolic resin with the SiC sol-gel system, using this compound in the filament winding stage. The results of this part of the study are presented in Chapter Five.

CHAPTER TWO
EXPERIMENTAL METHODS

This chapter describes the materials used in this work and the methods involved in the characterisation of these materials. Three types of composites were studied: (i) commercial CFRC composites, (ii) unidirectional CFRC composites prepared in the laboratory, (iii) unidirectional CFRC composite modified by incorporation of SiC obtained by a sol-gel method. Also methods used to obtain protective coatings for the CFRC composites are described.

2.1 - Materials

2.1.1 - Commercial carbon fibre reinforced carbon composites

Two commercial CFRC composites were utilized in the initial part of the work, KKarb Type A and Sigri CC1501G. KKarb Type A was provided by Kaiser Aerotech Inc, and it is a laminated composite with rayon-based carbon fibres in a 5-harness satin weave in a carbon matrix derived from a resin/pitch blend. General properties of this material, supplied by the manufacturer, are listed in Appendix I.

Sigri CC1501G was provided by Hoechst UK Ltd, and it is a laminated composite with PAN-based carbon fibres in a hopsack weave in a resin carbon matrix. General properties of this material, supplied by the manufacturer, are also listed in Appendix I.

Mercury intrusion porosimetry was carried out on both materials using a Quantachrome Autoscan 33 Porosimeter, in the pressure range 0.1-225 MPa, and in the pore entrance diameter range of 5-2500 nm. Apparent open

porosity of the same materials was determined by the water impregnation method, ASTM-D20.

2.1.2 - Carbon precursor matrix

The precursor matrix used in composite fabrication was a resol phenolic resin, Borden SC1008P; specifications supplied by the resin manufacturer are described in Appendix II. The curing schedule for bulk samples of that resin is also outlined in Appendix II.1. A resin sample was analysed by a Perkin Elmer 1720 FTIR spectrometer. A typical FTIR spectrum is presented in Appendix III, and the assignment of the main peaks is presented Appendix II.2.

The viscoelastic behaviour of a cured sample of the resin in the temperature range 20-200°C was analysed by dynamic mechanical analysis in a Metavib Instrument, in three point bending with a span/depth ratio of 10:1 at a frequency of 5.0 Hz, and a heating rate of 2°C/min.

X-Ray diffraction was recorded using a Philips PW1730 4kW X-Ray diffractometer with PC-APD software on samples of the resin heat treated at carbonising and graphitising temperatures, 1100°C and 2500°C respectively, to observe changes in the d_{002} peak.

2.1.3 - Carbon Fibres

Two PAN-based, high tensile strength, carbon fibre tows (12000 filaments) with different surface activities were used to manufacture the composites : (i) Courtaulds Grafil E/XA-S, which is surface treated and sized with an epoxy film, and (ii) Grafil XA/U, which has no surface treatment

and is unsized. The nature of the surface treatment of the E/XA-S fibre is proprietary. The fibres were used as-received and manufacturer's data for the properties are given in Appendix IV.

X-Ray diffraction was recorded for the as-received fibre and after heat treatment to 2500°C, using a Philips PW1730 4kW X-Ray diffractometer with PC-APD software, to observe changes in the d_{002} peak.

2.1.4 - Oxidation protection coatings

One refractory coating based on SiC and two different glassy coatings were used to obtain a multilayer oxidation protection coating over the CFRC composites. As a refractory coating a *sol-gel* system of SiC was used and as glassy layers *sol-gel* systems of SiO_2-TiO_2, and a borate coating based on B_2O_3 were used. Special care was taken not to modify either the *sol-gel* formulations or the application over the CFRC composite to ensure that results on different materials could be compared.

2.1.4.1 - SiC refractory coating

The SiC *sol-gel* was prepared according procedure developed by Castro (1991), Figure 2.1. The molar proportions in relation to tetraethyl orthosilicate (TEOS) - $Si(OC_2H_5)_4$ were as follows:

TEOS : Acetone : H_2O : HCl
1 : 3.2 : 8 : 0.01

A stoichiometric amount, in relation to the TEOS, of phenolic resin BP cellobond J2027L, with specification given in Appendix V, solubilized in acetone, was used as an external carbon source for the SiC reaction, assuming 50% carbon yield.

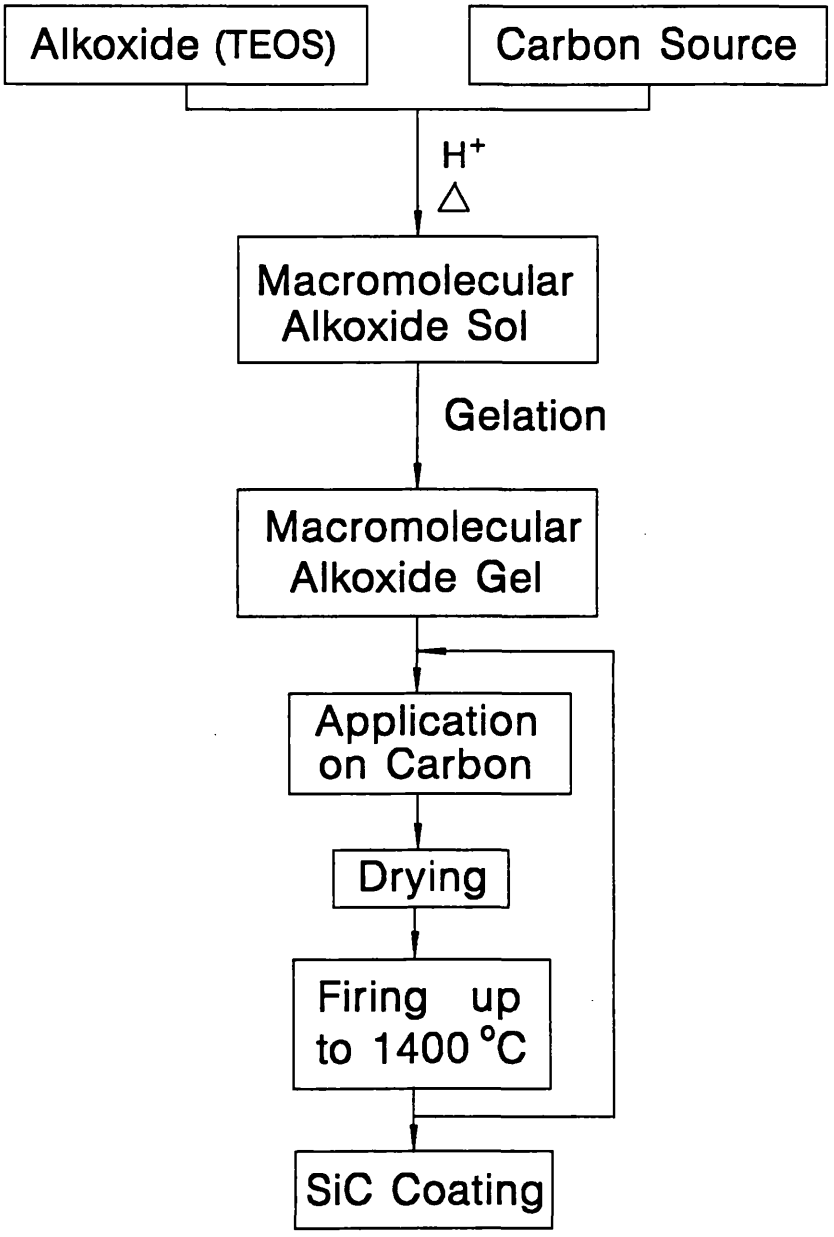

FIGURE 2.1 - Schematic diagram of SiC Sol-gel process

The procedure for applying the coating to the composites involved brushing three times before each firing procedure. After each brushing the samples were left at least 24 hours to dry at room temperature. After this period the samples were dried at 60°C in a oven for at least 3 hours. The SiC *sol-gel* system was fired in a horizontal Carbolite furnace in flowing argon, using a heating rate of 2°C/min up to 1450°C, with a soaking time of 4 hours at that temperature (White - 1987, Castro - 1991). Two other procedures were also used. The first was pressure impregnation/gelation and the second was vacuum impregnation followed by brushing.

In the pressure impregnation/gelation procedure a pressure vessel containing the samples was filled with the SiC *sol* system and a pressure of 3.5 bar was applied. The equipment was left 24 hours at 60°C in an oven until complete gelation occured. The samples were left to dry 24 hours at atmospheric pressure and room temperature and then fired to 1400°C as described above.

In the vaccuum impregnation/gelation procedure the samples were placed in an appropriate vessel and a vacuum applied using a rotary vacuum pump, and after filling with the *sol* system the equipment was left 24 hours at 60°C in an oven until complete gelation occured. After that the samples were dried for 24 hours at atmospheric pressure and room temperature and then fired to 1400°C in flowing argon as described above. After the vaccuum impregnation/gelation procedure, four more brushing/firing procedures were carried out in the same way as described above.

X-Ray difraction spectra of the uncoated and coated samples were recorded using a Philips PW1730 4kW X-Ray diffractometer with PC-APD software to observe characteristic peaks of the SiC.

2.1.4.2 - SiO_2/TiO_2 glassy layer

The *sol-gel* system for the SiO_2-TiO_2 glass was prepared using a procedure described by Castro (1991) with the following molar proportions:

TEOS : Ti[Iso] : Acetone : H_2O : HCl
1 : 3.2 : 9 : 9.35 : 0.01

where Ti[Iso] = titanium iso-propoxide.

The gelled *sol-gel* was applied using the same brush/drying procedure described for the SiC *sol-gel*. The SiO_2-TiO_2 *sol-gel* system was fired in a horizontal Carbolite furnace with the heating program shown in Figure 2.2. Because the horizontal furnace did not reach 1600°C, the final stage of heat treatment from 1250-1600°C was perfomed in a graphite resistance furnace (Astro), at a heating rate of 10-15°C/min with a soaking time of 15 min to melt the glassy layer.

2.1.4.3 - B_2O_3 glassy coating

The B_2O_3 glassy coating was prepared according to a procedure previously described by Ehrburger (1986). The procedure consists of diluting boric acid (H_3BO_3) in ethanol in the proportion of 18 wt%. The mixture is heated at about 60°C until a homogeneous solution is obtained.

The application of the solution over the CFRC composite was done by brushing, leaving to dry overnight, and this procedure was repeated three times. Firing was carried out at a heating rate of 120°C/h up to 700°C and holding at this temperature for one hour. Following the Ehrburger's procedure the samples were fired four times, and in the last firing an annealing of the B_2O_3 glassy coating was done for fifty hours at 700°C.

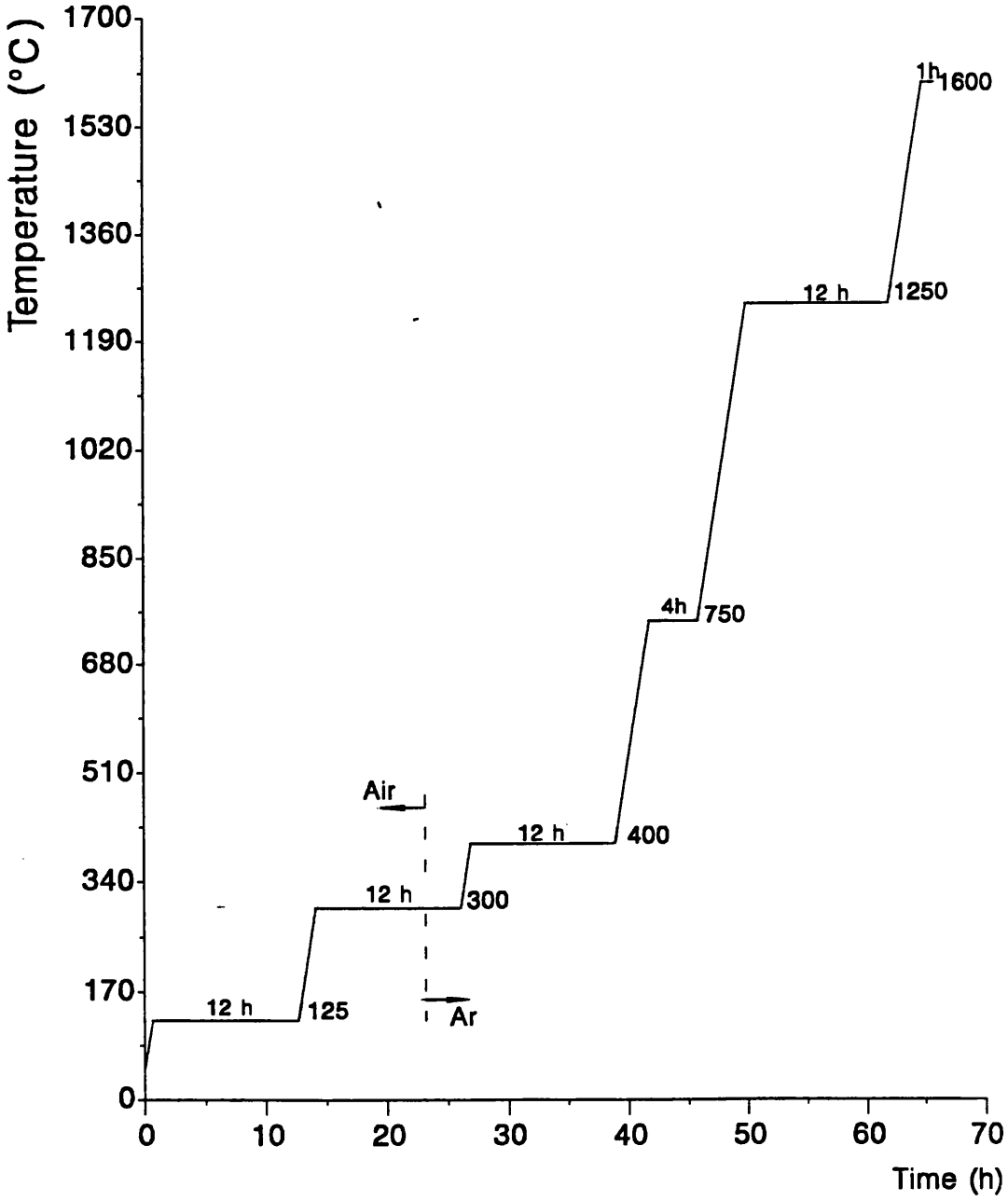

FIGURE 2.2 - Heat Treatment schedule for the SiO_2-TiO_2 sol-gel. Heating ramp between dwells = 120°C/min.

2.2 - Manufacturing methods for unidirectional composites

Unidirectional prepreg laminae were obtained from both types of fibres by the filament winding technique using a resol phenolic resin, Borden SC1008P. A schematic diagram of the process is shown on Figure 2.3. The prepreg laminae were protected with a polyester film to avoid contamination or dust. Before stacking, the polyester film was removed and the plies were left for half hour in a oven at 70°C to remove as much as possible of the resin solvent.

Laminate composites were produced by stacking ≈10 laminae of unidirectional prepregs with the fibres in parallel orientation. The stacked laminae were fitted in a square mould and then hot pressed with a multi-stage curing cycle up to 180°C. The cure cycle consists of a first stage at 80°C, allowing the resin flow, followed by a gel time at 135°C for half hour. The full hardening of the resin follows after heating at 165°C and at 180°C both for one hour. An over-cure at 165°C and 180°C, both for 24 hours, was carried out, as recommended by the resin manufacturer. All the as-cured *green* composites were trimmed to dimensions of approximately 3.2mmx8mmx135mm.

2.2.1 - Unidirectional CFRC composites

Three different classes of CFRC composites were prepared with the prepregs, as follows:

a) CFRC composite with 9 prepreg laminae of treated/sized fibres, designated as TS-1100 and TS-2500, depending upon the final heat treatment temperature.

b) CFRC composite with 9 prepreg laminae of untreated/unsized fibres, designated as UU-1100 and UU-2500;

c) CFRC composite using 5 prepreg laminae of treated/sized fibre and 4 prepreg laminae of untreated/unsized fibre, following the sequence TS/UU/TS/UU/TS/UU/TS/UU/TS, designated as T5U4-1100 and T5U4-2500.

The cured, resin matrix composites were packed in coke breeze in a graphite crucible and carbonised in a horizontal furnace in a flowing inert atmosphere, argon or nitrogen, up to 1100°C using a multi-stage heating schedule to produce CFRC composites. The heat treatment schedule for carbonised green unidirectional carbon fibre/phenolic matrix composites is shown in Figure 2.4. The development of this heat treatment schedule is described in Section 4.2, Chapter Four. Some CFRC composites were further heat treated in a flowing helium atmosphere at 10-15°C/min to 2500°C for 1 h in a graphite resistance furnace.

Bulk densities and shrinkage were measured by commensuration after the heat treatments at 1100°C and 2500°C. To minimise complications at the fibre/matrix interface, the samples were not densified by further impregnation/carbonisation cycles, as is usual with commercial CFRC composites. The fibre volume fraction of the CFRC composites was estimated by computer aided image analysis applied to a transverse cross section of the CFRC.

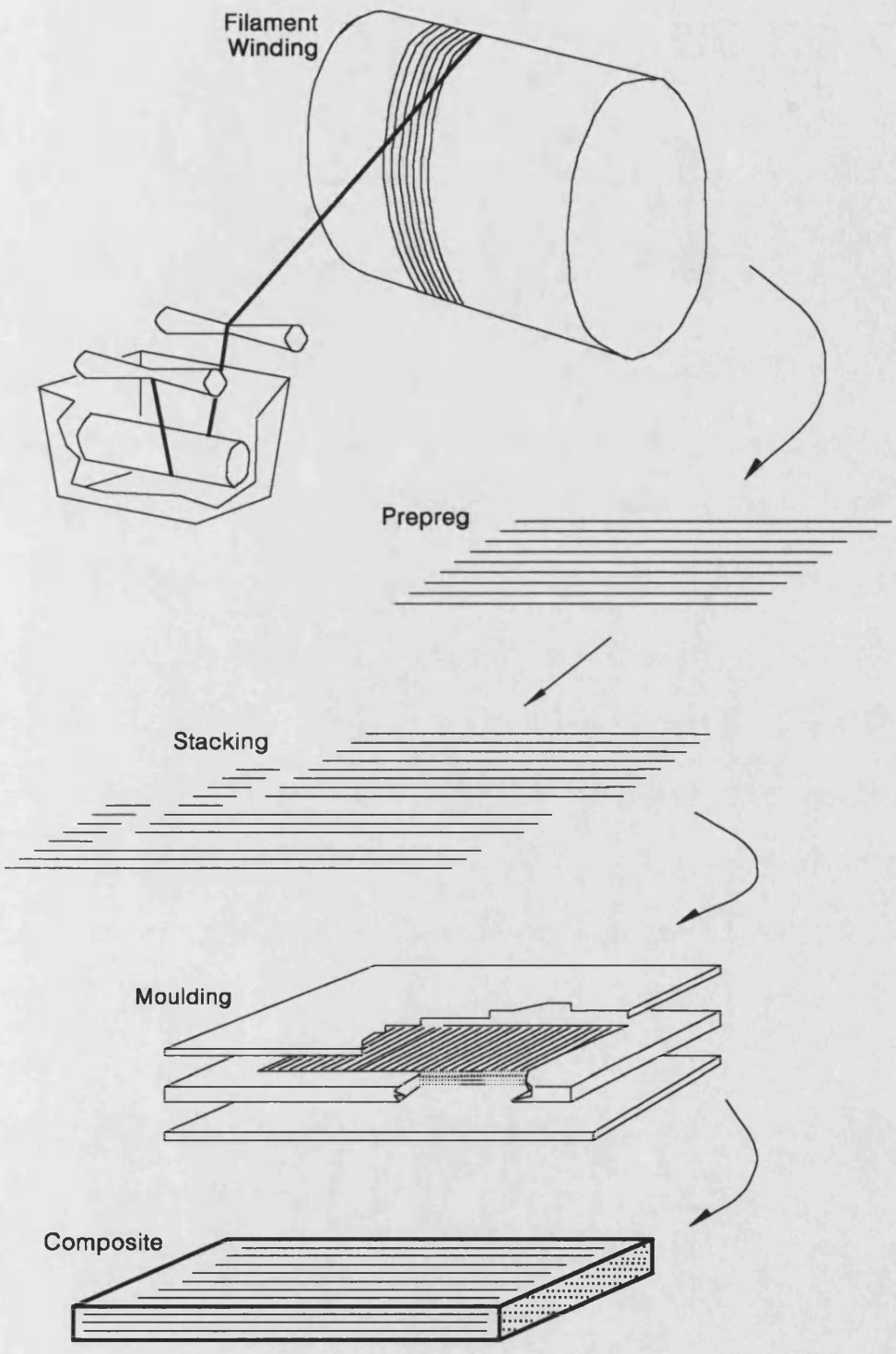

FIGURE 2.3 - Schematic diagram of the manufacturing process of unidirectional composites

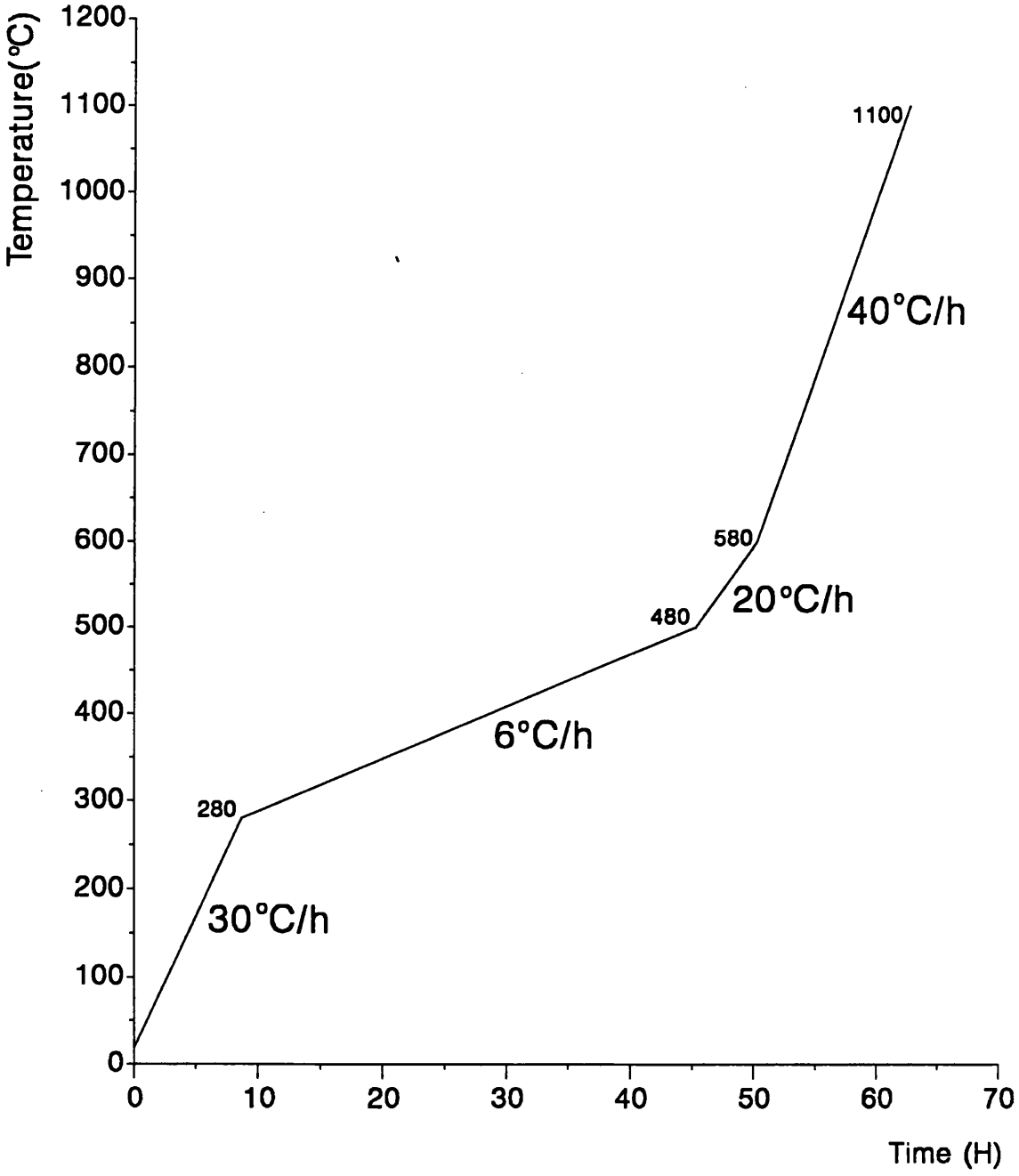

FIGURE 2.4- Heating program used for the carbonisation of carbon fibres/phenolic resin laminates.

2.2.2 - Modified SiC-Unidirectional CFRC composites

The unidirectional CFRC composites, prepared as described before in this section, were coated with the SiC *sol-gel* system using the procedure described in section 2.1.2.1.

Two other approaches were used to obtain hybrid C-SiC matrices. Firstly, the *sol-gel* system was applied between layers of the prepregs. After drying the *sol-gel* for nearly half hour at room temperature the plies were stacked and cured as described in section 2.2.1. Secondly, phenolic resin and the SiC *sol-gel* system were mixed in a defined proportion, resin/sol-gel:100/20 wt%, and the fibres were prepregged with this mixture. The phenolic/SiC *sol-gel* carbon fibre prepreg was left to dry, the plies were stacked, moulded and cured as described also in section 2.2.1. The specimens were packed and carbonised/fired as described in this section. Bulk density values of the samples were calculated from the weight and physical dimensions of specimens in air.

The heat treatment of the *green* carbon/SiC *sol-gel* system composite is a compromise between two different heat treatment schedules. So, two limiting parameters appear: (i) the carbonisation of the *green* body of the composite cannot be made at a high heating rate like the one utilized for sintering the SiC *sol-gel* coating (120°C/h), because the material may be ruptured by the stresses generated by the gases evolved during carbonisation, and (ii) the carbonisation of the hybrid C-SiC matrix cannot be made at a slow heating rate as utilized in the carbonisation of the green body composite (6°C/h), because SiC *sol-gel* cannot sinter at such a slow heating rate (White - 1987). So, the heat treatment cycle of the green C-SiC *sol-gel* system composite was carried according to the schedule shown in Figure 2.5.

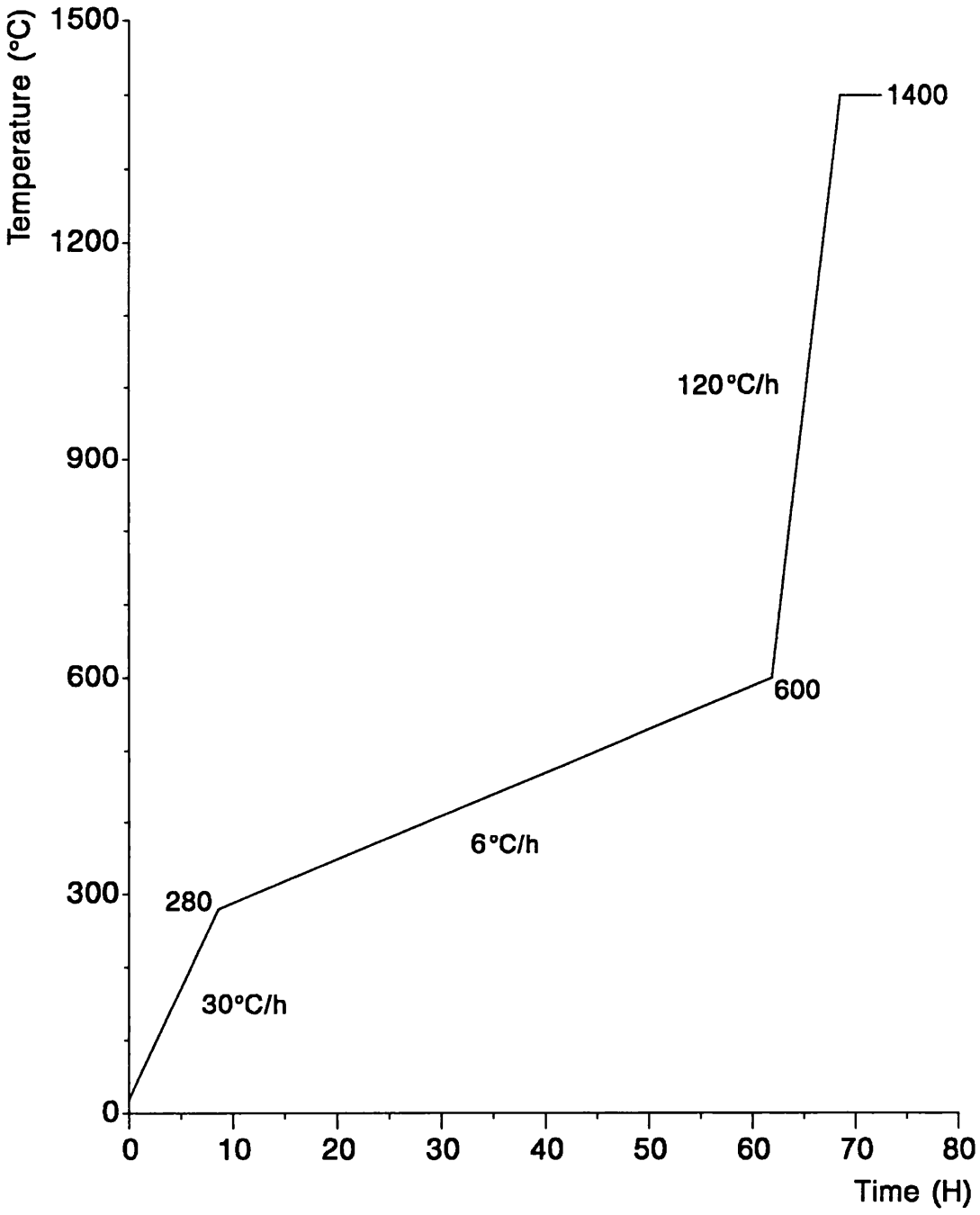

FIGURE 2.5 - Heating program used for the carbonisation/firing of carbon fibres/(phenolic resin-SiC sol-gel system) laminates.

This specific schedule was chosen taking account of two main facts. The first two steps of the carbonisation cycle are similar to those used for the carbonisation of the CFRC composite. The only difference is that the lower heating rate ramp (6°C/h) is extended up to 600°C. After that point the heating rate ramp is the one utilized for sintering the SiC *sol-gel* coating.

2.3 - Thermogravimetric Analysis

Thermogravimetric analysis (TGA) is the most important method for investigating the oxidation behaviour of the CFRC composites, the oxidation protection quality of the surface coatings and the weight loss of *green* moulded carbon fibre/phenolic laminates on carbonisation. These experiments were performed in a Setaram Thermobalance DTA92. The oxidation behaviour of the commercial CFRC Composites, Sigri and KKarb, and also coated samples were measured at 1200°C in flowing air with a flow rate of 1.5 l/h. The temperature was achieved using a heating rate of 100°C/min. The oxidation behaviour of the unidirectional CFRC composites manufactured in this work were measured in flowing air with a flow rate of 1.5 l/h, parallel to the composite fibres. For these materials the onset of oxidation and the weight loss were not so well defined using a heating rate of 100°C, and so a heating rate of 5°C/min was used to give more controlled oxidation behaviour. The weight loss of the *green* carbon fibre/phenolic resin composite on carbonisation was measured by heating in helium, at a heating rate of 5°C/min to 1100°C.

2.4 - Microstructural examination

Optical, scanning electron microscopy and X-Ray Dispersive Analysis

were used in this study to observe the microstructural features and chemical composition of the samples.

Samples of the commercial, as received or coated, and unidirectional CFRC composites were mounted in epoxy resin and polished in a automatic Motopol M12 polishing machine using the polishing routine outlined in Table 2.1.

The Zeiss ICM405 microscope was used for microstructural characterisation and for polarised light microscopy, using a full wave plate. Polarised light microscopy can be used to identify regions with strong basal plane orientation. The angle the basal plane makes with the optical system will determine the colour seen. When the basal plane is parallel to the optical system the colour seen is purple, Figure 2.6. If the basal planes are at an angle to the optical system they will be blue or yellow, on 90° rotation a blue region will change to a yellow region (Marsh - 1989).

The fracture surfaces and the microstructure of the gels were examined by scanning electron microscopy using a JEOL JSM T330 instrument. Carbon materials are reasonably conductive, therefore no special preparation was needed. The SiC *sol-gel*, after drying and before firing, was observed over the surface of the commercial CFRC composites with a coating of gold applied by sputtering for 3 min to increase electrical conductivity. The coatings and the internal modification produced by the *sol-gel* system were analysed and mapped for Si using the Scanning Electron Microscope, JEOL 35C, equipped with EDX (LINK AN10,000).

Table 2.1 - Basic polishing routine for SiC on CFRC composites. Sample cut through coating into substrate.

Planar Grinding Stage	Surface	Abrasive Size and type	Load per sample	Wheel speed	Head Rotation	Process Time
	paper	P320g SiC	5 lb	150	comp.	1 min

Sample Integrity Stage	Integrity Surface	Abrasive size and type	Load per sample	Wheel speed	Head Rotation	Process Time
	Metalap 4	9μm o/b	5 lb	25	contra	4 min
	Textmet 1.S.1	1μm o/b	5 lb	240	comp.	4 min
	Textmet 1.S.1& Si_2O	Coloidal Silica 0.06μm	5 lb	50	comp.	4 min

Polishing Stage	Polishing Surface	Abrasive Size and type	Load per sample	Wheel speed	Head Rotation	Process time
	Mastertex	Coloidal Silica 0.06μm	2.5 lb	50	contra	2 min

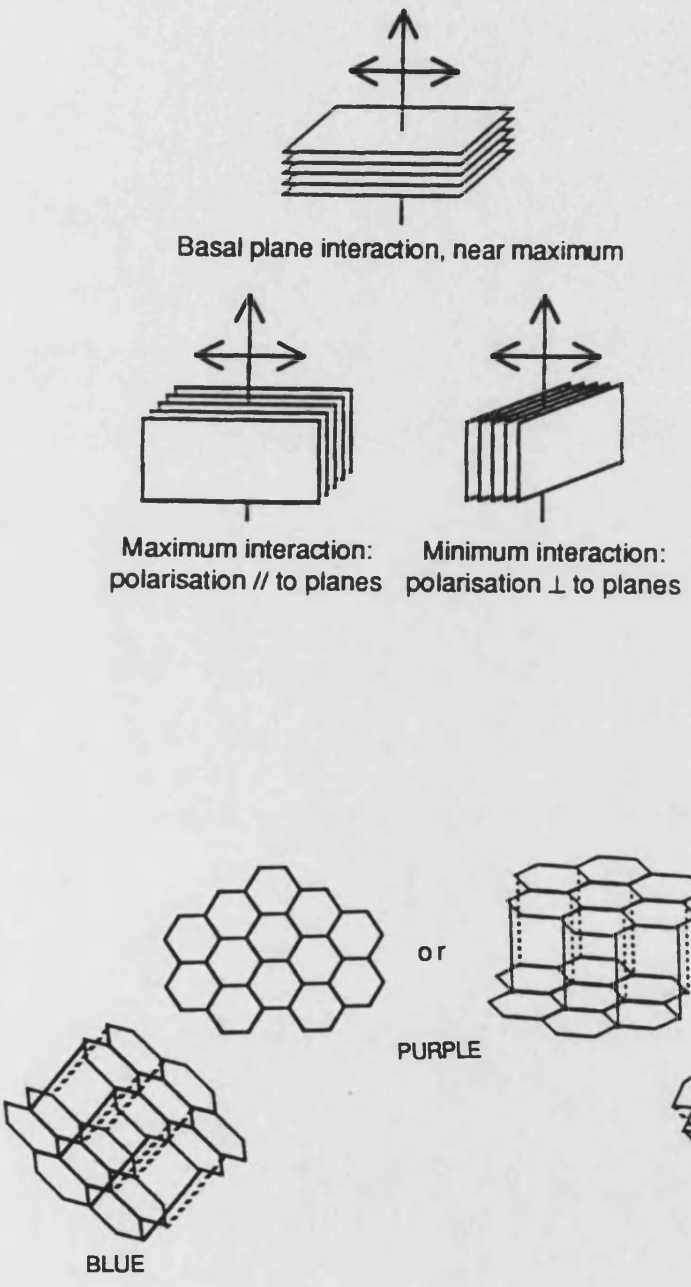

FIGURE 2.6 - Interference colours obtained by polarised light optical microscopy in carbon materials (Marsh - 1989).

2.5 - Mechanical Properties and Acoustic Emission

2.5.1 - Flexural Properties

Flexural strength of the specimens was measured in three point bending with load point rollers of 4 mm radius. The load was recorded at a cross head displacement of 0.5 mm/min used in all tests. The mid-span deflection of the specimen was taken as the cross head displacement, assuming the testing machine to be infinitely stiff compared with the sample. Flexural tests are of great convenience because they are performed with a modest consumption of test material, are extremely useful in obtaining preliminary data on systems not yet fully developed and are especially helpful in monitoring experimental progress. The flexural strength and elastic modulus were calculated using standard equations as defined in Appendix V.

In addition, for the purpose of internal comparison, a nominal fracture initiation energy of unnotched CFRC composites was calculated from force-deflection curves as follows

$$\gamma = U/2.w.d$$

where U is the area under the force-deflection curve for forces less than the maximum value, in Joules, and w and d are the width and depth of the specimen in meters.

The mid-span deflection at peak load was used as a measure of the nominal strain to initiate failure of the composites. Although the mid-span deflection is not a true strain, it provides a useful means of internal comparison.

2.5.1.1 - Commercial CFRC composites

For the KKarb material sample dimensions were 70 x 3.2 x 7 mm with the long axis in the warp direction. The span/depth (S/D) ratio was 19:1. It was demonstrated by Crocker (1991) for as-received specimens of the KKarb material that the flexural modulus was independent of S/D ratio for ratios greater than 10:1. For the Sigri material the sample dimensions were 90 x 2.9 x 7 mm. The flexural modulus of the Sigri material was shown to be independent of span/depth ratio for ratios greater than 25:1 (Rief - 1990, Crocker - 1991). As the Sigri CFRC composite has a hopsack weave, the fill and the fibre reinforcement in the warp directions are nominally identical, although previous work has shown that for 4 mm thick samples there is a difference in strength of about 15% between the warp and weft directions (Rief - 1991). Flexural properties of the commercial materials were measured using an Instron 1122 Universal Test Machine.

2.5.1.2 - Unidirectional CFRC composites

The flexural strength and modulus of the unidirectional CFRC composites and C/SiC modified composites were measured using an Instron 1195 with a span/depth ratio of 35:1. It will be shown in Section 4.4 of Chapter Four, that for this material the flexural modulus is approximately constant in the range of span/depth ratio of 25:1 - 55:1.

2.5.2 - Acoustic Emission Measurements

The experimental AE system is shown schematically in Figure 2.7. The AE events are detected by the response of a piezoelectric transducer coupled

to the surface of the stressed specimen using a thin layer of petroleum jelly. The transducer converts the stress waves into a sinusoidal electrical voltage of low amplitude, which is passed through a 60 dB pre-amplifier. The characteristics of the AE events are measured using a Marandy MR1004 system. The peak amplitude of each event is sorted into one of 25 amplitude channels, each of which is 2.4 dB wide relative to the threshold amplitude (10 mV). When a test is in progress, the MR1004 amplitude sorter/computer system records both analogue data, such as load or strain, and AE data in binary format. Data recording is optimised for speed of data acquisition, but, for subsequent analysis, the data must be decoded into an ASCII format which can then be read into a software package for production of graphs (Russel-Floyd - 1990).

The most frequent method for evaluating structural damage by AE monitoring is to count the signals emitted during deformation of the material and plot the results as count rate or total count as a function of some measure of the deformation such as pressure, stress, strain, or number of fatigue cycles (Stone - 1977).

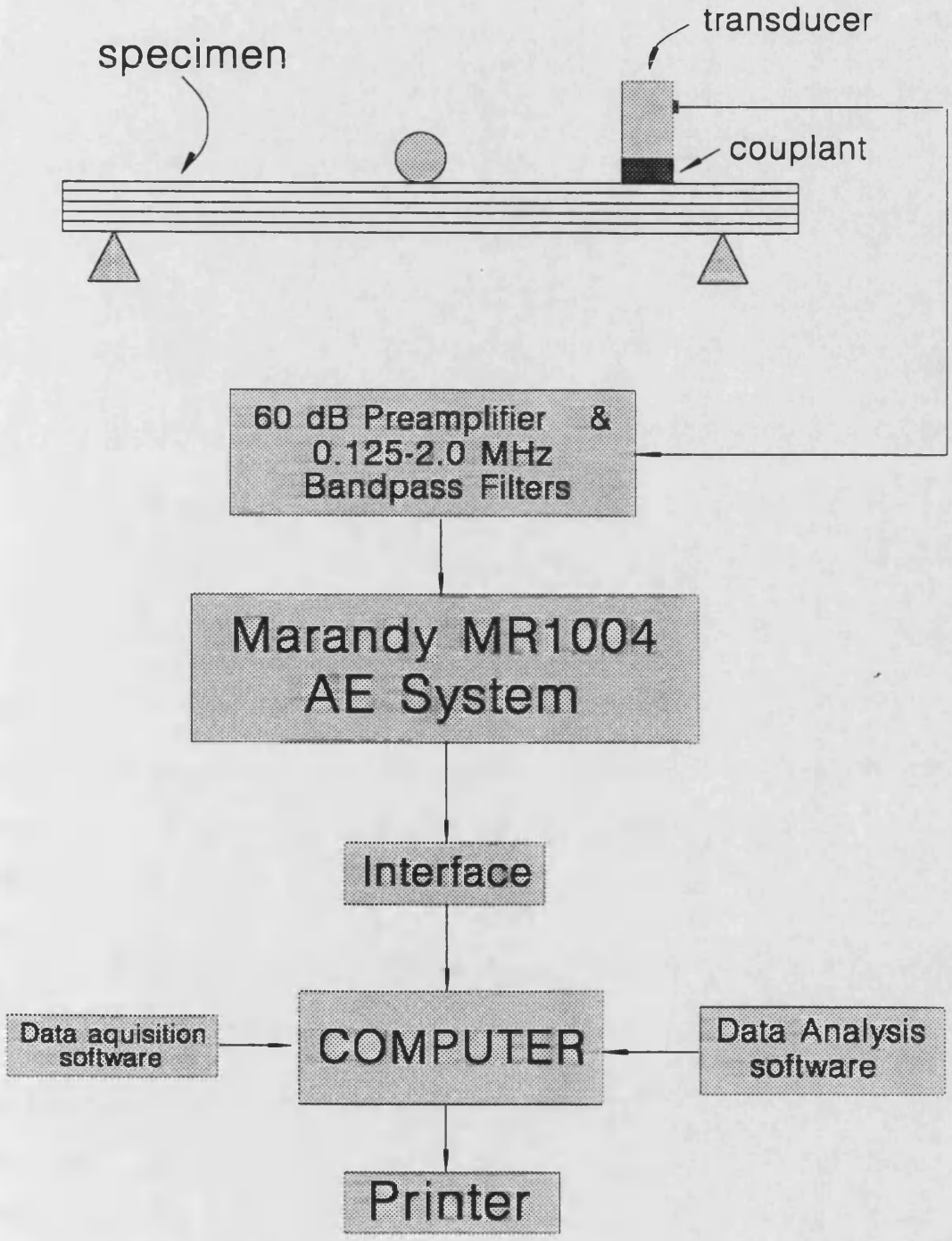

Figure 2.7 - Experimental set-up of the acoustic emissions measurements.

CHAPTER THREE
COMMERCIAL CFRC COMPOSITES RESULTS AND DISCUSSIONS

This chapter describes the results obtained from the commercial CFRC composites, Sigri and KKarb, utilized in the preliminary stage of this work. The effects on the mechanical properties, fracture behaviour and in the acoustic emission patterns during fracture were analysed on as-received and SiC sol-gel coated samples. Oxidation resistance tests on as-received and SiC coated samples with glassy layers were also investigated.

3.1 - Microstructure of the commercial CFRC composites

The microstructural features of the Sigri and KKarb CFRC composites were explored by Crocker (1991). The KKarb material, Figure 3.1, is reinforced with rayon carbon fibre bundles in a 5 harness satin weave. The matrix is formed from a blended mixture of pitch and resin and is graphitised. Optical micrography, Figure 3.1B, revealed also that there are many regularly-spaced, intrabundle cracks, ≈200 μm long, some of which extend across the whole width of the bundle (C), and little porosity is present. The fibre bundles can be easily identified by SEM, Figure 3.1A and a few small pores (P), ≈50 μm wide, can be seen.

The Sigri material, Figure 3.2, has a resin carbon matrix and ex-PAN carbon fibre bundles in a hopsack weave with very large pores, mainly at bundle/bundle interfaces that can be easily seen by optical and SEM micrographs. Possibly, these pores have formed because the resin has shrunk on carbonisation and/or bubbles of volatiles or air have been trapped on curing. Cross bundle cracks, similar to those found for the KKarb composite are also seen in Figure 3.2B.

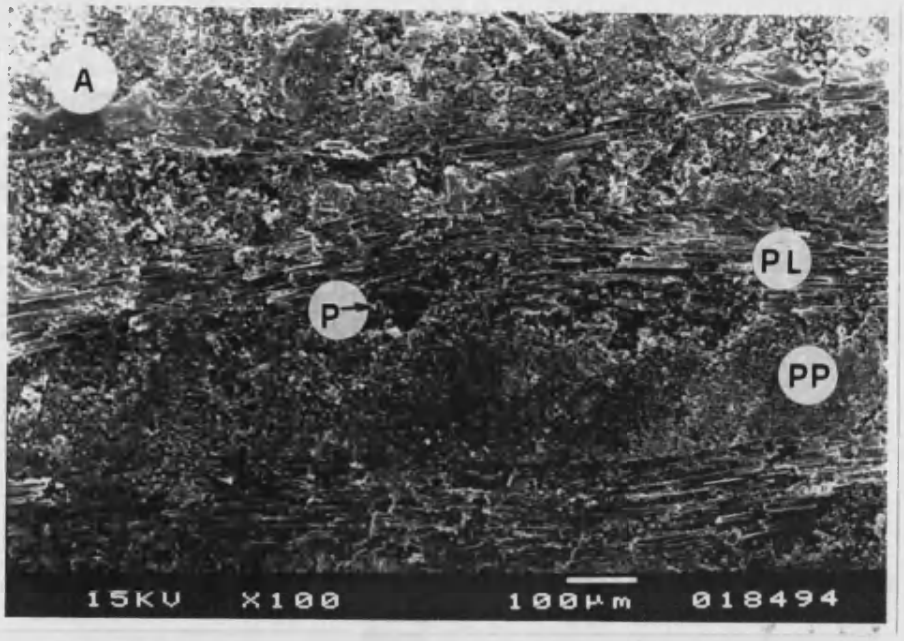

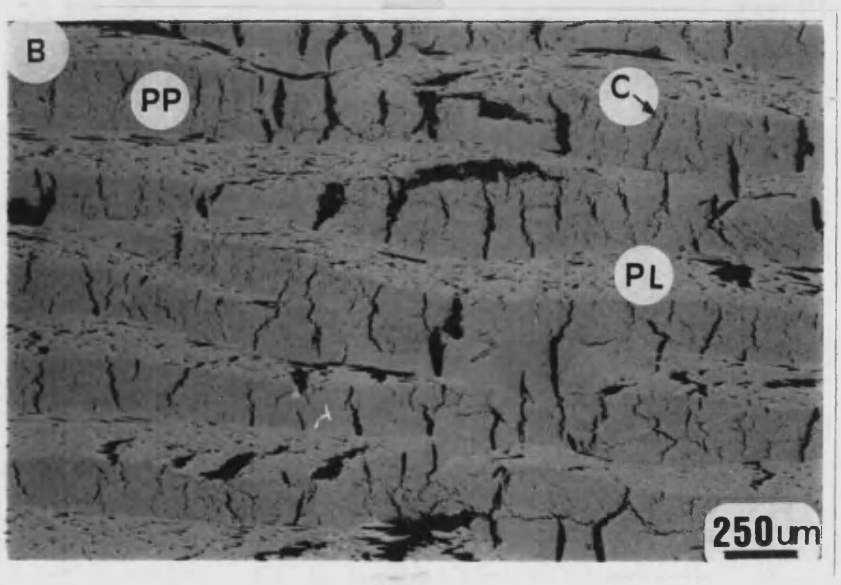

FIGURE 3.1 - Micrography of KKarb Type A CFRC composite. (A) Scanning Electron Microscopy and (B) Optical Microscopy showing fibre bundle parallel (PL), and perpendicular (PP) to the polishing plane, small pores (P), and cross bundle cracks (C).

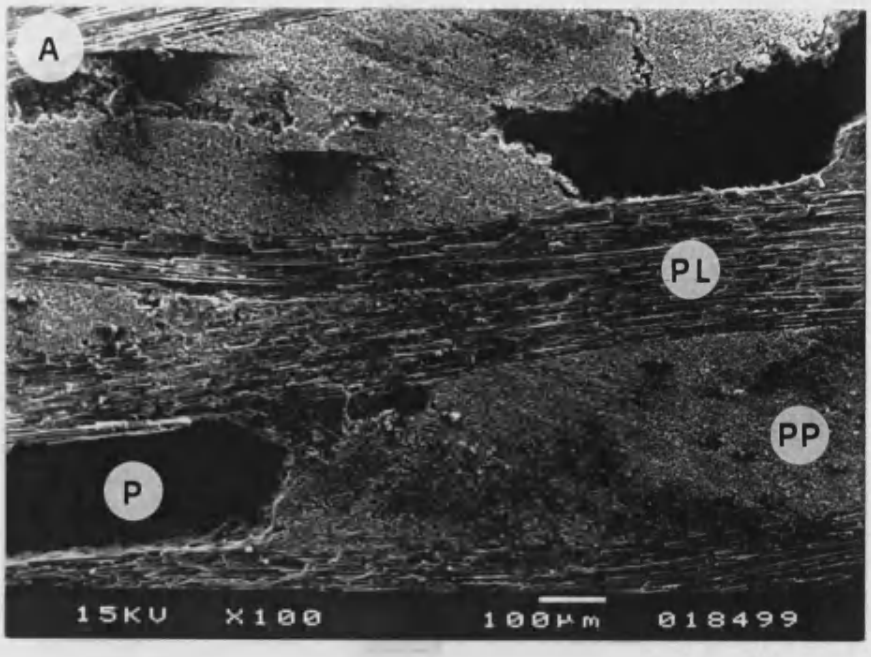

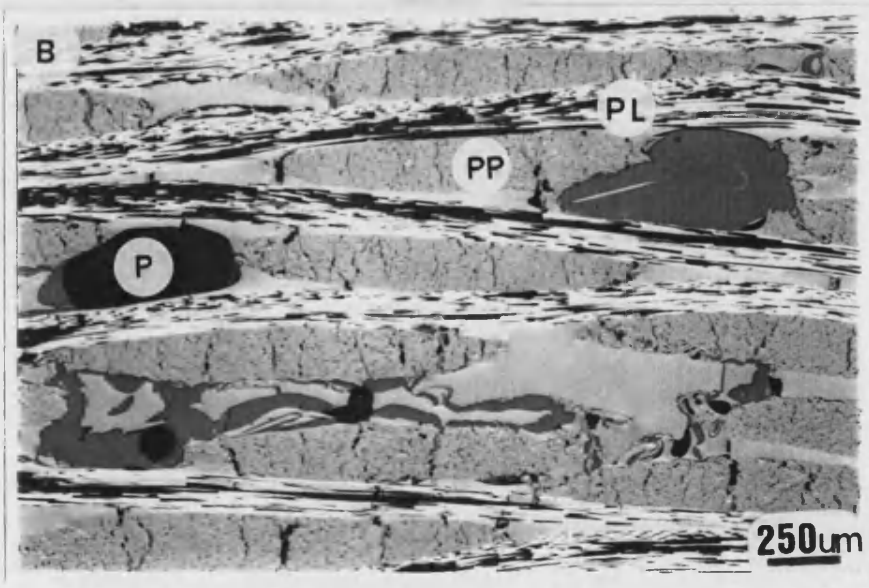

FIGURE 3.2 - Micrography of Sigri CC1501G CFRC composite. (A) Scanning Electron Microscopy and (B) Optical Microscopy showing fibre bundle parallel (PL) and perpendicular (PP) to the polishing plane and large pores (P), and cross bundle cracks (C).

Water penetration and mercury posimetry were used to estimate the porosity in the composites. The cumulative pore volumes obtained from mercury porosimetry are in Figure 3.3. The total open pore volume fraction, V^o_{total}, is given by:

$$V^o_{total} = V_{max} \cdot \rho_b$$

where V_{max} is the maximum value of cumulative pore volume in Figure 3.2, and ρ_b is the bulk density of the composites (ρ_b=1.43 and 1.36 g/cm^3 for Sigri and KKarb respectively). The fractions of open macropores and mesopores, V^o_{macro} and V^o_{meso} are obtained in a similar way using the IUPAC boundary at pore radius = 25μm between mesopores and macropores shown in Figure 3.3. Values of these pore volume fractions are compared with the total open pore volume fraction obtained by water penetration method, V^o_{H2O}, in Table 3.1.

	Sigri CC1501G	KKarb Type A
V^o_{H2O}	0.129	0.054
V^o_{total}	0.140	0.075
V^o_{macro}	0.075	0.025
V^o_{meso}	0.065	0.050

Table 3.1 - Porosity of Sigri CC1501G and KKarb Type A composite by mercury porosimetry and water penetration method (ASTM D-20).

The estimates of total open pore volume obtained by the two methods are in reasonable agreement for the Sigri material; the open pore volume fraction estimated by mercury porosimeter is slightly higher than that obtained by water penetration for the KKarb material.

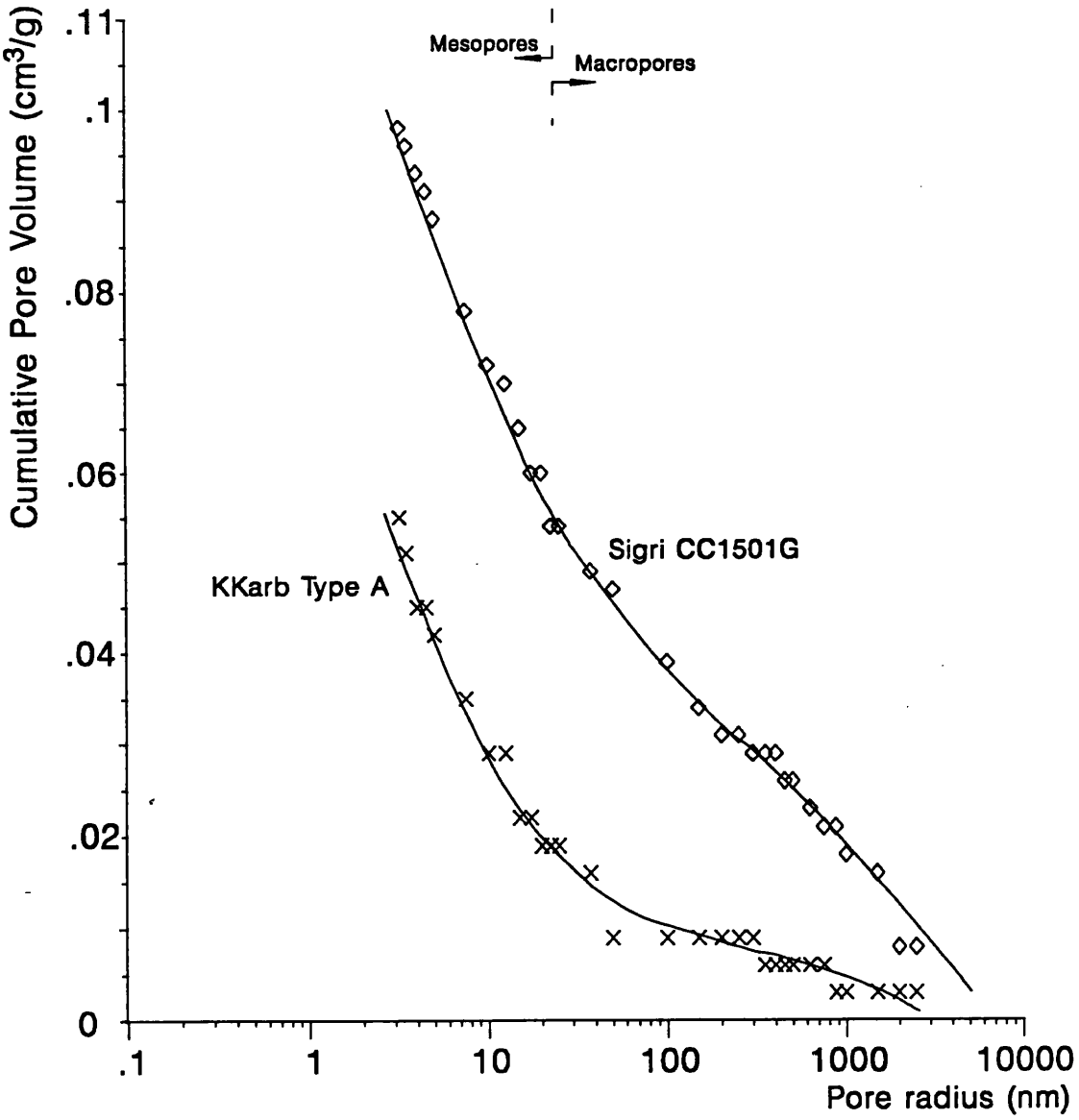

FIGURE 3.3 - Cumulative pore volume vs pore radius for KKarb Type A and Sigri CC1501G composites, by mercury porosimetry.

The macro pore volume fraction for Sigri composite is three times the value for KKarb material and this can be attributed to the presence of large pores in the Sigri material, Figure 3.2, and the few small pores in the KKarb material.

3.2 - Microstructure of SiC coated CFRC composites

Coatings of SiC prepared by the sol-gel method were applied to Sigri and KKarb composites, as described on Section 2.1.4.1 of Chapter Two. The microstructure of the alkoxide gel on Sigri and KKarb composites, observed by SEM, after drying and before firing shows similar mosaic textures for both materials, Figure 3.4. Elimination of the liquid phase leads to dry gels in the following sequence of events: progressive shrinkage and hardening, stress-development and fragmentation. Porous flat gel surfaces were found in both Sigri and KKarb composites brush coated with the alkoxide sol-gel.

Micrographs of Si X-ray maps for brush coated KKarb and vacuum impregnated KKarb materials after firing to produce SiC are shown in Figure 3.5. There is a continuous external coating of SiC which is approximately 10 μm thick on the brush coated material and aproximately 35 μm thick on the vaccuum impregnated material. In the vaccuum impregnated KKarb composite there is some penetration of the SiC through the microcrack network to a depth of ≈1 mm, suggesting that connectivity between pores and microcracks has a beneficial effect permitting penetration of the sol-gel system. A similar penetration of the crack network to ≈0.25 mm was found for the brush coated material. Thus, vacuum impregnation was clearly more effective in ensuring penetration of the CFRC by SiC sol-gel.

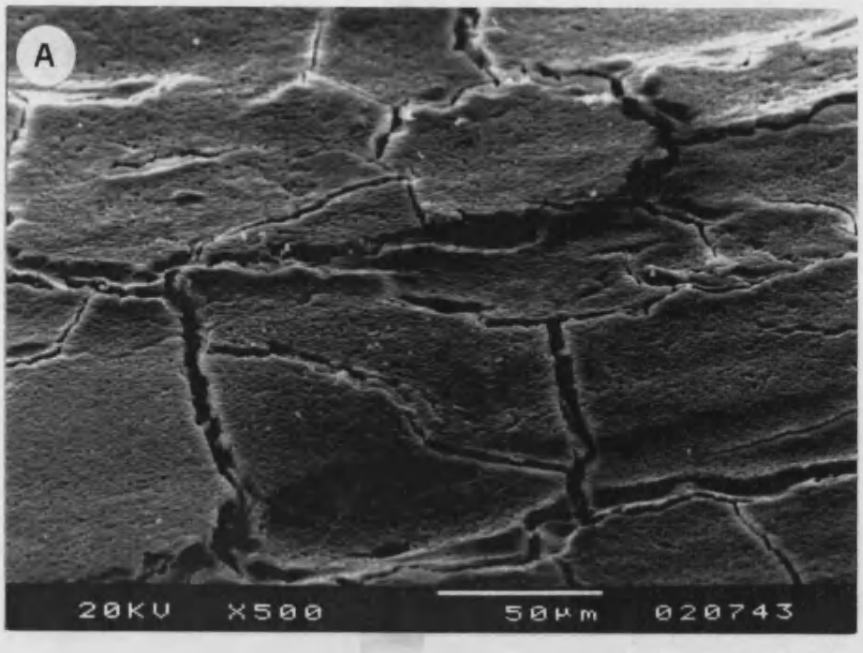

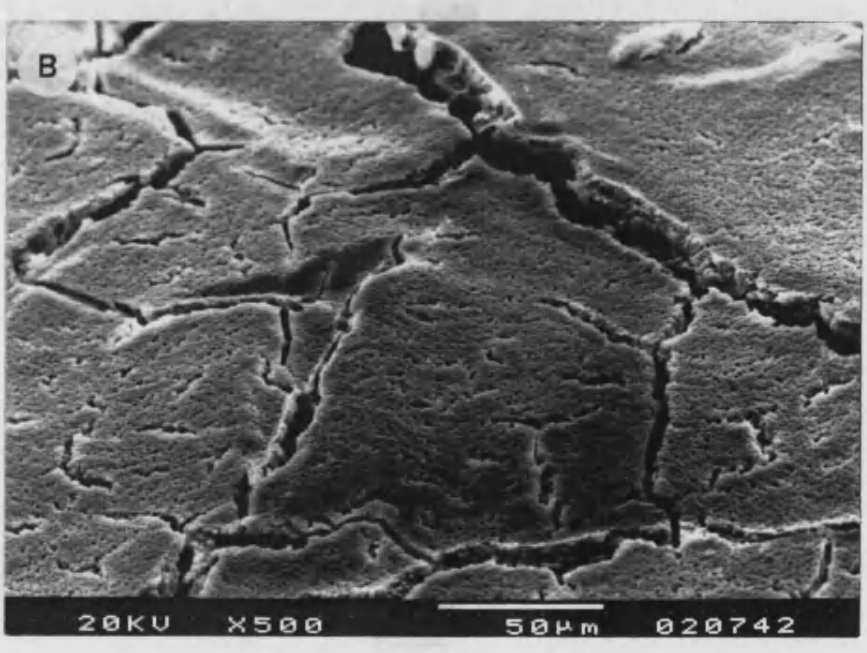

FIGURE 3.4 - Mosaic textures of the brush dried alkoxide gel, before firing, over the surface of CFRC composites. (A) KKarb composite, (B) Sigri composite.

Si X-ray maps of the coating on brush coated Sigri composite after firing, showed that it is thinner than was found for the KKarb material, Figure 3.6A, and it is not continuous. The surface of the brush coated Sigri material observed by SEM, Figure 3.6B, shows an irregular coating, suggesting that some discontinuous SiC agglomerates are formed. Even with seven firing procedures a thicker surface coating was not obtained, Figure 3.7A, but a greater extent of internal penetration was found, probably due to the large open porosity, Table 3.1. A similar large extent of internal penetration of SiC was found for samples submitted to pressure impregnation, Figure 3.7B.

The X-ray analysis of the uncoated and SiC coated Sigri material are shown in Figure 3.8. In addition to the characteristic X-ray peaks for carbon found on the uncoated Sigri composite on Figure 3.8A, the SiC coated Sigri material, Figure 3.8B, also shows characteristic X-ray peaks for SiC. There was no evidence from X-ray diffraction for other species in the coated material.

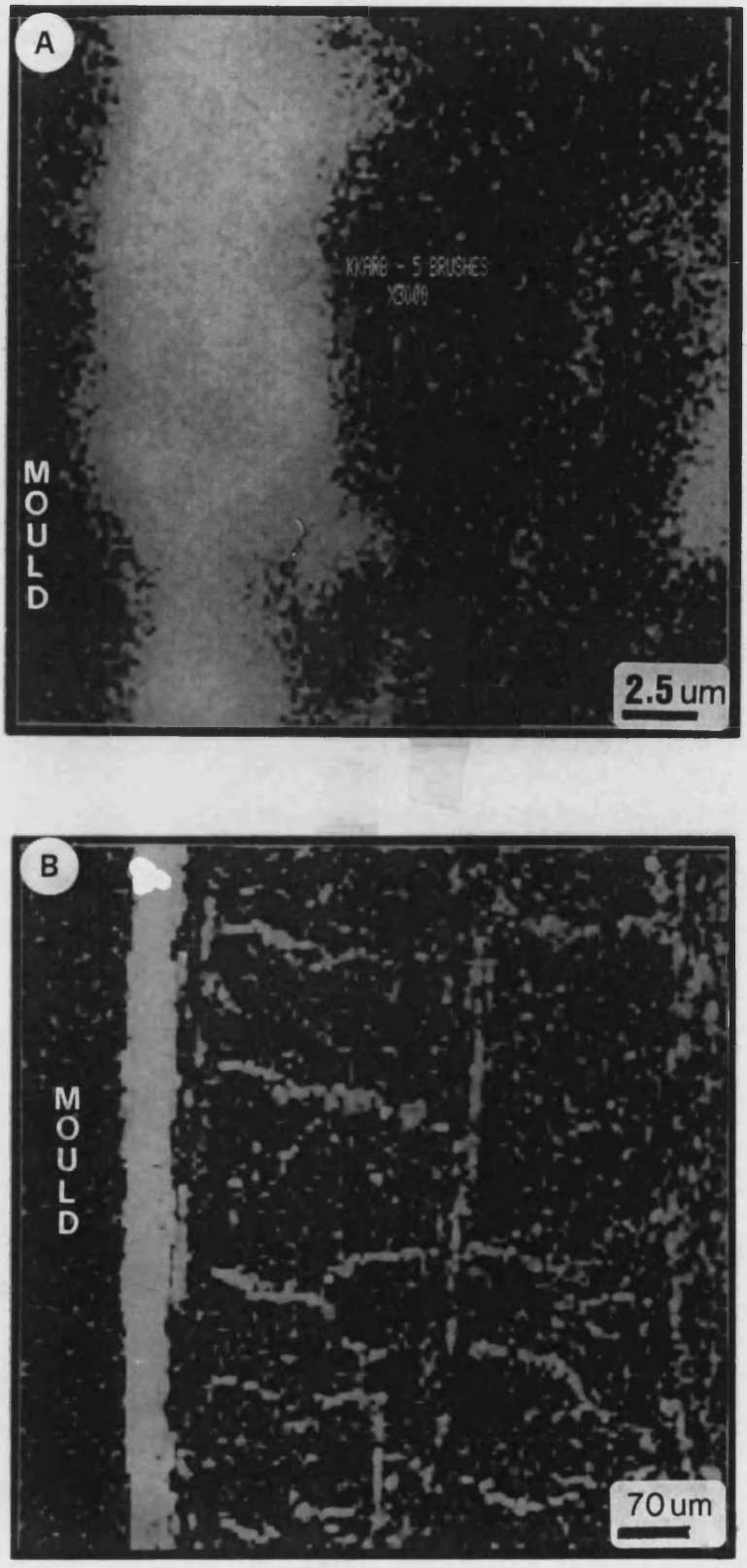

FIGURE 3.5 - X-Ray maps for Si on KKarb Type A composite. (A) Brush coated/5 firings; (B) Vacuum impregnated/firing, plus 4 brush coatings/4 firings.

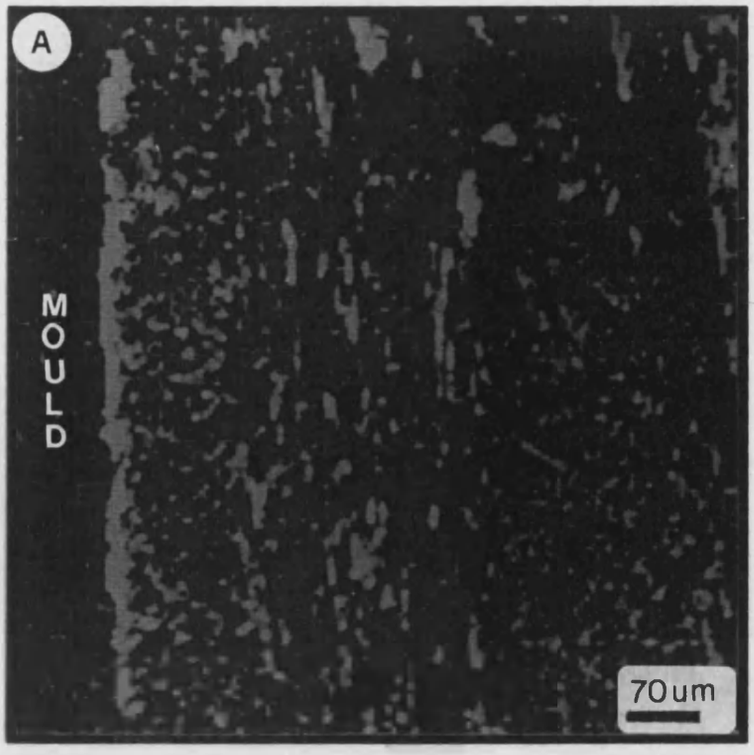

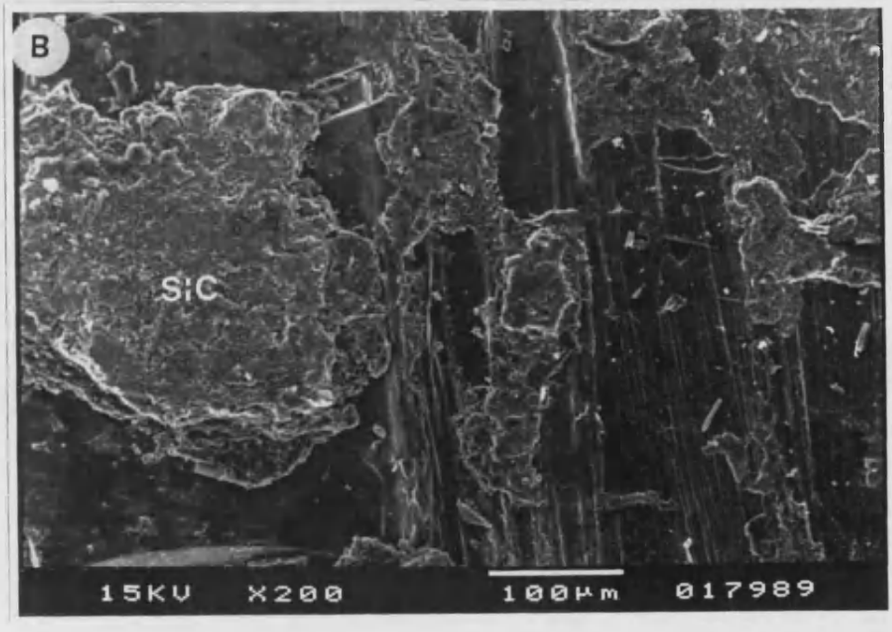

FIGURE 3.6 - (A) X-Ray map for Si on Sigri CC1501G composite brush coated/5 firings ; (B) SEM of the coating over the surface of the Sigri material brush coated/5 firings.

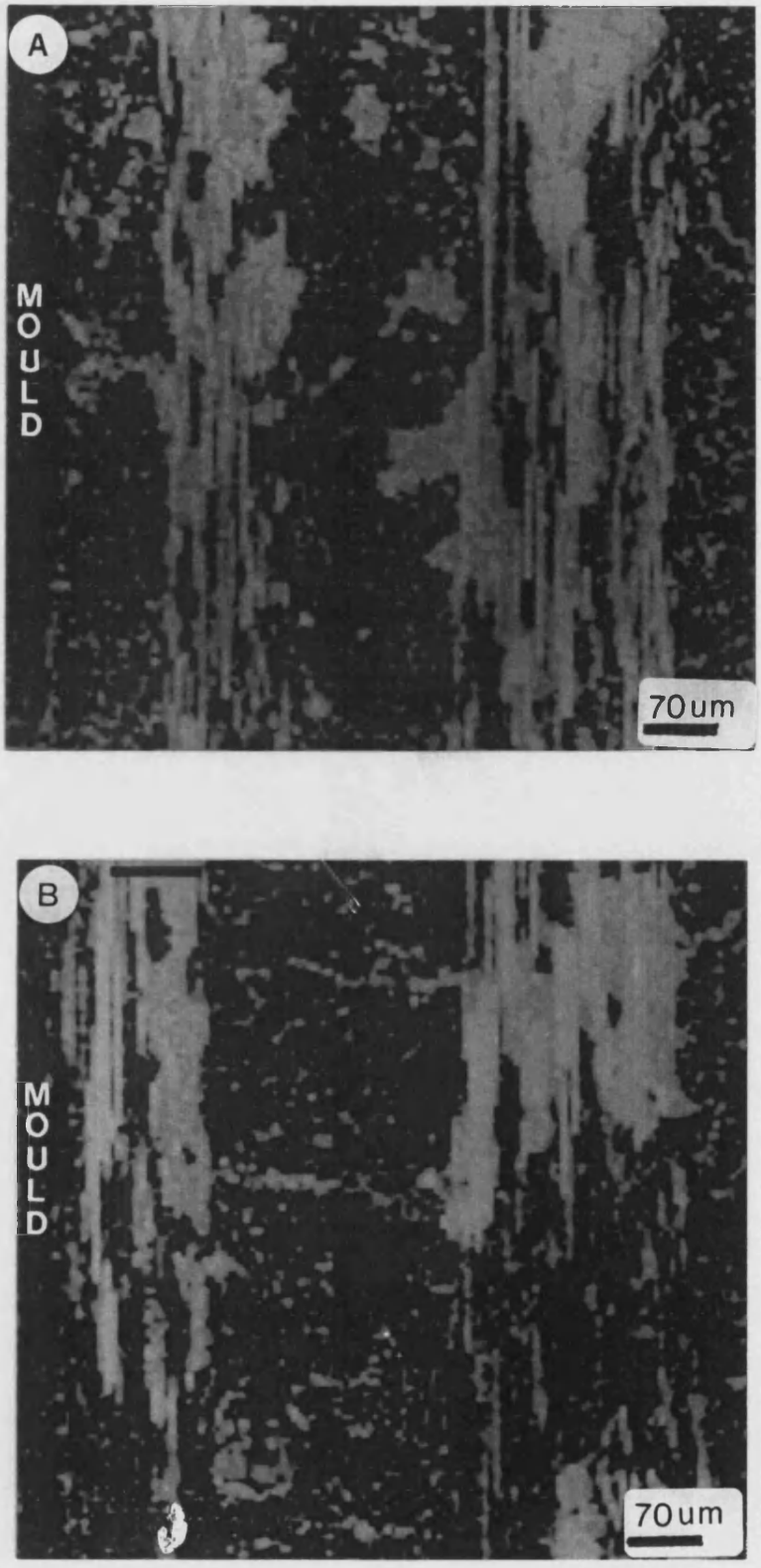

FIGURE 3.7 - (A) X-Ray map for Si on Sigri composite, 7 brush/7 firings; (B) X-Ray map for Si on Sigri, 3 pressure gelations/3 firings. Both showing extensive penetration of the SiC.

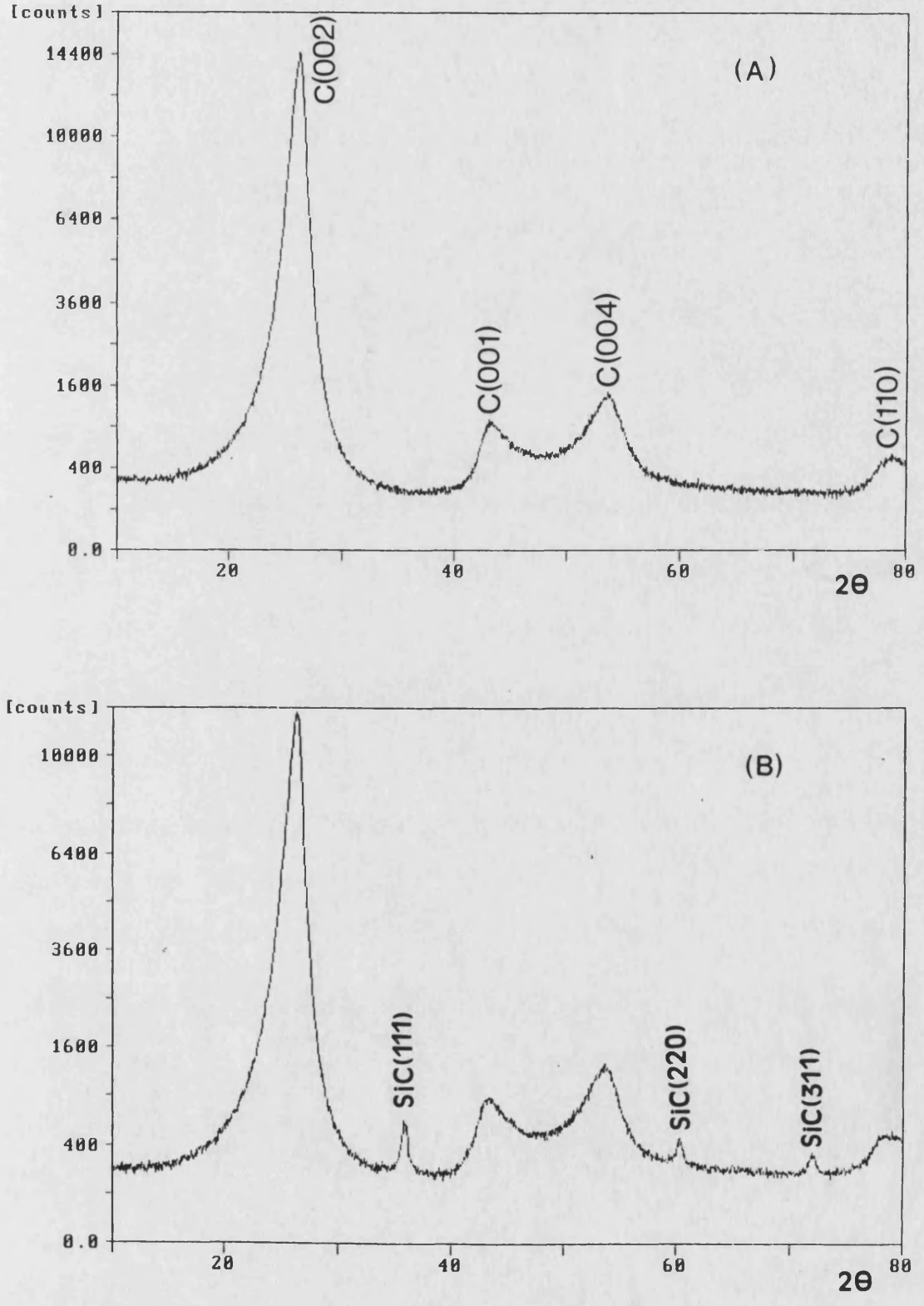

FIGURE 3.8 - X-ray analysis of the uncoated Sigri composite showing characteristic peaks for carbon (A) and SiC coated Sigri material (B), showing additional characteristic peaks of the SiC coating.

3.3 - Mechanical properties of commercial CFRC composites

Flexural strength and flexural modulus were measured for KKarb composite, Table 3.2, and Sigri material, Table 3.3, at a span/depth ratio of 25:1 and 19:1, respectively. The justification for using these span/depth ratios was given in Section 2.6.1.1 of Chapter Two, and definition of fracture initiation energy is given in Section 2.5.1 of the same Chapter. The mid-span deflection is taken at the peak stress.

3.3.1 - Uncoated samples

The specimens of Sigri or KKarb composites lose weight when subjected to heat treatment to 1500°C in helium, Figure 3.9. The curves show a small weight gain at ≈100°C due to a buoyancy effect during testing. A small but rapid weight loss (0.01-0.02%) probably due to loss of surface oxides (C[O] $\rightarrow$ CO_2 + CO) is observed after this temperature until ≈425°C. The materials are stable from 425°C-1000°C when they begin to lose weight at a similar rate and after 15 min at 1500°C a total weight loss of ≈0.03-0.04% was measured. Presumably calcination at the final heat treatment temperature during manufacture was not complete. As a precaution the coated and uncoated commercial composites were subject to an outgassing heat treatment at 1500°C for 12 hours before any measurements were made.

Typical plots of stress-deflection and sketches of the crack patterns after fracture for uncoated materials are shown in Figure 3.10. These curves and values of flexural strength and modulus, Tables 3.2 and 3.3, show that the Sigri material is stiffer and stronger than KKarb composite. On the other hand, the mid-span deflection of KKarb composite is almost the double that of the Sigri material, Tables 3.2 and 3.3 respectively.

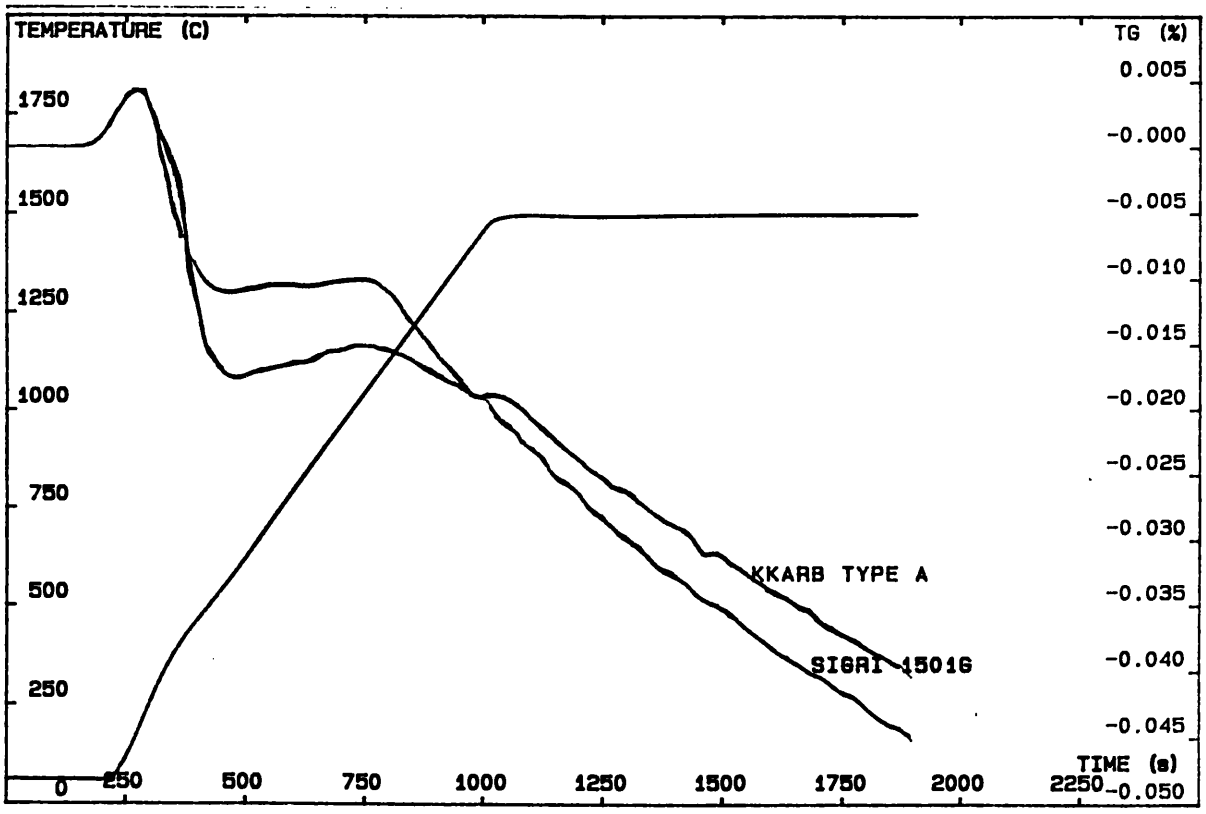

FIGURE 3.9 - Weight loss in helium at 1500°C of KKarb and Sigri CFRC composites.

The stress-deflection curves indicate that KKarb composite is tougher than Sigri material. KKarb composite has a nominal fracture initiation energy of 2.97±0.37 kJ/m^2 that is much higher than for Sigri material, 1.70±0.18 kJ/m^2. Similar results for the nominal fracture initiation energy of these materials were found by Crocker (1991).

It was also shown previously (Crocker - 1991) that flexural fracture of KKarb material is initiated by cross-ply cracking at the tensile surface of the specimen, but it is dominated by delamination between plies in the tensile stress field. Aveston (1971) showed that flexural failure by a process of repeated fracture arrest and delamination can contribute significantly to the toughness of reinforced composites so that the delamination type of fracture of KKarb composite may contribute to its superior toughness when compared to the Sigri material. Flexural fracture of uncoated Sigri materials is initiated in the compressive stress field and is dominated by 45° shear cracks running between large pores (Crocker - 1991). These failure modes were confirmed in the present work, Figure 3.10.

3.3.2 - SiC Coated samples

Mechanical properties of SiC coated KKarb and Sigri CFRC composites compared with the uncoated materials are presented in Table 3.2 and 3.3, respectively. Typical stress-deflection curves and sketches of the crack patterns after flexural failure for uncoated and SiC coated KKarb and Sigri CFRC composites are shown in Figure 3.11 and 3.13, respectively.

The fracture mechanism of SiC brush-coated KKarb is similar to the uncoated one, Figure 3.11A, except that ply delamination is more marked and extends to the neutral axis and the failure mode is characterized by a

more stepped reduction in stress after the peak load than is found for the uncoated KKarb material. Presumably, the negligible effect of SiC coatings on the strength of the KKarb material is because the fracture process is dominated by ply-delamination in regions of the composite where the SiC has not penetrated. The failure mode of the vacuum impregnated KKarb is characterized by a sharp reduction in stress after fracture, Figure 3.11B, being an indication that deeper penetration makes the material more brittle. This is also indicated by the lower mid-span deflection and fracture initiation energy of the vacuum impregnated SiC coated composite.

A SEM view of the tensile fracture face of the brush coated KKarb, Figure 3.14A, shows a sharp brittle crack of the SiC coating and fibre bundles are exposed, and no apparent delamination of the coating during fracture is observed. Although not pronounced, the mid-span deflection of the SiC vacuum impregnated and brush coated KKarb composite decrease in relation to the uncoated material giving rise to a lower nominal fracture initiation energy. The same trend is observed for the SiC pressure impregnated KKarb materials where a reduction in the mid-span deflection with the number of pressure impregnations gives rise to a decreasing value of the nominal fracture initiation energy.

	Uncoated	V.I./F*	Brush Coated	Pressure ——Impregnation——	
Number of Firings		4	5	1	2
Flexural Strength (MPa)	155.5±9.0	174.5±6.5	164.6±19.2	159.7±8.5	159.0±5.7
Flexural Modulus (GPa)	13.1±0.4	16.7±0.5	16.4±1.2	14.7±0.7	15.5±0.9
Mid-span deflection(a) (mm)	2.32±0.21	2.02±0.02	1.97±0.08	2.08±0.10	1.87±0.10
Nominal Fracture Initiation Energy (kJ/m^2)	3.45±0.40	3.04±0.08	2.82±0.39	2.83±0.23	2.58±0.23

*V.I./F - Vacuum impregnated/fired + 4 brush coatings

Table 3.2 - Mechanical Properties of KKarb Type A composites. Mean values ± are standard deviation; 7 samples. span/depth ratio = 19:1. (a) at peak stress.

	Uncoated	Brush Coated	Pressure Impregnation		
Number of Firings		5	1	2	3
Flexural Strength (MPa)	214.6±14.0	267.9±12.3	239.3±11.0	245.3±19.2	263.8±15.2
Flexural Modulus (GPa)	52.7±3.5	49.7±3.8	55.9±2.9	54.6±2.8	57.6±4.0
Mid-span deflection[(a)] (mm)	1.2±0.07	1.50±0.10	1.21±0.05	1.28±0.12	1.35±0.10
Nominal Fracture Initiation Energy (kJ/m^2)	1.69±0.17	2.5±0.22	1.95±0.16	2.07±0.31	2.35±0.27

Table 3.3 - Mechanical Properties of Sigri CC1501G composites. Mean values ± are standard deviation; 7 samples. span/depth ratio = 25:1. (a) at peak stress.

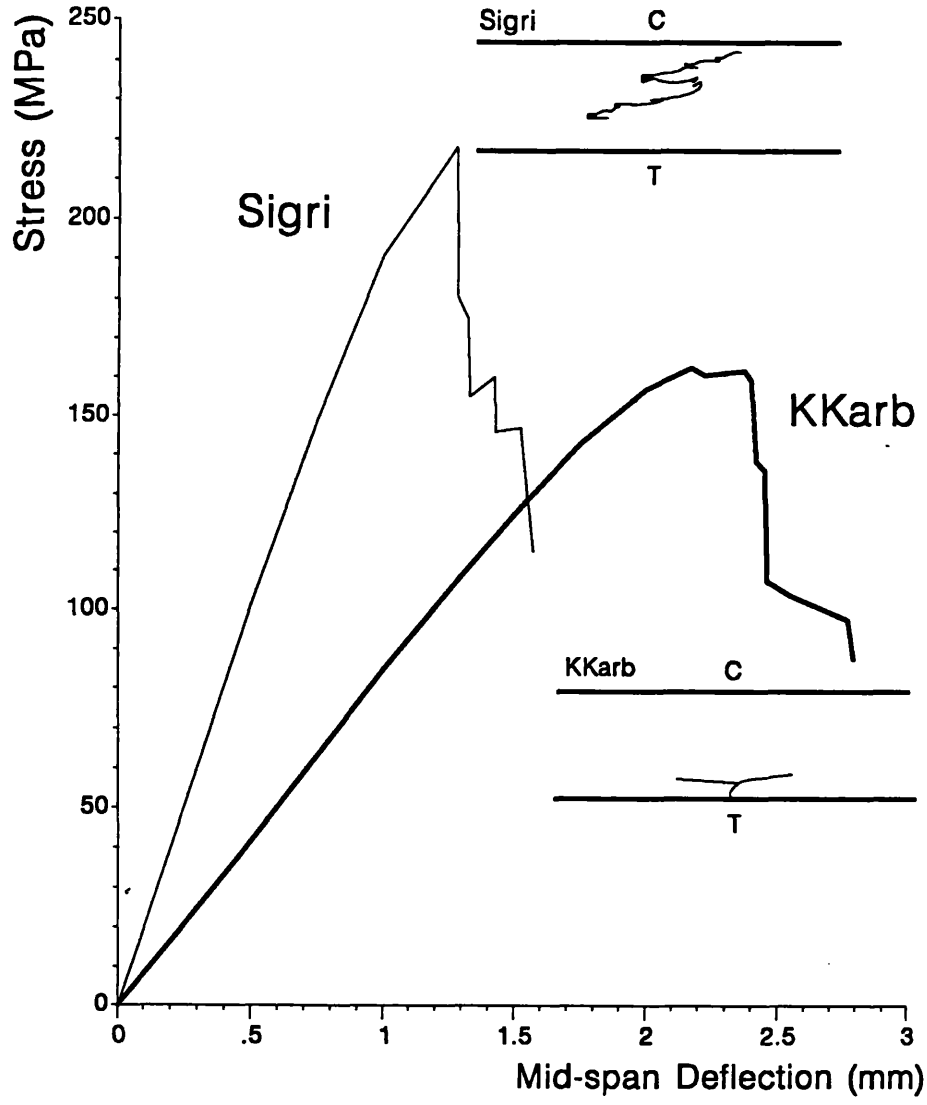

FIGURE 3.10 - Typical stress-deflection curves and sketches of the failure modes for uncoated specimens from KKarb Type A (span/depth = 19:1) and Sigri CC1501G (span/depth = 25:1). C=compressive face, T=Tensile face.

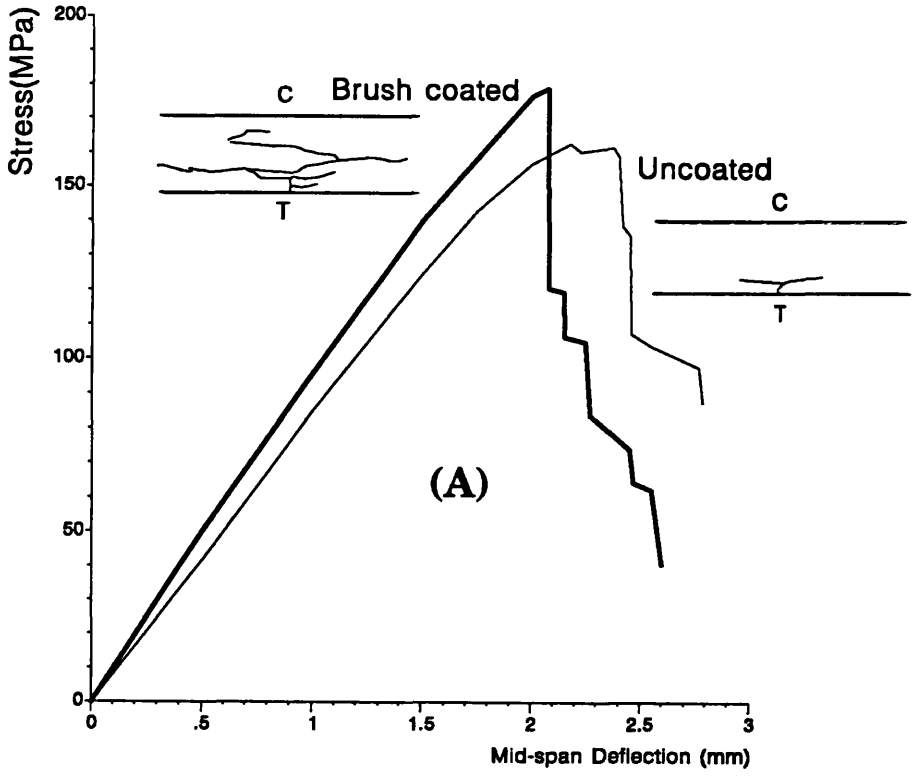

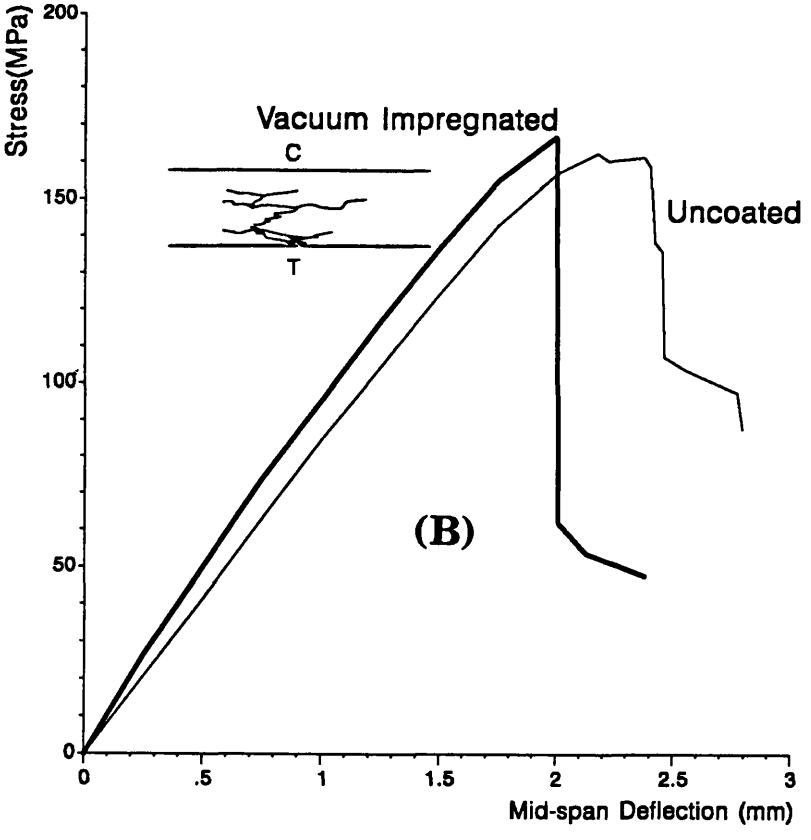

FIGURE 3.11 - Typical stress-deflection curves and sketches of the failure modes for KKarb composite with brush-coated/5 firings (A) and vacuum impregnated(firing)/4 firings (B). span/depth ratio = 19:1.

There is no significant change in the flexural strength after brush-coating and vaccum impregnating the KKarb material. On the other hand the flexural modulus increased by ≈25% after brush-coating, and by ≈28% after vacuum impregnation. Also the flexural modulus increased progressively with the number of pressure impregnations of the SiC *sol*, Table 3.2, but progressive impregnation has no effect on the flexural strength of KKarb material. This increase in flexural modulus may be attributed to the stiffening effect of the SiC coating. The stress-deflection curves and failure modes for the pressure impregnated KKarb composites are identical to the vacuum impregnated KKarb composite.

A simple way to consider the effect of SiC on the properties of the composites is to apply the rule of mixture. The micrographs of the SiC coated composites show that there is penetration of the open porosity by the SiC, which is more extensive for the Sigri material, due to its higher porosity, Table 3.1. There is also evidence of a significant external coating on the KKarb material.

The first assumption which can be made is that the total open porosity in both composites is completely filled by SiC. The effect on the strength and modulus of the coated composites, σ_{coat} and E_{coat}, can be represented by the rule of mixtures (Hull - 1981):

$$\sigma_{coat} = \sigma_{CFRC} \cdot V_{CFRC} + \sigma_{SiC} \cdot V_{SiC}$$

$$E_{coat} = E_{CFRC} \cdot V_{CFRC} + E_{SiC} \cdot V_{SiC}$$

where σ_{CFRC} and E_{CFRC} are the flexural strength and modulus of the uncoated composites, σ_{SiC} and E_{SiC} are the strength and modulus of SiC and V_{SiC} is the volume fraction of SiC which is assumed equal to the total open pore volume fraction determined by water penetration, Table 3.1. The

flexural strength of SiC varies between 280 - 930 MPa and the elastic modulus varies between 350 - 550 GPa (Srinivasan - 1989). Assuming values of σ_{SiC}=700 MPa and E_{SiC}=415 GPa gives the results shown in Table 3.4. The values of σ_{coat} obtained from the rule of mixtures for the two coated composites are in surprisingly good agreement with the experimental values, considering the simplistic nature of the assumptions. However, the rule of mixtures considerably overestimates the values of flexural modulus for both composites. This is not surprising since Crocker (1991) also found discrepancies between the calculated and the experimental elastic modulus for uncoated KKarb and Sigri composites using the rule of mixtures. Fibre degradation or fracture during manufacture and unbonded fibre and matrix were the main reasons proposed for the discrepancies.

In the case of the KKarb material the above analysis does not give the possible contribution that the external coating of SiC can make to the elastic modulus. The SiC coating over the surface of the KKarb material can be represented by a rectangular composite beam as shown in Figure 3.12. Figure 3.12 also gives the formula to estimate the equivalent flexural rigidity of the rectangular beam. In this calculation to take account of the porous nature of the SiC coating, Figure 3.5, the lowest value of the E_{SiC}=350 GPa was used. The thickness of the SiC coating is 10 μm. Application of the formula in Figure 3.12 gives a calculated elastic modulus for KKarb composite with SiC on both faces of 20 GPa, Table 3.4. This calculated value is somewhat higher than the experimental results found for the SiC coated KKarb materials but lower than the value calculated from the rule of mixtures. The SiC layer obtained by sol-gel method over KKarb composite is not homogeneous and it is porous and possibly for this reason the experimental value is lower than the calculated one.

	KKarb Type A	Sigri CC1501G
Flexural Strength (MPa) (experimental)	164.6±19.2	267.9±12.3
Flexural Strength (MPa) (rule of mixtures)	165.0	280.0
Flexural Modulus (GPa) (experimental)	16.4±1.2	49.7±3.8
Flexural Modulus (GPa) (rule of mixtures)	33.0	100.0
Flexural Modulus (GPa) (composite beam)	20	-

Table 3.4 - Experimental and calculated values for flexural strength and flexural modulus for KKarb and Sigri composites considering different approaches.

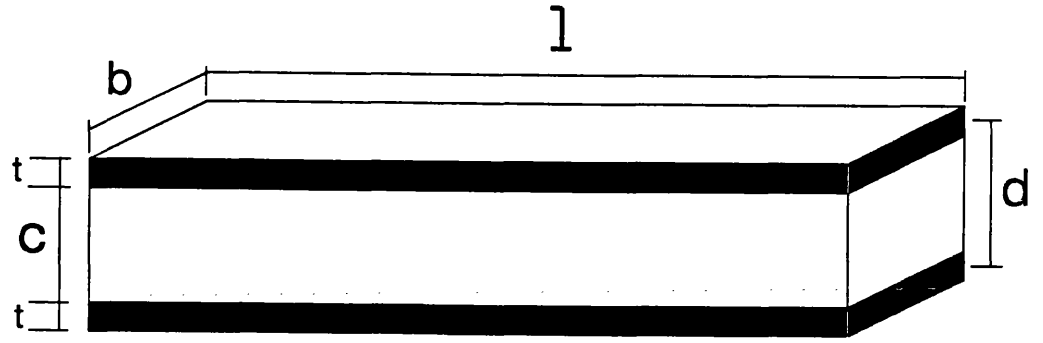

$$(EI)_{eq} = \frac{E_f b t^3}{6} + \frac{E_c b c^3}{12} + \frac{E_f b t d^2}{2}$$

where:

E_f = Young's modulus of the face = 350 GPa

E_c = Young's modulus of the core material = 13 GPa

b = width of a rectangular beam = 7.5 mm

t = face thickness of a rectangular beam = 10 μm

c = core thickness in a rectangular sandwich beam = 3.2 mm

d = distance between centroids of faces in a sandwich rectangular beam ≅ 3.2 mm

I = moment of a rectangular beam = $bc^3/12 = 2.05.10^{-11}$ m^4

This gives a value of the equivalent flexural rigidity, $(EI)_{eq}$ = 0.40064 $N.m^2$. This gives a calculated elastic modulus for the composite beam of 20 GPa.

Figure 3.12 - Equivalent flexural rigidity of a rectangular beam (Gibson - 1988)

SiC brush-coating Sigri material produces a change in the fracture mechanism, Figure 3.13A, and there is an increased amount of ply delamination, centred about the neutral axis, and the extent of shear cracking in the compressive stress field is reduced. This change in failure mode is accompanied by a change in the stress-deflection curve from a progressive failure to a more catastrophic failure. The flexural strength increases by ≈25% after brush-coating with SiC and it also increases progressively with the number of pressure impregnation cycles, Table 3.3. Presumably, the deeper penetration of SiC in the Sigri material increases its compressive strength by filling pores, with the result that, in 3-point bending, shear cracking in the compressive stress field is inhibited. No effect on flexural modulus of SiC impregnation of the Sigri composite was observed, Table 3.3, presumably because the SiC coating is thin and discontinuous and it does not behave as a composite beam. The failure mode for the vaccum impregnated SiC coated Sigri material is similar to that of the brush coated composite as seen on Figures 3.13A and 3.13B. Figure 3.14B shows a brittle fracture of the SiC coating on the side of the SiC brush coated Sigri material which runs parallel to the delamination cracks in the composite.

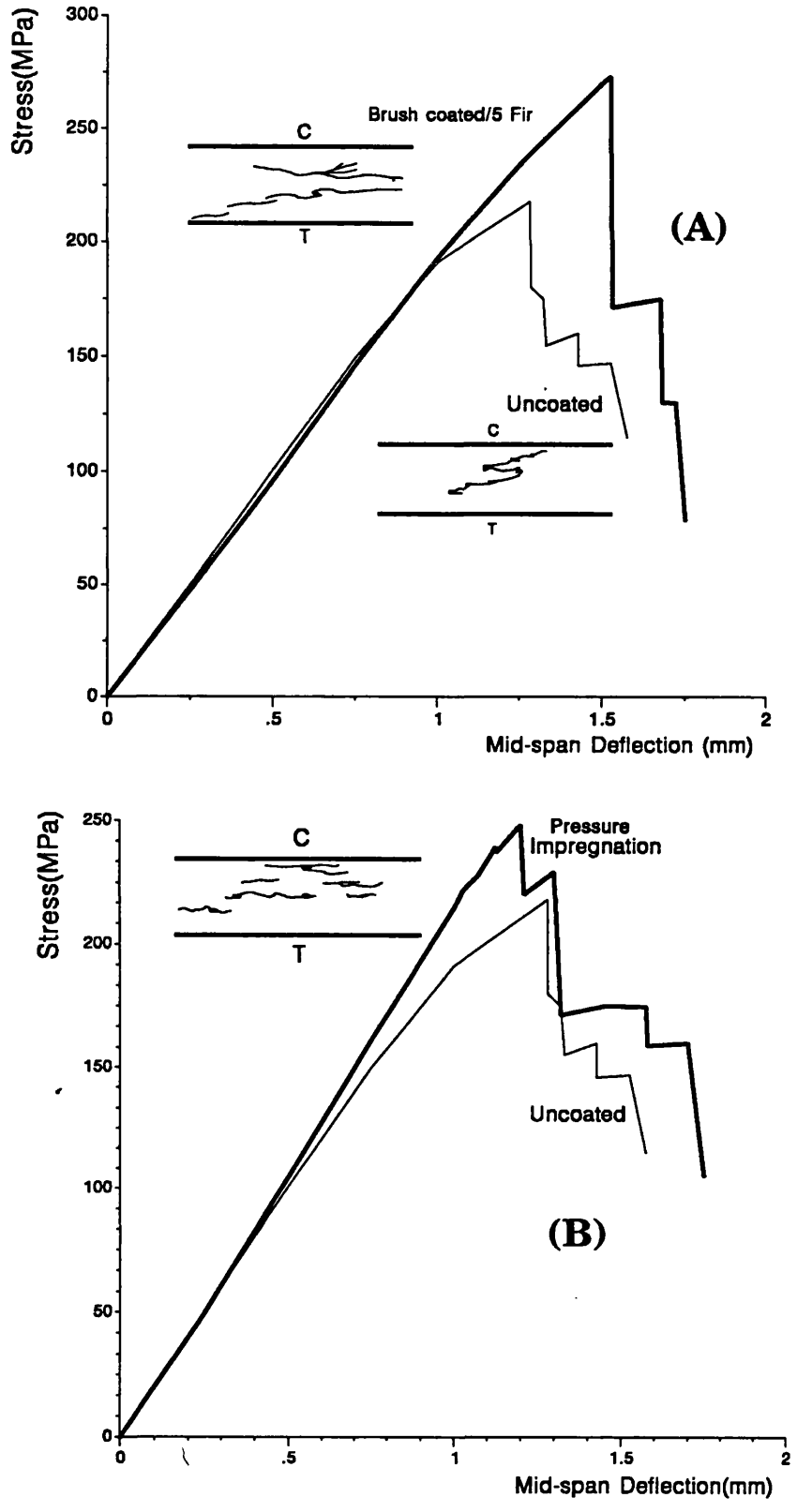

FIGURE 3.13 - Typical stress-deflection curves and sketches of the failure modes for Sigri, brush-coated/5 firings (A) and pressure impregnated/3 firings (B), span/depth ratio =25:1.

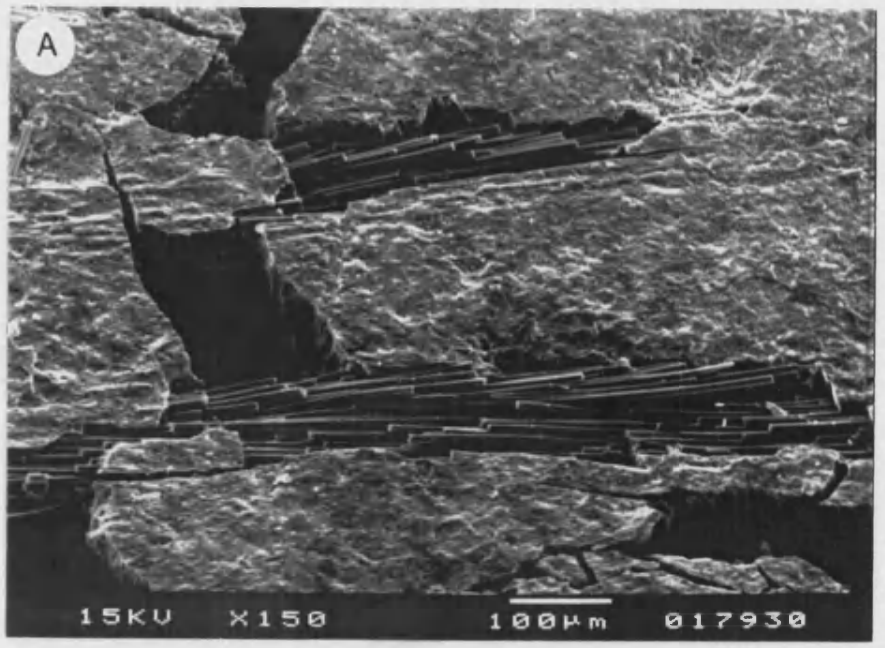

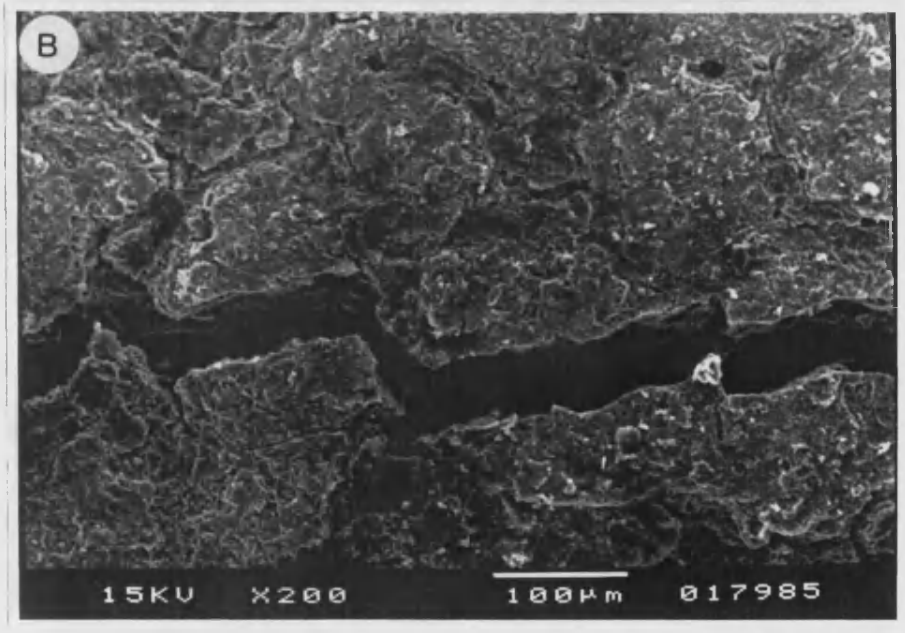

FIGURE 3.14 - (A) SEM view of the tensile fracture face of KKarb SiC brush-coated composite/5 Firings; (B) SEM side view of a delaminated region of Sigri SiC brush-coated/5 Firings.

3.3.3 - Acoustic Emission of the commercial CFRC composites

Acoustic Emission(AE) measurements during bend tests on the Sigri and KKarb CFRC composites, uncoated and SiC brush coated, were carried out using a span/depth ratio of 35:1; the results are in Table 3.5 and Table 3.6, respectively. This span/depth ratio was used so that the AE transducer could be attached without interference from the load points.

AE events were counted up to the failure stress. Examinations of the relative number of counts at different amplitudes can provide a useful means of distinguishing between individual failure mechanisms or between specimens of different quality (Stone - 1977). To describe the distribution of peak amplitude Pollock (1973) used a function $N(a)$ which defines the fraction of the emission population whose peak amplitude exceeds a, and showed how it is convenient to use an exponent b to characterize the amplitude distribution, as described in Appendix VIII. The Pollock plots in the form of log N(a) vs. amplitude level or channel number (equivalent to amplitude gain) were taken at the failure stress.

3.3.3.1 - Uncoated samples

Typical plots of stress-deflection and sketches of the crack patterns after fracture for uncoated KKarb and Sigri materials at a span/depth ratio of 35:1 are shown on Figure 3.15. The stress-deflection curve for KKarb material has a catastrophic reduction in stress in two steps, and the crack fracture pattern is usually characterized by two ply delaminating cracks connected to the tensile face region. For Sigri material the stress-deflection curve shows that it fails by a series of catastrophic steps and the crack fracture pattern is dominated by longitudinal shear cracks mainly in the

compressive region. Similar crack fracture patterns were found also by Crocker (1991). The value of flexural strength for KKarb material, Table 3.5, tested at a span/depth ratio of 35:1 was ≈15% higher, and the flexural modulus was ≈40% higher than the one tested at a span/depth ratio of 19:1. Crocker (1991) found similar values of flexural strength (200±40 MPa) which were independent of span/depth ratio in the range 10-50. However Crocker's measurements were subjected to greater scatter then the present results. It is possible therefore that her results masked an increase in flexural strength with span/depth ratio which is revealed in the more precise measurements presented in this work. It is also possible that the discrepancy between Crocker's results and the present results are due to batch to batch variability in these heterogeneous materials. The value of flexural strength for Sigri composite tested at a span/depth ratio of 35:1, Table 3.6, did not show any difference from the one tested at a span/depth ratio of 25:1. Crocker (1991) also found for the Sigri composite that flexural strength was independent of span/depth ratio in the range 20-50, although her value of flexural strength was somewhat lower (182.6±25 MPa). The nominal fracture initiation energy for KKarb composite is increased from 3.45±0.40 to 5.5±0.75 kJ/m^2 when the span/depth ratio increase from 19:1 to 35:1. A similar trend is found when comparing the Sigri material tested at span/depth ratios of 25:1 and 35:1. The increases in the nominal fracture initiation energy are attributable mainly to the increase in mid-span deflection, Tables 3.5 and 3.6.

Typical plots of cumulative acoustic emission counts and applied stress plotted against mid-span deflection for uncoated Sigri and KKarb composites are shown in Figure 3.16. For the KKarb material AE is detected from the onset of applied stress and it builds up continuously to produce ≈40000 AE counts at fracture. This indicates that deformation and failure of KKarb

composite is accompanied by a substantial amount of sub-critical activity.

The development of AE on stressing the Sigri composite is quite different from that found for the KKarb material and it can be divided in two stages. In the first stage there is a steady increase of AE until the onset of ply delamination at ≈160 MPa, when the stress-deflection curve deviates from elastic behaviour, and at that point the second stage begins in which there is a higher rate of AE counts until failure.

Typical Pollock plots of KKarb and Sigri composites are shown on Figure 3.17. The figure shows that AE from both materials conforms to the Pollock equation in the range $N(a) = 10^2$-10^4 (amplitude levels 2-15) but there is a greater number of low amplitude AE events from the KKarb material. This is reflected in the higher value of the Pollock exponent b, for KKarb, in Table 3.5.

	—(span/depth=35:1)—		—(span/depth=19:1)—	
	Uncoated	Brush Coated	Uncoated	Brush Coated
Flexural Strength (MPa)	180.4±15.0	185.0±21.7	155.5±9.0	164.6±19.2
Flexural Modulus (GPa)	18.2±1.3	20.2±0.3	13.1±0.4	16.4±1.2
Mid-span deflection[a] (mm)	6.38±0.24	5.84±0.60	2.32±0.21	1.97±0.08
Nominal Fracture Initiation Energy (kJ/m^2)	5.5±0.75	4.98±1.00	3.45±0.40	2.82±0.39
ΣAE at failure	43738±1425	103909±14167	——	——
Pollock exponent b	1.53	1.72	——	——

Table 3.5 - Mechanical Properties and AE parameters for KKarb Type A composites. Mean values ± are standard deviation; 7 samples. (a) at peak stress.

	—(span/depth=35:1)—		—(span/depth=25:1)—	
	Uncoated	Brush Coated	Uncoated	Brush Coated
Flexural Strength (MPa)	209.0±10.0	252.6±17.4	214.6±14.0	267.9±12.3
Flexural Modulus (GPa)	57.3±2.8	63.7±4.4	52.7±3.5	49.7±3.8
Mid-span deflection[a] (mm)	2.14±0.09	2.3±0.23	1.2±0.07	1.50±0.10
Nominal Fracture Initiation Energy (kJ/m^2)	2.1±0.16	2.73±0.44	1.69±0.17	2.5±0.22
ΣAE at failure	15468±5316	13552±9881	——	——
Pollock exponent b	1.30	1.37	——	——

Table 3.6 - Mechanical Properties and AE parameters for Sigri CC1501G. Mean values ± are standard deviation; 7 samples. (a) at peak stress.

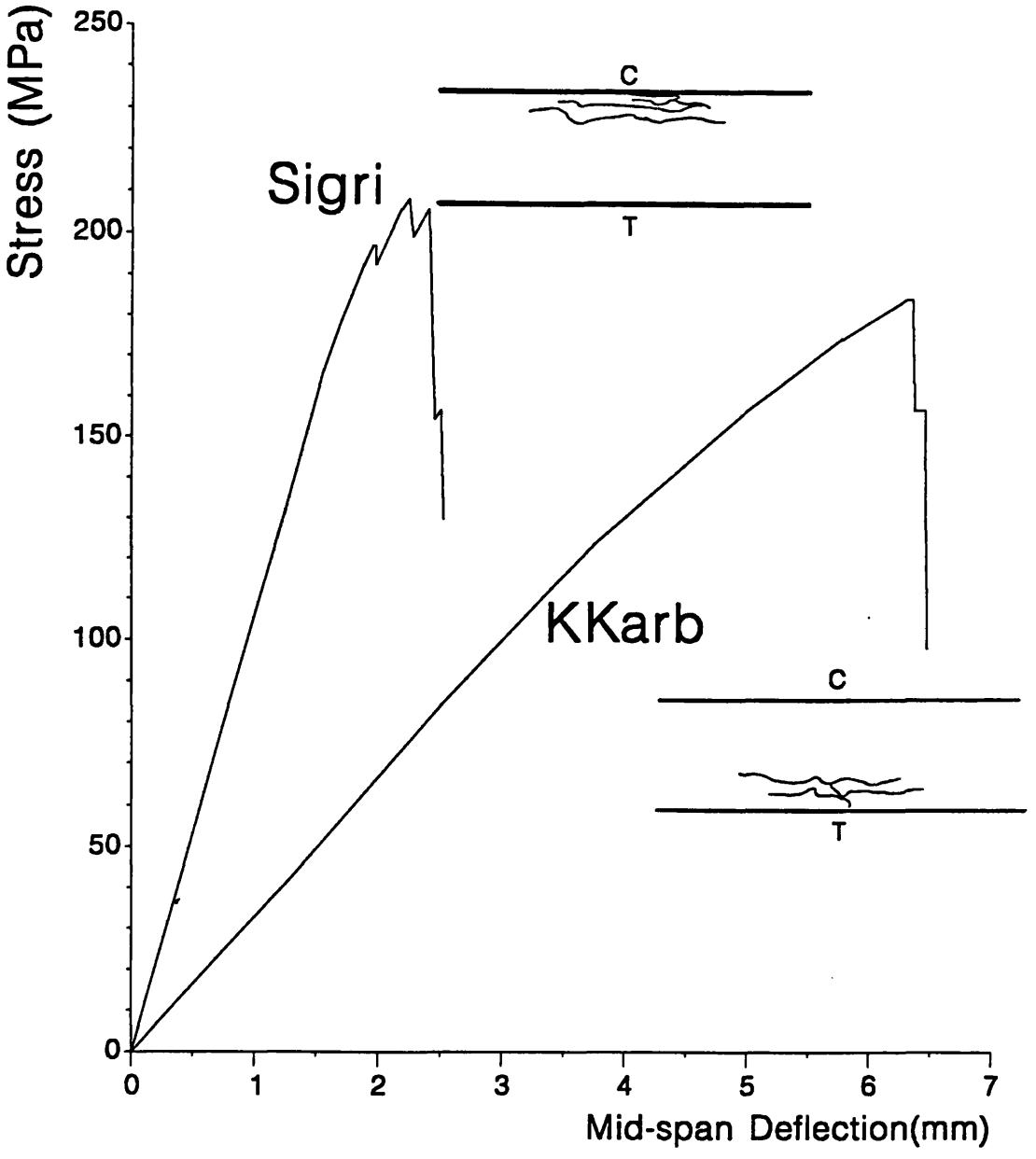

Figure 3.15 - Typical stress-deflection curves and failure mode sketches for Sigri CC1501G and KKarb Type A composites at a span/depth ratio=35:1.

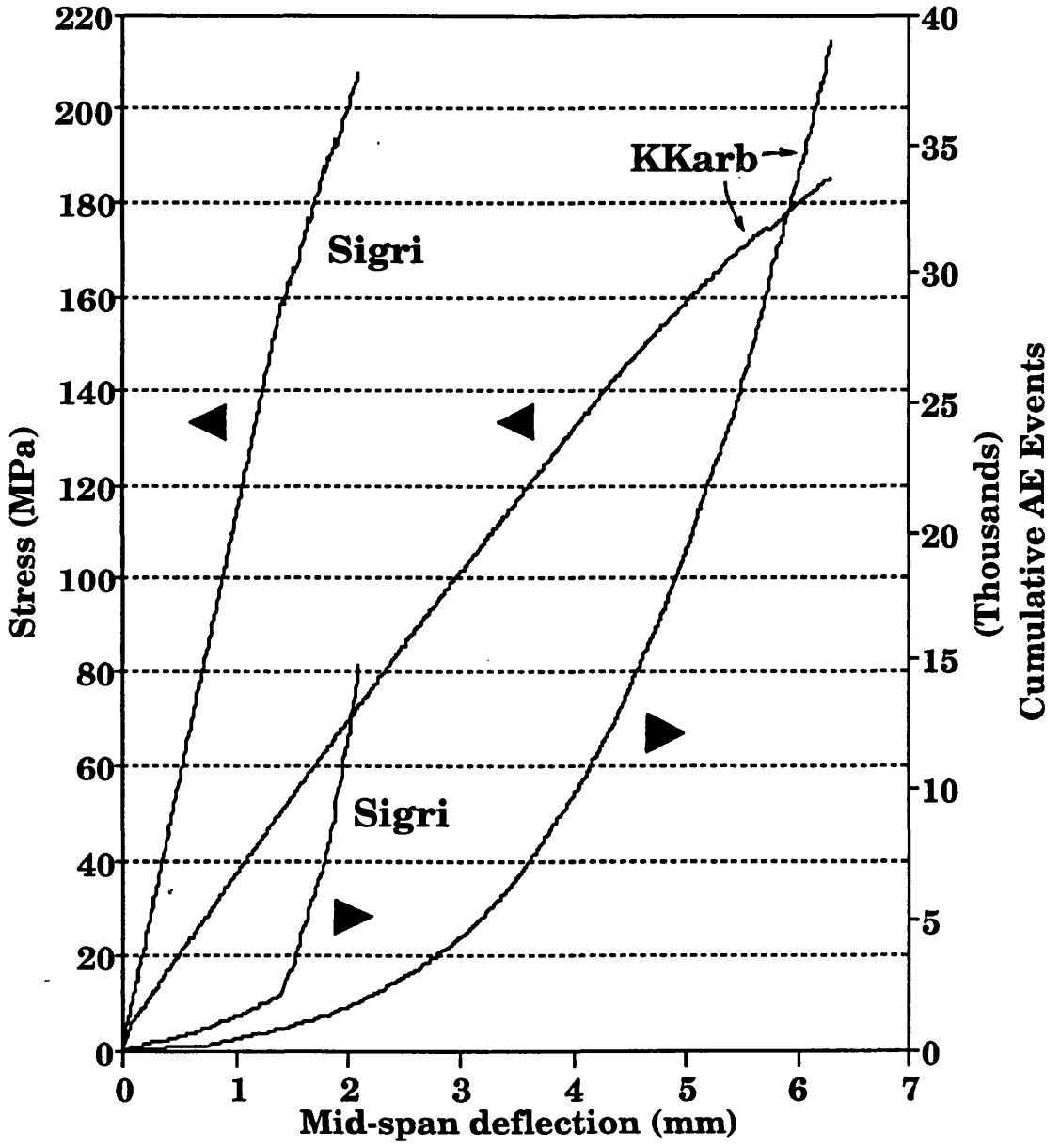

FIGURE 3.16 - Typical ΣAE and stress curves as a function of mid-span deflection of Sigri and KKarb composite, at a span/depth ratio of 35:1.

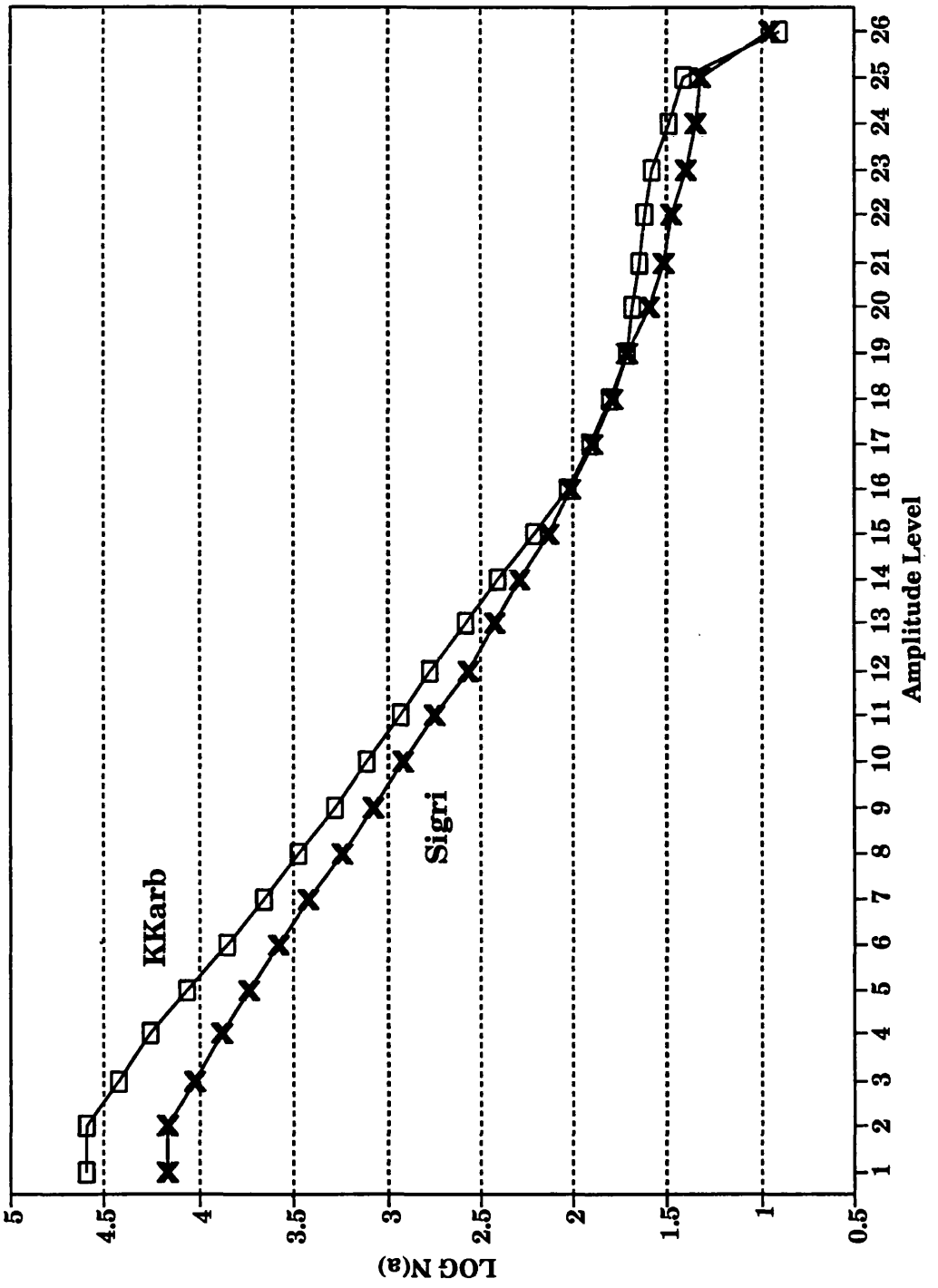

FIGURE 3.17 - Typical Amplitude distribution plots at failure stress for uncoated KKarb composite and Sigri composite, span/depth ratio = 35:1.

3.3.3.2 - SiC Coated samples

Mechanical properties and AE data for the uncoated and SiC coated KKarb composite at a span/depth ratio of 35:1 and 19:1 are given in Table 3.5. For the SiC coated KKarb composite there was practically no change in the flexural strength compared to the uncoated material, but there is a ≈20% increase in the flexural modulus with a lower mid-span deflection. These values follow the same trends observed in the properties of the SiC coated KKarb composites tested at a span/depth ratio of 19:1, *i.e.* there is no change in the flexural strength but there is an increase of ≈20% in the flexural modulus.

Figure 3.18A shows stress-deflection curves with respective failure modes for uncoated and SiC coated KKarb composites. It shows that the SiC coated KKarb composite undergoes a catastrophic failure in one step with the stress decreasing by about 45% of the maximum stress. The failure mode of SiC coated KKarb composite is characterized by ply delamination connected by cracks starting from the tensile face, similarly to the failure mode of the uncoated material. However the failure mode is different from that for the same material tested at span/depth ratio of 19:1, where extensive delamination extends to the neutral axis rather than being concentrated in the tensile face, Figure 3.11.

Results of mechanical properties and AE data for the uncoated and SiC coated Sigri composite at a span/depth ratio of 35:1 and 25:1 are given in Table 3.6. An increase in flexural strength of ≈25% was found but there is no pronounced difference in flexural modulus, and the failure proceeds at a similar mid-span deflection. The stress-deflection curve for SiC coated Sigri composite, Figure 3.18B, shows a reduction from the peak stress by a series of catastrophic steps until about ≈55% of the peak stress. The failure mode is

characterized by ply delaminations starting from the compressive face rather than concentrated in the neutral axis as was found for the same material tested at a span/depth ratio of 25:1.

Figure 3.19A shows the plot of AE and stress as a function of the mid-span deflection for SiC coated and uncoated KKarb composite. AE parameters are presented in Table 3.5. A much higher proportion of AE events, 104000 counts, was detected from the SiC coated KKarb composite compared to the same uncoated material, 44000 counts. During 3-point bending a beam is subject to compressive forces in the upper surface and tensile forces in lower surface. The development of the AE counts for the SiC coated KKarb composite is similar to the uncoated specimen, but at both surfaces of the beam of coated KKarb composite SiC is present and so the load points can generate compressive and tensile stresses on the coating. This generalized microcracking of the SiC coating gives rise to a high number of AE counts even at low stress levels, as demonstrated by the deviation of the two AE curves at low mid-span deflection.

Figure 3.19B shows the plot of AE and stress as a function of the mid-span deflection for SiC coated and uncoated Sigri composite. AE parameters are presented in Table 3.6. The patterns of AE from Sigri and SiC coated Sigri composites are in sharp contrast to those obtained from the equivalent KKarb composites. AE counts from the SiC coated Sigri composite follow approximately the same trend as found for the uncoated Sigri composite with two distinct regions. At low stresses similar values of flexural modulus for the coated and uncoated Sigri composite are reflected in the superposition of the two AE curves. In the case of the coated Sigri composite the onset of ply delamination is shifted to a higher stress level, clearly seen in the stress-deflection curve at ≈230 MPa. This ply delamination is accompanied by a sharp increase in the rate of AE. The incorporation of SiC

in Sigri composite delays the onset of ply delamination and reduce the amount of AE events at failure.

AE amplitude plots conform to the Pollock equation in the range N(a) = 10^2-$10^{4.5}$ and 10^2-10^5 for uncoated and SiC coated KKarb composites respectively, Figure 3.20A. For SiC coated KKarb there is a higher proportion of low amplitude AE events, reflected in the higher value of the Pollock exponent b, Table 3.5. These low amplitude AE events are presumably associated with microcracking of the SiC coating.

AE amplitude plots for the uncoated and SiC coated Sigri material, Figure 3.20B, also conform to the Pollock equation in the range N(a) = 10^2-10^4 where the two plots are nearly parallel. This shows that there is no significant change in the nature of the sub-critical events giving rise to AE, that is also suggested by Figure 3.19B.

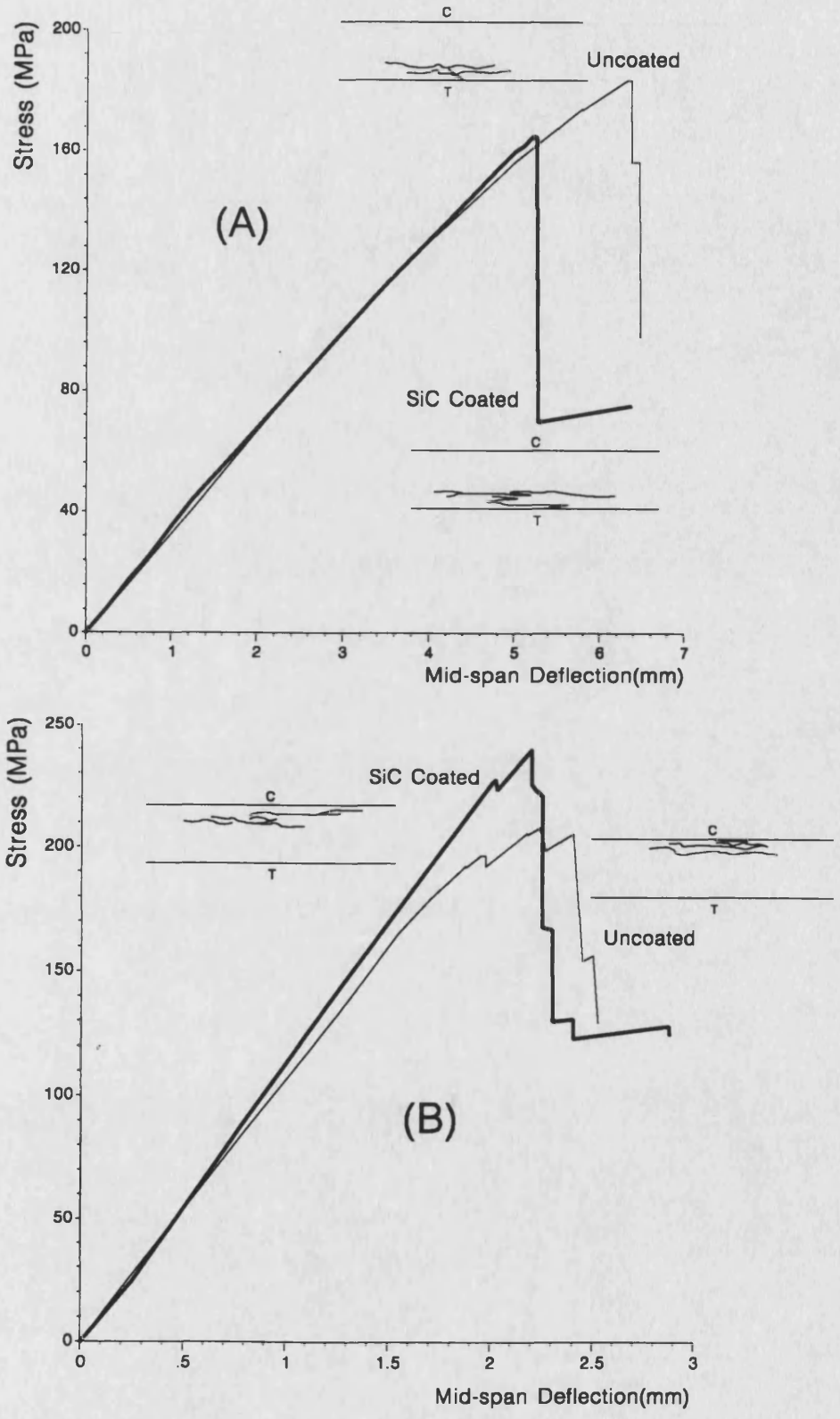

FIGURE 3.18 - Typical stress-deflection curves and failure modes or SiC coated KKarb (A) and Sigri (B) composites at a span/depth ratio of 35:1.

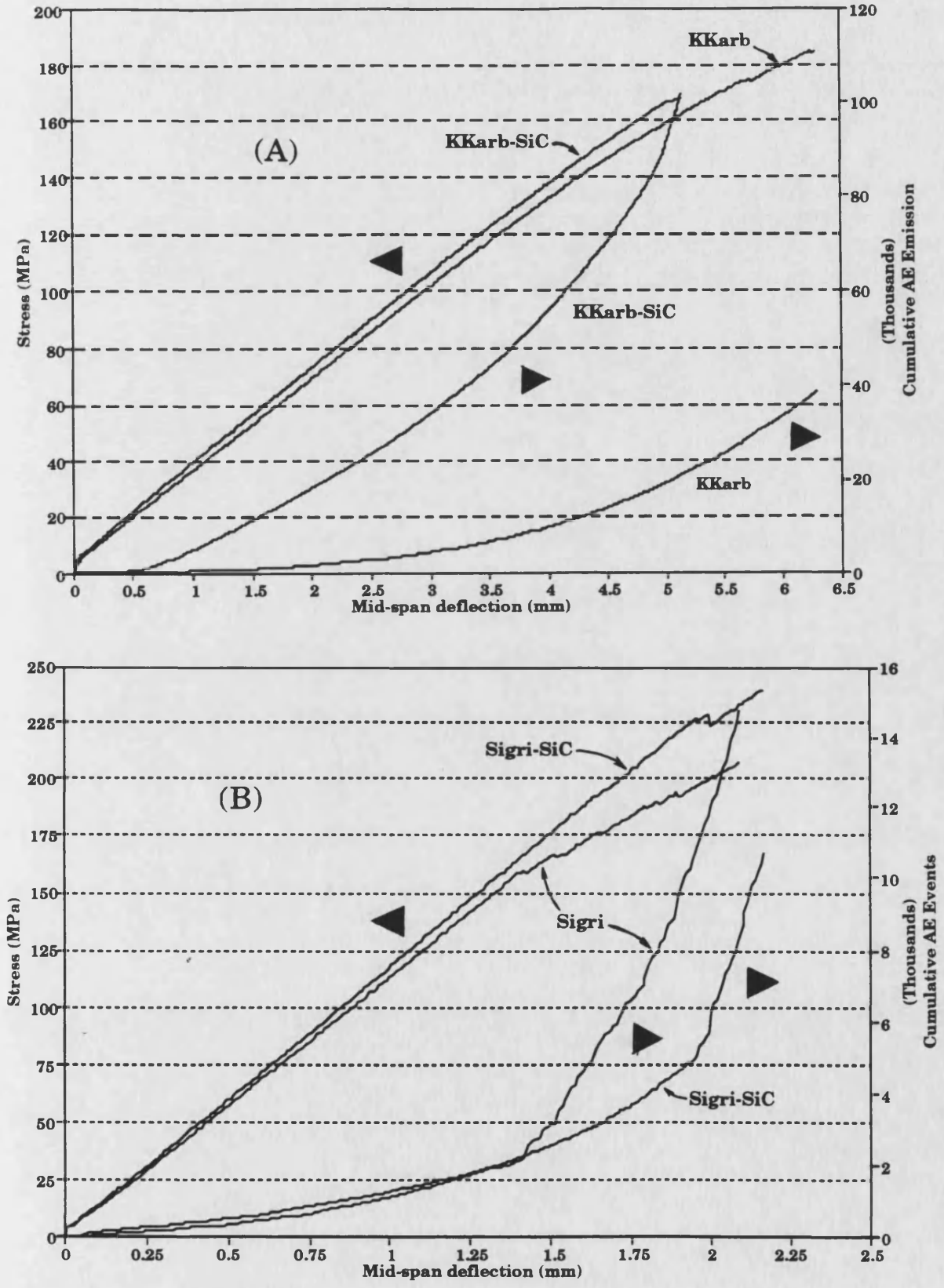

FIGURE 3.19 - Typical ΣAE and stress as a function of mid-span deflection of SiC brush coated KKarb composite (A) and SiC brush coated Sigri material (B), span/depth ratio of 35:1.

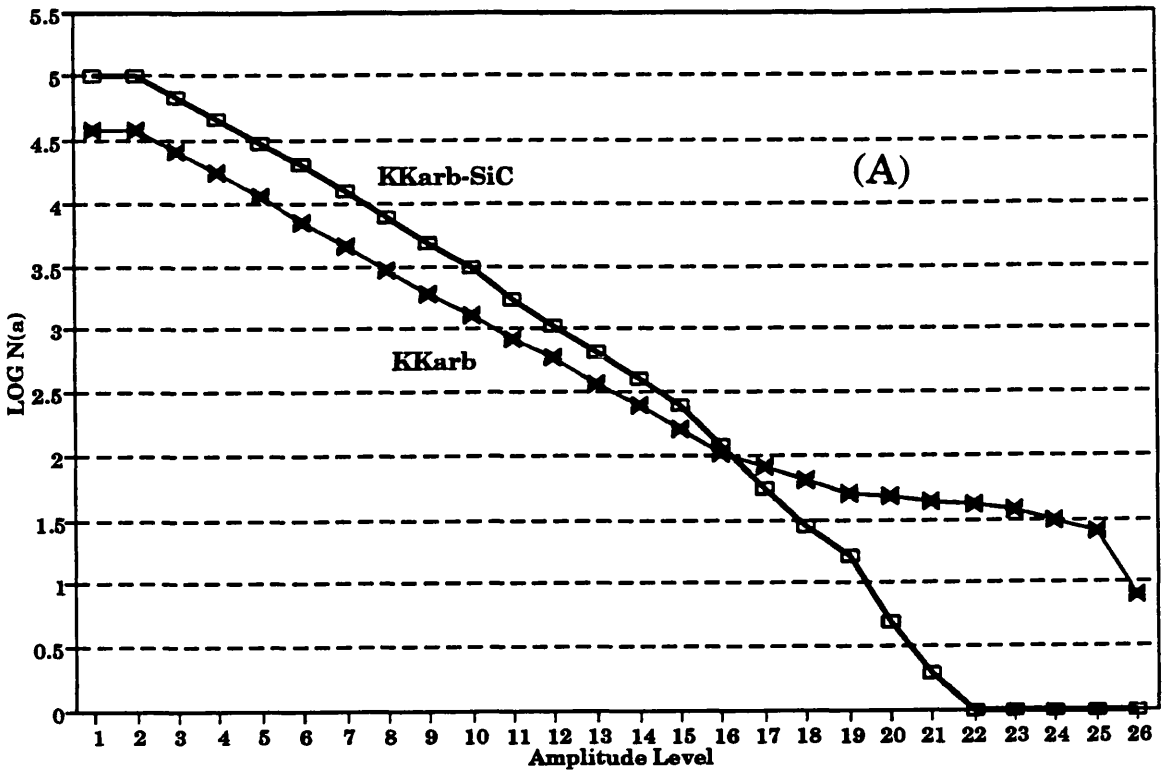

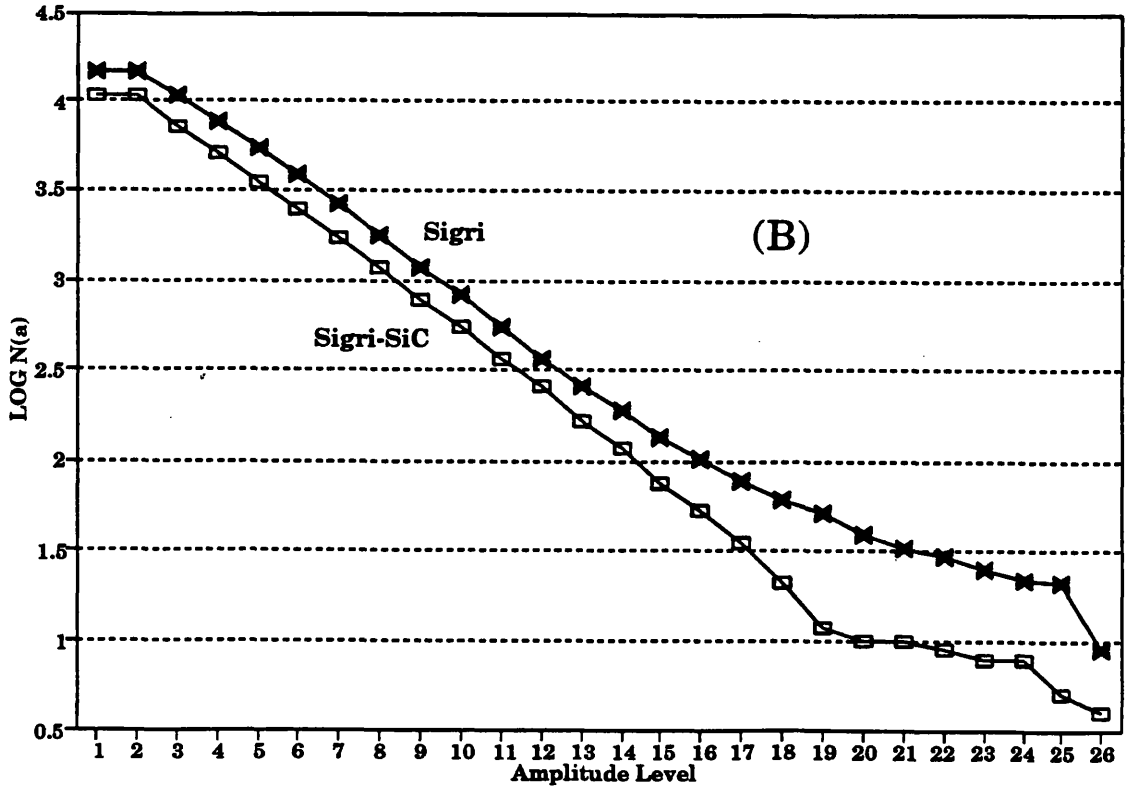

FIGURE 3.20 - Typical Amplitude distribution plots at failure stress for SiC brush coated KKarb composite (A) and Sigri composite (B), span/depth = 35:1.

3.4 - Thermogravimetric Analysis

The purpose of this section is to compare the oxidation performance of the surface coatings on the Sigri and KKarb CFRC composites. In the first part the oxidation behaviour of the uncoated KKarb and Sigri composites are considered and in the following sections the oxidation behaviour of the coated specimens of these composites are discussed. As mentioned earlier, Section 3.3.1, all the specimens were submitted to a calcination treatment before oxidation measurements or coating procedure. The TGA curves shown both the thermogravimetric curve (TG), percent weight loss as a function of temperature and the differential thermogravimetric curve (DTG), *i.e.* the derivative of the TG curve.

3.4.1 - Uncoated KKarb and Sigri composites

In Figure 3.21 a comparison is shown of the oxidation behaviour of the uncoated Sigri and KKarb materials heated in flowing air at a rate of 100°C/min followed by isothermal conditions at 1200°C. The results for the oxidation behaviour of KKarb and Sigri composites are summarized in Table 3.7. The TG curve shows that KKarb composite starts to oxidize at ≈535°C and the Sigri composite at ≈570°C, region A in Figure 3.21. The presence of a resin carbon matrix in Sigri composite is a possible reason for the slightly higher oxidation onset temperature exhibited by this material in relation to the KKarb material, which contains a resin/pitch blend carbon matrix. Crocker (1991) found similar values for the onset of oxidation of powdered samples of KKarb and Sigri composites using a heating rate of 20°C/min. Both composites have a transient in the DTG curve between 750-1100°C related to Zone I oxidation, region B in Figure 3.21, before reaching a steady state oxidation rate at ≈1200°C. Sigri composite oxidizes faster than the

KKarb material, possibly because the larger amount of open porosity, and consequently higher surface area, makes it more susceptible to oxidation. In the steady state oxidation at ≈1200°C, region C, the Sigri material oxidizes about 30% faster than the KKarb composite.

Material	Oxidation onset temperature (°C)	Steady state rate at 1200°C %/min	Total wt loss after 25 min
KKarb	535	-0.44	8.6
Sigri	570	-0.62	10.9

Table 3.7 - Parameters of oxidation behaviour for KKarb and Sigri CFRC composites.

3.4.2 - SiC coated samples

To evaluate the SiC coated specimens in relation to the uncoated ones it was decided to use as models the SiC brush coated KKarb composite, and brush coated and pressure impregnated Sigri composite.

The results of the oxidation behaviour for the SiC coated samples are summarized on Table 3.8. The performance of a coating will be defined by the benefit factor:

$$BF = \frac{WL_{UNC} - WL_{COAT}}{WL_{UNC}}$$

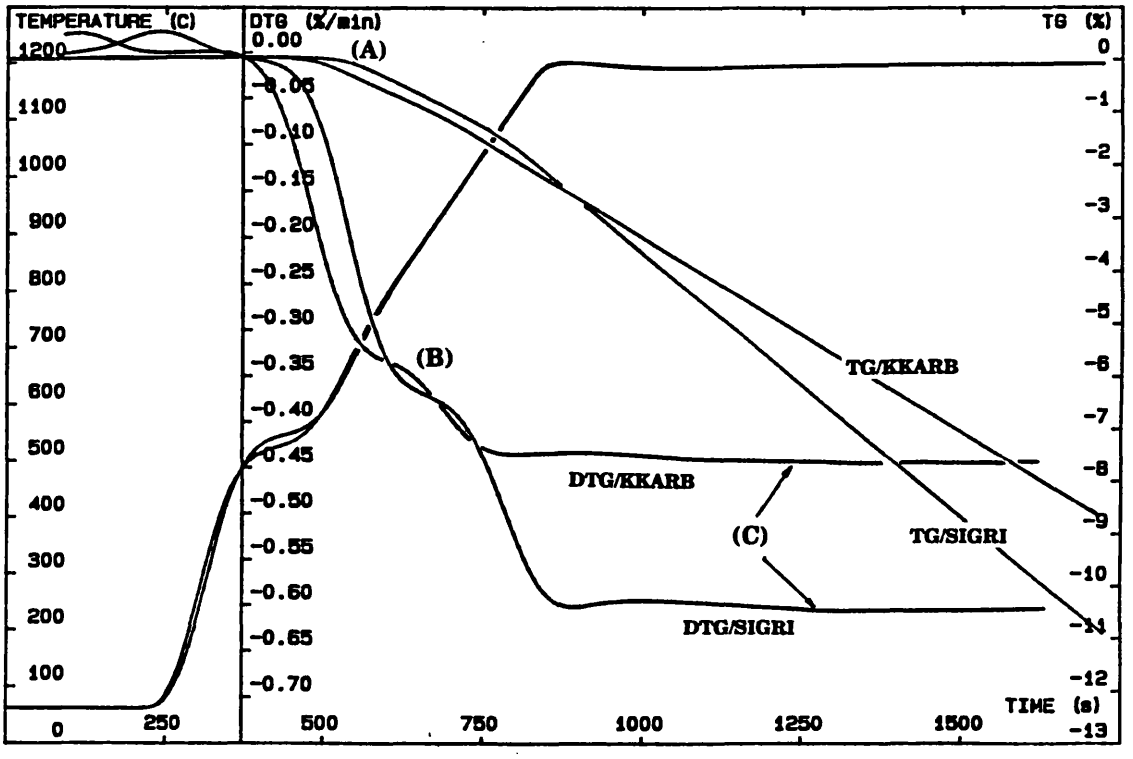

FIGURE 3.21 - TGA analysis of uncoated KKarb composite (m= 850.26 mg) and uncoated Sigri composite (m=737.6 mg) at 1200°C, in flowing air (1.5 l/min).

where WL_{UNC}= total weight loss of the uncoated composite after the completion of the experiment, and WL_{COAT}= total weight loss of the surface coated composite after the completion of the experiment.

Material	Oxidation onset temperature (°C)	Steady state rate at 1200°C %/min	Total %wt loss after 25 min	Benefit Factor
KKarb	535	-0.44	8.6	1.00
KKarb 5SiC(BC)	600	-0.34	6.4	1.25
Sigri	570	-0.60	10.9	1.00
Sigri 5SiC(BC)	570	-0.45	8.1	1.25
Sigri 3SiC(PI)	570	-0.38	7.2	1.34

Table 3.8 - Parameters of oxidation behaviour of SiC coated Sigri and KKarb CFRC composites. Numbers preceding the coating are number of firings. BC = brush coating, PI = pressure impregnation.

Figure 3.22A shows that for the SiC brush coated KKarb composite the temperature of onset of oxidation was slightly increased from ≈535°C to ≈600°C, in relation to the uncoated KKarb material. Similarly, the oxidation rate at 1200°C was reduced from -0.45% to -0.35%/min, giving rise to a benefit factor of 1.25. The depression on the DTG curve after the transient in Zone I oxidation was also reduced in the brush coated KKarb. This improvement in both oxidation onset temperature and oxidation rate can be attributed to the SiC layer over the surface of the KKarb composite

retarding, to some extent, the contact of the material with oxygen. Although the improvement in the onset temperature of oxidation for SiC coated KKarb material was similar to the one found by Castro (1991), the oxidation rate found in his work (-2%/min) was much higher than the one found in this work (-0.44%/min) possibly because a different sample geometry was used.

Figure 3.22B shows the TG and DTG curves for the uncoted and SiC brush coated Sigri composite. The SiC coating did not improve the oxidation onset temperature but reduced the oxidation rate at 1200°C from -0.62% to -0.45%/min, giving rise to a benefit factor of 1.25, similar to that provided by brush coated SiC on the KKarb material. The DTG curve for SiC coated Sigri composite shows a reduction in the rate of oxidation in between 900-1050°C, possibly due to formation of SiO_2, followed by an increase in the rate of oxidation with a slow approach to the steady state.

Figure 3.23 shows that a greater improvement in reducing the oxidation rate of Sigri composite was achieved by the pressure impregnation method. After the third pressure impregnation the onset of oxidation was not improved but a lower oxidation rate was achieved, giving rise to a benefit factor of 1.34. Also, a reduction in the rate of oxidation in between 900-1050°C was found. As the SiC layer over Sigri composite is discontinuous and not homogeneous, its presence only reduces the oxidation rate rather than delays the onset of oxidation. It is clear that the coating procedure by the pressure impregnation method is more efficient, reducing the processing time with less firing procedures and achieving less weight loss during oxidation. Vix-Guterl (1993) found also that the in-depth oxidation of the carbon interlayer in SiC/C/SiC composites (SiC matrix separated from the SiC fibres by a pyrolitic carbon layer) is strongly decreased at 900°C due to a limited transport rate of oxygen due to the formation of silica layers.

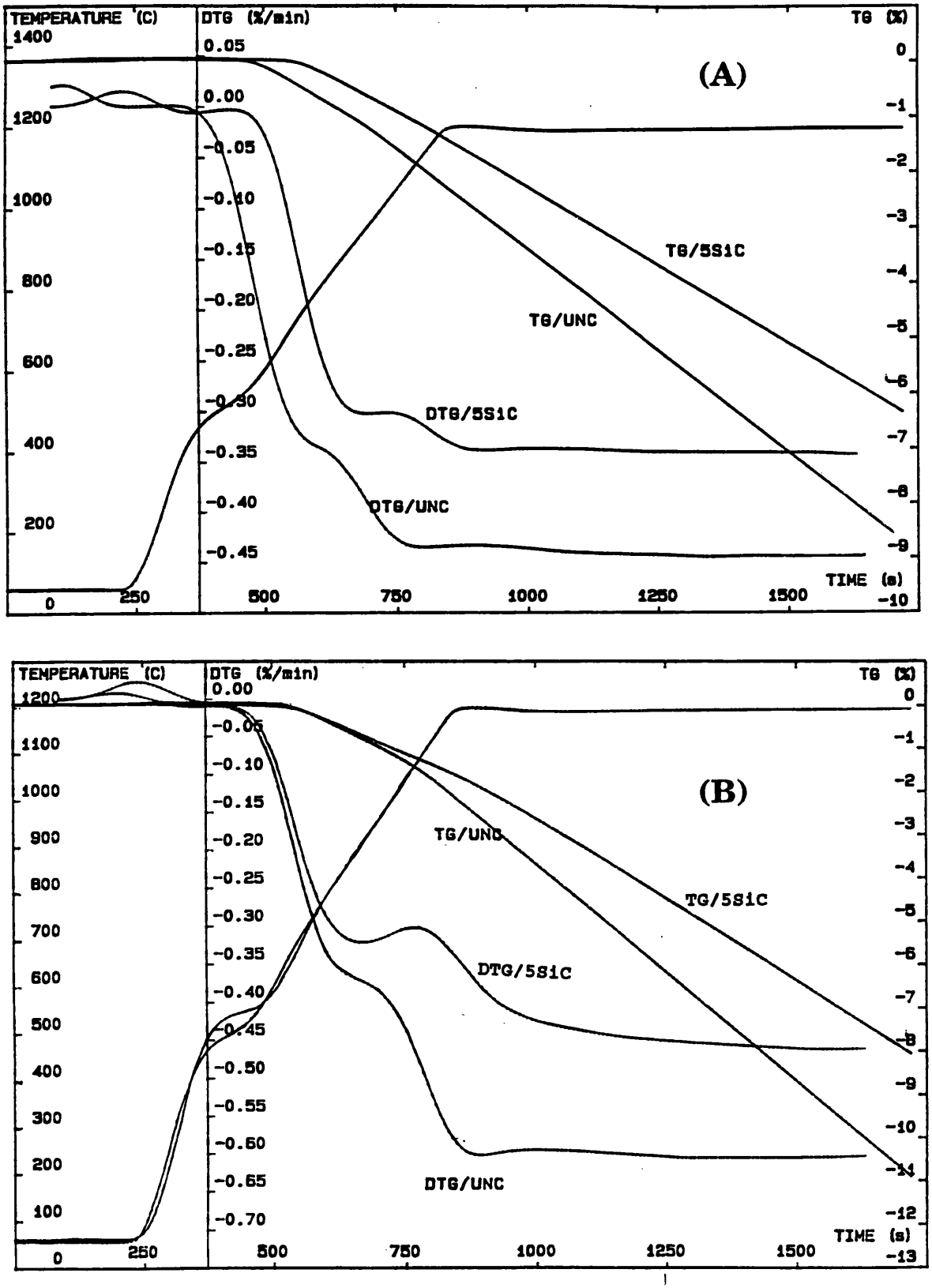

FIGURE 3.22 - TGA of (A) SiC brush coated KKarb composite (m=833.5 mg) and (B) SiC brush coated Sigri composite (m=749.4 mg) at 1200°C, in flowing air (1.5 l/h).

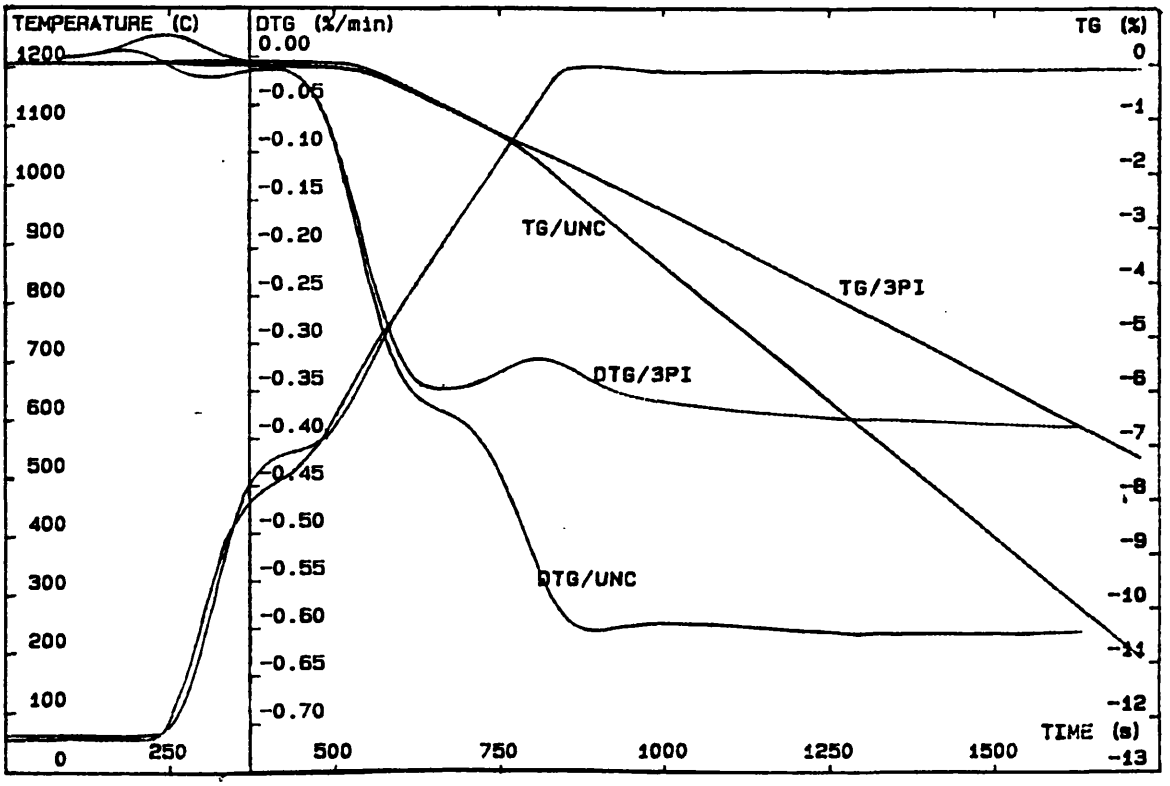

FIGURE 3.23 - TGA analysis of SiC coated Sigri composite by pressure impregnation method (m=766.2mg) at 1200°C, after the third pressure impregnation/gelation/firing procedure, in flowing air (1.5l/h).

Figure 3.24 shows an SEM micrograph of a SiC coated KKarb composite oxidised for 15 min at 1200°C. Although an improvement in oxidation resistance of KKarb material coated with SiC by sol-gel method is achieved, the porous SiC coating allows the ingress of oxygen and a clear debonding and erosion of the coating from the carbon substrate is seen after oxidation. This is possibly a result of excavation of the underlying carbon material.

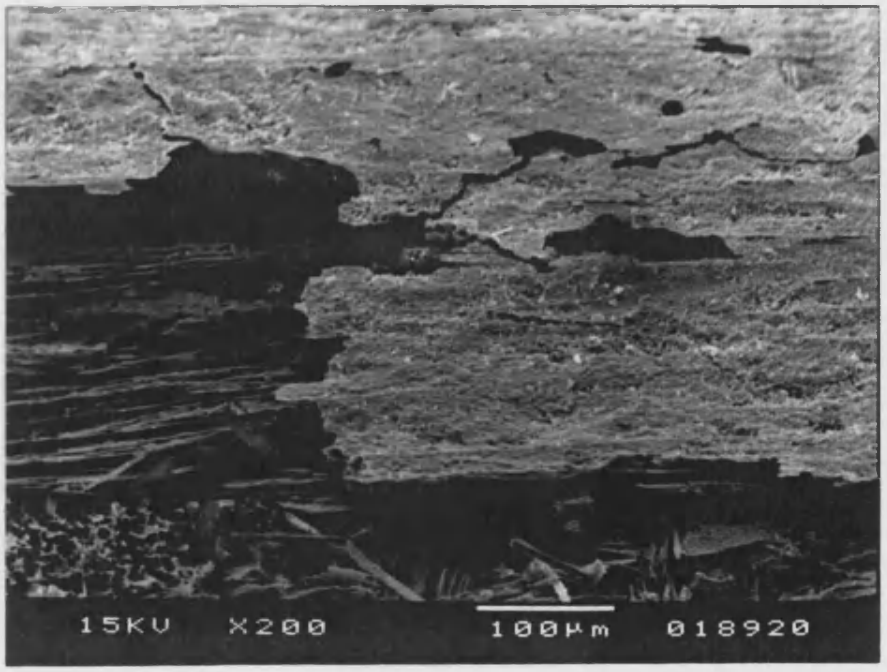

FIGURE 3.24 - SEM micrograph showing erosion of the SiC coating on KKarb composite by excavation of the underlying carbon material.

3.4.3 - Multilayer refractory/glassy coatings

In this work, oxidation studies of KKarb and Sigri CFRC composites coated by SiC/B_2O_3 and SiC/SiO_2-TiO_2/SiC were carried out at 1200°C to make a comparison with previouly uncoated and SiC coated samples tested at this temperature. The results of the oxidation behaviour of KKarb and Sigri CFRC composites coated by the multilayer refractory/glassy coatings are summarized in Table 3.9. It has been shown by Castro (1991) that the SiC/SiO_2-TiO_2 glassy coating over the SiC refractory coating, both obtained by the sol-gel method, improves the oxidation resistance of CFRC composites. Differences in the oxidation behaviour of the KKarb and Sigri CFRC composites were investigated using a SiC refractory coating over the previously mentioned coating schedule, i.e. five firings of brush coated SiC and four firings of brush coated SiO_2-TiO_2, plus three firings of brush coated SiC. This SiC overlayer is expected to provide enhanced oxidation protection to the CFRC composite. The full potential of the SiO_2-TiO_2 glassy coating should be evaluated at 1600°C, when it melts and can fill cracks both from SiC refractory coating and from the CFRC composite, but it was not possible to achieve this temperature in the equipment available.

Figure 3.25A shows TG curves for SiC/B_2O_3 coated KKarb composites. A clear delay in the temperature of oxidation onset from ≈535°C to ≈840°C for the KKarb composite coated is observed, giving a benefit factor of 1.40. The characteristic inflections in the DTG curve observed in the uncoated and SiC brush coated KKarb composite were pratically supressed when the glassy borate coating is used.

Figure 3.25B shows TG curves for coated Sigri composites. The TG curve exhibits a delay in the temperature of oxidation onset from ≈570°C to ≈950°C, giving rise to a benefit factor of 1.53.

Material	Oxidation onset temperature (°C)	Steady state rate at 1200°C %/min	Total %wt loss after 25 min	Benefit Factor
KKarb	535	-0.44	8.6	1.00
KKarb SiC/B_2O_3*	840	-0.32	5.1	1.40
KKarb SiC/SiTi/SiC**	600	-0.32	6.0	1.30
Sigri	570	-0.60	10.9	1.00
Sigri SiC/B_2O_3*	950	-0.32	5.1	1.53
Sigri SiC/SiTi/SiC**	570	-0.40	7.0	1.36

* - 5 firings of SiC plus 4 firings of B_2O_3

** - 5 firings of SiC, 4 firings of SiO_2-TiO_2, 3 firings of SiC

Table 3.9 - Parameters of oxidation behaviour of multi-layer coated Sigri and KKarb CFRC composites.

In both borate coated samples the presence of moisture was detected by a small depression in the DTG curve at ≈120°C. The melting point of the boron oxide glassy coating is around 450°C and during heating it fill cracks both from the SiC refractory layer and from the CFRC composite consequently blocking the ingress of oxygen. The shapes of the DTG curve from KKarb and Sigri borate coated composites are also similar. The oxidation in the Zone I region (≈450-800°C) is practically supressed, until the boron oxide begins to volatilize at ≈850°C. A more significant delay in the oxidation onset is observed for the borate coated Sigri composite, but similar oxidation rates (-0.32%/min) and weight loss (≈5.1%) were found for both borate coated KKarb and Sigri composites. This can be explained by the fact that the temperature of the oxidation onset for the borate coated Sigri composite is

higher than for the KKarb composite and so it compensates the higher weight loss for the uncoated Sigri composite in relation to KKarb material.

Exposure of borate glasses to ambient moisture produces gradual hydrolysis which results in swelling and crumbling of the glass (Strife - 1988) and this can result in coating spallation at room temperature during heating. It has been shown (McKee - 1986, Ehburger - 1986) that borate glass are effective oxidation inhibitors at temperatures up to 1000°C. Additions of alkali oxides, such as Li_2O, can significantly reduce the ambient moisture sensitivity of B_2O_3 (Savage - 1993).

The TG curves at 1200°C for KKarb composite coated with 5SiC/4SiO_2-TiO_2/3SiC, Figure 3.26A show no improvement in the temperature of oxidation onset in relation to the uncoated and SiC coated KKarb composites. The DTG curve shows a clear decrease in oxidation rate in the temperature range of 1000-1200°C due possibly to SiO_2 formation, and after an increasing oxidation rate is found which slowly approaches the steady state rate. The benefit factor for this coating design was 1.30.

The same trends were observed by the Sigri composite coated with 5SiC/4SiO_2-TiO_2/3SiC, Figure 3.26B. In relation to this coating the temperature of oxidation onset was not modified, and also the DTG curve shows a decrease in oxidation rate in the temperature range of 900-1050°C, but to a lesser extent than the SiC coated ones, followed by an increase in the oxidation rate which slowly approaches the steady state. This coating gives a benefit factor of 1.36.

At 1200°C, the SiC coating reduces the oxidation of CFRC composites by at least 25%. Using a borate glassy coating over the SiC coating, the oxidation is reduced by at least 40% with a significant improvement in the oxidation onset temperature by more than 300°C.

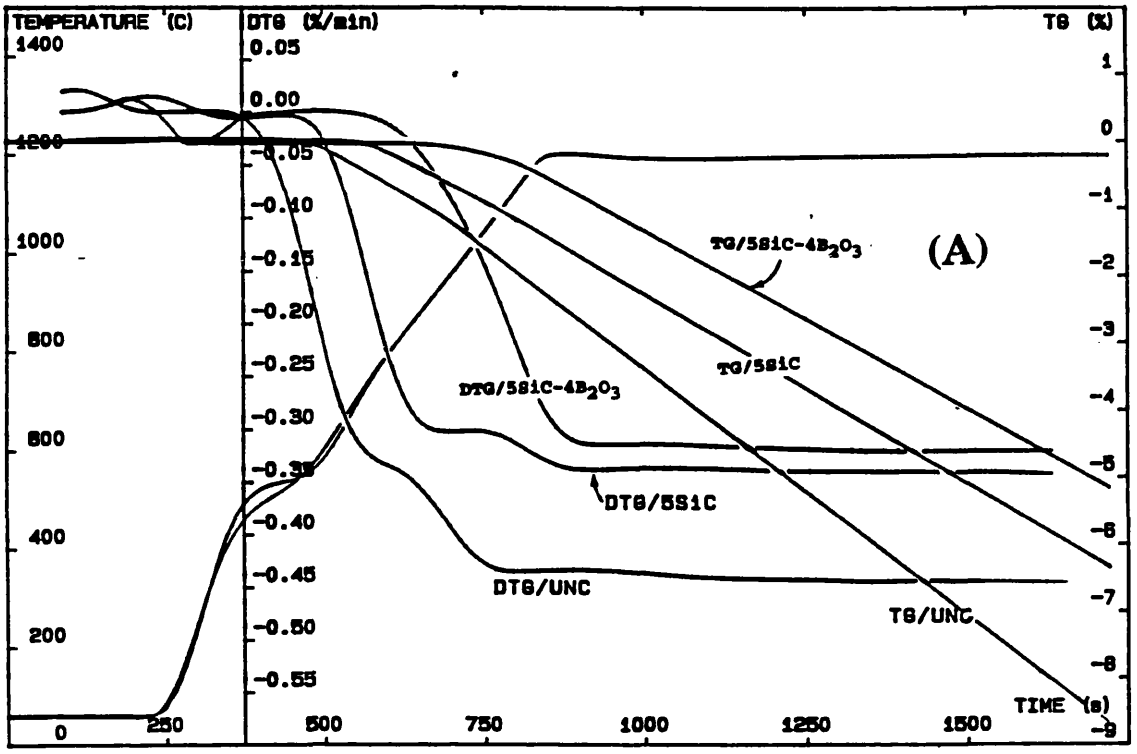

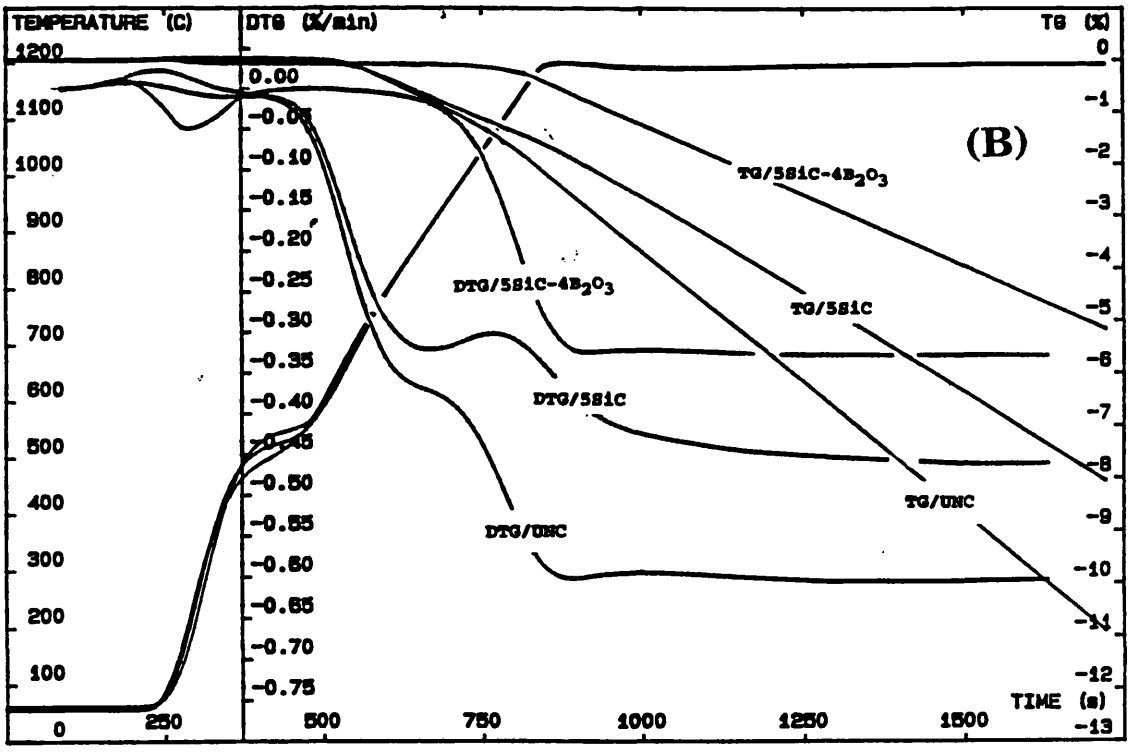

FIGURE 3.25 - TGA analysis of CFRC coated composites, at 1200°C in flowing air (1.5 l/h). (A) KKarb, (B) Sigri. Number of firings are indicate before coatings specification. Mass of the Sigri/5SiC-$4B_2O_3$ (m=806.2 mg), mass of the KKarb/5SiC-$4B_2O_3$ (m=868.4 mg).

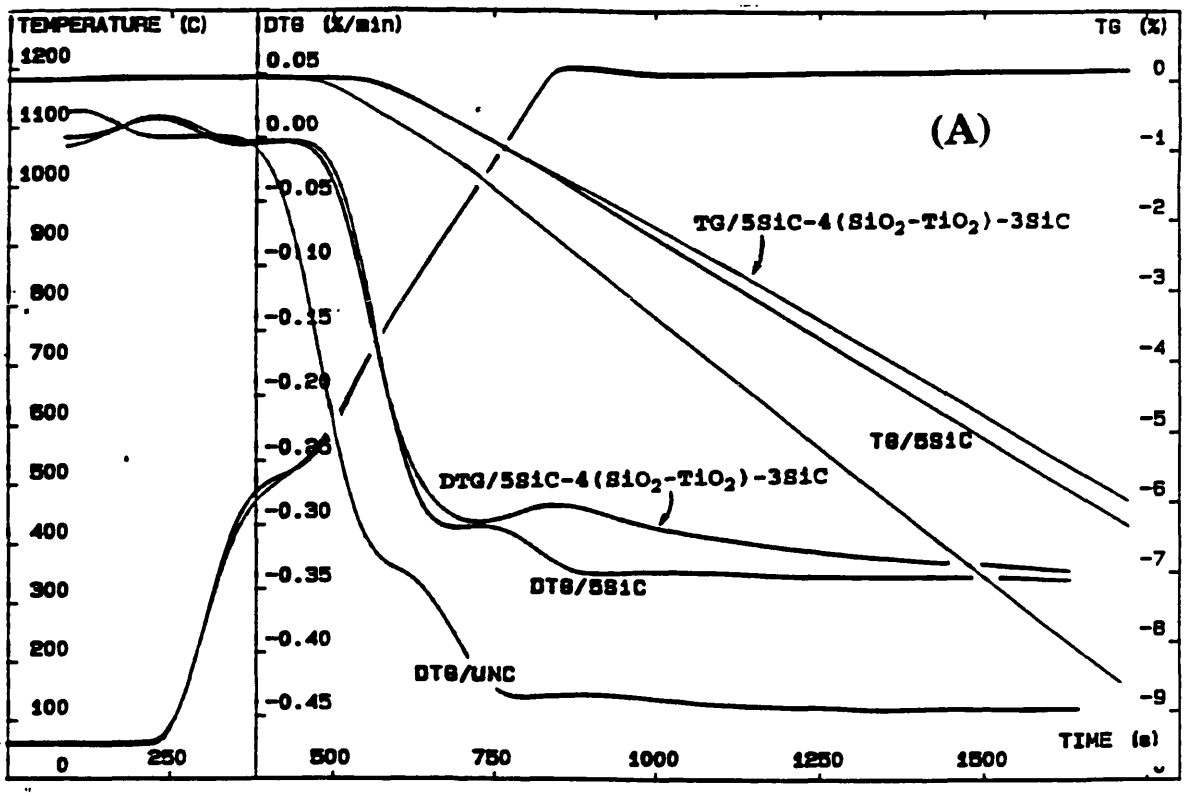

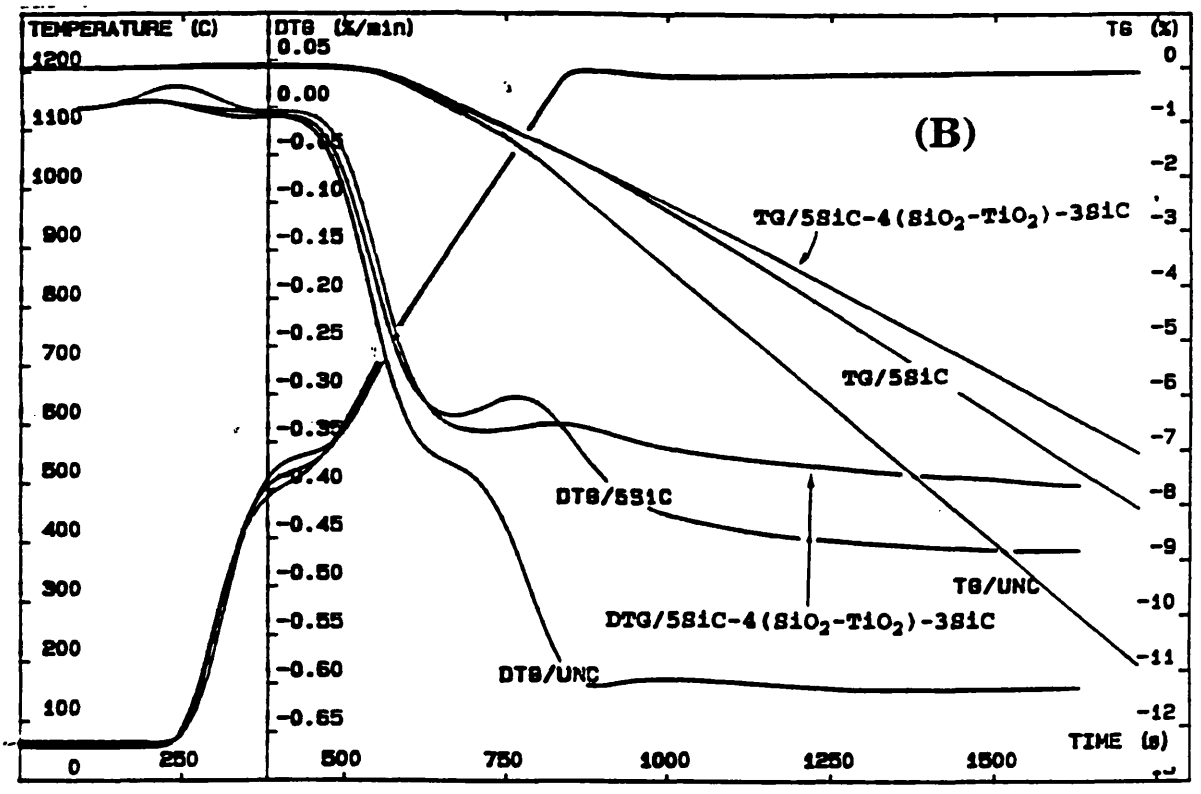

FIGURE 3.26 - TGA analysis of CFRC composites at 1200°C in flowing air (1.5 l/h). (A) KKarb, (B) Sigri. Number of firings are indicate before coatings specification. Mass of the Sigri/5SiC-4SiO_2-TiO_2/3SiC (m=789.6 mg), mass of the KKarb/5SiC-4SiO_2-TiO_2/3SiC (m=895.5 mg).

CHAPTER FOUR
UNIDIRECTIONAL CFRC COMPOSITES RESULTS AND DISCUSSIONS

This chapter discusses the results achieved on the fabrication of unidirectional carbon fibre reinforced carbon composites. Their microstructures obtained by a defined heat treatment schedule were analysed and their mechanical properties were evaluated using the acoustic emission technique.

4.1 - Microstructure of the precursor carbon fibre/phenolic composite

The carbon fibre/phenolic composite precursor (CFRP) is the *green* raw material used to obtain CFRC composites. The classes of *green* composites prepared were described in Chapter Two, Section 2.2. The microstructures of these composites were investigated by optical microscopy in order to correlate them with the microstructures of the CFRC obtained after heat treatments at 1100°C. Both transverse and longitudinal sections through the fibres were investigated.

The transverse cross section of the *green* composites, with treated and sized carbon fibres, Figure 4.1A, shows pores (P) with size around 100 μm between well bonded fibre bundles. These pores are probably a result either of air trapped during the stacking of the prepreg layers before moulding, or of volatiles trapped during the curing process of the composite. The large pores are mainly located adjacent to the interlamellar resin rich regions. For the *green* CFRP composite with untreated and unsized carbon fibres, Figure 4.1B, the microstructure is similar to that of the CFRP *green* laminate with

treated and sized carbon fibres, Figure 4.1A. Interlaminar pores with size around 100 μm are also observed in a clustered fibre packing array. These pores are also probably a result of trapped air during the stacking of the prepregs. Longitudinal views of the *green* TS-CFRP and the *green* hybrid T5U4-CFRP can be seen in Figure 4.2. In the TS-CFRP *green* composite, Figure 4.2A, the resin rich interface layer (I) between fibre plies (T) can be identified. In the hybrid T5U4-CFRP composite, Figure 4.2B, the T laminae with well bonded fibres and the poorly bonded fibres in the U laminae together with the interface between the U laminae and the T laminae can all be clearly identified. The different extents of bonding between fibres in the T laminae and U laminae are not so clearly seen in the cross sections through the fibres, Figure 4.1.

4.2 - Development of the heat treatment schedule for Unidirectional CFRC composites

The main chemical reactions that probably take place in the carbonisation of a typical phenolic resin are shown in Figure 4.3 (Burger - 1975). In the temperature range 120-180°C the dominant processes are condensation reactions with the elimination of water. At higher temperatures (380-800°C) further condensation reactions occur in with the elimination of other volatiles (CO, CO_2, CH_4 and H_2). The conversion of organic compounds to carbon by means of pyrolysis such as these is controlled by reaction parameters such as temperature, heating rate, residence time at the pyrolysis temperature, and possibly the total gas pressure.

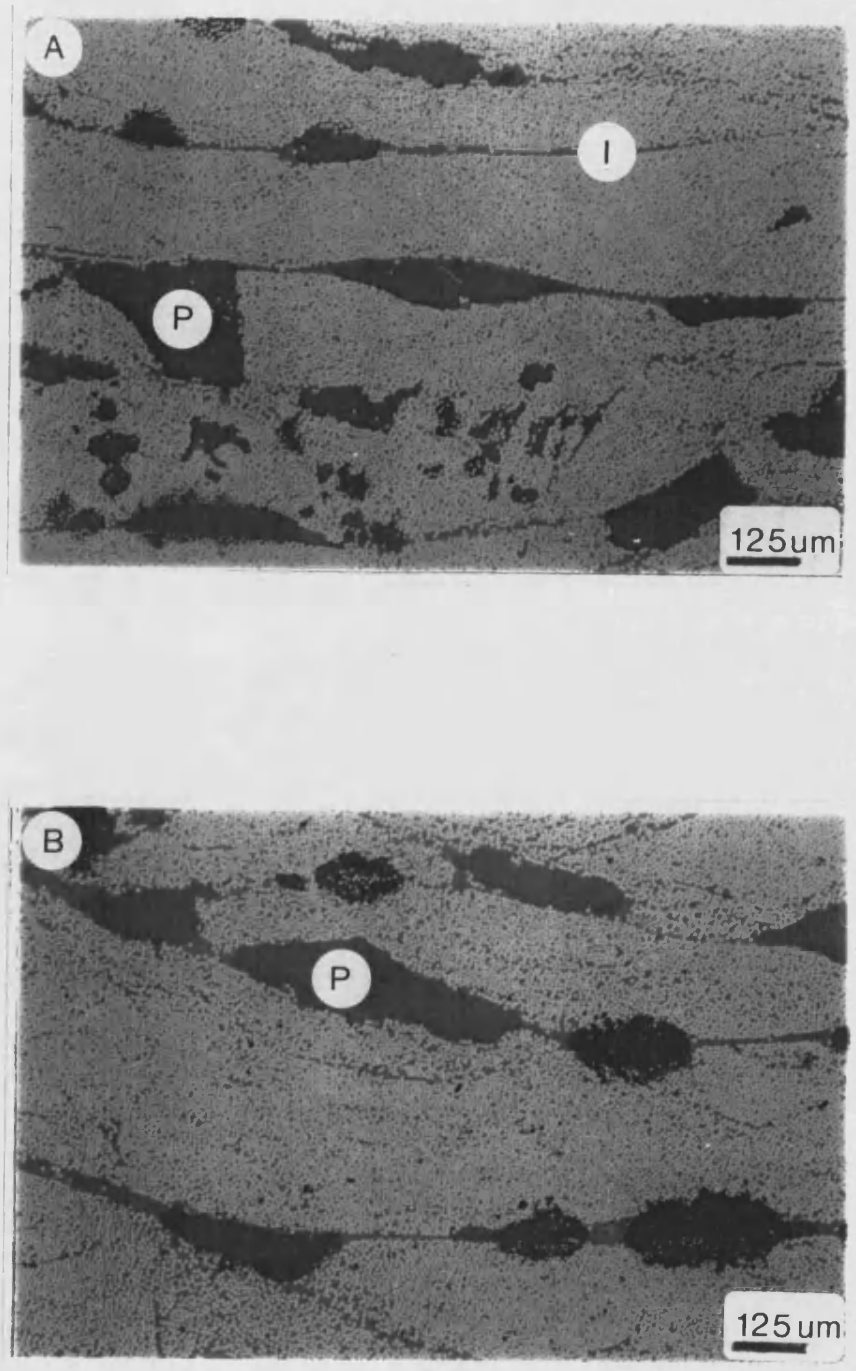

FIGURE 4.1 - Optical micrographs of transverse cross sections through the fibres of the *green* carbon fibre/phenolic resin composites with treated/sized fibres (A) and untreated/unsized fibres (B). P=Pores. I= interlamellar regions.

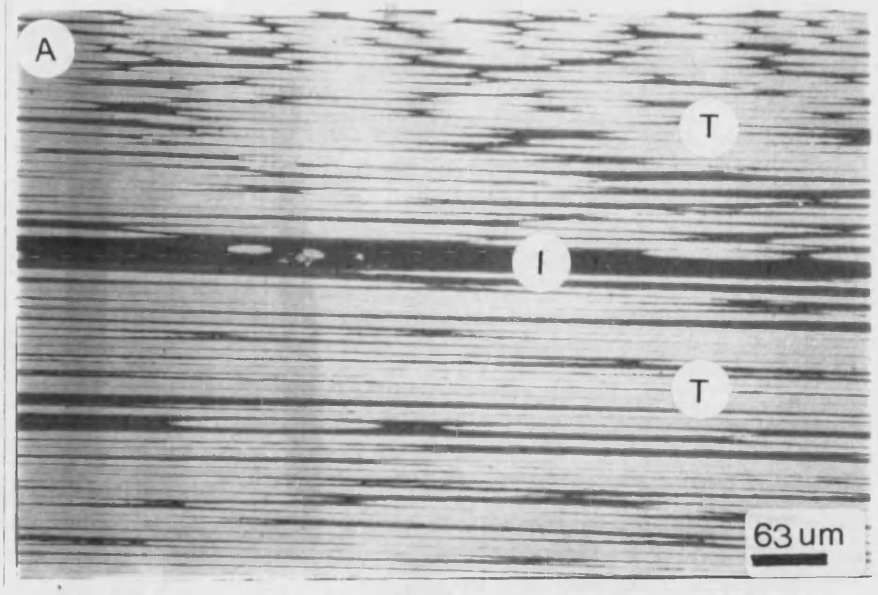

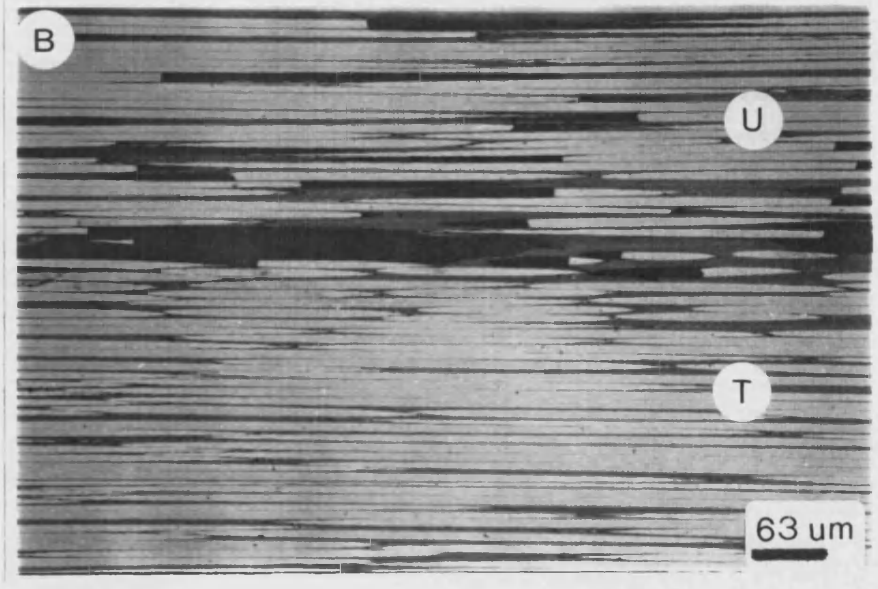

FIGURE 4.2 - Optical micrographs of longitudinal sections of (A) *green* carbon fibre/phenolic composite with treated and sized fibres; I=interlaminar resin matrix, T=fibre laminae. (B) *green* hybrid carbon fibre/phenolic composite with alternating laminae containing treated and size fibres (T) and untreated and unsized fibres (U).

The porous structure, due to evolved pyrolysis gases, is affected by the rate of gas evolution and the rate of diffusion of the evolved gases, which are closely related to the carbonisation conditions, such as heating rate and sample dimensions.

The development of a carbonisation schedule depends on the weight loss profile of the carbon matrix precursor and a thermogravimetric analysis was carried out for a bulk sample of the Borden SC1008P resin, and for the reinforced phenolic composite with the same resin, Figure 4.4. These results show that the major weight loss in the pure resin and in the composite occur in the approximate temperature range 250-550°C when the materials are heated at 5°C/min. Considering these two experiments the proposed heating schedule was devised, Figure 2.5, and the main events that take place in the carbonisation of the composite are as follows.

** 20°C till 280°C - Heating rate : 30°C/h*

In this region the polymer passes through its glass transition, where the matrix exhibits normal viscoelastic behaviour up to 200°C, demonstrated by a continuous decrease in the storage modulus (E') from 5.6 GPa at 20°C to 3.8 GPa at 115°C when the rate of decay of E' increases sharply approaching the glass transition of the phenolic resin, Figure 4.5. In this region the resin starts to release water, Figure 1.7, and the glass transition of the resin taken at the maximum of the Tan δ peak (≈0.5) was 165°C.

** 280°C till 480°C - Heating rate : 6°C/h*

In this temperature range phenolic resins experience a pronounced shrinkage, Figure 4.6, and weight loss, Figure 4.4. During this first degradation stage, random chain scission occurs, where the gas products are mainly H_2, CH_4, CO_2 and CO, Figures 1.8 and 4.3. Maximum gas pressure develops in this stage because the porosity and the permeability of the

porous composite are both small and a slow heating rate is necessary in order to avoid damage induced by the pressure build-up of the gases inside the laminate. When the gas evolution is higher than that of diffusion of evolved gases, gas pressure builds up in the bulk solid. In this case if the mechanical strength of the samples under carbonization does not overcome the gas pressure, some of the evolved gases would diffuse out explosively from the bulk, creating irregular pores. Fissuring is also likely to occur, because of the stress resulting from the accumulation of evolved gases (Choe - 1992).

** 480°C till 580°C - Heating rate : 20°C/h*

In this temperature range the rate of shrinkage and weight loss decrease and a higher heating rate can be used. Gases such as CH_4, CO, and CO_2, continue to be evolved. The methylene groups are known to react with each other, generating methane. CO is also produced by decompositition of ether bonds.

** 580°C till 1100°C - Heating rate : 40°C/h*

In this temperature range the shrinkage and weight loss are almost complete. Char formation reactions primarily take place, producing CO, CH_4, and H_2. The porosity of the component will depend on the carbonization temperature and on subsequent temperature treatment.

After heat treatment at 1100°C, a batch of each group of samples was further heat treated for one hour at 2500°C, in flowing argon, in a graphite resistance furnace (Astro) using a heating rate of 10-13°C/min.

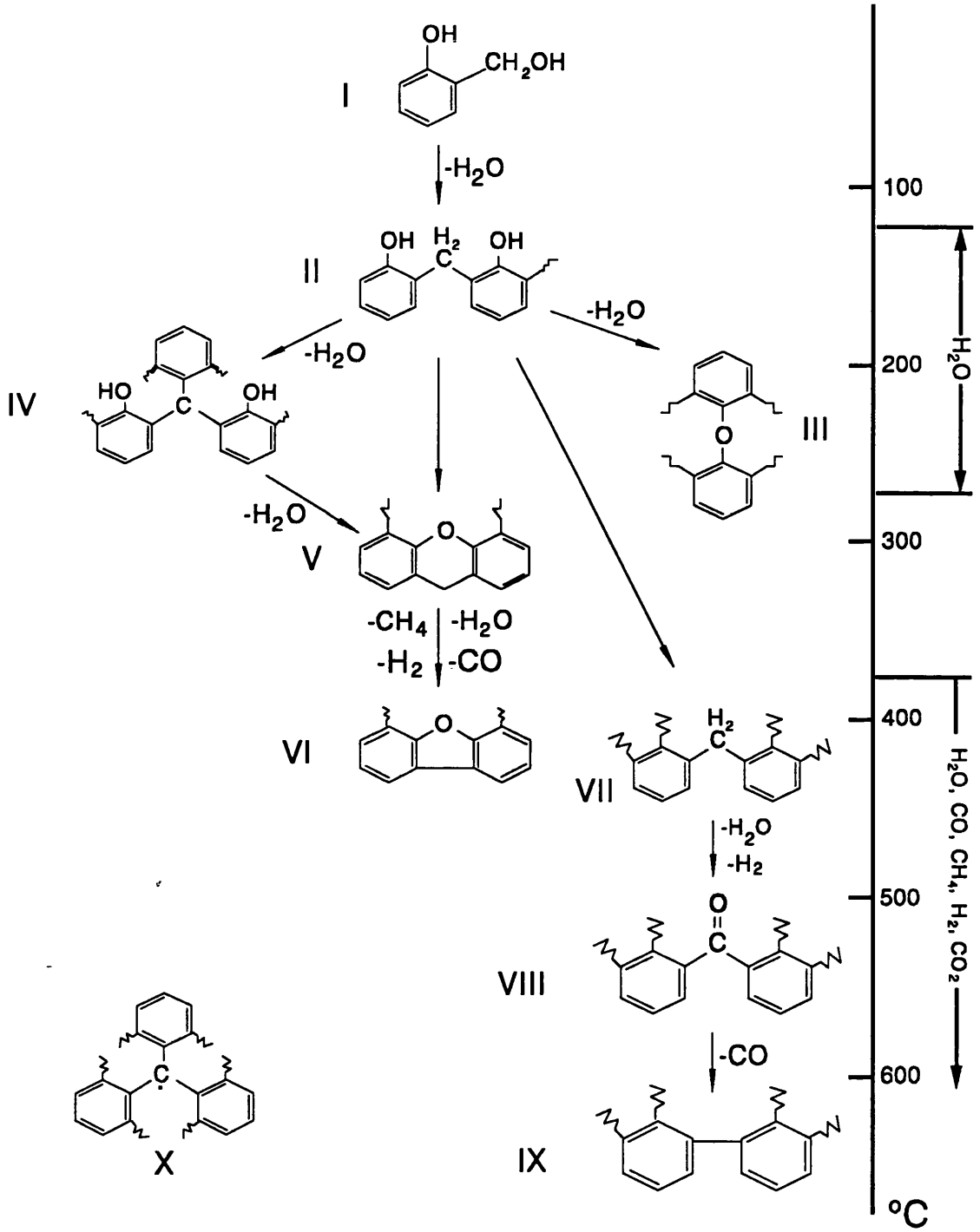

FIGURE 4.3 - Reactions that possibly takes place in the carbonisation of a typical phenolic resin (Burger - 1975).

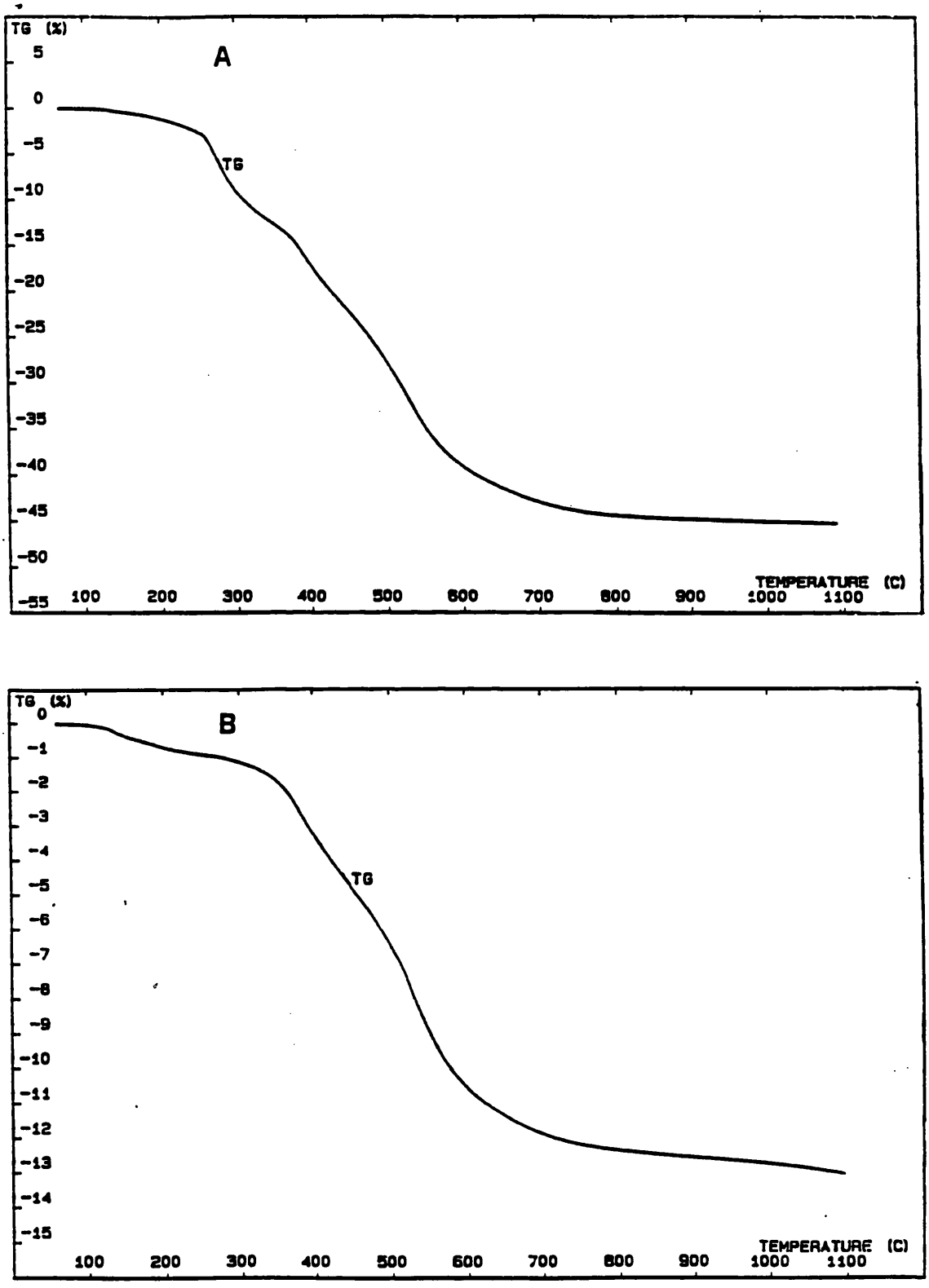

Figure 4.4 - (A) TGA for Borden SC1008P phenolic resin (mass=67.922mg) and (B) TGA for a CFRC composite reinforced with treated sized fibres with the same resin (mass=153.435mg), in helium (flow rate:1.5 l/min), heating rate: 5°C/min.

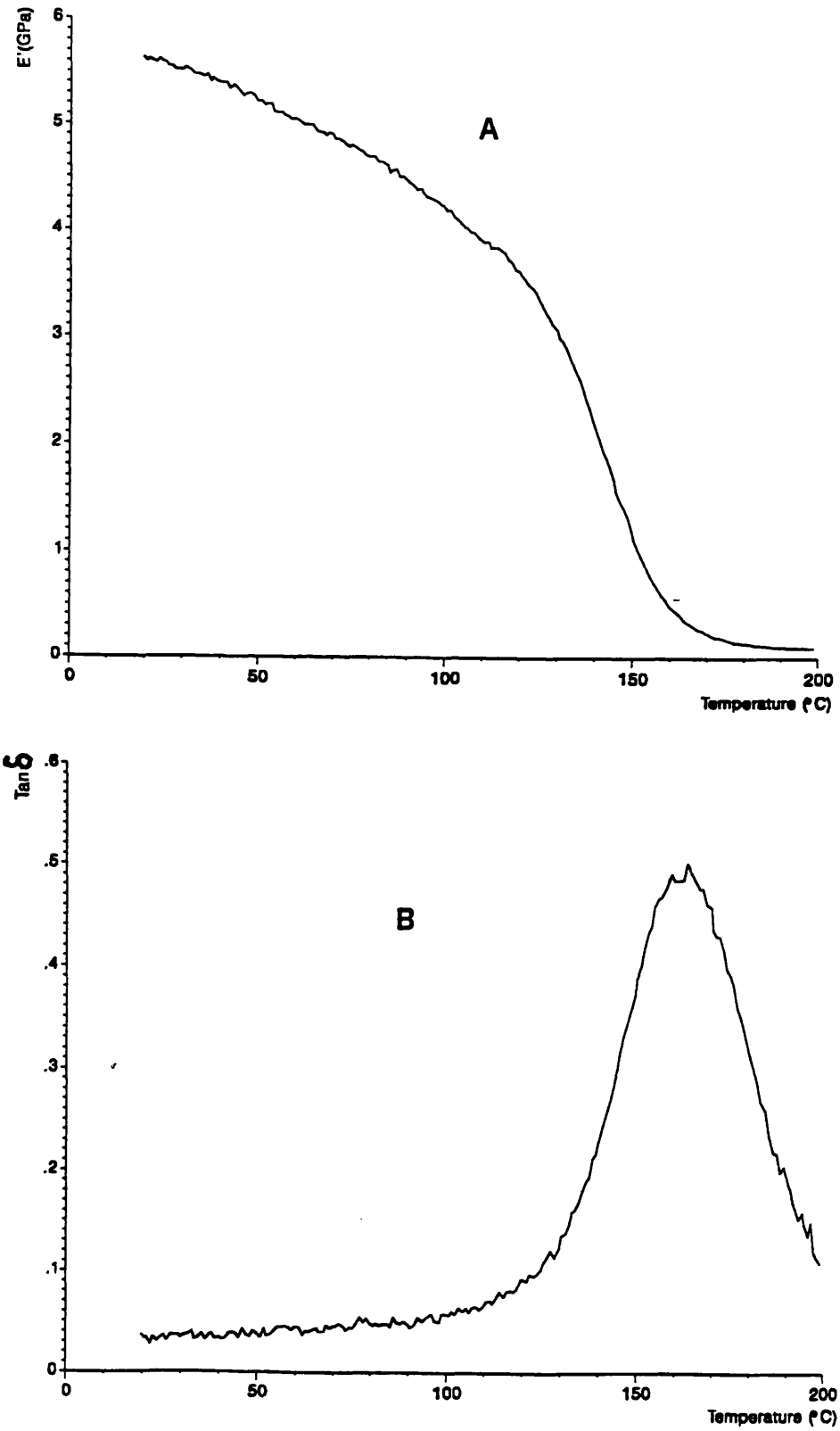

FIGURE 4.5 - Dynamic mechanical analysis of Borden SC1008P phenolic resin at a span of 44.00mm (width=15.05mm, thickness=4.77mm). (A) Storage Modulus(E'); (B) Tan δ.

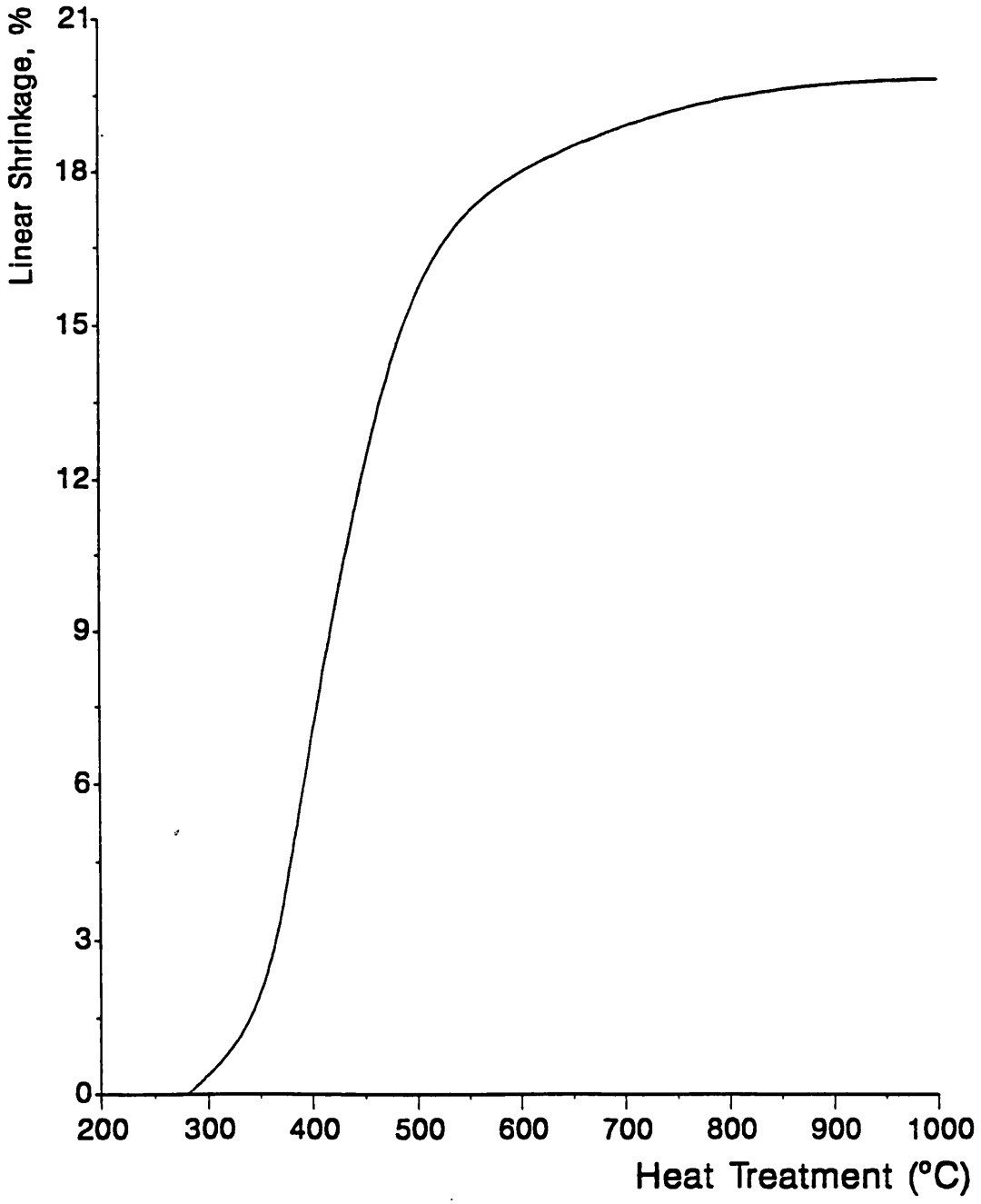

Figure 4.6 - Shrinkage profile of a typical phenolic resin (Burger - 1975).

4.3 - Microstructure of CFRC composites

4.3.1 - Microstructures of the CFRC composites heat treated to 1100°C

The Figure 4.7 shows typical transverse optical micrographs of the unidirectional CFRC composites heat treated up to 1100°C. The fibre laminae (F) of the TS-1100 composite, Figure 4.7A, and the matrix carbon (M) can be clearly distinguished. Fibres and matrix carbon within fibre laminae appear to be well-bonded. The presence of carboxylic groups on the treated and sized carbon fibre surface can possibly provide chemical bonding with the hydroxyl groups of the phenolic resin and form a strong covalent ester type of bond that is maintained during the carbonisation process (Fitzer - 1980, Kowbel - 1990). There are large pores (P) and the matrix contains regularly spaced microcracks, C1, running perpendicular to the laminae; these are possibly volumetric shrinkage cracks which are formed by stress relief on shrinkage of the matrix and they could be observed as well in the longitudinal view of the same composite, Figure 4.8A. There are similar, narrow cracks, C2, running from the large smooth pores (P) through the matrix into the laminae. The large pores (P) appear to be relics of those formed in the carbon fibre/phenolic resin precursors, Figure 4.1A, although their shapes are modified by carbonisation. Estimated values for fibre volume fraction determined by image analysis, weight loss, open and close pores for the TS-1100 composite can be seen in Table 4.1.

The microstructure of the UU-1100 composite, Figure 4.7B, is quite different from that of TS-1100 material. The large pores (P) are also seen but the fibre laminae and the interlaminar matrix are not clearly distinguished. The most characteristic feature of the microstructure of the UU-1100 composite is an extensive microcrack network enclosing clusters of fibres, measuring approximately 60 μm, and individual fibres. This microcrack

network probably results from carbonisation shrinkage of the matrix due to the low degree of fibre/matrix bonding in the *green* composite, Figure 4.2B. The relatively weak bond, if any, between fibre and matrix is readily broken, and a gap is formed at the fibre-matrix interface. This results in an "opening-up" of the composite, as it is sometimes called, and an increase in apparent porosity (Perry - 1974). Estimated values for fibre volume fraction determined by image analysis, weight loss, open and close pores for the TS-1100 composite can be seen in Table 4.1.

TABLE 4.1 - Shrinkage, weight loss and porosity of CFRC composites heat treated at 1100°C

CFRC Composite	TS-1100	UU-1100
Cross sectional shrinkage (%)	9.0 - 14.0	2.5 - 4.5
Weight Loss(%)	10 - 12	10 - 12
Total porosity(%)	24	38
Fibre volume fraction	0.73	0.60

The original features of the TS-1100 and UU-1100 composites were preserved in the hybrid T5U4-1100 CFRC, Figure 4.7C, where the two characteristic laminae made from treated and sized fibres (T), and untreated and unsized fibres (U) can be clearly identified. Large smooth pores (P) are present mainly in the U laminae. The fibre volume fractions were 0.60 and 0.70 for the U laminae and T laminae respectively.

The weight loss value for the TS-1100 material (10-12%) is similar to that recorded by TGA (≈13%), Figure 4.4B. The larger porosity of the UU-1100 composite, Table 4.1, is attributed to the more extensive microcrack

and pore network present in this material. The shrinkage of a CFRC composite is affected by many factors, such as fibre content, reinforcement architecture, carbon yield of the precursor, heating rate and final heat treatment, and surface characteristics of the carbon fibre (Jortner - 1991, Fitzer - 1986). Table 4.1 shows that the CFRC composite made with treated and sized fibres exhibited higher shrinkage than the CFRC composite made with untreated and unsized fibres.

Similar trends were observed by Manocha (1988) and Fitzer (1986), who both attributed the lower bulk shrinkage of the composites made with untreated and unsized fibres to poorer fibre/matrix adhesion, which allows matrix to shrink away from the fibres, leaving voids. Using unidirectional CFRC composites with high modulus fibres (fibre volume fraction = 0.55) and carbonising up to 1100°C, Manocha (1988) found a volumetric shrinkage of 30% for a CFRC composites made with treated and sized fibres with 5% open pores. A volumetric shrinkage of 18% was found for a CFRC composite with untreated and unsized fibres with 18% open pores. Fitzer (1986) found a cross sectional shrinkage of 17% for a unidirectional CFRC composite made with treated and sized fibres heat treated also at 1000°C, and a cross sectional shrinkage of 14% for a unidirectional CFRC composite made with untreated and unsized fibres. The quantitative differences in bulk shrinkage found by different workers can be attributed to the differences in microstructure of the composites and their heat treatment temperatures.

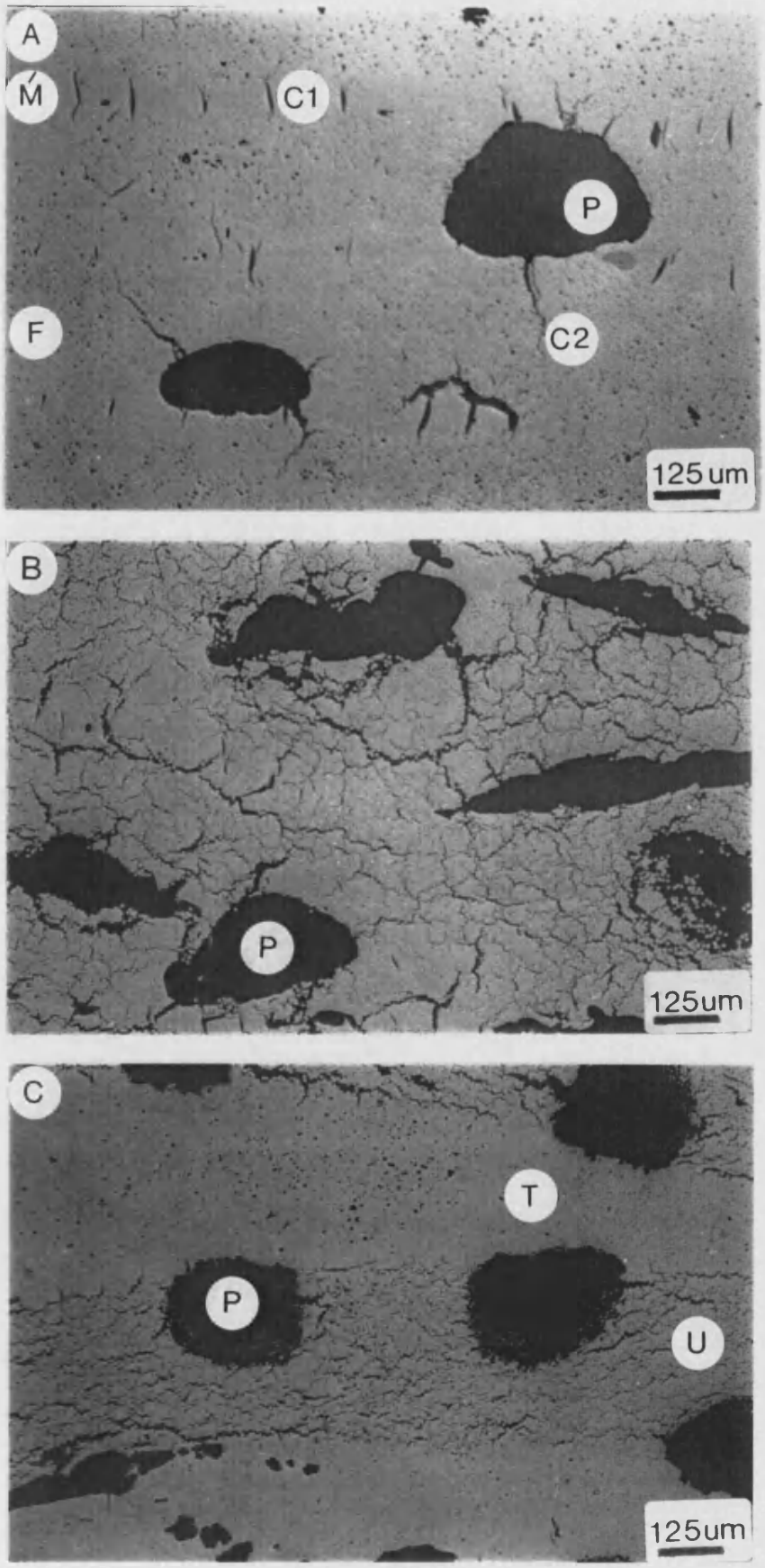

FIGURE 4.7 - Optical micrographs of the unidirectional CFRC composites, heat treated up to 1100°C, perpendicular to fibre axis. (A) TS-1100; (B) UU-1100; (C) T5U4-1100.

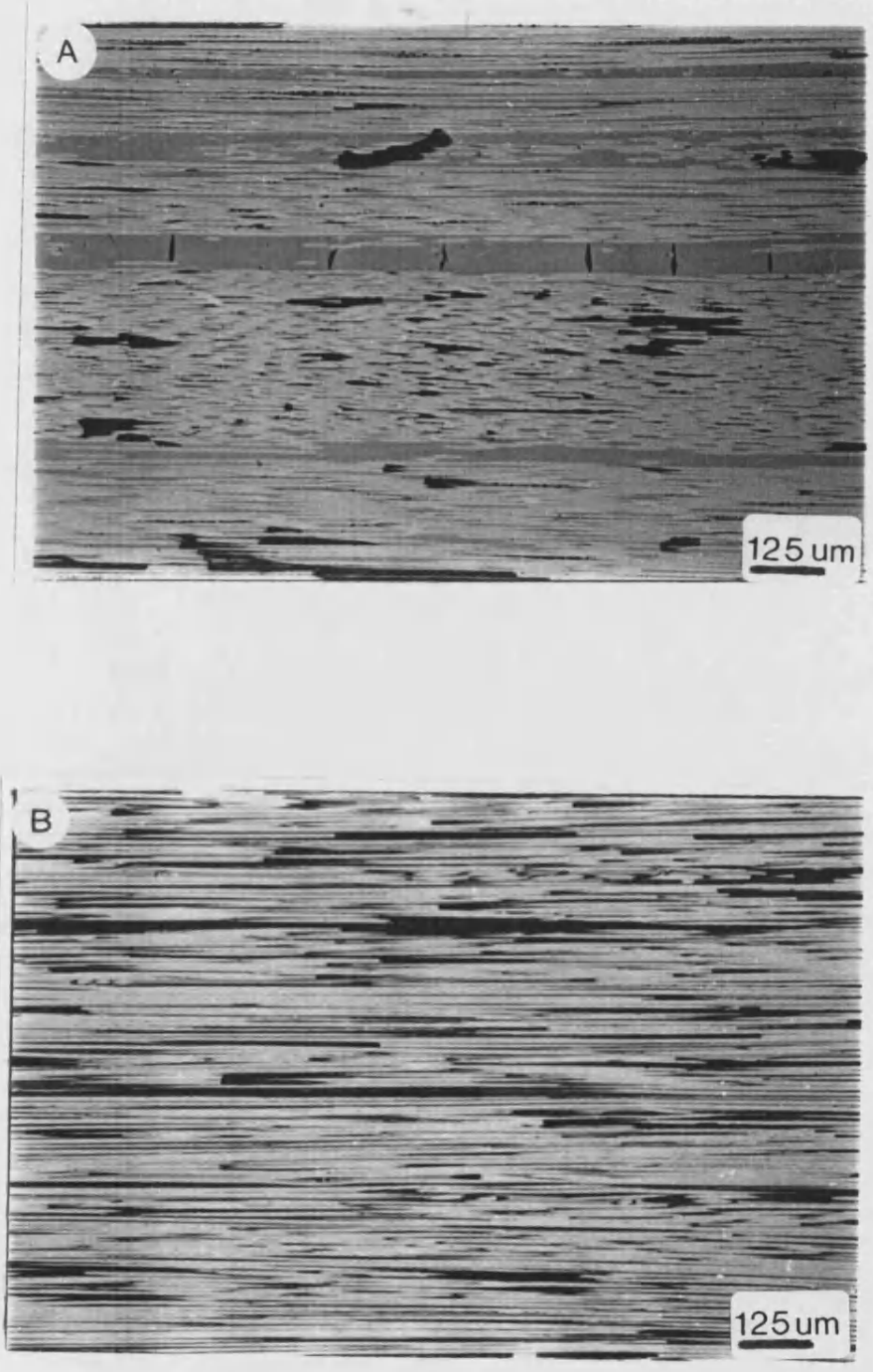

FIGURE 4.8 - Optical micrographs of the unidirectional CFRC composites heat treated at 1100°C, longitudinal to fibre axis. (A) TS-1100, (B) UU-1100.

4.3.2 - Microstructure of CFRC composites heat treated to 2500°C

Estimated values for fibre volume fraction determined by image analysis, weight loss, total porosity for the CFRC composite heat treated at 2500°C can be seen in Table 4.2. A subsequent heat treatment at 2500°C on samples previously heat treated at 1100°C results in additional weight loss. A different picture was found for shrinkage when heat treating the CFRC composites to 2500°C, after treatment at 1100°C. Small increases in total porosity were found and they can be related to the weight losses.

The Figure 4.9 shows microstructures of the CFRC heat treated at 2500°C. The microstructure of the composite made from treated and sized fibres is substantially modified by heat treatment to 2500°C. The lamellar microstructure of the TS-1100 composite, Figure 4.7A, is not retained in the TS-2500 material, Figure 4.9A, which shows a branched, crack network with major cracks lying parallel to the lamellar plane. The large pores which are near-equiaxed in the TS-1100 composite have become elliptical in the TS-2500 material. Small equiaxed pores, of size 10-20 μm, are also developed upon heat treatment to 2500°C. By contrast, the microstructure of the composite made from untreated and unsized fibres is little changed upon heat treatment from 1100°C to 2500°C, except that the crack network is more developed, Figures 4.7B and 4.9B.

The lamellar morphology of the hybrid composite is retained upon heat treatment from 1100°C to 2500°C. Figure 4.9C shows that features found in the TS-2500 and UU-2500 materials are also found in the T and U lamellae respectively of the T5U4-2500 hybrid composite. The fibre volume fraction in between large pores found for the U laminae was 0.58 and for the T laminae 0.68.

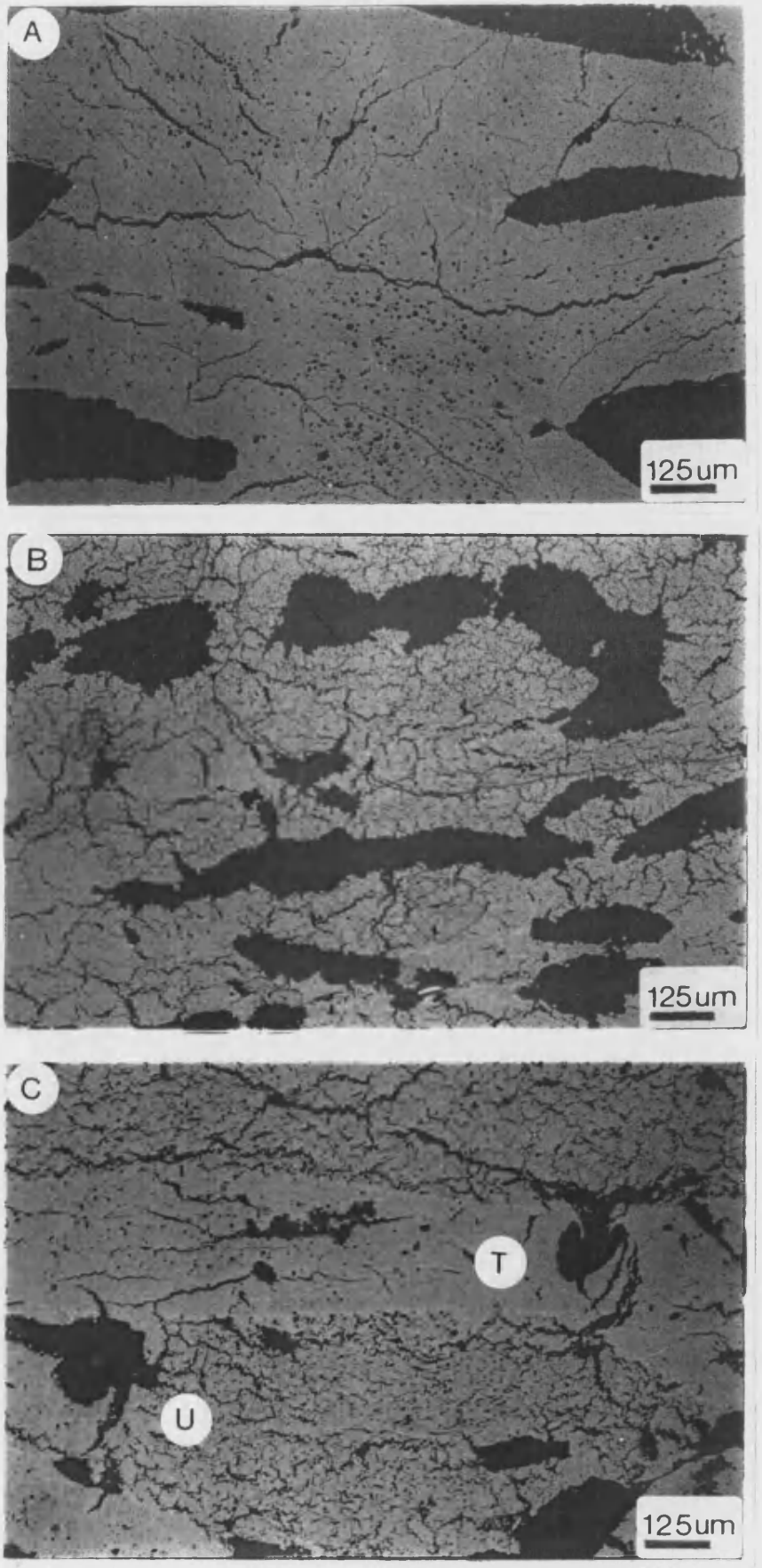

FIGURE 4.9 - Optical micrographs of CFRC composites heat treated at 2500°C, (A) TS-2500, (B) UU-2500, (C) T5U4-2500.

TABLE 4.2 - Shrinkage, weight loss and porosity of CFRC-1100 composites heat treated at 2500°C.

CFRC Composite	TS-2500	UU-2500
Cross sectional shrinkage (%)	13.3 - 16.8	19.3 - 24.0
Weight Loss (%)	3.5	4.0
Total porosity (%)	28	41.0
Fibre volume fraction	0.70	0.58

The high heating rate (≈10-13°C/min) used in the heat treatment up to 2500°C probably was responsible for the development of extensive networks of pores and cracks, as it was not possible to use low heating rates in the equipment used. Lower heating rates are desirable to avoid excessive damage to the samples.

High tensile strength carbon fibres are obtained by heat treatment to 1100-1500°C. Heat treating these fibres at higher temperatures produces a more graphitic structure. This structural modification can be detected by X-ray analysis, as shown on Figure 4.10. The characteristic 002 peak in the as received carbon fibre corresponds to a $d_{(002)}$ spacing of 0.355 nm. After heat treatment at 2500°C the value of $d_{(002)}$ decreases to 0.346 nm and the (002) peak becomes sharper, indicating that a more graphitic structure is achieved. A similar structural modification occurs in the resin carbon used as matrix, Borden SC1008P, heat treated at graphitising temperature, Figure 4.11. The resin carbon heat treated at 1100°C shows a broad $d_{(002)}$ peak at 0.39 nm and after heat treatment at 2500°C the position of the peak (002) corresponds to a $d_{(002)}$ of 0.361 nm and the peak is also sharper.

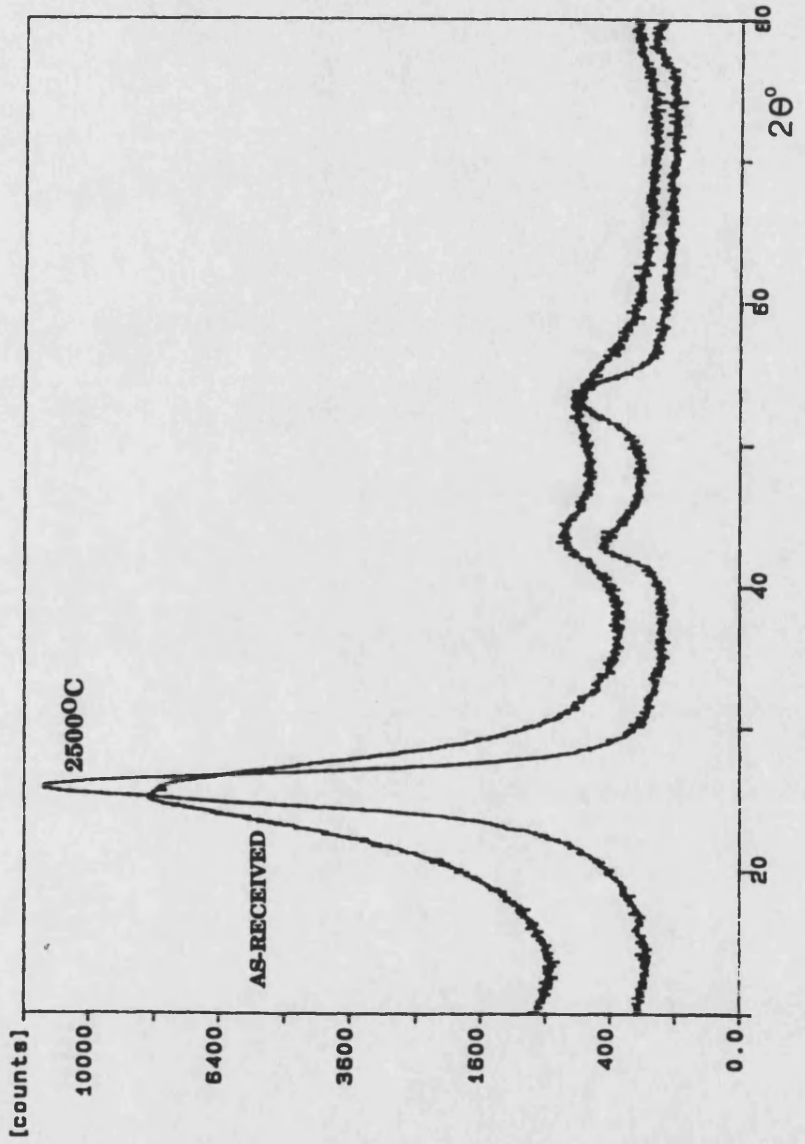

FIGURE 4.10 - X-ray analysis of as-received Courtaulds Grafil E/XA carbon fibre, and the same carbon fibre heat treated at 2500°C.

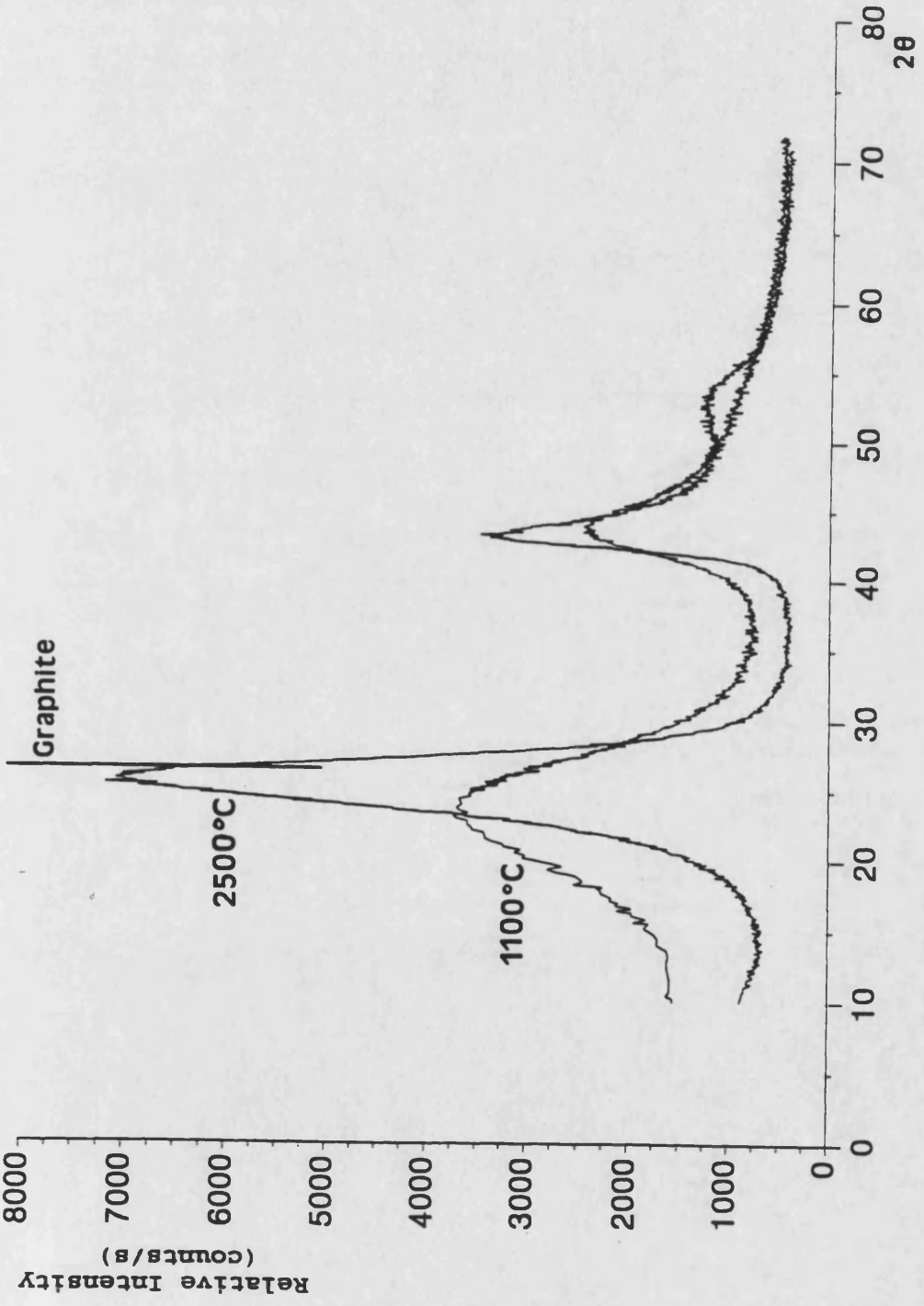

FIGURE 4.11 - X-ray analysis of a bulk Borden SC1008P resin heat treated at 1100°C, and the same resin heat treated at 2500°C.

A clear example of the change in the interlayer spacing ($d_{(002)}$) and in the crystallite size normal to the c axis (Lc) of graphitized and non-graphitized carbon materials with heat treatment temperature is shown in Figure 4.12 (Otani - 1991).

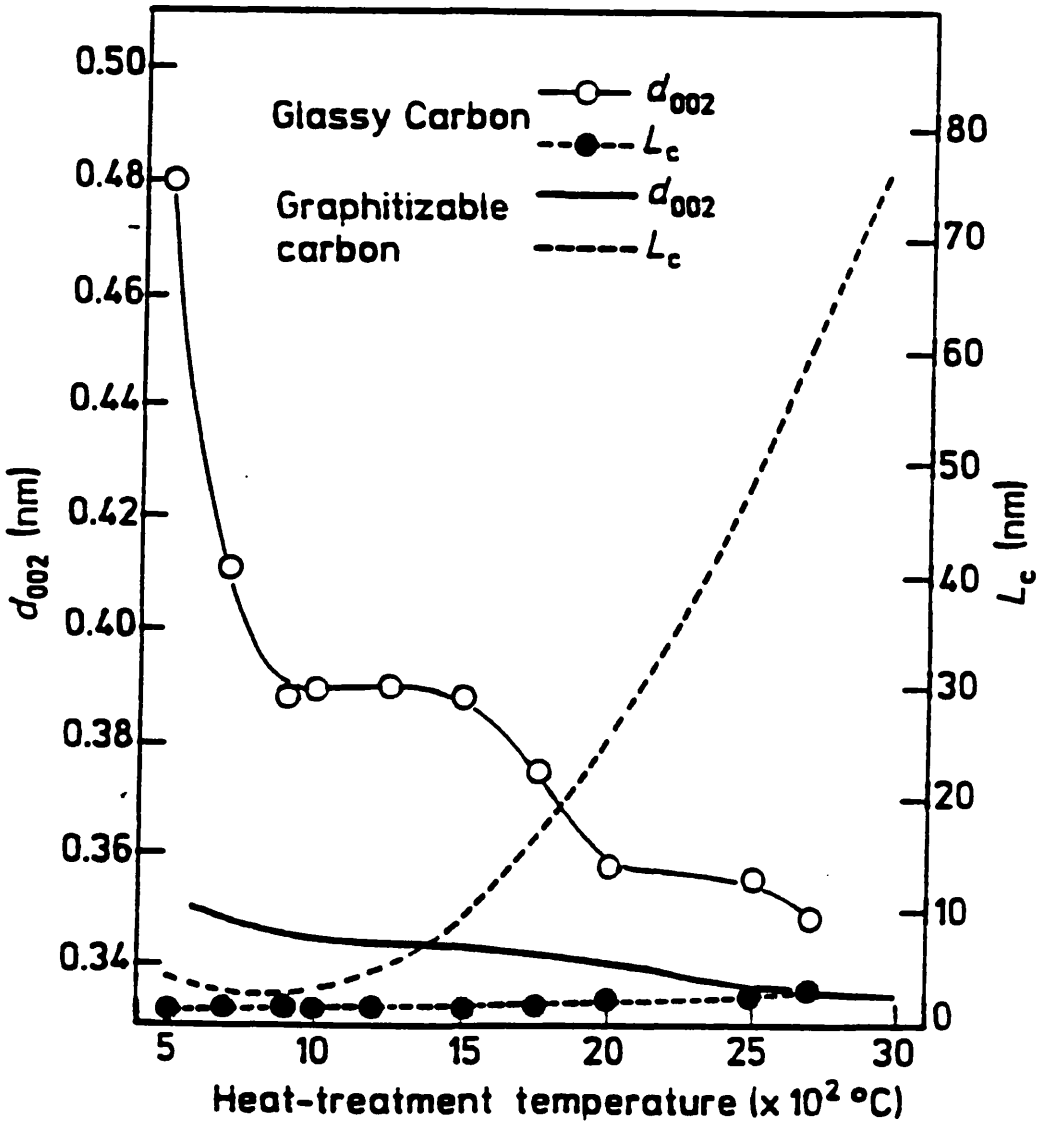

FIGURE 4.12 - Changes of X-ray parameters of glassy carbon and a typical graphitizable carbon as a function of the heat treatment temperature (Otani - 1991).

The heat treatment at 2500°C of the CFRC composites will promote stress graphitisation, *i.e.* a relative orientation of the resin carbon matrix radially to the fibres, usually as a sheath-like structure adjacent to the fibre and 1-3 μm deep (Zaldivar - 1991c). Optical activity was detected by polarised light microscopy, Figure 4.13, where regions of graphitic order can be identified. Optically anisotropic regions of the graphitic structure, *i.e.* areas of strong basal plane alignment, appear in a bright white pattern around fibres. Figure 4.13B shows that the crack network in the UU-2500 composite breaks up the fibre tows into small bundles containing up to ≈30 fibres; there is stress graphitisation of the matrix carbon within these bundles, but not at the crack surfaces, where the stress field is inadequate to induce graphitisation. Optical activity is also detected by coloured polarised light microscopy, Figure 4.14, where the colours (yellow or blue) appear according to their orientation with respect to the polariser and the analyser. Such localised graphitization, is believed to be the result of thermally induced tensile or compressive stresses acting at the fibre-matrix interface (Huettner - 1990). The source of the stresses is clearly the mismatch between fibre and matrix deformations on heating. It is not clear however, whether the major contribution to stress graphitization is by stresses caused by matrix shrinkage during pyrolysis, by thermal stresses occurring after the matrix is carbonised, or by creep-induced flow and stress relaxation at high temperatures (Peebles - 1988). The lack of optical anisotropy after pyrolysis below 1000°C suggests that stress itself is the main factor, rather than stress-induced molecular alignment during pyrolysis. Manocha (1988) found that CFRC composites with treated and sized fibres show a columnar-like carbon matrix, whereas those made with untreated and unsized fibre possess a lamellar type carbon matrix that is well oriented around carbon fibres when heat treated at graphitizing temperatures (T>2500°C).

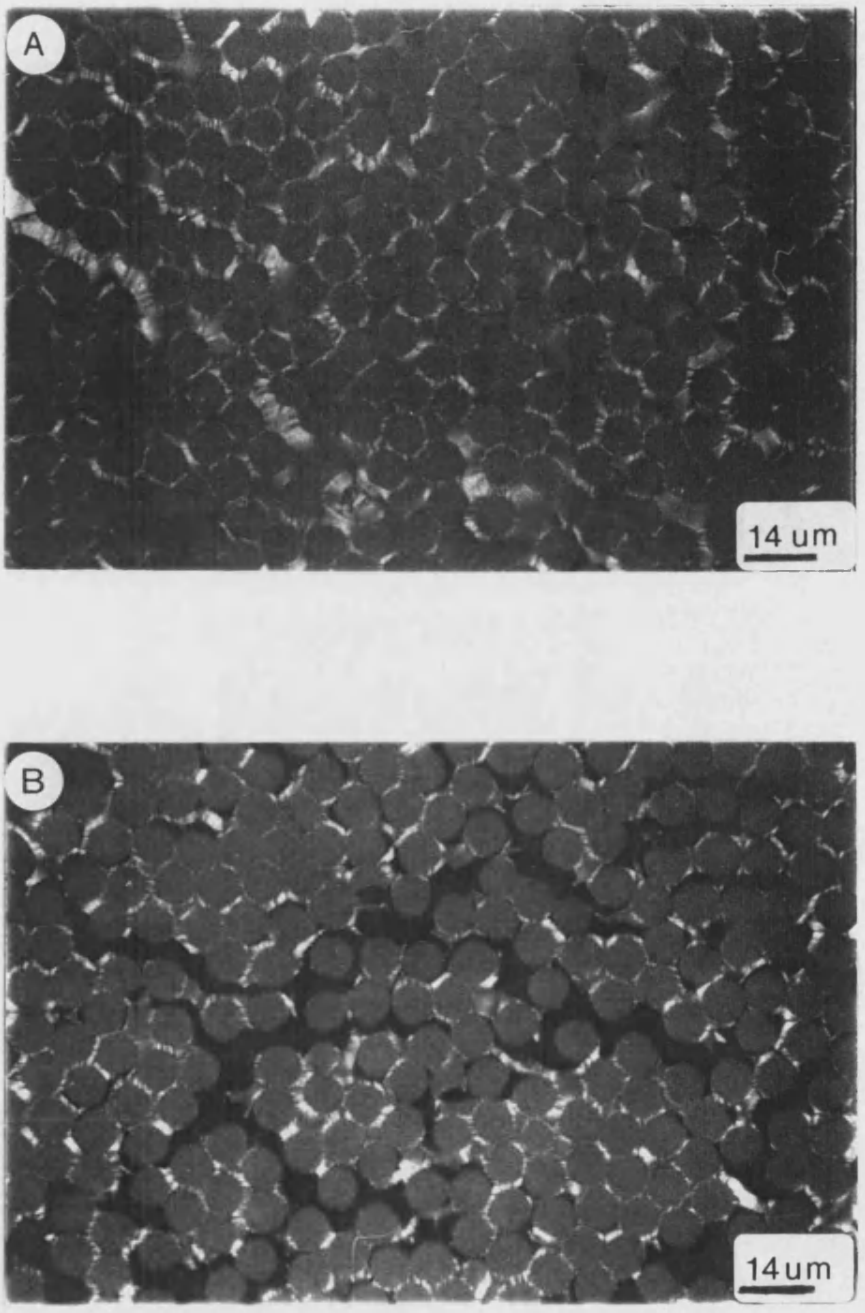

FIGURE 4.13 - Polarized light micrographs of TS-2500 composite (A) and UU-2500 composite (B).

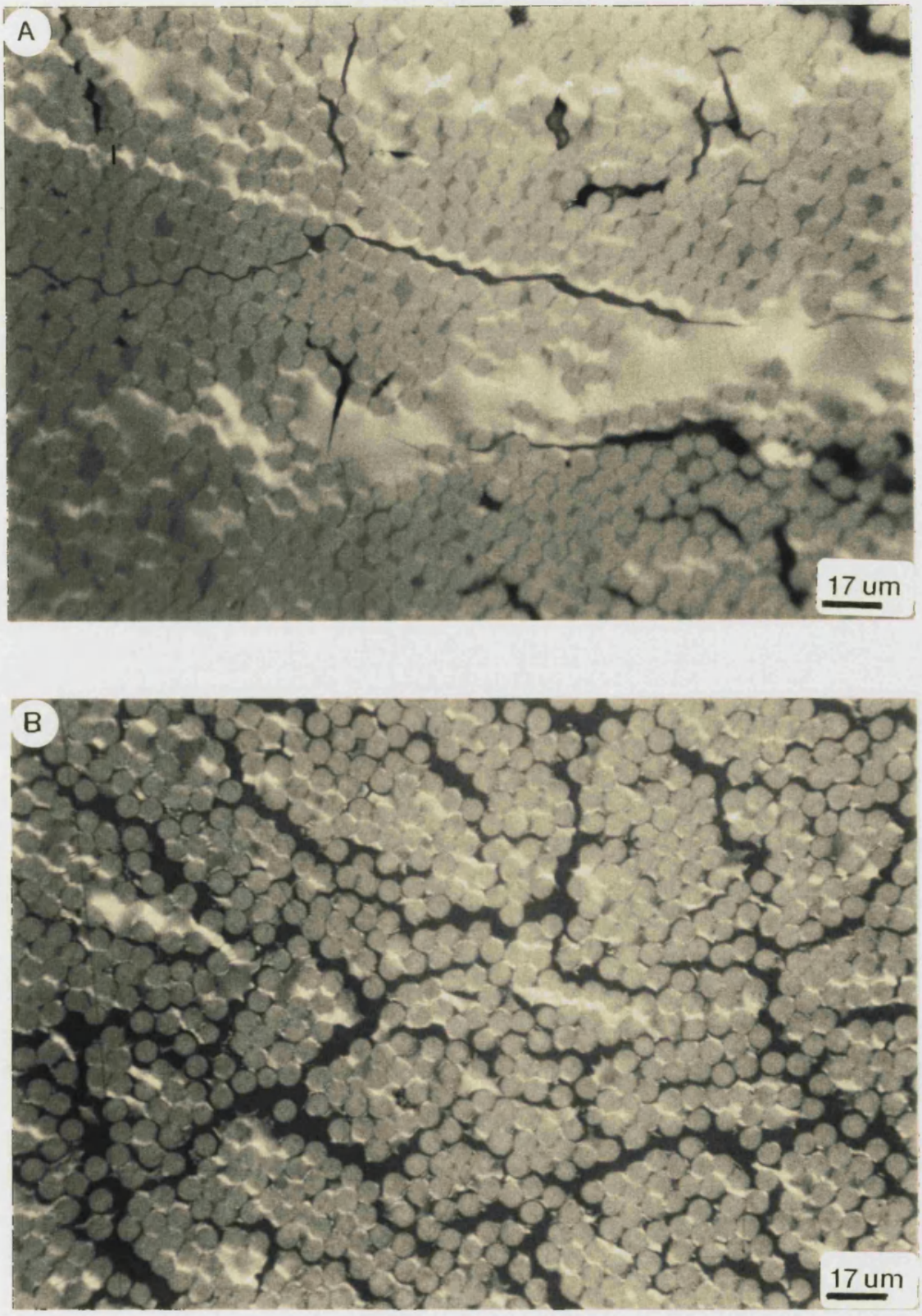

FIGURE 4.14 - Coloured polarized light micrographs of TS-2500 composite (A) and UU-2500 composite (B).

4.4 - Mechanical Properties of Unidirectional CFRC composites

4.4.1 - Mechanical properties of the CFRC composites heat treated to 1100°C

In order to establish a convenient span/depth ratio for testing the unidirectional CFRC composites, 3-point bend tests were carried out at various span/depth ratios for the TS-1100 composite. It was found that the flexural modulus for this material increases progressively until it remains approximately constant in the range of span/depth ratios greater than 25:1, Figure 4.15; similar results have been found for other CFRC composites (Crocker - 1991). Therefore, a standard value of span/depth ratio of 35:1 was adopted for the 3-point bend tests of all unidirectional CFRC composites. The flexural properties obtained for the unidirectional CFRC composites heat treated up to 1100°C are listed in Table 4.3. Typical plots of the stress-deflection curves and sketches of the failure modes for each CRFC heat treated at 1100°C can be seen in Figure 4.16.

A strong chemical bonding between the fibre and matrix in CFRC composites, as in the TS-1100 material, leads in general to a poor flexural strength and low strain to failure. The restrained shrinkage of the matrix during carbonization process, due to a strong interfacial bonding, induces regularly spaced pyrolysis cracks in the interlamellar resin carbon matrix, Figure 4.7, that are perpendicular to the lamellar plane. The strong fibre/matrix bond leads to a catastrophic brittle failure promoted by a fast crack propagation, Figure 4.16. A sharp smooth fracture surface with negligible fibre pull-out is found due to the strong bond between fibre and matrix, Figure 4.17. Fitzer (1980) suggests that when using surface treated fibres the matrix cannot crack by absorbing fracture energy, because the energy at the tip of the notches or cracks is possibly smaller than the bonding energy between fibre and matrix. The cracks therefore do not stop at the fibre surface but run straight through the composite.

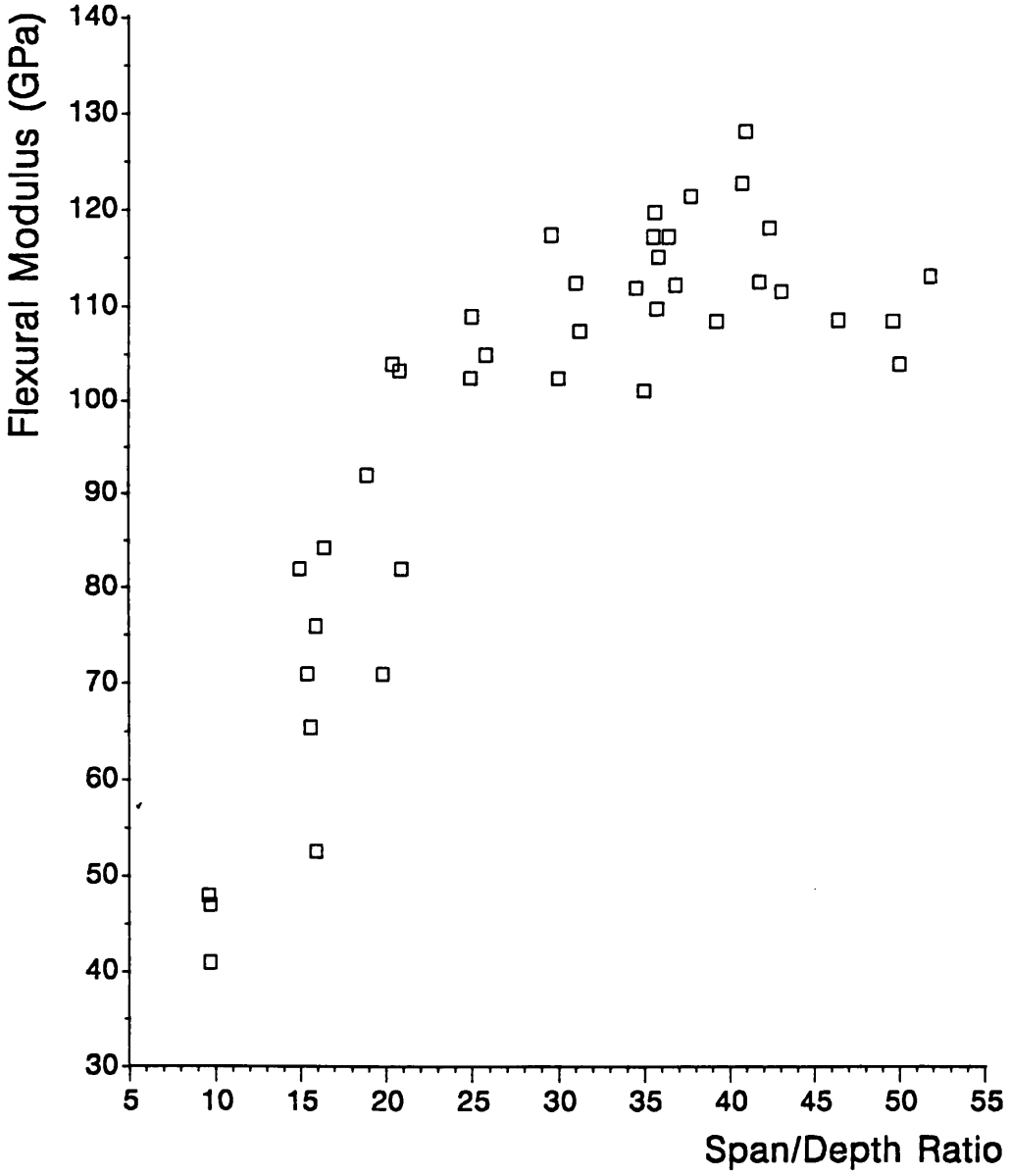

FIGURE 4.15 - Flexural modulus as a function of the span/depth ratio a TS-1100 CFRC composite.

CFRC Composite	TS-1100	UU-1100	T5U4-1100
Bulk Density (g/cm^3)	1.38±0.06	1.35±0.04	1.35±0.01
Flexural Strength (MPa)	134.0±22	142.5±16	165.0±10
Flexural Modulus (GPa)	114.0±7.0	60.0±6.0	69.0±4.0
Mid-span deflection[(a)] (mm)	0.85±0.1	1.80±0.23	1.74±0.2
Nominal Fracture Initiation Energy (kJ/m^2)	0.56±0.13	1.43±0.18	1.37±0.19
ΣAE counts at failure	1738±1103	13101±5227	54364±13323
Pollock exponent b	0.66	1.82	1.67

TABLE 4.3 - Mechanical properties and AE parameters of CFRC composites heat treated at 1100°C. ± values are standard deviation of 7 samples, (a) at peak stress.

Although the flexural strengths of the TS-1100 and UU-1100 composites are not significantly different (95% confidence), Table 4.3, the weak interfacial bonding in the UU-1100 material, allows deformation to occur in the matrix during heat treatment, so fibre breakage can only occur when the tensile strength of the fibres is exceeded (Fitzer - 1980). A weak interfacial bond, seen in Figure 4.7B, leads to crack deflection at the fibre/matrix interface and/or pull-out of small fibre bundles, and fibre sliding in both the tensile and compressive stress fields without fracture into two pieces, Figure 4.16. This type of failure mode results in an increased failure strain and a lower flexural modulus, Table 4.3. The failure behaviour of the UU-1100 is defined as pseudo-plastic and it is characterised by a continuous reduction in stress after the peak stress, eventually reaching almost a plateau value, Figure 4.16. Values of nominal fracture initiation energy for the TS-1100 and UU-1100 materials, Table 4.3, show that the latter undergoes a tougher failure mode, as is also suggested from a comparison of the shapes of the stress-deflection curves for the two materials, Figure 4.16.

The hybrid T5U4-1100 composite has the highest flexural strength of the materials heat treated at 1100°C, Table 4.3, suggesting that the combination of alternating laminae, in that disposition, containing fibres with different surface treatments has a synergistic effect on flexural strength. An intermediate strain to failure was also found, although the modulus was just slightly higher than the UU-1100 composite and far from the value found for the TS-1100 material, showing that there is not a proportional increase in modulus when using such laminae. The fracture mode of the T5U4-1100 composite was initiated by a brittle failure of the T laminae on the tensile face of the specimen that was marked by a discontinuity in the stress-deflection curve at about 130 MPa, Figure 4.16.

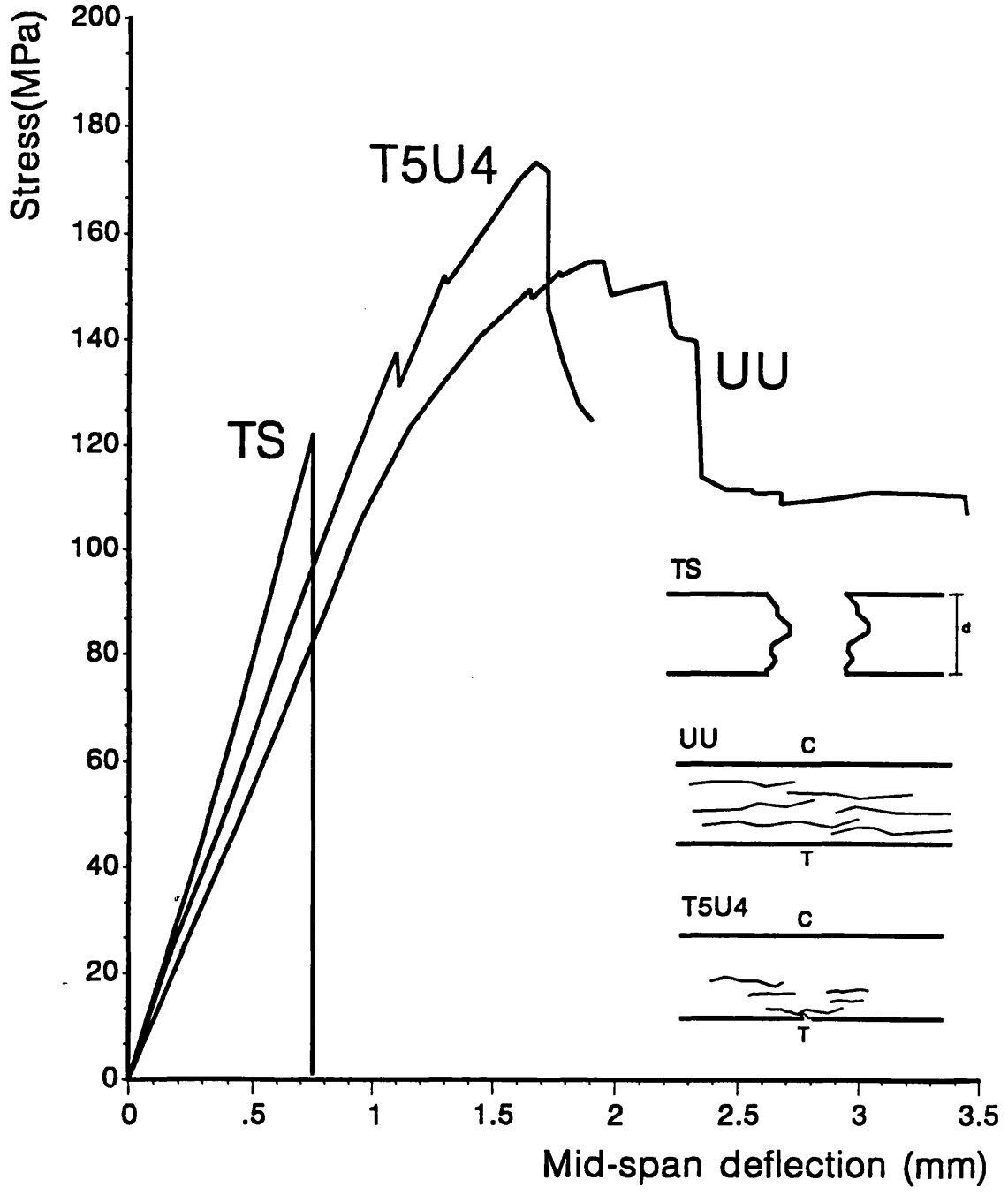

FIGURE 4.16- Typical 3-point bend stress-deflection curves for unidirectional CFRC composites, heat treated to 1100°C. Insert: schematic failure modes, C=compressive face, T=tensile face.

Afterwards extensive ply delamination between the T and U laminae is observed and fibre pull-out in the U laminae extending to the neutral axis, before the ultimate failure stress is reached. Different dispositions of the fibre laminae in the hybrid composite with the same proportion of plies are expected to provide different fracture patterns.

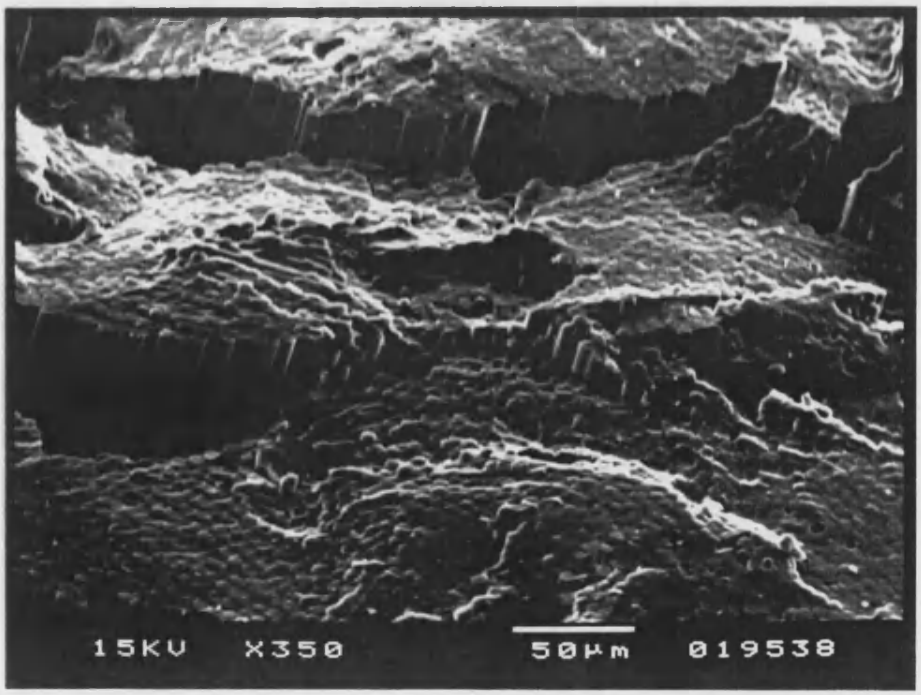

FIGURE 4.17 - Surface topography of a TS-1100 CFRC composite showing smooth fracture after failure.

4.4.2 - Mechanical properties of the CFRC composites heat treated to 2500°C

Typical plots of stress-deflection curves for the unidirectional CFRC composites heat treated at 2500°C and flexural properties are in Figure 4.18 and Table 4.4, respectively. Heat treating CFRC composites made with treated and sized fibres at graphitising temperatures (>2500°C) has a beneficial effect on its flexural strength and failure strain, being more than twice as great as those of the TS-1100 material, although the flexural modulus is not changed significantly (95% confidence). As a result, the nominal fracture initiation energy is increased from 0.56 to 2.2 kJ/m^2 on heat treatment from 1100 to 2500°C, Table 4.4. Increases in mechanical properties have been reported upon heat treatment of CFRC composites to graphitising temperatures (Thomas - 1978a, Fitzer - 1980). Manocha (1988) found that the stress graphitisation effect is particularly strong in CFRC composites made with treated and sized carbon fibres and heat treated at graphitising temperatures (T > 2500°C), where small domain crystallites in the matrix grow up and crack branching can occur. There is also evidence in the present work for more extensive stress graphitisation in the TS-2500 composite compared to the UU-2500 material. This is because there is a strong bond between fibre and matrix in the TS-2500 composite. Although bulk resin carbons have an amorphous structure, heat treatment at 2500°C will allow an intermediate stage, where the microstructure is sufficiently ordered to accommodate some slip from shear forces, but is disorded enough to prevent long range slip. In that way energy absorption and so toughness is higher permitting extensive microcracking in the matrix and the chance for multiple fracturing is the greatest. Therefore, heat treatment from 1100 to 2500°C also produces a change from a brittle failure mode to a tougher one which is characterised by extension of the crack system, seen in Figure 4.18.

CFRC composite	TS-2500	UU-2500	T5U4-2500
Bulk Density (g/cm^3)	1.20±0.04	1.20±0.03	1.25±0.01
Flexural Strength (MPa)	296.6±46	116.5±16	187.0±16
Flexural Modulus (GPa)	120.0±18	61.0±11	92.7±10
Mid-span deflection[(a)] (mm)	1.53±0.08	1.20±0.13	1.53±0.08
Nominal Fracture Initiation Energy (kJ/m^2)	2.2±0.39	0.63±0.10	1.23±0.09
ΣAE counts at failure	8908±2890	8572±3066	16668±8370
Pollock exponent b	0.97	1.83	1.67

TABLE 4.4 - Mechanical properties and AE parameters of unidirectional CFRC composites heat treated at 2500°C. ± values are standard deviation of 7 samples. (a) at peak stress

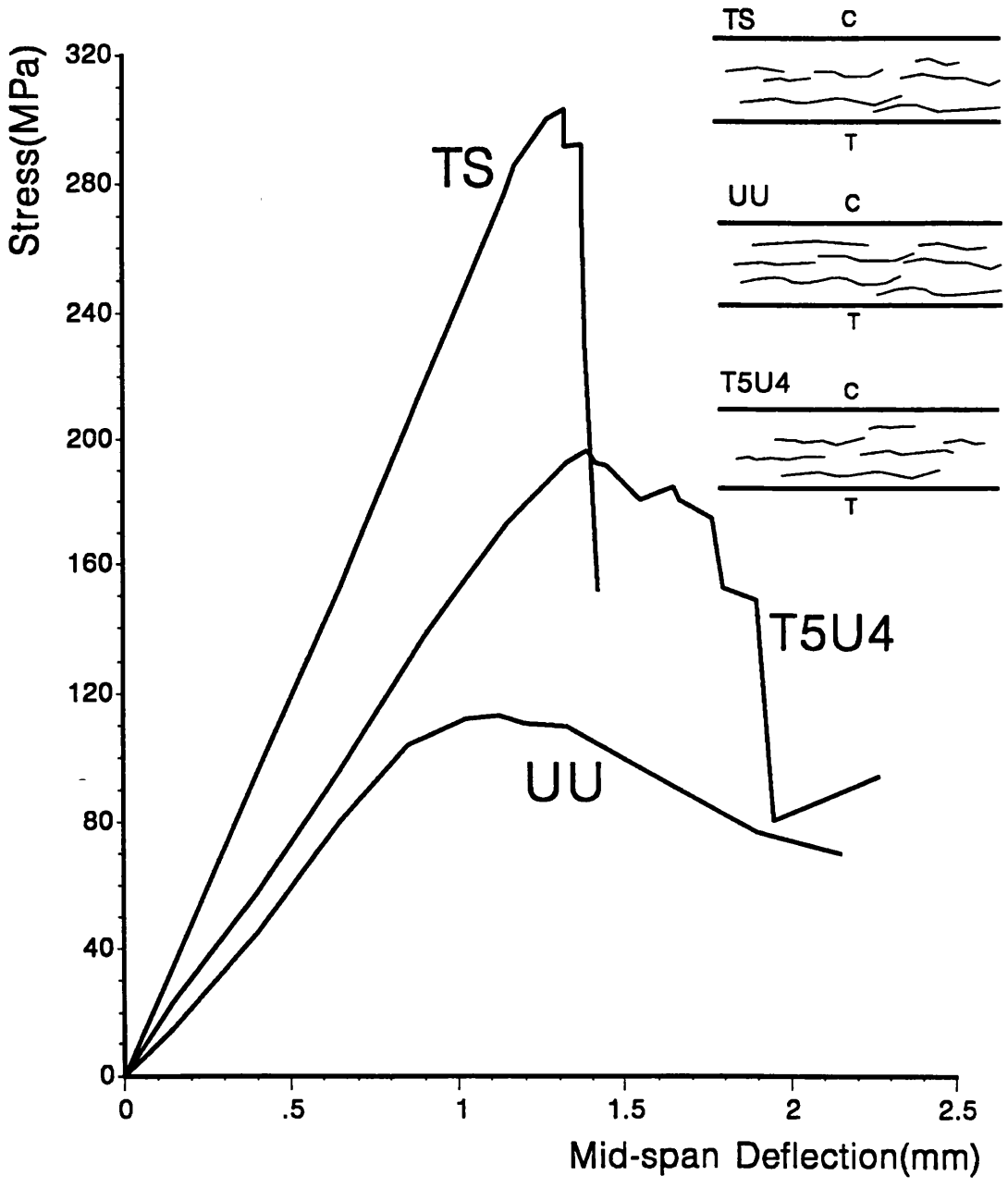

FIGURE 4.18 - Typical 3-point bend stress-deflection curves for unidirectional CFRC composites, heat treated at 2500°C. Insert: schematic failure modes, C=compressive face, T=tensile face.

Graphitic order is present in the UU-2500 composite also, but it was not sufficient to improve mechanical properties, Table 4.4. Although the flexural modulus is unchanged, the flexural strength and the nominal failure strain of the UU-2500 composite are reduced compared to those for the UU-1100 material. The flexural strength decrease is probably a result of an increase amount of debonding and fibre pull-out. The fracture pattern of the UU-2500 composite is similar to the UU-1100 material and is characterized by extensive delamination. It is possible that the development of a graphitic microstructure in the vicinity of the fibre/matrix interface in the UU-2500 composite facilitates fibre bundle sliding, so leading to the observed reduction in flexural strength.

Although a similar nominal failure strain was found for the hybrid T5U4-2500 composite, the strength and modulus increased in relation to the T5U4-1100 material. If we consider valid the conclusions drawn previously for the individual TS-2500 and UU-2500 composites in relation to mechanical properties, the increase in the properties of the hybrid T5U4-2500 composite can be attributed mainly to the presence of the T laminae. The failure of the first ply in the tensile face of the T5U4-1100 composite was removed by heat treatment at 2500°C, resulting in a tougher failure mode. For both hybrid composites heat treated at 1100 and 2500°C the initiation of failure appears to be dominated by the T laminae, but, once failure is initiated, the stress-deflection behaviour is dominated by fibre bundle sliding and micro fracture of the U laminae.

4.5 - Acoustic Emission of unidirectional CFRC composites

4.5.1 - Acoustic emission from the CFRC composites heat treated to 1100°C

Typical plots of stress-deflection data and the associated cumulative AE

counts for the composites heat treated to 1100°C are in Figure 4.19. Although the extent of AE differs for the three composites, in each case there is a progressive increase in AE during bend tests and there is no threshold stress for the onset of AE. For the TS-1100 and UU-1100 composites the development of AE with strain is very similar up to a mid-span deflection of ≈0.6 mm. The number of AE events at fracture from the hybrid T5U4-1100 composite is much greater than from the other two composites and the development of AE with applied strain is of a similar form to that for UU-1100 material.

Amplitude distributions of AE at fracture in the form log N(a) vs. amplitude level (channel number) are in Figure 4.20. The figure shows that there is a greater number of AE events of large amplitude from the TS-1100 composite than from the UU-1100 material for which there are no AE events with amplitudes > 40dB (channel number > 16). However, for the UU-1100 composite there are more AE events of amplitude < 12.5 dB (channel number < 5). These trends are consistent with the different fracture modes of these two composites. The failure mode of the UU-1100 composite involves extension of the microcrack network seen in Figure 4.7 and fibre bundle sliding which give rise to many stress waves of low energy and low amplitude. By contrast, the brittle failure mode of the TS-1100 is presumably, characterised by rapid microfracture events, which are fewer in number than those from the UU-1100, but which release stress waves of high energy and amplitude. Although the number of AE events from the hybrid T5U4-1100 composite is greater than from the other two composites, the AE amplitude distribution is similar to that for the TS-1100 composite at high amplitudes and similar to that for the UU-1100 material at low amplitudes, reflecting the contributions to AE from sub-critical processes in the T and U laminae in the hybrid composite.

The AE amplitude distributions from flexural loading have been quantified using the empirical Pollock power law : $N(a) = (a/a_0)^{-b}$, as explained in Appendix VIII, where a_0 is the threshold amplitude and b is a parameter which characterises the amplitude distribution. For UU-1100 and T5U4-1100 composites the AE amplitude distributions fit the power law in the range $N(a) \approx 10^2$ - $\approx 10^4$ counts, Figure 4.20; values of the parameter b = 1.82 and 1.67 for UU-1100 and T5U4-1100 composites respectively are similar, reflecting the near-parallel alignment of the AE amplitude curves for these materials at low channel number, Figure 4.20. The AE amplitude distributions for the TS-1100 composite do not fit the power law, except for a narrow range of N(a) values > $\approx 10^3$ which give a low value of b = 0.66.

The AE amplitude distributions were also taken in the linear elastic range at a strain to failure represented by the mid-span deflection of ≈0.5 mm for the CFRC composites, Figure 4.21. For TS-1100 and T5U4-1100 composites the AE amplitude distributions fit the power law in a narrow range of N(a) values > $\approx 10^{2.5}$. For UU-1100 composite the AE amplitude distributions fit the power law for $N(a) > 10^{1.5}$. These AE distribution curves gives b values for TS-1100 and UU-1100 composites of 0.68 and 1.67 respectively. These b values are similar to the ones calculated at failure stress, Table 4.4, indicating that the proportion of AE events in channel numbers < ≈10 are similar. There are no AE events with amplitudes > 45 dB (channel number > 18) for TS-1100 composite. The AE distribution curves for the T5U4-1100 composite fit the power law in the narrow range of N(a) > $\approx 10^{2.5}$ giving a value of b = 1.31, indicating that compared with the same composite at the failure stress there is a high of proportion of high amplitude events in the linear elastic range. The higher value of b at fracture (b = 1.67) is due to an increase in the number of low amplitude AE events, possibly associated with fibre bundle sliding in the U laminae.

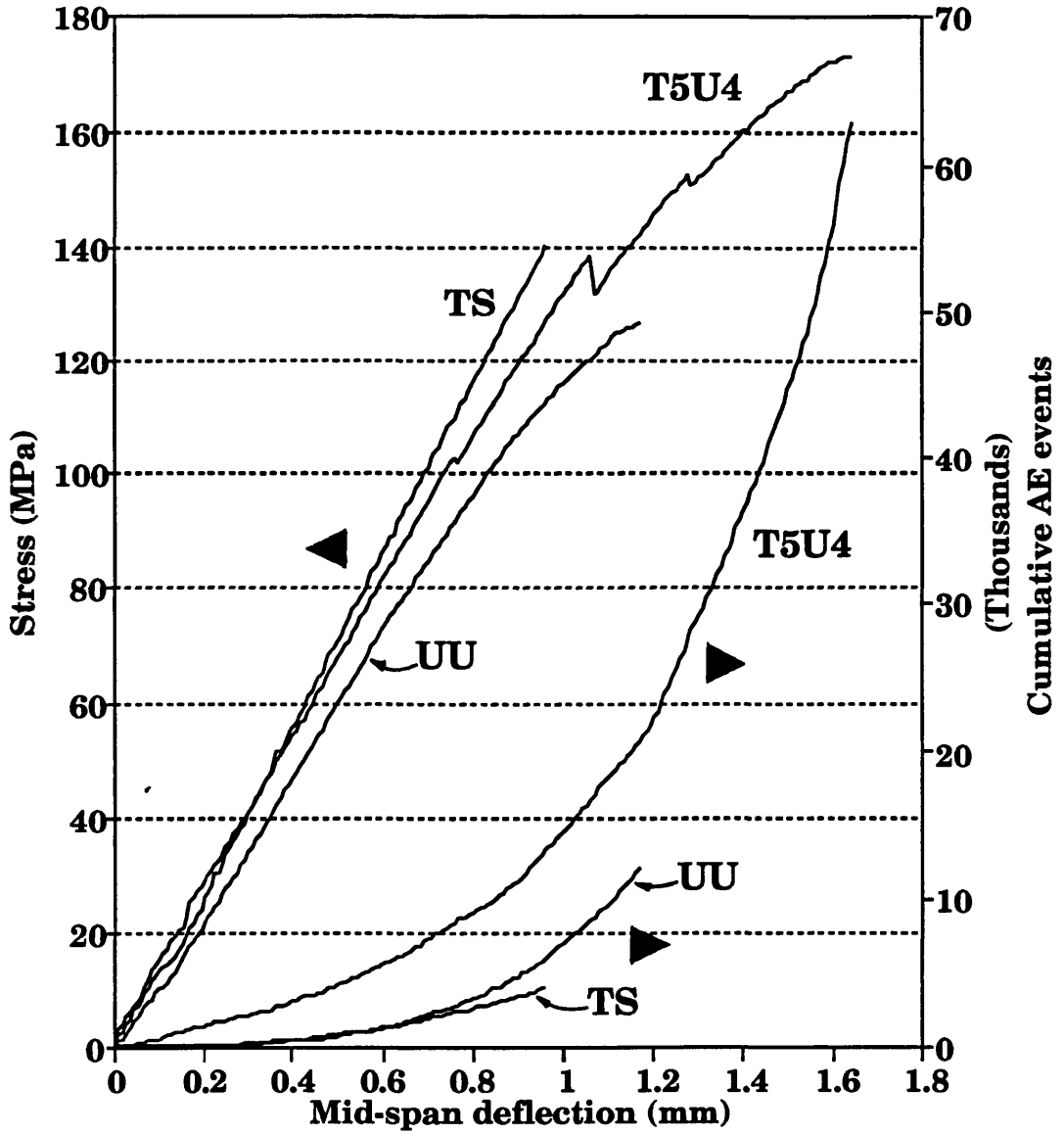

FIGURE 4.19 - Typical plots of stress and AE counts as a function of the mid-span deflection for unidirectional CFRC composites heat treated to 1100°C, subjected to loading to failure in flexure.

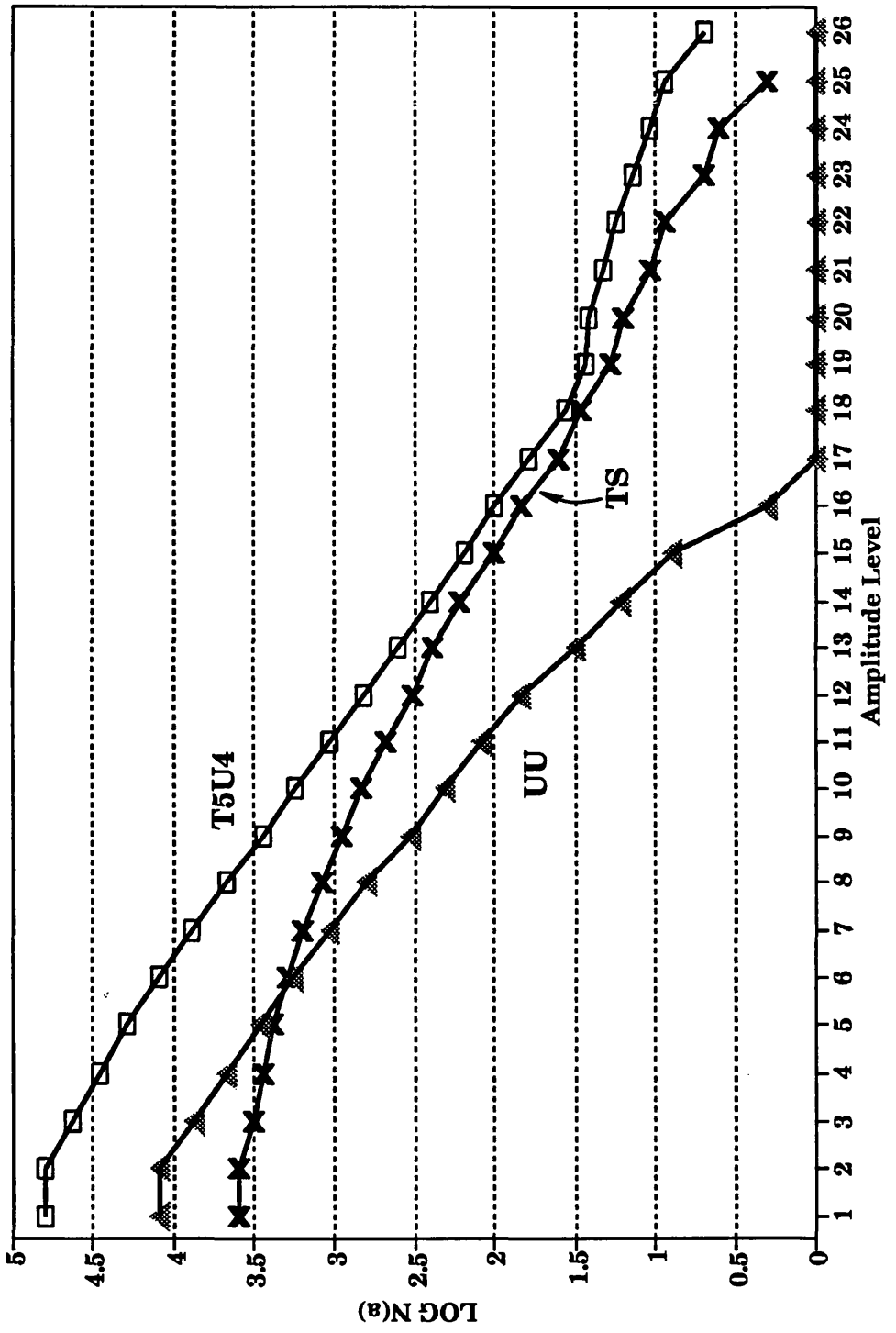

Figure 4.20 - Typical plots of AE amplitude distribution at failure stress for unidirectional CFRC composites heat treated at 1100°C.

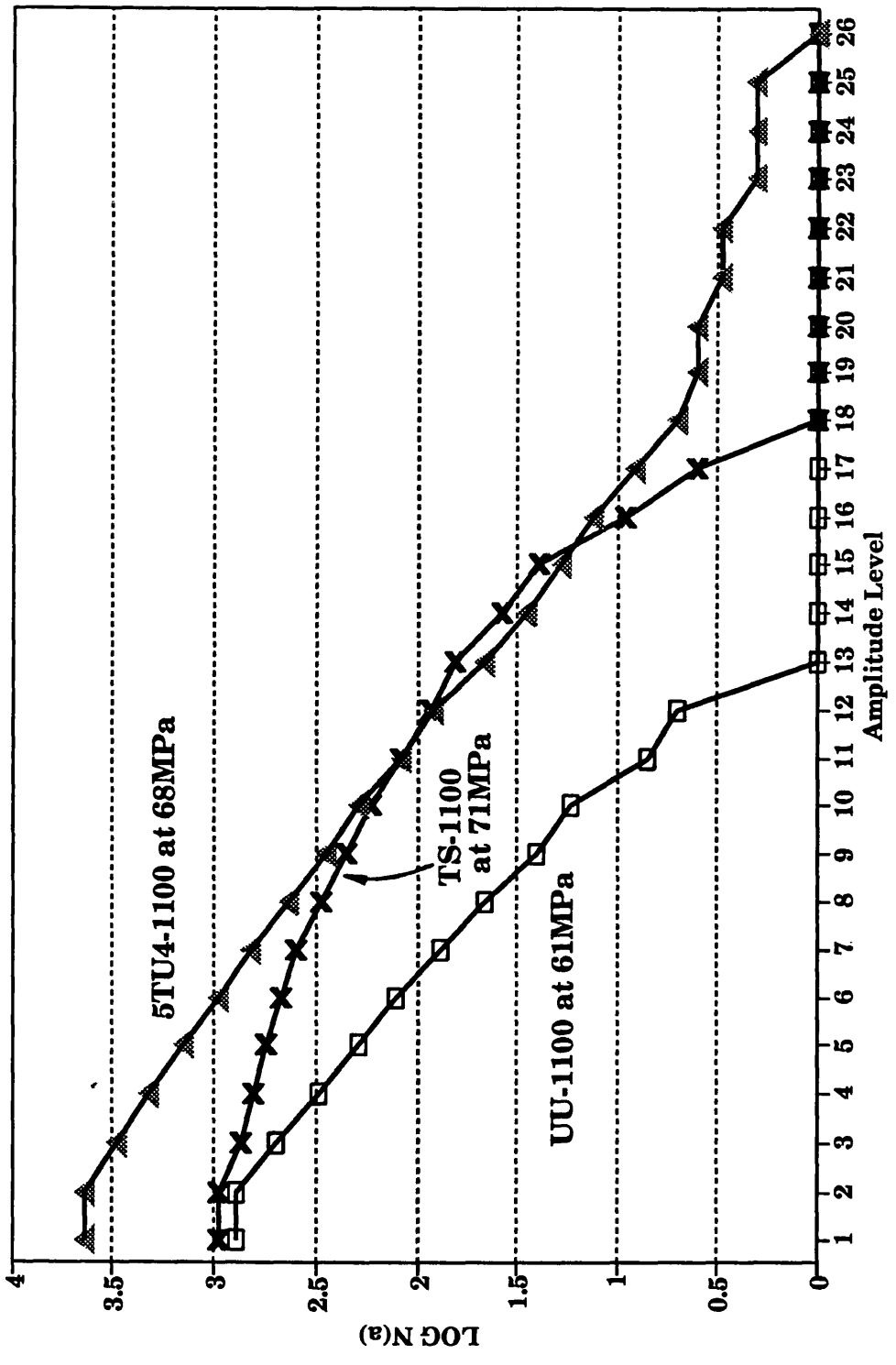

Figure 4.21 - Typical plots of AE amplitude distribution taken at the linear elastic range for unidirectional CFRC composites heat treated at 1100°C, at a mid-span deflection of 0.5 mm.

4.5.2 - Acoustic emission from CFRC composites heat treated to 2500°C

Typical stress-deflection curves with their associated AE are shown in Figure 4.22. Although for each of the composites the development of AE during the bend tests is similar in form to those found for the CFRC composites heat treated to 1100°C, in the case of the TS-2500 composite there is an increase in the total number of AE events at fracture compared to the TS-1100 composite, Table 4.4, but for the other two materials there is a reduction in AE events upon heat treatment. The development of AE found for the T5U4-2500 composite follows closely that found for the UU-2500 material, Figure 4.22, suggesting that the number of AE events from the hybrid material is dominated by those from the U laminae. The changes in AE from the three composites after heat treatment may be attributed to the effects of stress graphitisation. In the case of the TS-2500 material the development of shrinkage cracks at the fibre-matrix interface increases the extent of sub-critical microcracking, so generating additional AE. For the other two materials the development of a graphitic structure facilitates fibre bundle sliding, in the U laminae in the case of the hybrid material, leading to reductions in AE.

The AE amplitude distributions for the UU-2500 and T5U4-2500 composites, Figure 4.23, fit the Pollock power law in the range N(a) $\approx 10^2$ to $\approx 10^4$ counts and the values of the exponent b for these materials are similar to those for the UU-1100 and T5U4-1100 composites, Table 4.3. The AE amplitude distribution for the hybrid material lies roughly parallel to that of the UU-2500 composite at low amplitudes and parallel to that of the TS-2500 at high amplitudes; a similar result was also found for the T5U4-1100 hybrid composite, Figure 4.21. Thus, there appears to be only a small effect of heat treatment from 1100 to 2500°C upon the AE amplitude distributions for these composites, perhaps reflecting the similar fracture modes of the

materials heat treated to 1100°C and 2500°C. The AE amplitude distributions for the TS-2500 material fit the Pollock law for N(a) > $\approx 10^3$, giving an exponent b=0.96. This is a higher value of b than was found for the TS-1100 composite, and it reflects an increase in the proportion of low amplitude AE events. It is possible that this increase is the result of an increasing proportion of low energy events in the fracture process, such as extensions of the microcrack network seen in Figure 4.9A and cracking at the fibre/matrix interface.

Figure 4.24 shows AE distributions taken in the linear elastic range for CFRC composites heat treated at 2500°C at a strain to failure represented by a mid-span deflection of ≈0.5 mm. For UU-2500 composite the AE amplitude distribution fits the power law in the range ≈10 to $\approx 10^3$ counts and for the T5U4-2500 composite in the range $\approx 10^{1.5}$ to $\approx 10^3$ counts giving b values of 2.10 and 1.78, respectively. There are no AE events with amplitudes greater than 30 dB (channel numbers > 12) for the UU-2500 composite or greater than 37 dB (channel numbers > 15) for T5U4-2500 material. For the TS-2500 composite the AE amplitude distribution fits the power law in the range $\approx 10^{2.5}$ to $\approx 10^4$, giving a b value of 1.08. These b values are only slightly higher than the counterparts at the failure stress, Table 4.4, suggesting that a higher proportion of low energy AE events are dominant in the linear elastic range.

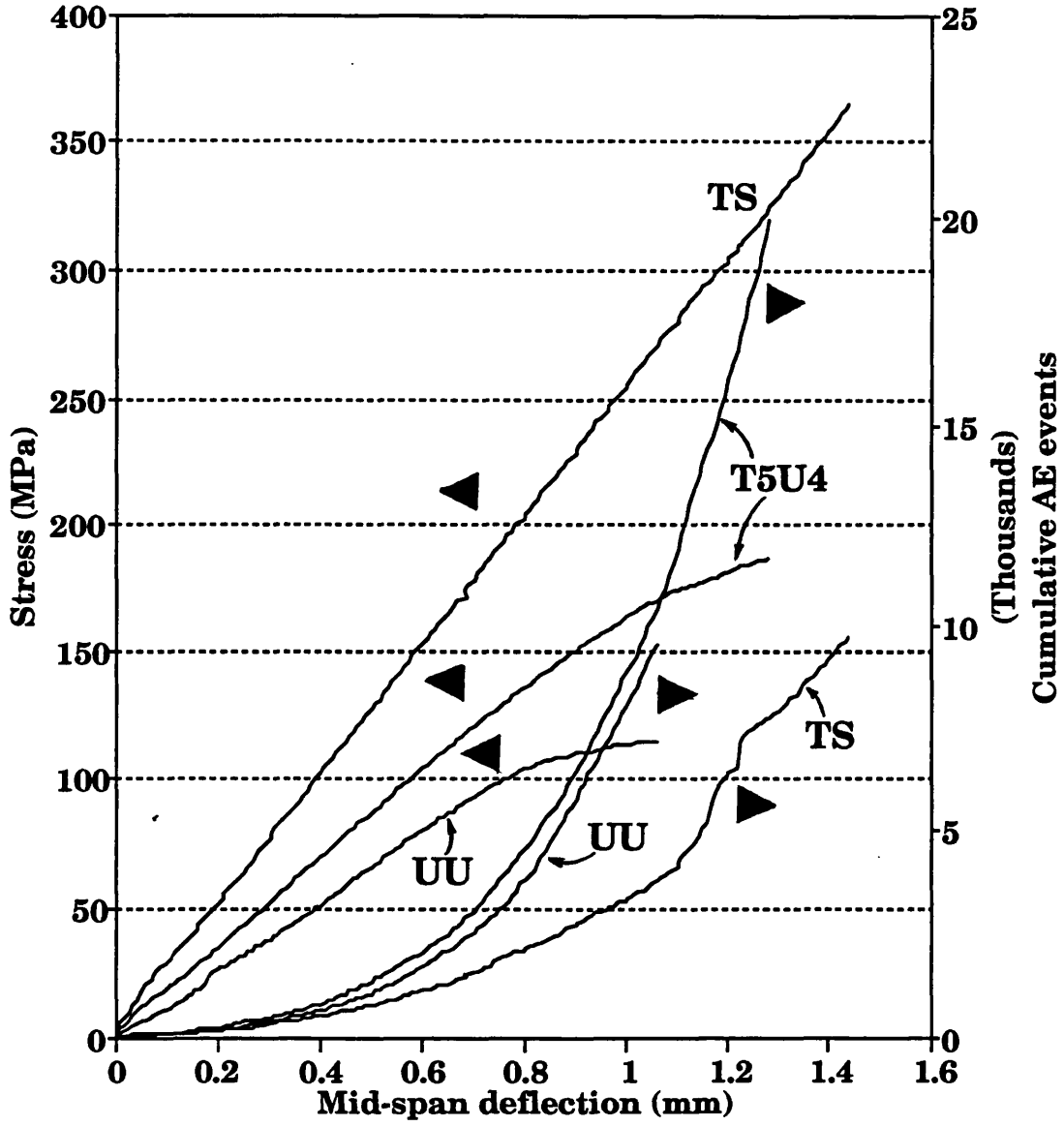

FIGURE 4.22 - Typical plots of stress and AE counts as a function of the mid-span deflection for unidirectional CFRC composites heat treated to 2500°C, subjected to loading to failure in flexure.

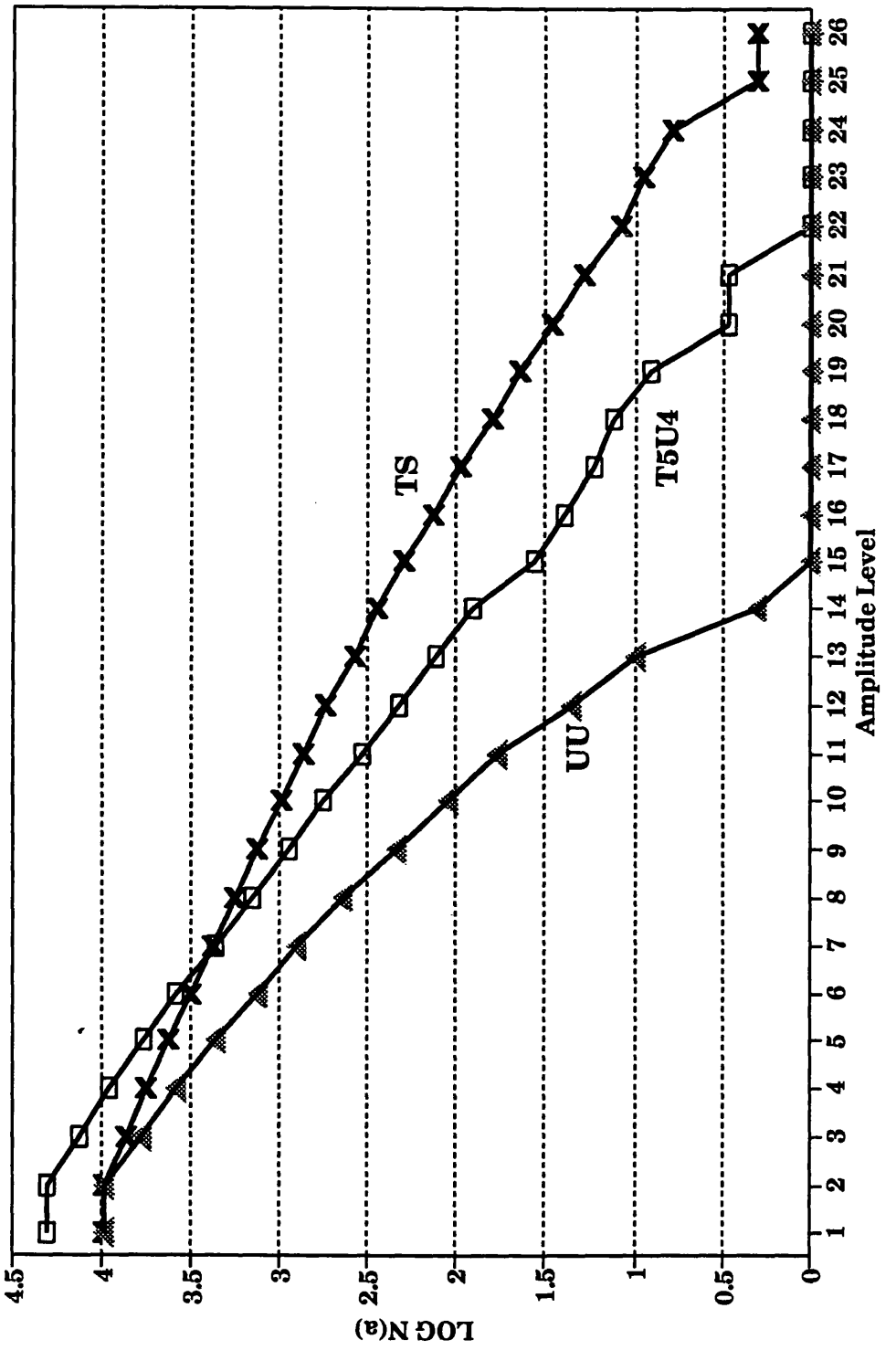

FIGURE 4.23 - Typical plots of AE amplitude distribution at failure stress for unidirectional CFRC composites heat treated to 2500°C.

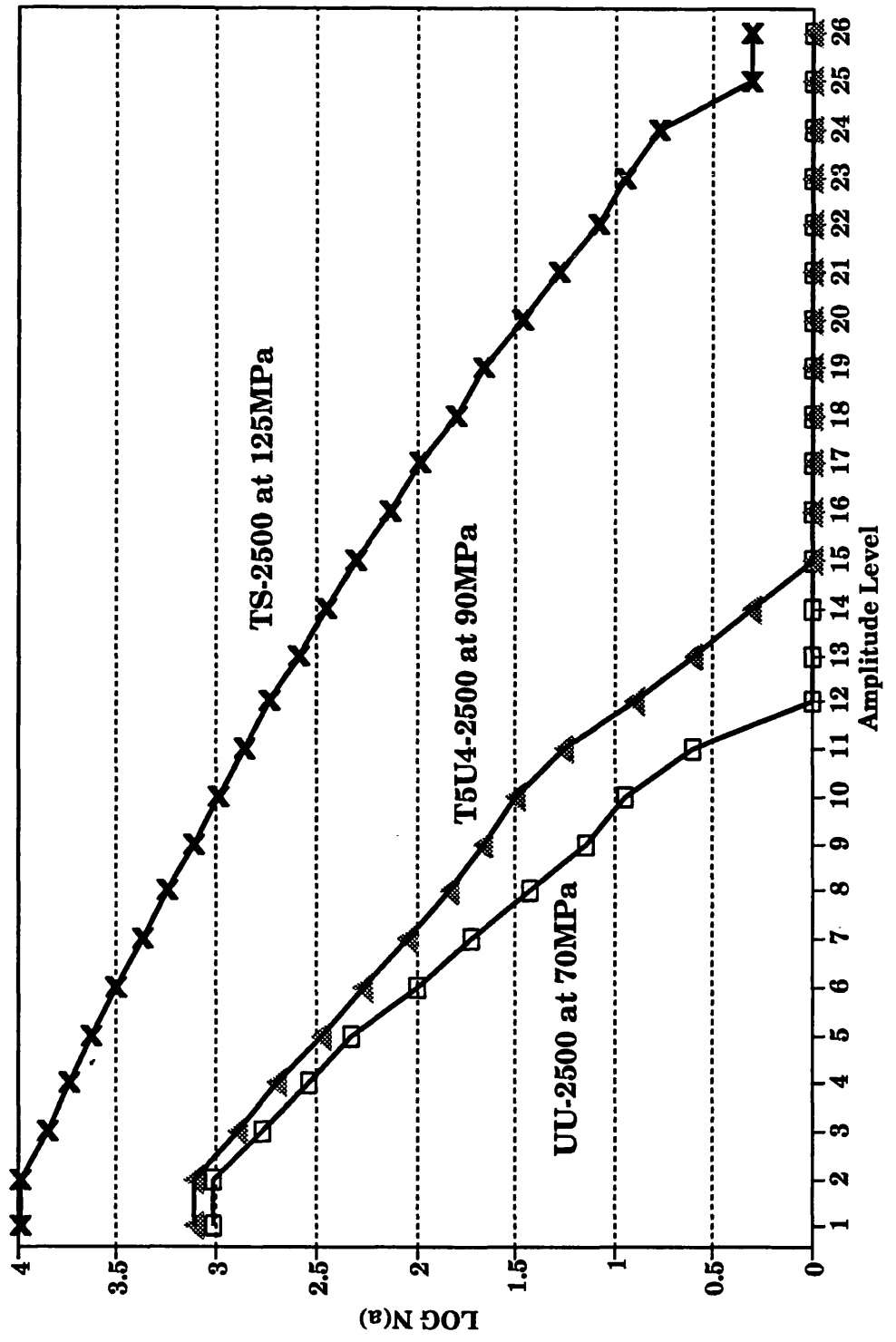

Figure 4.24 - Typical plots of AE amplitude distribution taken at the linear elastic range for unidirectional CFRC composites heat treated at 2500°C, at a mid-span deflection of 0.5 mm.

4.6 - Thermogravimetric analysis of unidirectional CFRC composites

The oxidation behaviour of the unidirectional CFRC composites under a heating rate of 5°C/min is shown in Figure 4.25. Four model composites were chosen to perform the analysis, TS-1100, UU-1100, TS-2500 and UU-2500 material. The results are presented in Table 4.5. Composites heat treated to 1100°C, Figure 4.25A, lost absorbed moisture at ≈100°C, indicated by a small depression in the TG curve and a peak in the DTG curve. For the TS-1100 composite the onset of oxidation is at ≈460°C and for the UU-1100 material the onset of oxidation starts is ≈440°C. Also the limiting oxidation rate reached at ≈750°C is greater for the UU-1100 composite (≈-0.79 %/min) than for the TS-1100 (≈-0.64%/min). These differences are explained by the fact that the UU-1100 composite has more open porosity, caused by unbonded fibres, Figure 4.7, and as a consequence it has a high exposed surface area; therefore the UU-1100 composite is more susceptible to the oxygen attack.

An improvement in the oxidation resistance by delaying the oxidation onset temperature and reducing the limiting oxidation rate is clearly observed, when heat treating the unidirectional CFRC composites from 1100°C to 2500°C. Figure 4.25B shows the TG and DTG curves for TS-2500 and UU-2500 composites. These composites shows no evidence of evolution of moisture at ≈100°C. The presence of absorbed water in the CFRC composites heat treated at 1100°C is probably due to the presence of polar oxygen-containing groups which were eliminated on heat treatment to 2500°C. The oxidation temperature onset of the TS-2500 composite increased to ≈660°C and the limiting oxidation rate decreased from ≈-0.64%/min to ≈-0.50%/min compared with the TS-1100 composite. For the UU-2500 composite the oxidation onset temperature also increased to ≈600°C and the limiting oxidation rate decreased from ≈-0.79 %/min to ≈-0.69%/min. These results show that there is an overall increase in the

oxidation onset temperature of ≈40% and an overall decrease in the limiting oxidation rate of ≈12% for both composites. Reductions in reactivity of all types of carbon on heat treatment to graphitising temperatures is a well-know phenomenon.

Table 4.5 - Thermogravimetric data for oxidation of unidirectional CFRC composites

CFRC composite	Oxidation onset temperature (°C)	Limiting oxidation rate (%/min)
UU-1100	440	- 0.79
TS-1100	460	- 0.64
UU-2500	600	- 0.69
TS-2500	660	- 0.50

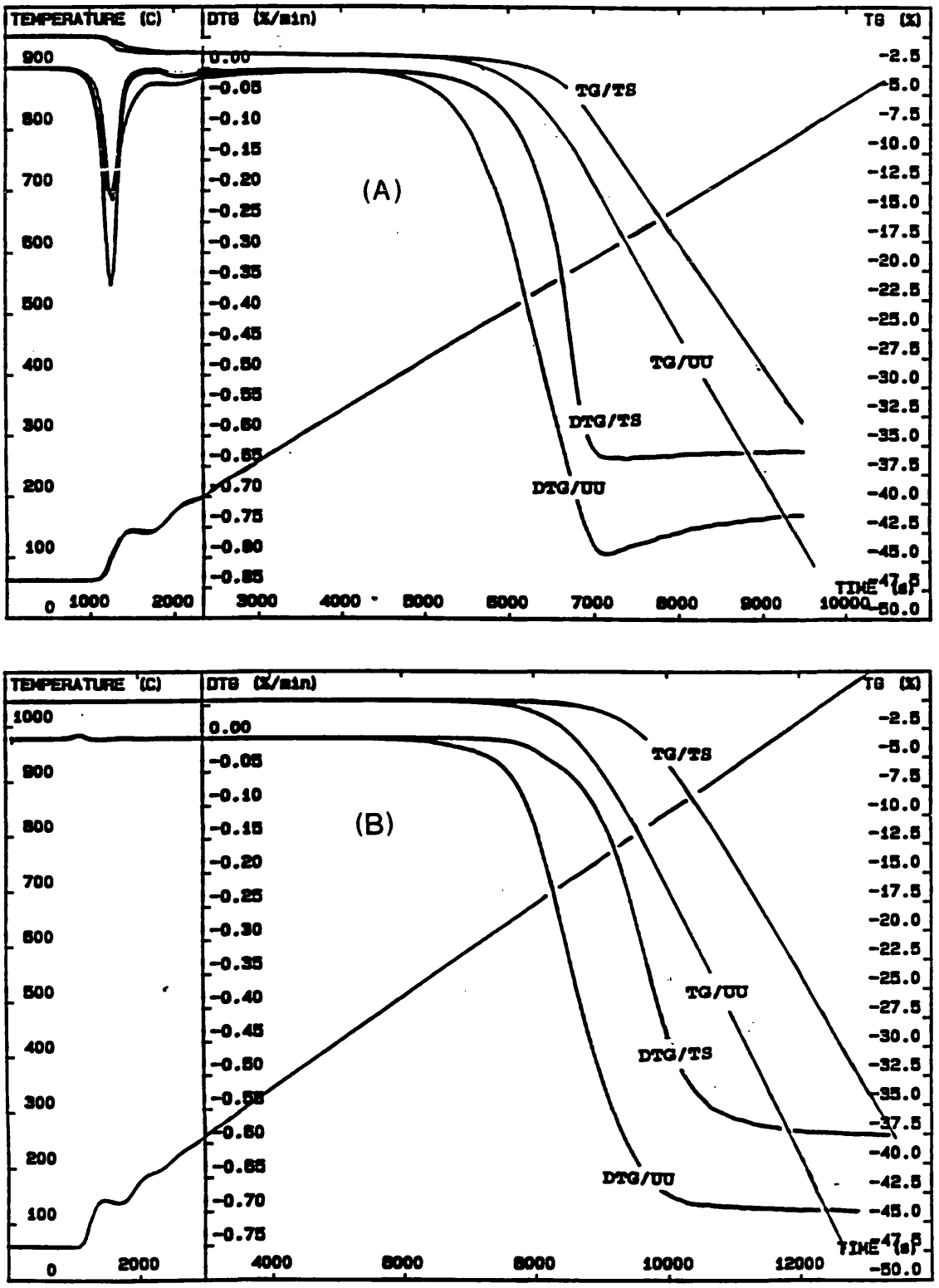

FIGURE 4.25 - Thermogravimetry (TG) and Differential Thermogravimetry (DTG) of unidirectional CFRC composites heated in flowing air. A - TS-1100 (wt = 441.02 mg), UU-1100 (wt = 392.15 mg); B - TS-2500 (wt = 453.3 mg), UU-2500 (wt = 385.9mg).

CHAPTER FIVE
MODIFIED UNIDIRECTIONAL C-SiC COMPOSITES RESULTS AND DISCUSSIONS

This chapter describes the experiments that were carried out to obtain a carbon fibre reinforced carbon composites modified by the SiC sol-gel system. A specific heat treatment schedule was developed for carbonisation/firing of the unidirectional composites and their mechanical properties were evaluated. Results on acoustic emission monitored during bending in some of the specimens are also presented.

5.1 - Introduction

The hybrid composites consisting of carbon fibre reinforced carbon-SiC matrix were obtained using the formulation of the SiC sol-gel system described in Chapter Two, Section 2.1.4.1. Three methods were used to obtain a C-SiC composite using the SiC sol-gel system, and these are shown schematically in Figure 5.1, as follows:

(A) incorporation of the SiC sol-gel system into the impregnating phenolic resin at the filament winding stage;

(B) incorporation of the SiC sol-gel system in between plies of the *green* composite at the lay-up stage;

(C) incorporation of the SiC sol-gel system by brushing the surface of the CFRC composite.

The method (A) was carried out using the fabrication steps of the *green* body unidirectional carbon fibre/phenolic resin laminate and the SiC sol-gel system was incorporated as a mixture with the phenolic resin in the filament

winding stage. The composite was moulded in a similar way to the conventional carbon fibre/phenolic laminate but a different heat treatment schedule was used, as described in Chapter Two, Section 2.4.2. The method (B) was carried out also using the fabrication steps of the *green* body of the carbon fibre/phenolic resin laminate. The SiC sol-gel system was brushed in between plies of carbon fibre/phenolic prepregs before the lay-up stage. The moulding steps used to obtain the *green* matrix composite were similar to the one used for the conventional carbon fibre/phenolic laminates. The heat treatment schedule used in this method was the same as that used in method (A). Method (C) was carried out as a consequence of the results obtained with the commercial CFRC composites, Chapter Three, and with the unidirectional CFRC composites, Chapter Four, which were brush coated and fired with the SiC sol-gel system, following the procedure described in Chapter Two, Section 2.1.4.1.

The preliminary results obtained using method (A) were not satisfactory. The mixture of phenolic resin in the SiC sol-gel system was suitable to impregnate the carbon fibre tows during the filament winding procedure, but, after the carbonisation/firing of the unidirectional C-SiC laminate, a very porous material was obtained with poor integrity and, consequently, it was not suitable to measure mechanical properties. The porous structure of the unidirectional C-SiC reinforced material is possibly caused by the large amount of solvent of the SiC sol-gel system that was not easily removed during the early processing stages of the composite. Therefore, it was decided not to carry on work with method (A). Composites with good integrity using method (A) can possibly be obtained using other fibre preforms, such as bidirectional and fibre felts, and also using hypercritical drying as a processing method, but such work is outside of the scope of this research project. Methods (B) and (C) are discussed in the next sections.

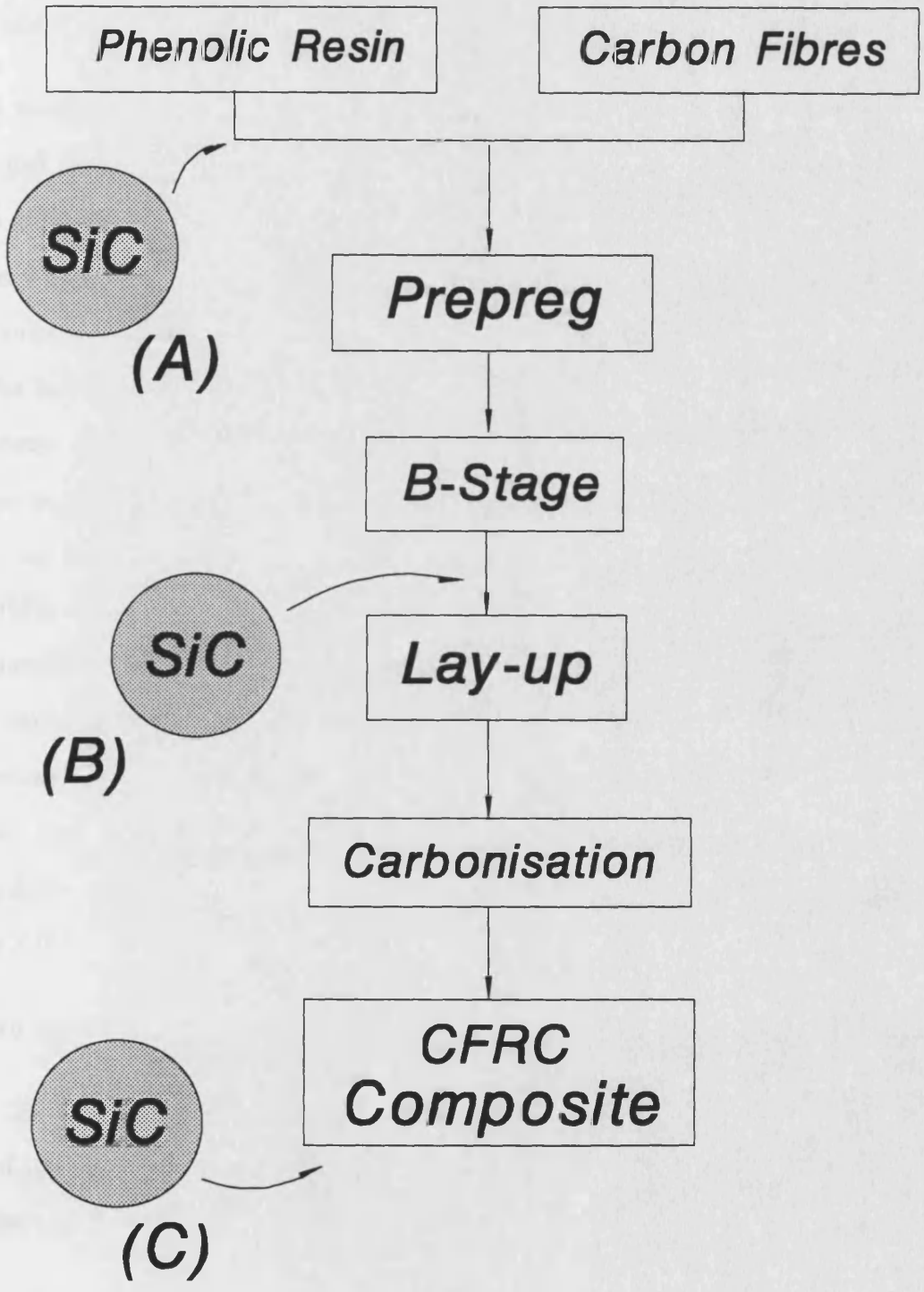

FIGURE 5.1 - Schematic diagram of possible ways of incorporation of SiC sol-gel system on carbon fibre reinforced composites.

5.2 - Unidirectional CFRC composites modified by interlaminar SiC

5.2.1 - Introduction

The modification of unidirectional CFRC composites by the interlayer SiC sol-gel system (method B) was carried out using similar techniques as used to obtain the conventional unidirectional CFRC composites. Prepreg laminae were obtained by the filament winding technique. Also the solvent of the impregnating resin was removed until a tacky lamina was obtained. Once the laminae were ready for the lay-up step of the process, the SiC sol-gel system was applied by brushing on each face of the laminae. These laminae were left to dry at room temperature for nearly half an hour before the lay-up was carried out. The uncured laminate is then hot pressed and cured following the heating schedule given in Chapter Two, Section 2.2. After complete curing, the as-cured *green* composite was then trimmed to the same approximate dimensions as used for the conventional CFRC composites (≈3.5mmx8mmx135mm), packed in coke breeze in a graphite crucible and carbonised/fired in a horizontal furnace in a flowing argon atmosphere, up to 1400°C, using the multi-stage heating schedule shown in Figure 2.5.

Two model composites were prepared:

a) 10 unidirectional laminae, with treated and sized fibres, where the SiC sol-gel system was brushed in between each ply, and identified as TS-1400-SG, and

b) 10 unidirectional laminae, with untreated and unsized fibres, where the SiC sol-gel system was brushed in between each two plies of the laminate, and identified as UU-1400-SG. The SiC sol-gel was brush coated in between each two plies because, at that stage of the work, the untreated

and unsized carbon fibre tows were filament wound twice before being removed from the winding drum.

5.2.2 - Microstructure of the *green* CFRC composites modified by the interlayer SiC sol-gel system

Figure 5.2 shows optical micrographs of cross and longitudinal sections of a green CFRC composite modified by the interlayer SiC sol-gel made with untreated and unsized fibres. The interlaminar region (I) can be also clearly identified. This composite is also characterized by the presence of unbonded fibres as found for previous CFRC composites made with untreated and unsized fibres. The characteristic pattern of unbonded fibres can only be clearly seen in the longitudinal view of the composite, Figure 5.2B, with large slit pores in between fibre bundles. The thickness of the fibre laminae both in cross (U1) and longitudinal (U2) sections varies between 400-500 μm.

Figure 5.3 shows optical micrographs of cross and longitudinal sections of a *green* CFRC composite modified by the interlayer SiC sol-gel made with treated and sized fibres. Similarly to Figure 5.2, the interlaminar region (I) composed of the alkoxide sol-gel and phenolic resin matrix can be clearly seen in both micrographs, having a thickness between 60-120 μm and it seems to be uniform. The laminae of the composite, T1 in the cross section, Figure 5.2A, and T2 in the longitudinal section, Figure 5.2B, have a thickness of 250-350 μm. A comparison of Figure 5.2B and 5.3B shows that the fibres are well-bonded to the matrix in the latter case. The micrographs described above are similar to those of the conventional CFRC composites discussed in Chapter Four. However in the case of composites with interlaminar alkoxide gel the interface between laminae are more clearly distinguished.

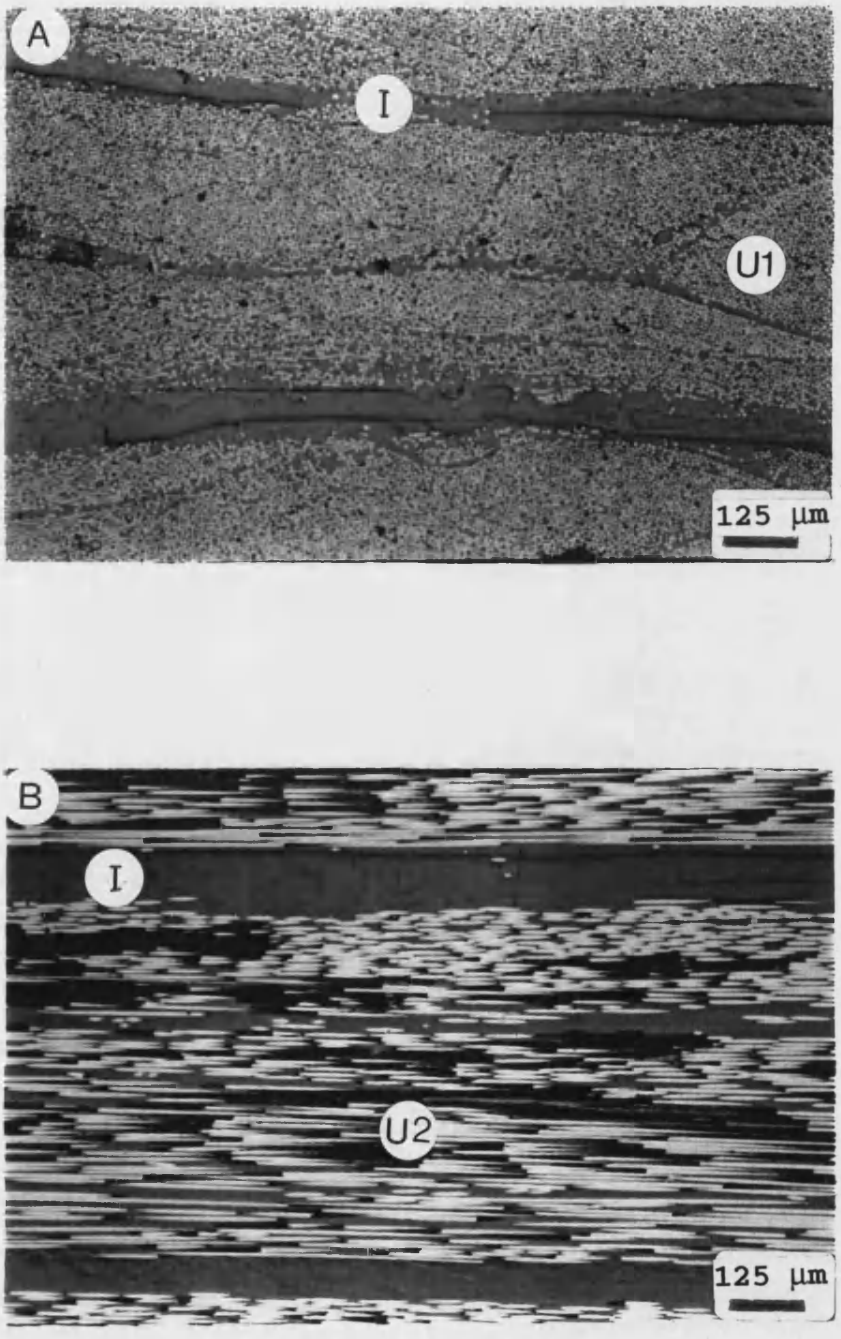

Figure 5.2 - Transverse (A) and longitudinal (B) section of a *green* CFRC composite modified by interlaminar SiC made with untreated and unsized fibres. U1 - transverse laminae, U2 - longitudinal laminae, I - interlaminar region.

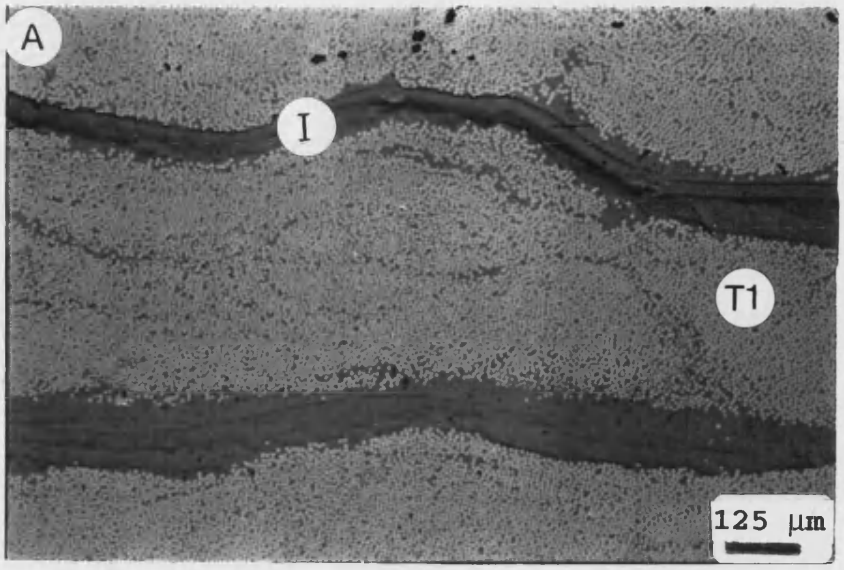

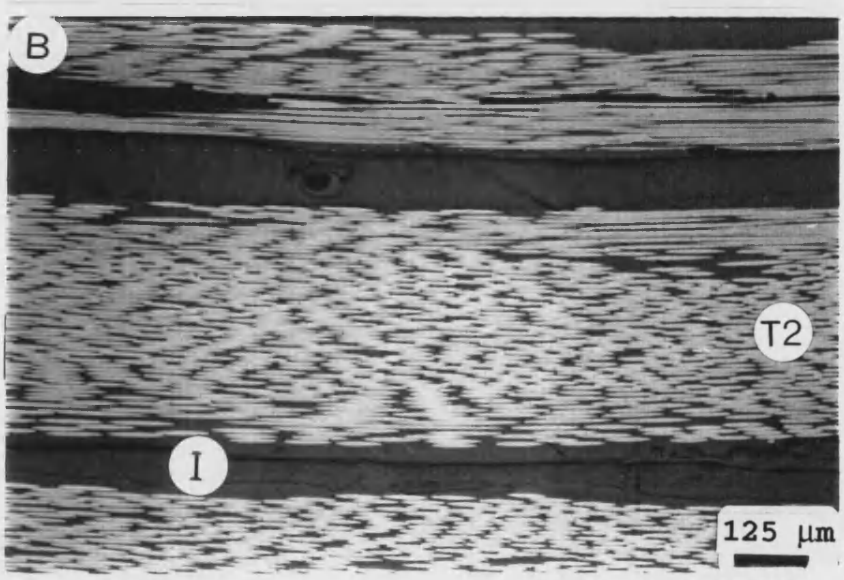

Figure 5.3 - Transverse (A) and longitudinal (B) sections of a *green* CFRC composite modified by interlaminar SiC made with treated and sized fibres. T1 - transverse laminae, T2 - longitudinal laminae, I - interlaminar region.

5.2.3 - Microstructure of fired unidirectional CFRC composites modified by the interlayer SiC sol-gel system

Figure 5.4 shows typical optical micrographs for (A) cross and (B) longitudinal sections for a fired CFRC composite with interlayer SiC. The general features of CFRC composites made with untreated and unsized fibres are also seen in the present one, *i.e.* unbonded fibres and an extensive microcrack network. The interlayer SiC plus carbon residue (I_{SiC}) is clearly distinguished in both micrographs and it is cracked. These cracks in the interlayer SiC are formed during firing to 1400°C since they are not seen in the green composites, Figure 5.2. The laminae (U) are also clearly distinguished having a thickness of ≈750 μm, and the interlaminar region (I) where SiC is present has a thickness of 50-70 μm. There is also an interface (I_L) inside the laminae (L) formed during the filament winding stage, as in this composite the fibre tows were filament wound twice before removal from the winding drum. Pores (P) are also seen in the interlayer SiC, possibly formed during the carbonisation/firing of the *green* composite.

Figure 5.5 shows a typical optical micrograph of (A) cross and (B) longitudinal sections of a TS-1400-SG composite. The lamina (T) is clearly identified in both micrographs but its thickness is not regular, as seen in the cross section, Figure 5.5A. The SiC in the interlaminar region (I) appears to be formed as clusters rather than as a continuous layer with pores (P). The micrograph also shows that the laminae have a thickness between 150-350 μm, and the interlaminar region (I) has a thickness between 120-250 μm. Slit cracks are also seen within and running parallel to the laminae. These slit cracks are not seen in the *green* stage, suggesting that they are formed during the carbonisation/firing stage.

Figure 5.6 shows an X-ray map for a longitudinal section of a

UU-1400-SG composite. These micrographs provided the first evidence that the heating schedule devised for carbonising/firing this composite resulted in the formation of SiC. The SiC is identified in the micrograph by the white areas in the bulk composite following the contours of the laminae (L). Some agglomerates of SiC (A) are formed inside the laminae, possibly filling pores. This indicates that some of the alkoxide sol-gel has infiltrated in the lamina during the early stages of lay-up and moulding. Unbonded fibres can facilitate infiltration of the alkoxide sol-gel brush coating, but infiltration is more difficult in the TS-1400-SG composite where well bonded fibres obstruct infiltration of the alkoxide sol-gel during brushing.

An X-ray map for Si on a longitudinal section of the TS-1400-SG composite, Figure 5.7. The interlaminar SiC is identified in the micrograph by the white areas in between fibre laminae (L). The interlaminar SiC is not a continuous layer having a thickness up to 100 μm and it is cracked. Possibly these cracks are formed during the carbonisation/firing of the composite. A secondary electron image (SEI) for the TS-1400-SG composite, Figure 5.7B, also shows bright areas which are related to the SiC in Figure 5.7A. Like the conventional CFRC composites, these hybrid C-SiC materials are porous materials. The microcracks and pores generated during the heat treatment schedule are then suitable for subsequent infiltration of the *sol* alkoxide.

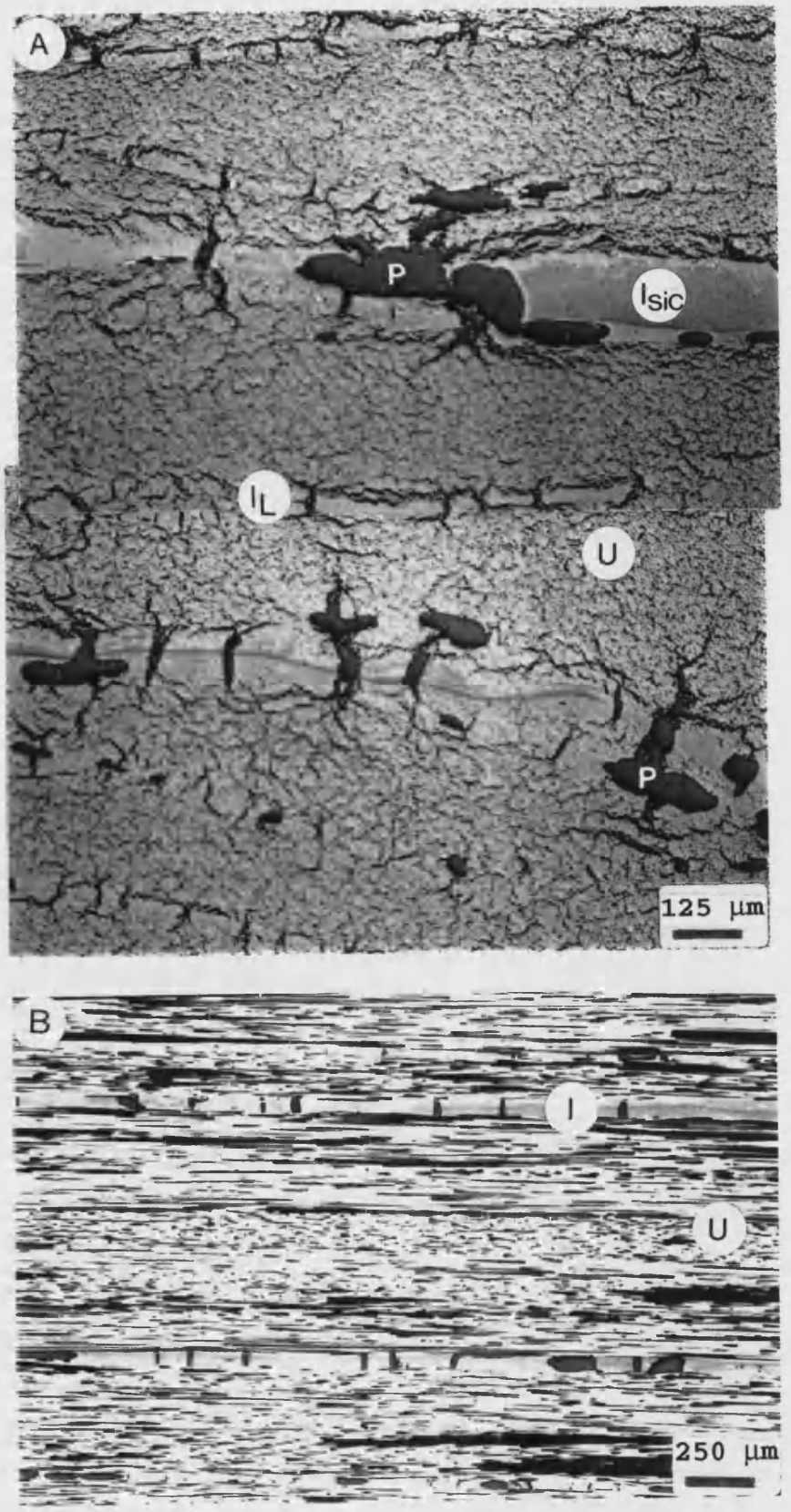

FIGURE 5.4 - Optical micrograph of (A) cross and (B) longitudinal sections of a UU-1400-SG composite, showing features of the SiC in between fibre laminae. Sol-gel brushed in between each two plies. U = lamina, I_L=interlaminar region, I_{SiC}=interlaminar region where SiC is present, P=pore.

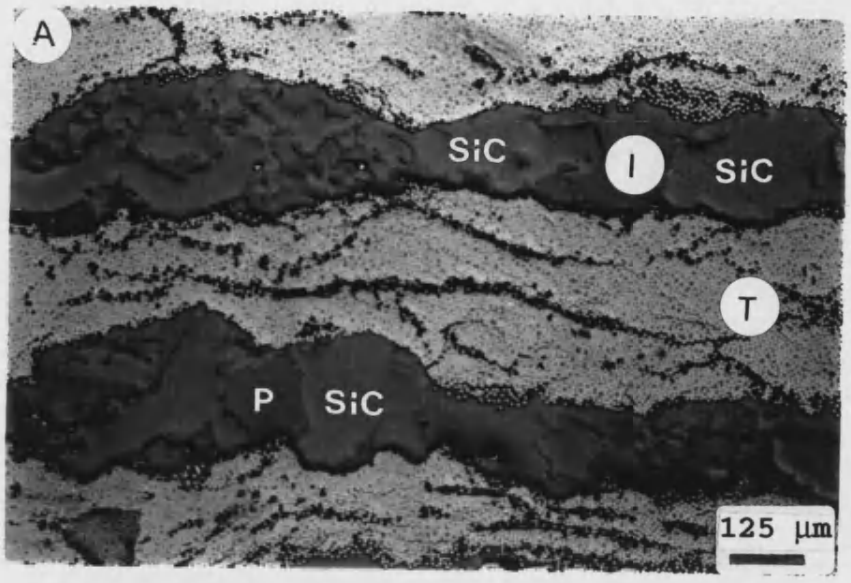

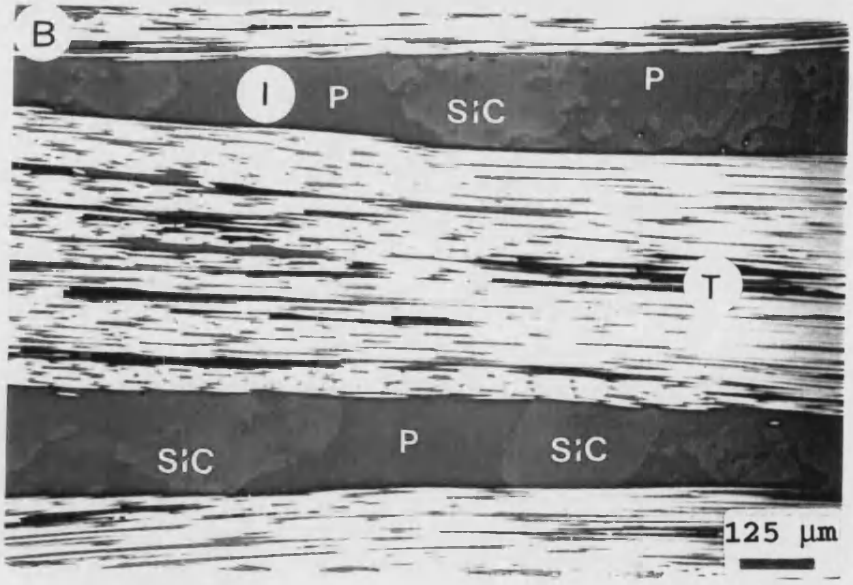

Figure 5.5 - Optical micrograph of a longitudinal section of a TS-1400-SG composite, showing features of the SiC in between fibre laminae. Sol-gel brushed in between each ply. T = lamina, I = interlaminar region, P = pore.

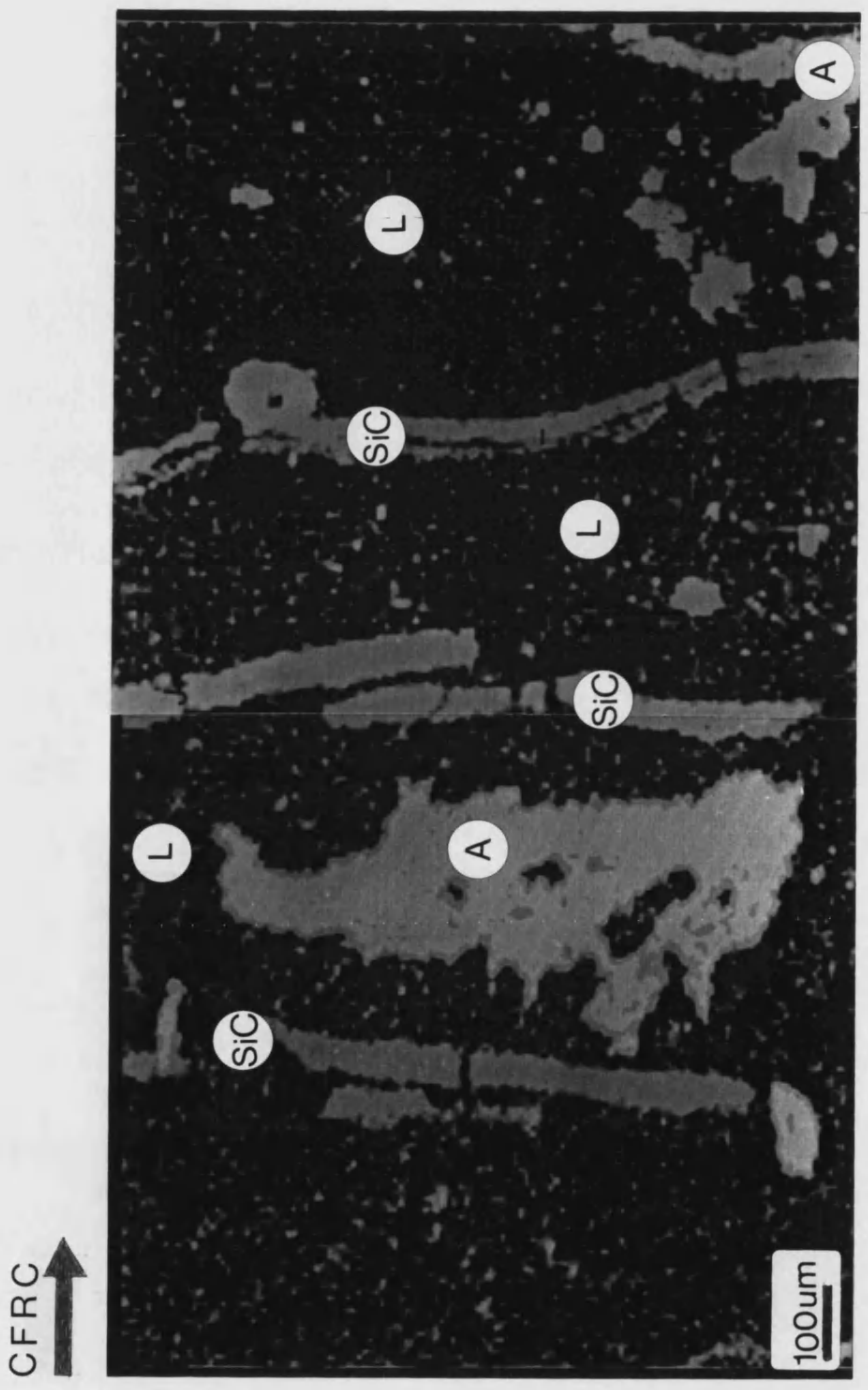

FIGURE 5.6 - X-Ray maps for Si on a longitudinal sectional through the bulk UU-1400-SG composite. L = lamina, A = agglomerates of SiC.

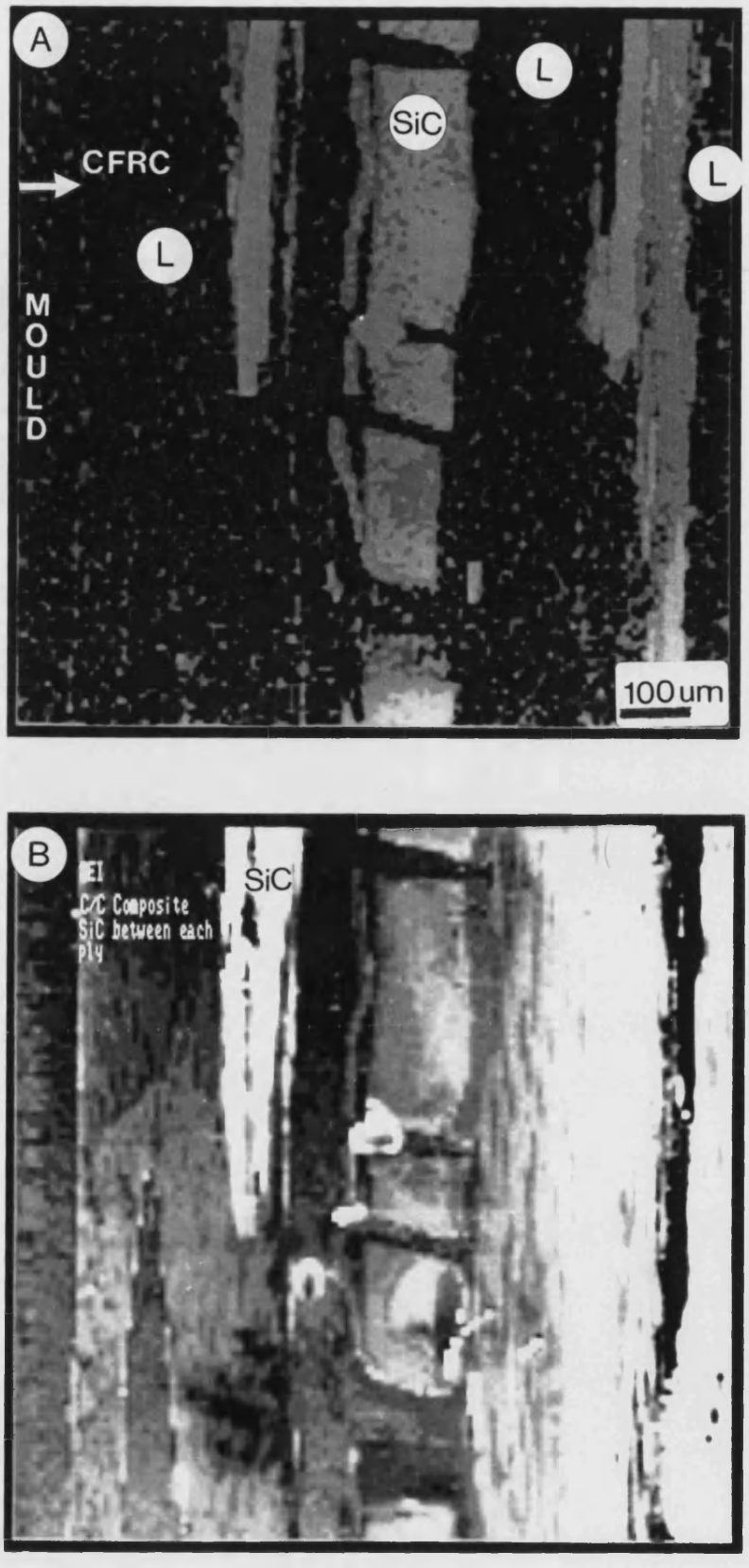

FIGURE 5.7 - (A) Si X-Ray map and (B) corresponding secondary electron image for a longitudinal section through TS-1400-SG unidirectional composite. Sol-gel brushed in between each individual ply. L = lamina.

5.2.4 - Mechanical properties of CFRC composites modified by interlayer SiC sol-gel system

The mechanical properties of the unidirectional composites modified by interlayer SiC sol-gel system are compared to the conventional TS-1100 and UU-1100 CFRC composites, described to Chapter Four, in order to observe differences that arise from the intercalation of SiC sol-gel system in the bulk composite, Table 5.1. The CFRC composites modified by interlayer SiC were heat treated to 1400°C with the heating schedule shown in Figure 2.5, and further weight loss is observed.

No change was found in the flexural strength of the TS-1400-SG composite compared to the TS-1100 composite (95% confidence), although the flexural modulus of the TS-1400-SG material was lower, Table 5.1. The lower density of the TS-1400-SG composite is possibly due to the porous structure created by the interlayer SiC formed during moulding and also by higher heat treatment. Possibly this porous structure is also responsible for the decrease in the modulus of the TS-1400-SG composite compared to the TS-1100 material.

Figure 5.8A shows stress-deflection curves and sketches of failure modes for the TS-1100 and TS-1400-SG composites. Both materials have a brittle failure mode as seen by the sharp drop in the stress after failure. The stress after failure for the TS-1400-SG falls sharply to nearly 5% of the peak stress, but the failure mode of the composite shows that the material does not fall apart like the TS-1100 composite. Delamination cracking in the TS-1400-SG composite suggests that the interlaminar SiC becomes the weak plane leading to a failure mode that can be defined as catastrophic delamination.

Composite	TS-1400-SG	TS-1100	UU-1400-SG	UU-1100
Bulk density (g/cm^3)	1.35±0.02	1.38±0.07	1.33±0.01	1.35±0.04
Flexural Strength ((MPa)	140±10.0	134±22.0	155±9.0	142.5±16
Flexural Modulus (GPa)	90±6.0	114±7.0	82.5±5.0	60±6.0
Mid-span deflection[(a)] (mm)	1.10±0.14	0.85±0.10	1.40±0.13	1.80±0.23
Nominal Fracture Initiation Energy (kJ/m^2)	0.90±0.25	0.56±0.13	1.02±0.13	1.43±0.18

TABLE 5.1 - Mechanical properties of CFRC composites modified by interlayer SiC, derived from the sol-gel system, and compared with conventional unidirectional CFRC composites. (a) at failure stress.

The lower flexural modulus, due to the low density, and higher strain to failure of the TS-1400-SG lead to a higher nominal fracture initiation energy, Table 5.1, suggesting that the interlayer SiC results in an increase in toughness, but the fracture pattern is still catastrophic.

Figure 5.8B shows stress-deflection curves and failure modes for UU-1100 and UU-1400-SG composites. The failure modes from both composites look similar from these curves and fracture modes, suggesting that fibre bundle sliding is still the dominant mechanism in the failure pattern. The UU-1400-SG composite has a significant increase in flexural modulus, Table 5.1, possibly due to the stiffening effect of the interlaminar SiC. A reduction in the strain to failure of the UU-1400-SG possibly due to the embrittling effect of the interlayer SiC leads to a lower fracture initiation energy.

The mechanical property results obtained on CFRC composites modified by interlayer SiC suggests that the flexural modulus of these CFRC composites is mainly governed by the presence of the interlayer SiC, despite the different positions that the SiC sol-gel was brushed in between fibre laminae of the TS-1400-SG and UU-1400-SG composites. There is practically no effect of SiC on the flexural strength of the composites that could be detected, possibly due to the large scatter of data.

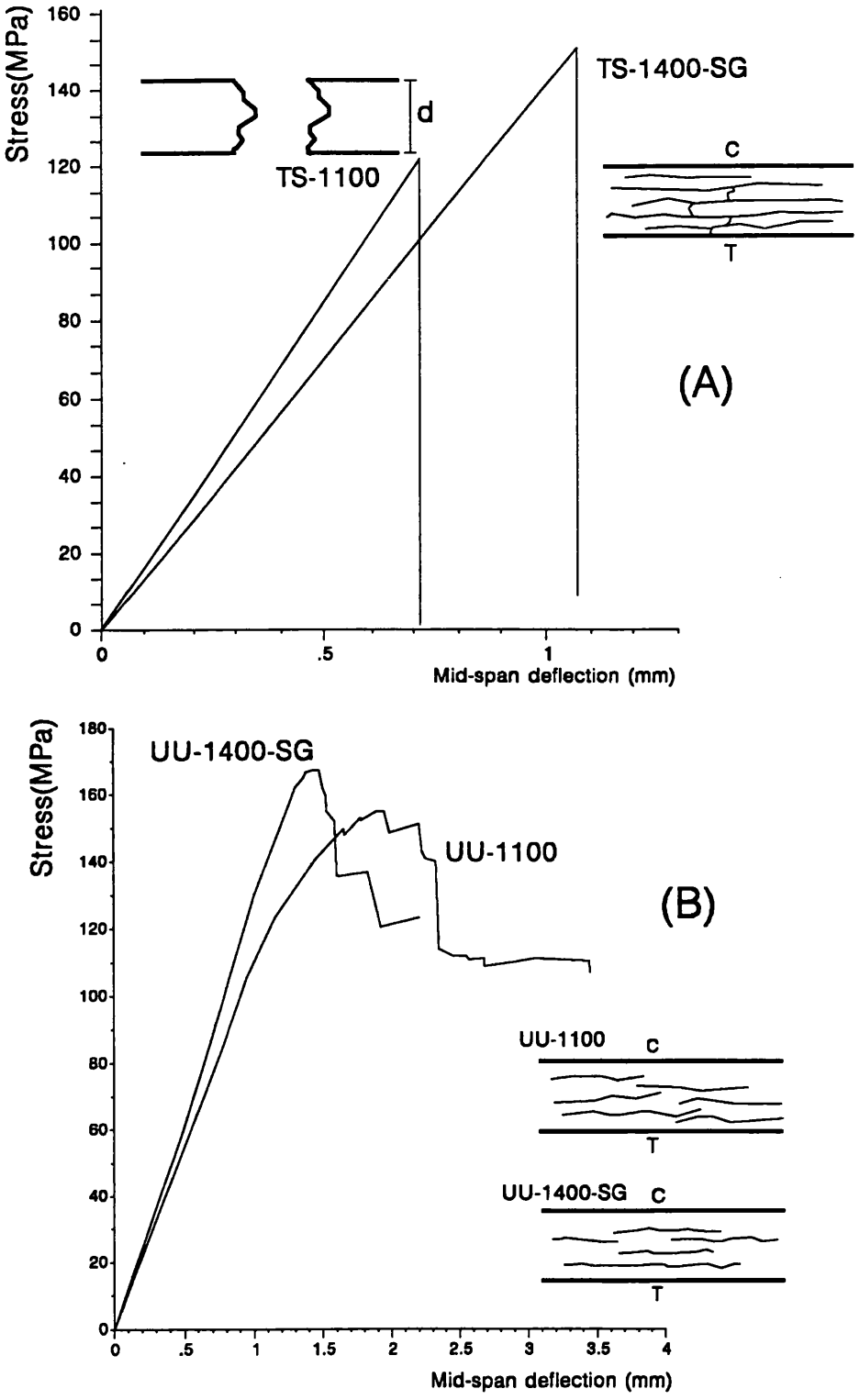

FIGURE 5.8 - Stress-deflection curves and failure modes for a CFRC composites. (A) CFRC composite made with treated and sized carbon fibres modified by interlaminar SiC (TS-1400-SG), (B) CFRC composite made with untreated and unsized fibres modified by interlaminar SiC (UU-1400-SG).

5.3 - CFRC composites modified by SiC sol-gel brush coating

Four contrasting unidirectional CFRC composites were used in this part of the work:

(1) TS-1400-SiC is a unidirectional CFRC composite made with treated and sized fibres heat treated to 1100°C and then subject to brush coating with SiC sol-gel system and fired to 1400°C five times;

(2) UU-1400-SiC was prepared in a similar way to TS-1400-SiC, except that untreated and unsized fibres were used.

(3) TS-2500-SiC is a unidirectional CFRC composite made from treated and sized fibres heat treated to 2500°C and then subject to brush coating with SiC sol-gel system and fired to 1400°C five times.

(4) UU-2500-SiC was prepared in a similar way to TS-2500-SiC, except that untreated and unsized fibres were used.

5.3.1 - Microstructure of SiC brush coated CFRC composites

The characterization of the SiC coating in the unidirectional CFRC composites was done using optical microscopy and Si X-ray mapping. Figure 5.9A shows an optical micrograph of a transverse section through the bulk UU-1100 composite, and the UU-1400-SiC composite, Figure 5.9B. The fractal nature of the microcrack network pattern of the UU-1100 composite almost disappears when this material is brush coated and fired with SiC sol-gel. This shows that the SiC sol-gel penetrates deeply inside the composite filling many of the microcracks. The area R-R' shows a SiC rich region linking pores in the UU-1400-SiC composite suggesting that the SiC penetrates via the network of large pores in the composite.

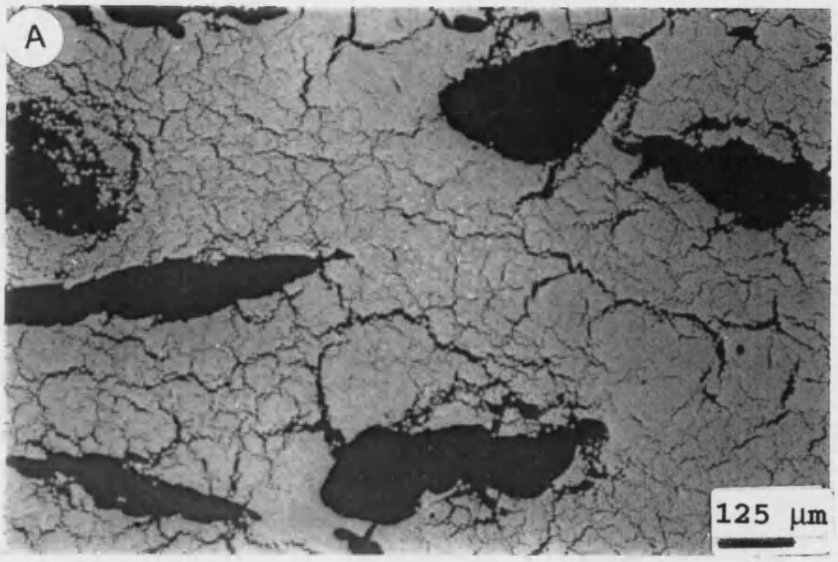

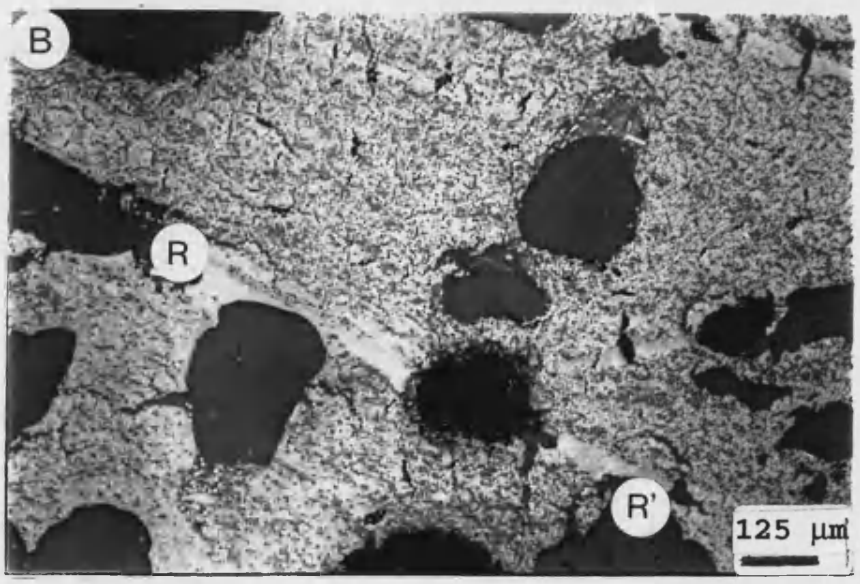

FIGURE 5.9 - Comparative optical micrographs of a transverse section of an uncoated UU-1100 composite (A) and brush coated UU-1400-SiC composite (B). R-R' = SiC rich region linking pores.

The micrographs also suggests that the elliptical shaped pores, 400 μm wide in the UU-1100 composite, are turned to more round ones, 250 μm width, in the UU-1400-SiC with SiC filling corners of these pores.

Figure 5.10 shows optical micrographs of transverse sections of the surface of a TS-1400-SiC at different positions in the sample after applying five brush coatings of SiC sol-gel. It is clear from Figure 5.10A that the ≈120 μm thick SiC coating is not homogeneous as it contains many pores and also has a lamellar character due to multiple coatings. The porous SiC coating is not continuous, as can be seen from Figure 5.10B, which shows an uncoated part of the composite surface, but with SiC filling some of the open cracks. Figure 5.10A also shows a resin rich region, R. SiC coatings form more readily at crack free surfaces of the composite. Where there are cracks, the SiC penetrates into the composite and only a thin, discontinuous coating, or no coating, is formed.

Figure 5.11 shows optical micrographs of transverse cross sections of the UU-2500-SiC composite in a bulk region (A) and on the surface of the sample after applying five brush coatings of SiC sol-gel. It is clear from Figure 5.11B that the ≈120 μm thick SiC coating is similar to that formed on the TS-1400-SiC composite, *i.e.* it is not homogeneous as it contains many pores and also has lamellar character due to multiple coatings. The porous SiC coating is not continuous, as can be seen from Figure 5.11B, which shows a partially coated surface of the composite, but with SiC filling some of the open cracks, T'. SiC rich regions are seen in both micrographs, and are indicated by regions S-S' and T-T'.

Similarly, an optical micrograph of the TS-2500-SiC, Figure 5.12, shows a porous discontinuous coating ≈120 μm thick with an irregular surface contour and with porous SiC bridging some open pores. Figure 5.13 shows a

typical through thickness Si X-ray map for the transverse cross section (≈3.7 mm thick) of a unidirectional TS-2500-SiC composite. The SiC penetrates throughout the thickness of the composite including regions far from the surface, but in a discontinuous and irregular manner. The Si X-ray mapping also shows that deep penetration of SiC into the composite is facilitated by interconnected pores.

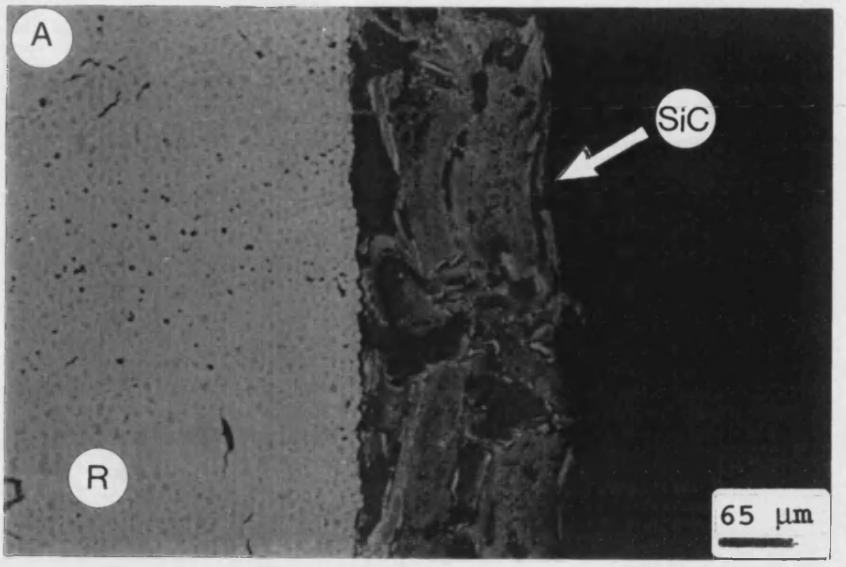

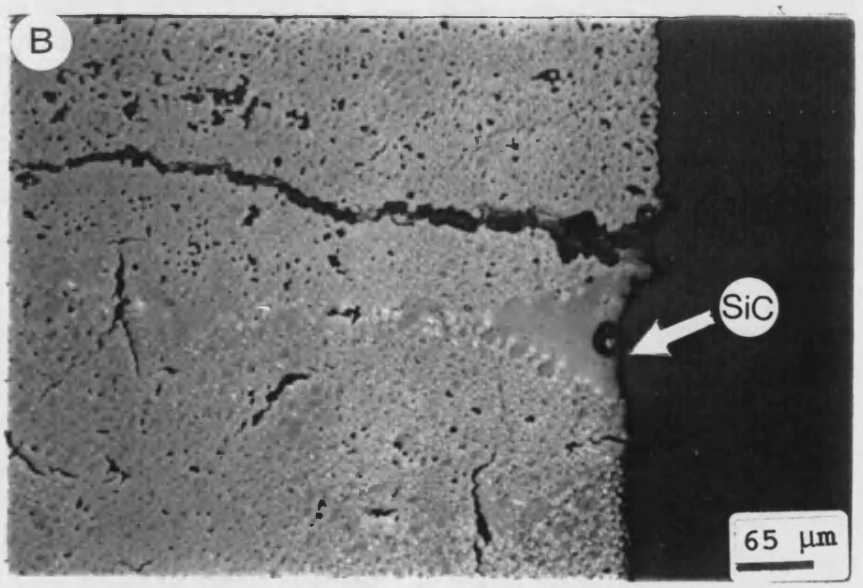

FIGURE 5.10 - Optical micrographs of a transverse section of a brush coated TS-1400-SiC at different positions in the same sample. R= resin rich region.

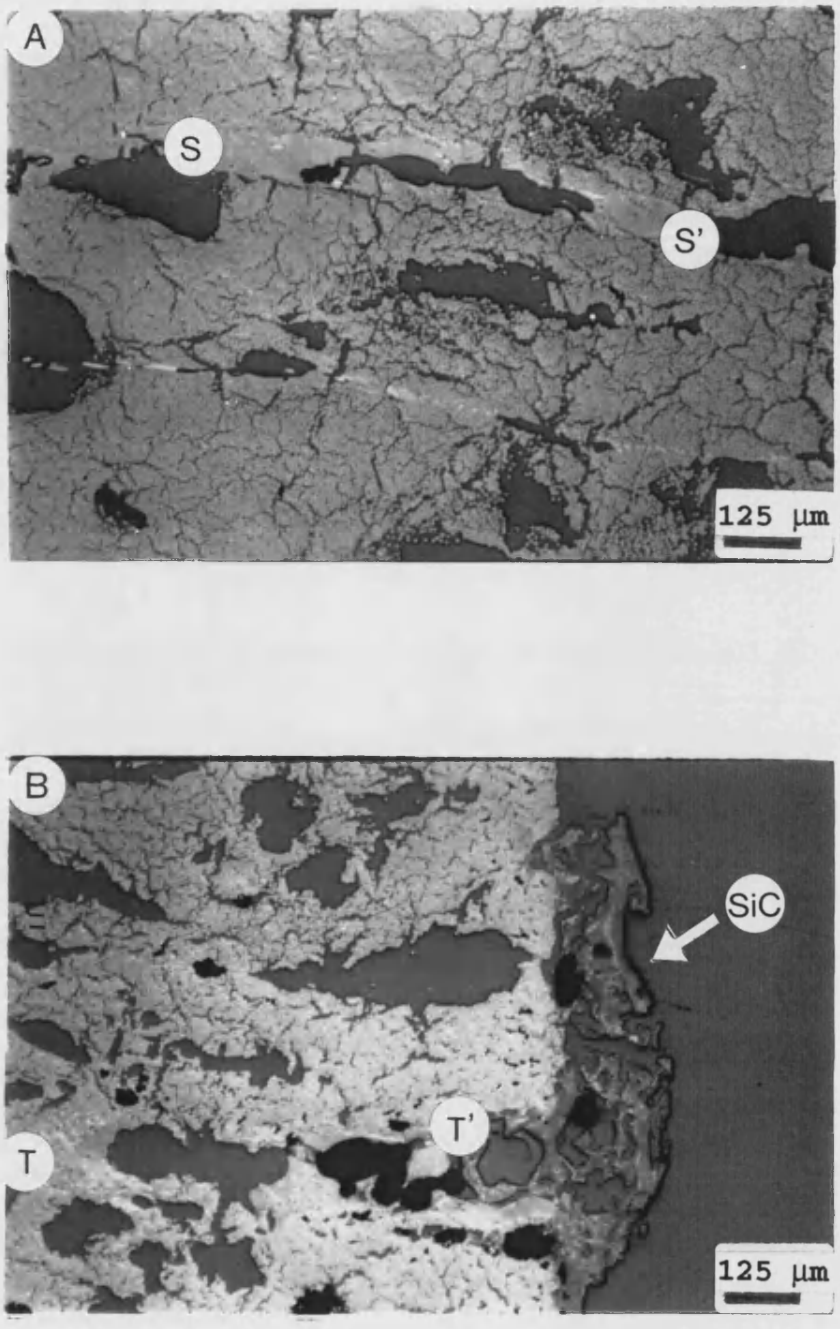

FIGURE 5.11 - Optical micrographs of a transverse section of a SiC coated UU-2500 composite at different positions in the same sample. S-S' and T-T' = SiC rich region.

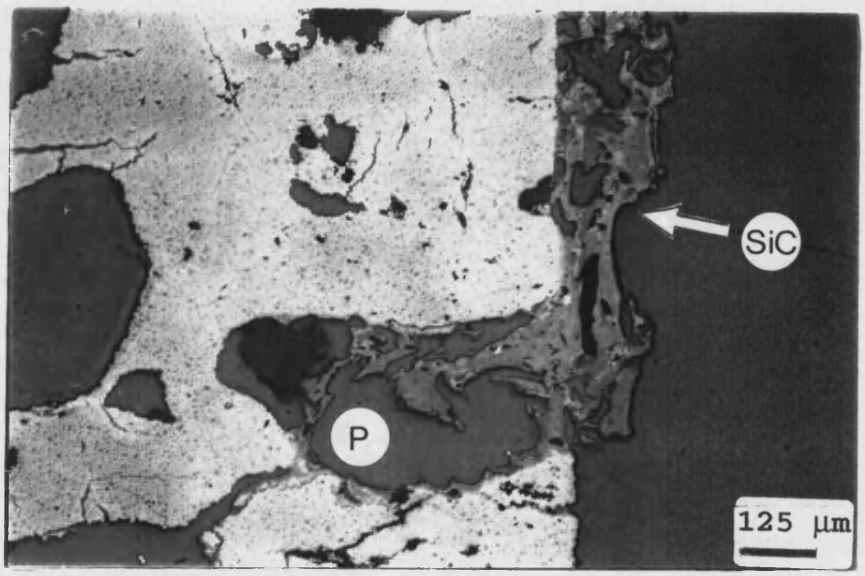

FIGURE 5.12 - Optical microscopy of a TS-2500-SiC showing the SiC coating bridging an open pore. P = pore.

FIGURE 5.13 - Typical Si X-ray map for a transverse through thickness cross section of a brush coated TS-2500-SiC composite.

5.3.2 - Mechanical properties of SiC brush coated unidirectional CFRC composites

5.3.2.1 - SiC coated CFRC-1400 composites

The flexural testing data and AE parameters obtained for the TS-1400-SiC and UU-1400-SiC composites are compared to those of the uncoated composites in Table 5.2. Although the SiC coated unidirectional CFRC composites were subject to successive heat treatments up to 1400°C, comparisons are made with the conventional uncoated unidirectional CFRC composites heat treated to 1100°C, as described in Chapter Four. AE signals were monitored during bend testing using a span/depth ratio of 35:1. Figure 5.14 shows typical stress-deflection curves and sketches of the failure modes of the SiC coated and uncoated TS-1100 and UU-1100 composites. Due to multiple firings up to 1400°C the SiC coated composites have lower densities, Table 5.2. Possibly a large amount of porosity is generated which offsets the greater density of the SiC.

Figure 5.14A shows stress-deflection curves and failure modes for TS-1100 and TS-1400-SiC composites. The failure modes for TS-1100 composite, as described on Chapter Four, is dominated by fast fracture characterized by a flat fracture surface with negligible fibre pull-out and the failure mode of TS-1400-SiC material is similar. The fracture surface of the TS-1400-SiC is therefore identical to TS-1100 composite, Figure 4.17. The stress-deflection curves are also similar although the strain to failure of the TS-1400-SiC composite is larger and therefore the fracture initiation energy is almost doubled in comparison with TS-1100 material. The SiC brush coating of TS-1100 composite fills pores and cracks resulting in a TS-1400-SiC composite with increased strength. This behaviour is similar to that found for SiC brush coated Sigri composite, Chapter Three. The increase in strength and

nominal fracture initiation energy for the TS-1400-SiC composite are remarkable when bearing in mind the low density of the this material due to multiple firings.

Figure 5.14B shows stress-deflection curves and failure modes for UU-1100 and UU-1400-SiC composites. The failure modes are similar for both CFRC composites, being an indication that fibre bundle sliding is also the dominant failure process in the UU-1400-SiC material. Consequently the stress-deflection curves for UU-1100 and UU-1400-SiC have similar shapes. A lower failure strain was found for the UU-1400-SiC composite, although the flexural strength and modulus did not changed in comparison with the UU-1100 material.

The stress-deflection curves for TS-1400-SiC composite, Figure 5.14A, is similar in form to that of TS-1400-SG material, Figure 5.8A, and shows a modest increase in flexural strength and failure strain due to SiC filling pores in the TS-1400-SiC composite and SiC in between plies in the TS-1400-SG composite. The fracture mode for both composites is catastrophic, although for TS-1400-SG the failure mode is dominated by a catastrophic delamination in the SiC interlayer, rather than a fast crack fracture through the composite as for TS-1400-SiC and TS-1100 composites. An increase in flexural modulus and a reduced mid-span deflection is found both for UU-1400-SiC composite, Figure 5.14A, and UU-1400-SG composite, Figure 5.8B, in comparison to the UU-1100 material, and consequently the fracture initiation energy is reduced for both composites due to the embrittling effect of the SiC. The fracture initiation energy of the UU-1400-SiC material decreased by ≈35% compared to UU-1100 composite.

Composite	TS-1400-SiC	TS-1100	UU-1400-SiC	UU-1100
Bulk density (g/cm^3)	1.26±0.02	1.38±0.07	1.18±0.01	1.35±0.04
Flexural Strength (MPa)	198±28	134±22.0	140.5±10	142.5±16
Flexural Modulus (GPa)	105.6±6.7	114±7.0	67.0±10	60±6.0
Mid-span deflection (mm)	1.17±0.11	0.85±0.10	1.41±0.15	1.80±0.23
Nominal Fracture Initiation Energy (kJ/m^2)	1.09±0.28	0.56±0.13	0.91±0.11	1.43±0.18
ΣAE at failure	7613±3338	1738±1103	19788±8767	13101±5227
Pollock exponent b	1.00	0.66	1.50	1.82

TABLE 5.2 - Mechanical properties and AE parameters of SiC brush coated unidirectional CFRC composites, previously heat treated to 1100°C, compared with CFRC composites heat treated at 1100°C.

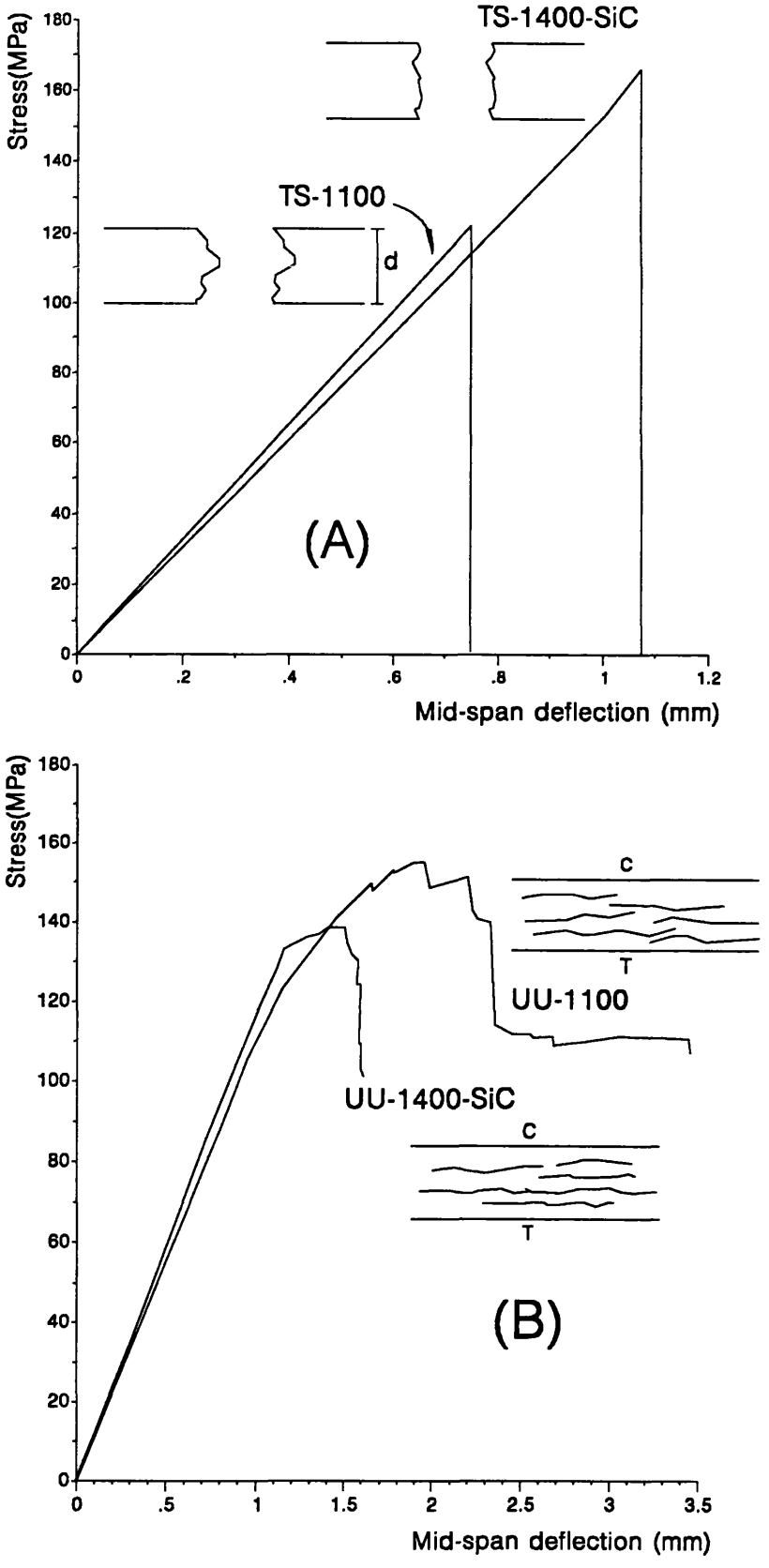

FIGURE 5.14 - Typical stress-deflection curves and failure modes for TS-1400-SiC (A) and UU-1400-SiC composites (B) compared with conventional TS-1100 and UU-1100 composites.

5.3.2.2 - SiC coated CFRC-2500 composite

The flexural testing data and AE parameters obtained for the TS-2500-SiC and UU-2500-SiC composites are listed in Table 5.3. Typical stress-deflection curves and sketches of the failure modes of the SiC coated and uncoated TS-2500 and UU-2500 composites are shown in Figure 5.15. There is no significant difference in density between uncoated and SiC coated TS-2500 and UU-2500 composites. Presumably, the large amount of porosity in both SiC coated composites offsets the greater density of SiC.

Figure 5.15A shows stress-deflection curves and sketches of the failure modes for the TS-2500-SiC and TS-2500 composites. The SiC brush coating does not affect significantly the deformation and fracture of the TS-2500 material because the coating is not continuous and mainly fill pores and cracks, as can be seen by the optical micrograph of Figure 5.11 and the Si X-Ray map of Figure 5.13. Both TS-2500 and TS-2500-SiC CFRC composites have similar stress-deflection curves and therefore flexural strength and flexural modulus are similar (95% confidence), Table 5.3, leading also to a similar failure strain and fracture initiation energy. The failure modes, shown by sketches in Figure 5.15A, indicate that the presence of SiC in the TS-2500-SiC composite confines the extension of the microcrack network (see Figure 4.9A) about the neutral axis, suggesting that most of the SiC is in the outer parts of the TS-2500-SiC composite.

Figure 5.15B shows stress-deflection curves and sketches of the failure modes for the UU-2500-SiC and UU-2500 composites. The SiC brush coating on the UU-2500 composite does not affect the fracture pattern of the UU-2500-SiC material showing that the failure mechanism is also dominated by fibre bundle sliding due to unbonded fibres. Therefore, very similar stress-deflection curves, flexural strength and modulus were found, Table 5.3,

although the strain to failure was slightly lower leading to a decrease in the fracture initiation energy due to an embrittlement effect of the SiC.

The results shows that TS-2500-SiC composite is still stronger than UU-2500-SiC material, although a slightly tendency of the SiC to embrittle both composites is revealed by the lower mean nominal fracture initiation energy, Table 5.3. The significance of the mean nominal fracture initiation energy was offset by the large scatter of data. The failure mode of TS-2500-SiC composite is more catastrophic and it is still a tougher material than UU-2500-SiC material, Table 5.3, as evidenced by the higher fracture initiation energy. In general the SiC coatings on CFRC composites, heat treated at 2500°C, do not have an effect as strong on the mechanical properties as the effect found for the CFRC composites heat treated at 1100°C.

Composite	TS-2500-SiC	TS-2500	UU-2500-SiC	UU-2500
Bulk density (g/cm^3)	1.20±0.03	1.20±0.04	1.09±0.02	1.20±0.03
Flexural Strength (MPa)	267.4±24	296.6±46	116±7.4	116.5±16
Flexural Modulus (GPa)	115.4±10.4	120.0±18	66.4±9.3	61.0±11
Mid-span deflection[a] (mm)	1.57±0.14	1.53±0.08	1.03±0.11	1.20±0.13
Nominal Fracture Initiation Energy (kJ/m^2)	1.97±0.29	2.2±0.40	0.55±0.08	0.63±0.10
ΣAE at failure	23288±7811	8908±2890	16447±5798	8572±3066
Pollock exponent b	0.97	0.97	1.67	1.83

TABLE 5.3 - Mechanical properties and AE parameters of SiC brush coated CFRC composites, previously heat treated to 2500°C, compared with CFRC composites heat treated at 2500°C. (a) at failure stress.

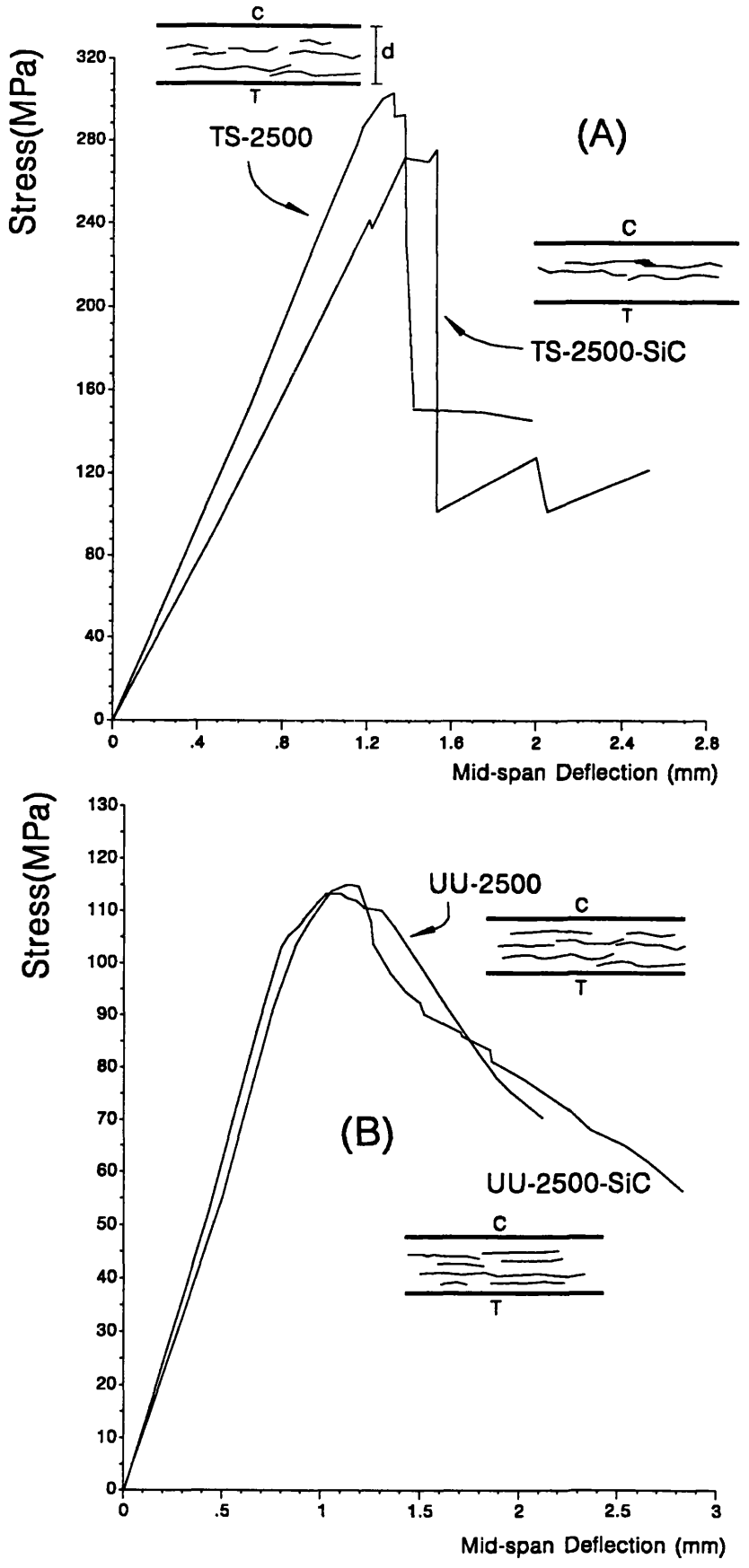

FIGURE 5.15 - Typical stress-deflection curves and failure modes for TS-2500-SiC composite (A) and UU-2500-SiC (B) composites compared with conventional TS-2500 and UU-2500 composites.

5.3.3 - Acoustic Emission of SiC coated CFRC composites

5.3.3.1 - SiC coated CFRC-1400 composites

Typical plots of stress and AE counts as a function of the mid-span deflection for the TS-1400-SiC and UU-1400-SiC composites are shown in Figure 5.16 and Figure 5.17 respectively. Similar curves for uncoated specimens, TS-1100 and UU-1100 are also shown for comparative purposes.

Figure 5.16 shows that the development of the AE events with strain (mid-span deflection = d) for TS-1100 and TS-1400-SiC composites is very similar up to d = 0.4 mm. Above this value of strain the rate of AE from the TS-1400-SiC is significantly greater than for the TS-1100 material. This difference is attributed to microcracking of SiC, although this increase in the AE event counts does not appear to influence the shape of the stress-deflection curve, Figure 5.14A. As a result of these factors the number of AE events at fracture from the TS-1400-SiC composite exceeds that from the TS-1100 material by a factor of approximately four, Table 5.2.

Similar trends are also found when comparing the AE from the UU-1100 and UU-1400-SiC composites, Figure 5.17. The accumulation of AE with strain for the two materials is similar up to the failure strain for the UU-1100 composite, but thereafter there is a very rapid increase in AE in the UU-1400-SiC composite until the cumulative AE counts at failure exceed those from the UU-1100 material by a factor of approximately two, Table 5.2. As with the TS-1100 and TS-1400-SiC composites, the larger amount of AE events from the UU-1400-SiC composite is attributed to SiC microcracking, which appears to take place without affecting significantly the principal mechanisms of deformation and fracture of the SiC coated composite.

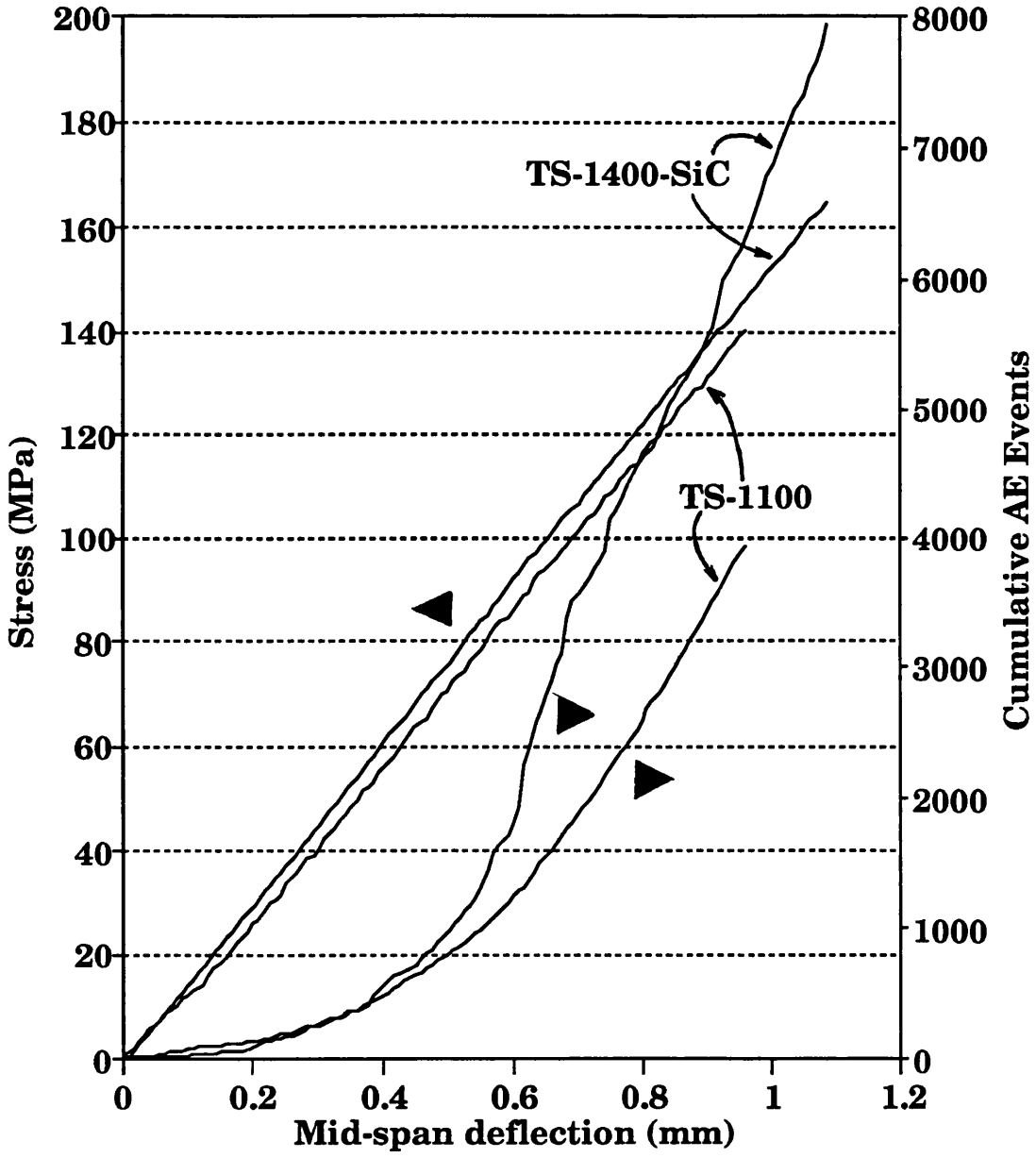

FIGURE 5.16 - Typical plots of stress and AE counts as a function of mid-span deflection for TS-1400-SiC and TS-1100 CFRC composites, subjected to loading to failure in flexure.

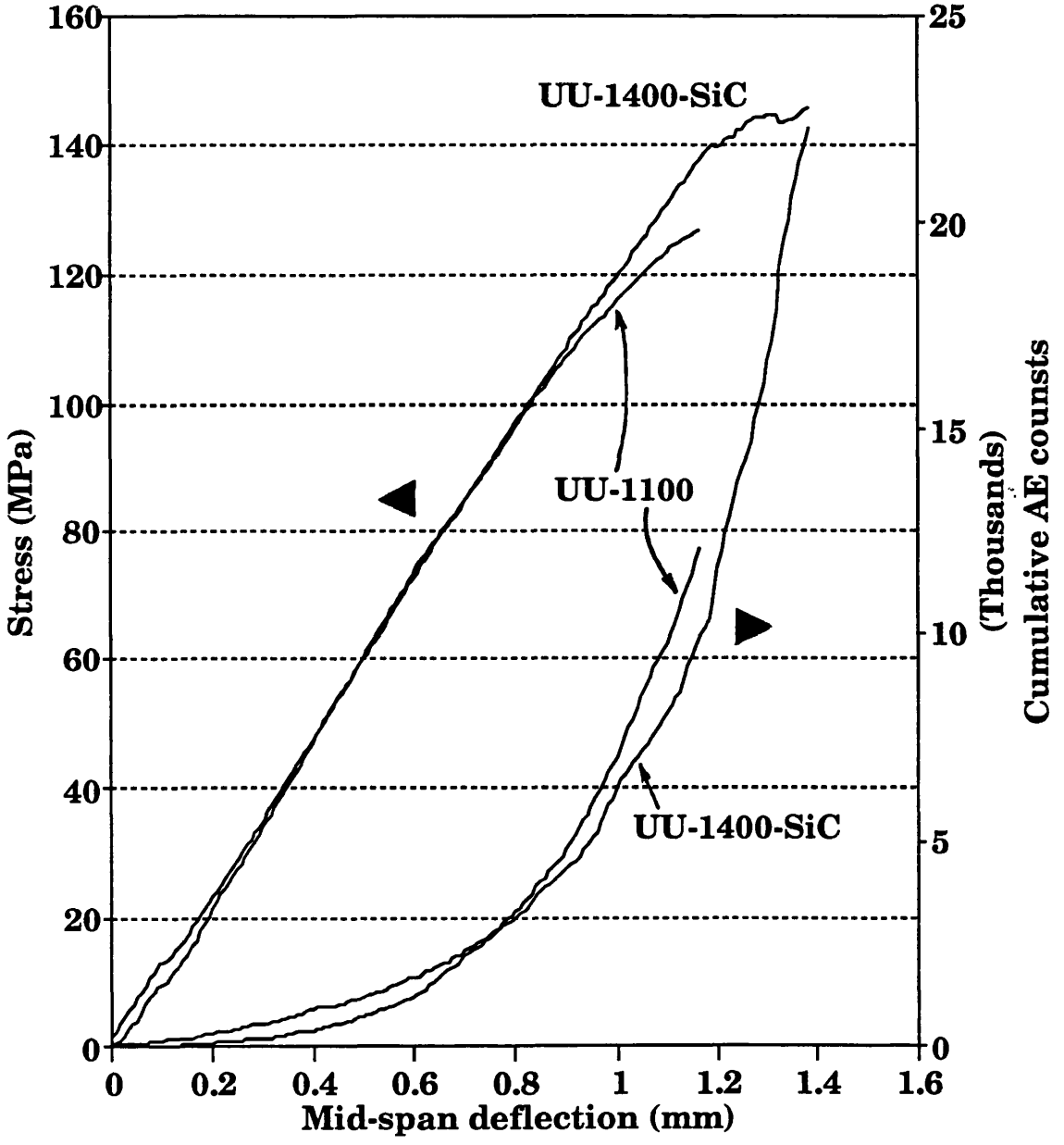

FIGURE 5.17 - Typical plots of stress and AE counts as a function of mid-span deflection for UU-1400-SiC and UU-1100 CFRC composites, subjected to loading to failure in flexure.

Figure 5.18A shows typical plots of AE amplitude distribution at failure stress for (A) TS-1400-SiC composite compared with TS-1100 material, and (B) UU-1400-SiC composite compared with UU-1100 material. The figure shows that higher AE event counts from the TS-1400-SiC has resulted in a shift in the amplitude distribution to higher values. However, the slopes of the lines are similar in the range 150 - 1500 counts (amplitude levels 8 - 14), with more AE events at high (> 35 dB) and low amplitudes (< 20 dB) for TS-1400-SiC composite. The amplitude distributions for TS-1400-SiC and TS-1100 composites are complex curves that do not fit the Pollock equation in the complete range of amplitudes (amplitude levels 2 - 26) at all. A reasonably linear range is found for TS-1400-SiC for counts in the range $\approx 10^3$ - $\approx 10^4$, giving a b value of 1.00, Table 5.2.

Figure 5.18B is similar to Figure 5.18A in that the large number of AE counts from UU-1400-SiC composite has resulted in a shift in the amplitude distributions to higher values. However, the slopes of the lines are similar in the range 10 - 10^4 counts (amplitude levels 2 - 17). The amplitude distribution for UU-1400-SiC composite fits the Pollock law in the narrow range of values N(a) > $\approx 10^3$, giving a b value of 1.50, Table 5.2, which is lower than the b value for the UU-1100 composite (b = 1.82) taken in the range $\approx 10^2$ - $\approx 10^4$ counts.

There are no AE events for amplitude levels > 19 in the UU-1400-SiC composite, while for TS-1400-SiC material the AE counts extend across the entire range of amplitudes (channels 2 - 26). These differences reflect the fracture modes of these materials, *i.e.* failure process dominated by shear deformation (fibre bundle sliding) in the case of the UU-1400-SiC composite, and microcracking in the TS-1400-SiC material, which are equivalent to the uncoated CFRC counterparts.

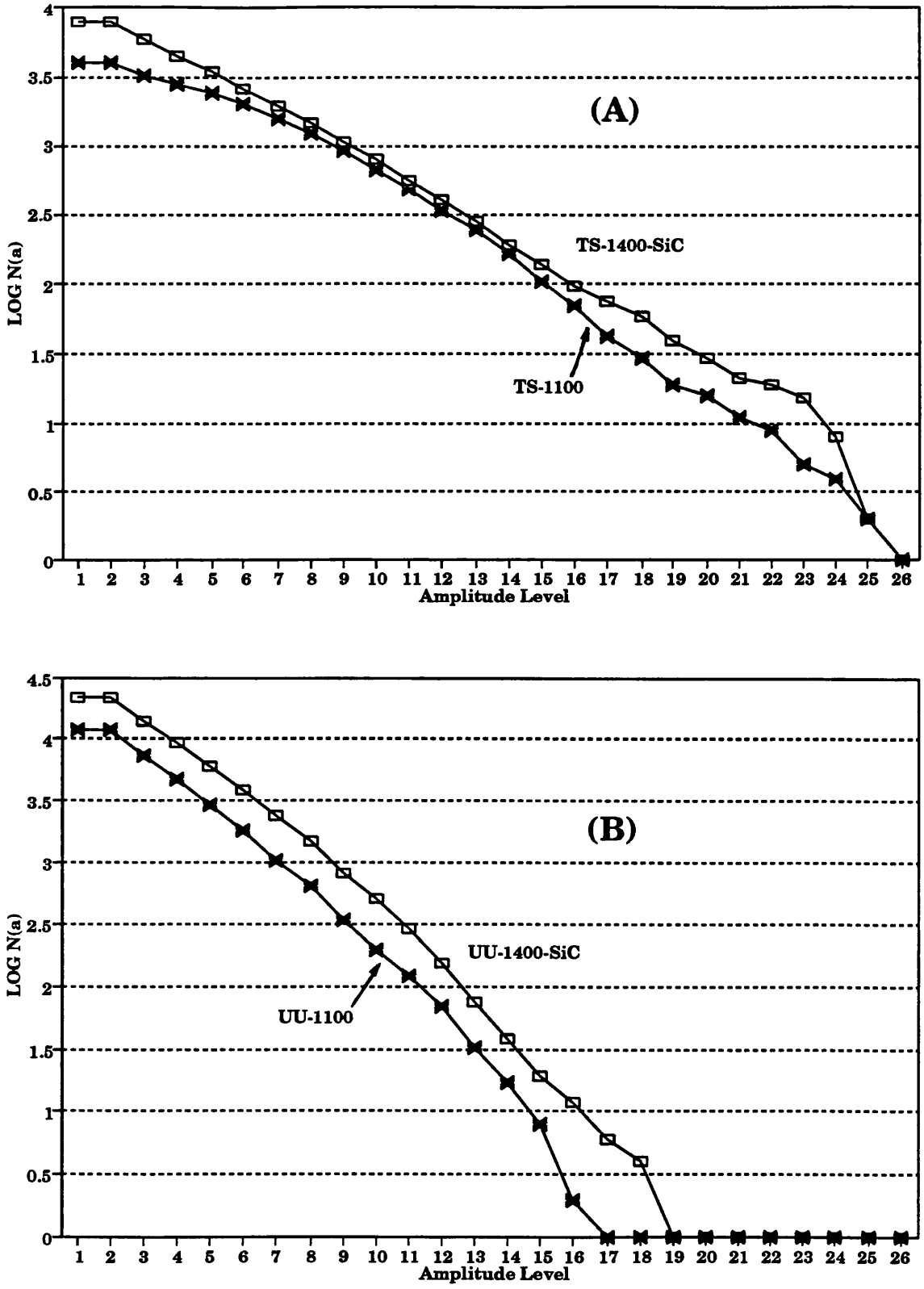

FIGURE 5.18 - Typical plots of AE amplitude distribution at failure stress for SiC coated CFRC composites. (A) TS-1100, TS-1100-SiC; (B) UU-1100, UU-1100-SiC.

5.3.3.2 - SiC coated CFRC-2500 composites

Typical plots of stress and AE counts as a function of the mid-span deflection for the TS-2500-SiC and UU-2500-SiC composites are shown in Figure 5.19 and Figure 5.20 respectively. Similar curves for uncoated specimens are also shown for comparative purposes. The development of AE during the bend test for the TS-2500-SiC composite is similar in form up to ≈120 MPa to that for the TS-2500 material. In contrast to the TS-1100 and TS-1400-SiC composites, Figure 5.16, AE from the TS-2500-SiC material diverges from that for the TS-2500 composite at low strain values. There is also a very rapid increase in AE as fracture is approached so that total number of AE events at fracture for TS-2500-SiC composite is 2.5 times that of the AE at fracture of the TS-2500 material. As with the materials heat treated to 1100°C the additional AE counts may be attributed to microcracking of the SiC incorporated in the composite.

The development of AE found for the UU-2500-SiC composite, Figure 5.20, diverges at low strain value but follows the same pattern found for the UU-2500 material reflecting the small change in flexural strength and flexural modulus. There is also an increase in the total number of AE counts attributed to microcracking of the SiC incorporated in the composite.

Amplitude distributions of AE at fracture in the form log N(a) vs. amplitude level (channel number) are in Figure 5.21. The figure 5.21A shows that the amplitude distributions for TS-2500-SiC and TS-2500 composites are parallel over a wide range of amplitude levels (amplitude levels 2 - 24) indicating that the proportions of high and low amplitude energy events are similar, but for TS-2500-SiC material the amplitude distribution is shifted to a higher position in relation to the TS-2500 material. For TS-2500-SiC composite the AE amplitude distribution fits the

Pollock power law for $N(a) > \approx 10^3$, giving an exponent b = 0.97, that is the same value found for TS-2500 composite, Table 5.3, reflecting the parallelism of the curves.

The AE distribution for the UU-2500-SiC composite, Figure 5.20B, shows also a shift to higher position due to an increase in AE counts attributed to additional SiC microcracking in the composite structure; there are no AE events with amplitude levels higher than 20 (gain > 50 dB). Therefore the AE amplitude distribution for UU-2500-SiC composite fits the power law for just one decade, $N(a) > \approx 10^3$ counts, giving a exponent b = 1.67 that is lower than the value for the UU-2500 material (b = 1.83), Table 5.3.

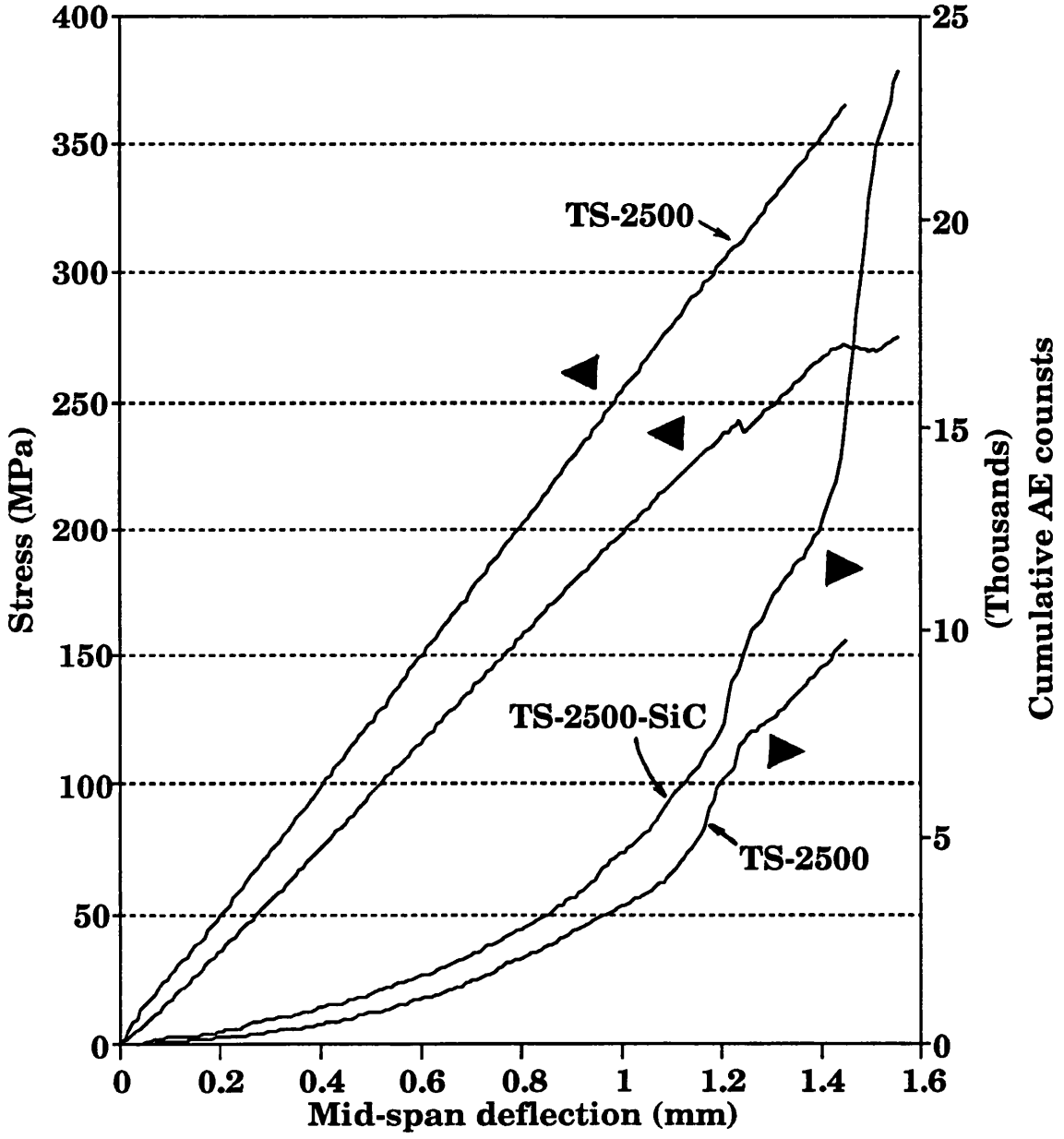

FIGURE 5.19 - Typical plots of stress and AE counts as a function of mid-span deflection for TS-2500 and TS-2500-SiC CFRC composites, subjected to loading to failure in flexure.

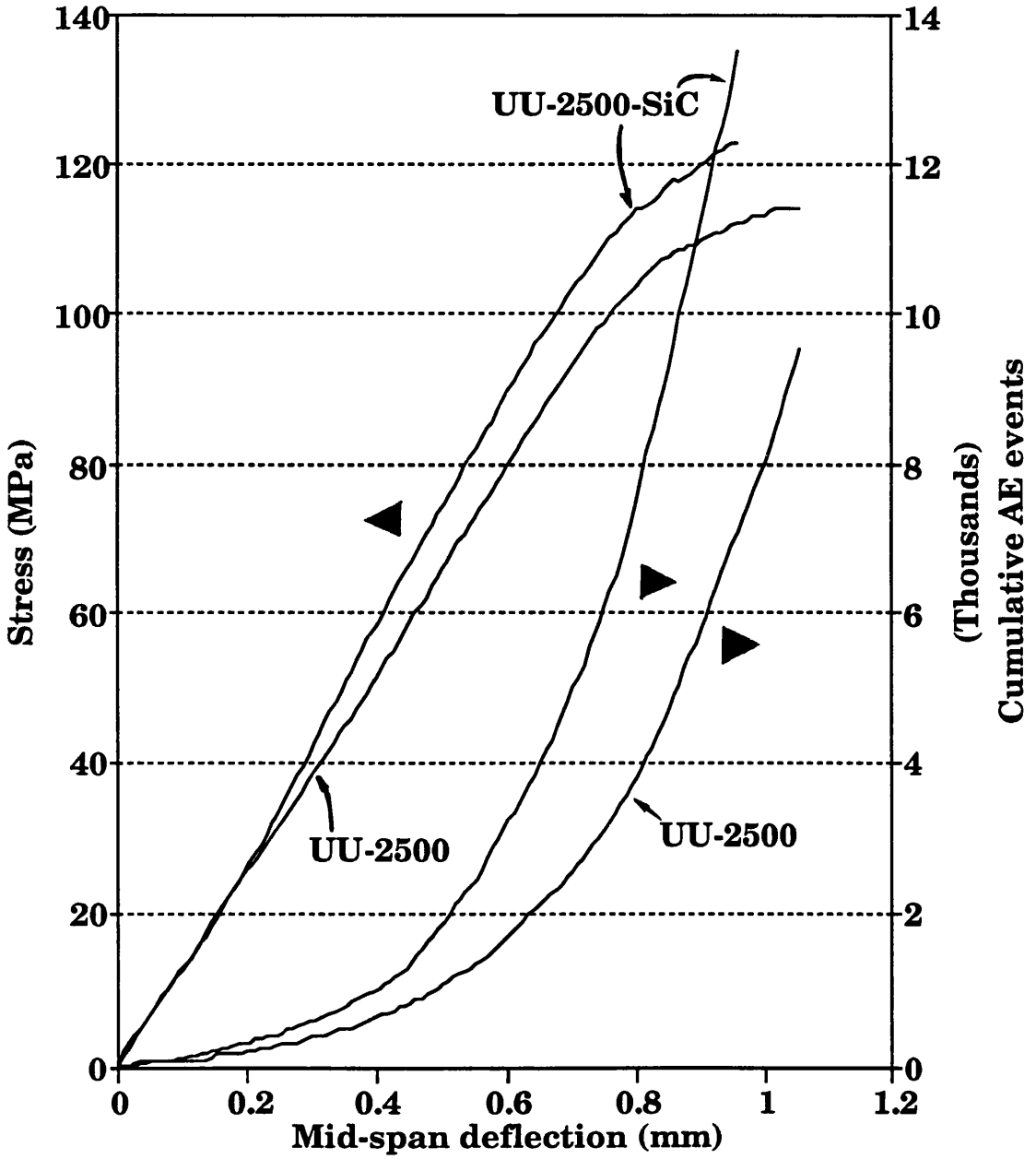

FIGURE 5.20 - Typical plots of stress and AE counts as a function of mid-span deflection UU-2500 and UU-2500-SiC CFRC composites, subjected to loading to failure in flexure.

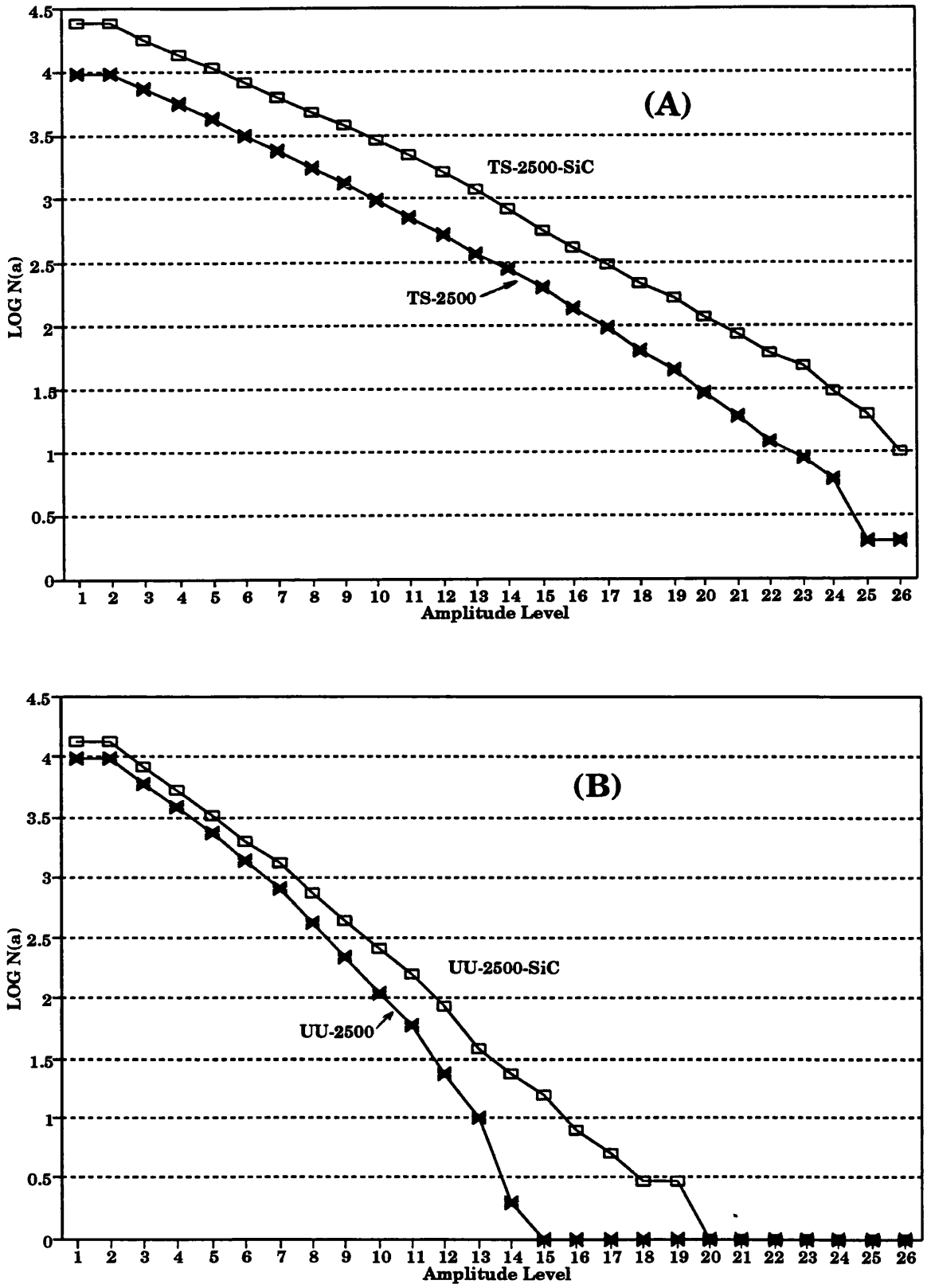

FIGURE 5.21 - Typical plots of AE amplitude distribution at failure stress for SiC coated CFRC composites. (A) TS-2500, TS-2500-SiC; (B) UU-2500, UU-2500-SiC.

CHAPTER SIX
SUMMARISING DISCUSSIONS AND CONCLUSIONS

In this chapter the principal findings of the work presented in Chapters Three to Five are summarized and some general points of discussion are made. In section 6.1 the microstructural features of uncoated and SiC coated Sigri and KKarb woven CFRC composites are discussed, followed by their mechanical properties and oxidation resistance. In section 6.2 results achieved on unidirectional CFRC composites in relation to microstructure, mechanical properties and oxidation resistance are discussed. In section 6.3 results obtained using different approaches to obtain and hybrid C-SiC composites are discussed. In Section 6.4 the principal conclusions of the work are stated.

6.1 - Commercial Woven CFRC composites

6.1.1 - Microstructure

The microstructures of KKarb and Sigri composites are illustrated in Figures 3.1 and 3.2 respectively, and are described in Chapter Three, Section 3.1. A detailed discussion of the microstructures of these composites was given by Crocker (1991) and therefore this subject is not considered in detail here.

Common features found in Sigri and KKarb composites are the intrabundle (or cross-bundle) cracks, *e.g.* C in Figure 3.1B. The cross bundle cracks in both composites are mainly straight and perpendicular to the longitudinal yarns. The cross-bundle cracks in KKarb composite are closer together and more regularly spaced (≈150 μm) than in the Sigri composite (≈ 200 μm).

These cross-bundle cracks originate as a result of volumetric shinkage on carbonization of the matrix, although they are also be modified on cooling as a result of differences in thermal expansion coefficient of the parallel (PL) and perpendicular (PP) fibre bundles seen in Figures 3.1 and 3.2. As an example, the volumetric shrinkage, ΔV, of a pure resin on carbonisation is $\Delta V \approx -0.50$ (Jortner - 1991). The maximum volumetric shrinkage strain in a fibre bundle is given in Figure 6.1, and can be represented by $\varepsilon_v \approx \Delta V.V_m$, where V_m is the volume fraction of matrix in the fibre bundle. (ε_v may be less then this maximum value if porosity is generated within fibre bundles on carbonisation). Typically $V_m \approx 0.4$ and so $\varepsilon_v \approx -0.20$. Matrix carbon being a weak and brittle material is unable to withstand such shrinkage strains and therefore cracking is inevitable.

The type of cracking which occurs in woven CFRC, illustrated schematically in Figure 6.2, depends upon the relative magnitude of the strength of the bundle-bundle interface bond, σ_i, and the strength of the matrix carbon, σ_c. If $\sigma_i > \sigma_c$ then stress relief cracks are initiated in the matrix carbon within perpendicular bundles, Figure 6.2A, and the cracks will run perpendicular to the PL bundles (*i.e.* Z axis in Figure 6.2). This type of cracking is clearly seen in Figures 3.1 and 3.2. Conversely, if $\sigma_i < \sigma_c$ then cracks will be initiated at the bundle-bundle interface, Figure 6.2B. This type of cracking is not seen in the case of the Sigri and KKarb composites, presumably because this type of cracking (if extensive) would result in a CFRC composite which was unaceptable for commercial use. If however, $\sigma_i \geq \sigma_c$ then cracks may be initiated within fibre bundles but further shrinkage may lead to their extension into the bundle-bundle interfaces. This type of cracking is seen for KKarb composite, Figure 3.1, but not for the Sigri composite, Figure 3.2. In practice the nature of the cracking will also be influenced by factors such as the fibre and matrix types, weave pattern and processing conditions.

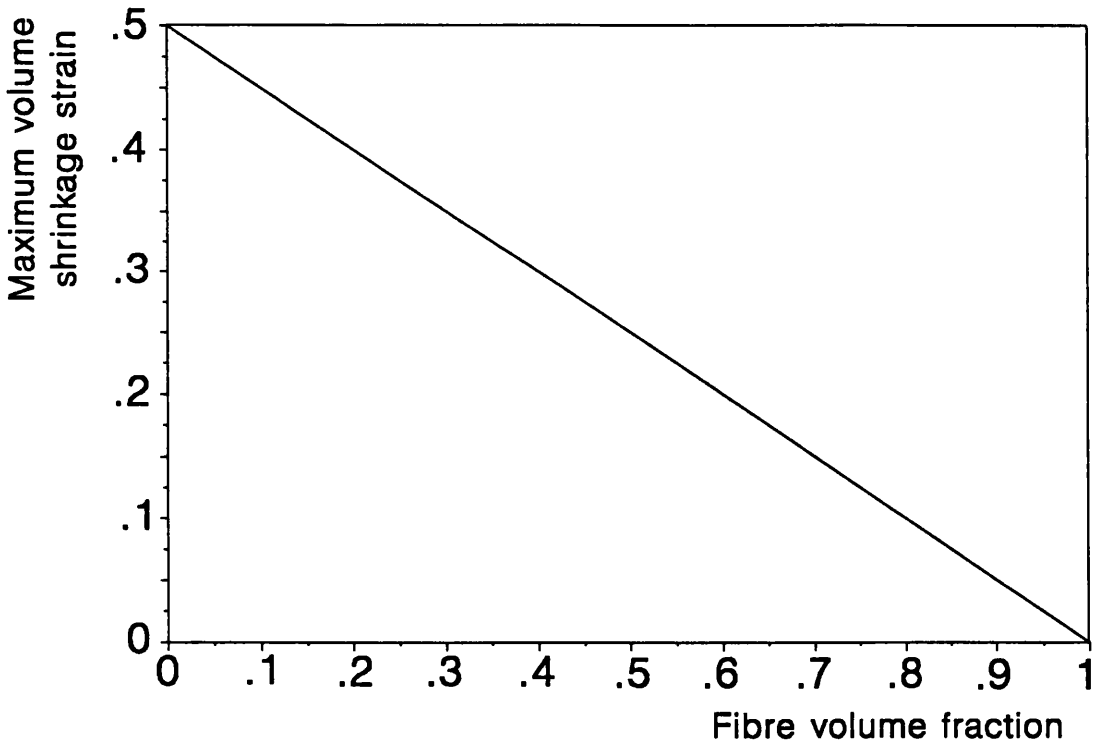

Figure 6.1 - Effect of fibre volume fraction on maximum volumetric shrinkage strain on carbonising a carbon fibre reinforced phenolic resin, assuming matrix volume yield = 0.50 and no porosity generation (adapted from Jortner - 1991).

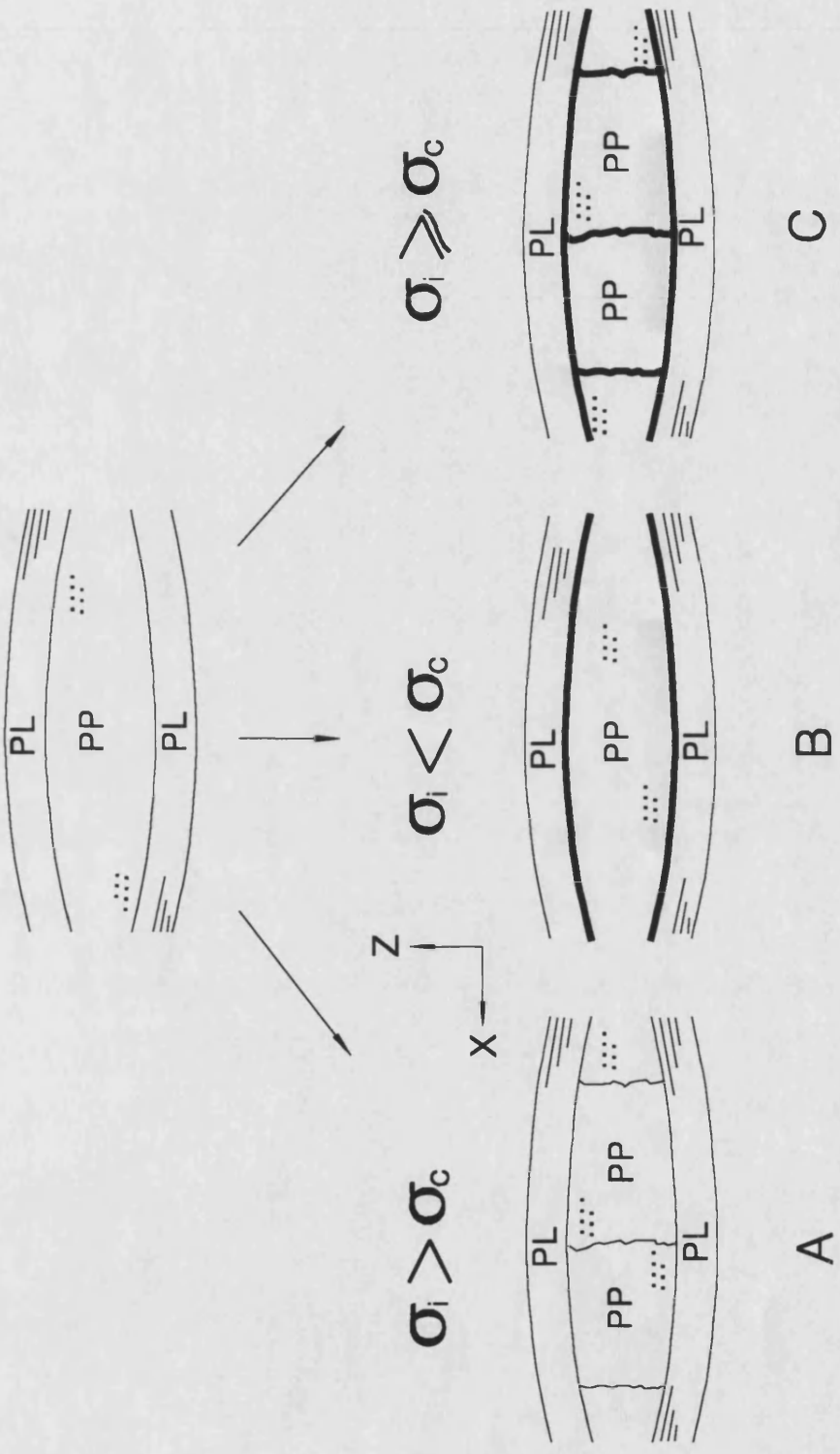

Figure 6.2 - Types of cracks that occurs on woven CFRC composites. σi = strength of bundle-bundle interface bond, σc = strength of the matrix carbon.

Considering SiC impregnation, the most important differences in the microstructure of the KKarb and Sigri composites are the different extents of porosity, Table 3.1 and Figure 3.3. The Sigri material, Figure 3.2, contains many large pores which are not found in the KKarb composite, Figure 3.1. The EDX images for Si in SiC coated composites, show that very thin SiC coatings (≈10 μm) are produced on the surface of brush coated KKarb CFRC composites, Figure 3.5A, and on the Sigri material, Figure 3.6, the SiC sol-gel is mainly consumed by filling pores, leaving only a small amount of SiC to form a discontinous surface coating (< 5 μm). Vacuum impregnation of alkoxide *sol* was used on KKarb composite and this method produced an increased thickness of the coating and the microcrack network was filled by the alkoxide *solution*, Figure 3.5B. During vacuum impregnation some of the sol-gel solvent, *i.e.* acetone, vaporises possibly reducing the gelation time of the alkoxide sol-gel. Pressure impregnation of the alkoxide sol-gel into the KKarb and Sigri materials forced the solution to go deeper inside the composites. The EDX mapping for Si for pressure impregnated Sigri composite shows an increased amount of SiC in the bulk composite, Figure 3.7B. The higher open porosity and inherent connectivity between these pores are key factors in enhancing the impregnation by providing pathways for the alkoxide *sol*. These results suggest that enhanced impregnation of the SiC sol-gel can be achieved by vacuum impregnation followed by pressurisation.

Determinations of the SiC content made by ASTM - C561 (ash, in Graphite) found that the Sigri composites has ≈1.35±0.22%wt of SiC, and KKarb composite has ≈0.63±0.15%wt. These weight fractions take around 10 - 15 days to be obtained using the brush coating method. The volume fraction corresponding to these weight fractions will be lower, due to the high density of SiC (ρ = 3.2 g/cm$^{3)}$. The measurements showed that,

after the total removal of the carbon material in the SiC coated Sigri composite, the SiC appears to be an interconnected network of fibrillar nature. For KKarb composite it was found that the SiC forms a hollow sheath after the burn-off of the carbon material. This morphology reflects the fact that SiC only partially penetrates the KKarb composite.

6.1.2 - Mechanical Properties of woven CFRC composites

6.1.2.1 - Uncoated composites

The mechanical properties of CFRC composites are influenced by many factors, such as fibre type, weave pattern and microstructure. The flexural modulus of KKarb and Sigri composites are independent of span/depth ratio for ratios greater than 19:1 and 25:1, respectively (Crocker - 1991). The differences in flexural modulus (13 GPa for KKarb material and 53 GPa for Sigri composite), Tables 3.2 and 3.3, are attributed mainly to the type of carbon fibre used, since Sigri composite has ex-PAN carbon fibres ($E \cong 300$ GPa) whereas KKarb composite has low modulus rayon carbon fibres ($E \cong 30$ GPa).

These composites also have different flexural failure modes, that are summarized as sketches in Figure 6.3 for the uncoated and SiC brush coated materials. These differences occur because differences in microstructure lead to different microcracking mechanisms. The failure modes of KKarb composite, either at a span/depth ratio of 19:1 or at 35:1, are mainly characterised by longitudinal ply delamination cracks which develop on the tensile side of the specimen, Figure 6.3A. The stress-deflection curves for KKarb composite, Figure 3.10 and Figure 3.15, at these span/depth ratios consist of an increase in stress to a single peak followed by a catastrophic

reduction in stress mainly by two steps. Kowbel (1990) and Crocker (1991) found that for woven CFRC composites tested in flexure at span/depth ratios higher than 30:1, the tensile stresses between the fibre bundles increase, eventually pulling them apart in a delaminating mode. These interfaces are weaker than the transverse fibre bundles, and it is therefore easier for cracks to delaminate plies than to propagate across bundles.

The failure modes of Sigri composite, either at a span/depth ratio of 25:1 or 35:1, Figure 6.3C, are similar to each other and can be characterised as a combination of delamination,and cross bundle shear cracks running between pores in the compressive stress field, although large longitudinal cracks are more dominant in the Sigri composite tested at a span/depth ratio of 35:1. The stress-deflection curves for both span/depth ratios, have multiple peaks, indicative of subcritical cracking, and the reduction in stress after the peak value involves a multi-step process, Figure 3.10 and Figure 3.15. These differences in behaviour between the KKarb and Sigri composites are strongly influenced by the greater extent of porosity in the Sigri material, Table 3.1.

6.1.2.2 - SiC coated composites

The influence of the incorporation of SiC sol-gel on the mechanical properties of KKarb and Sigri composites depends upon the extent of open porosity. The flexural modulus of SiC coated KKarb composite was increased by ≈25%, Table 3.2, when brush coating and vacuum impregnation/brushing are used, but there was no pronounced effect on flexural strength. By contrast, for the SiC coated Sigri composite there was an increase of ≈20% in the flexural strength over the uncoated material, either by brush coating or

pressure impregnation, but no change in the flexural modulus was observed, Table 3.3.

KKarb composite has less open porosity (≈5.5%), Table 3.1, so a thicker surface SiC coating was obtained, and consequently, the flexural modulus was higher than for the uncoated composite, Table 3.2. The increase in flexural modulus was explained by considering the composite and the SiC coating as a composite beam, Figure 3.24 and Table 3.4. On the other hand, the greater open porosity (≈14%) of the Sigri material resulted in deeper penetration of the SiC sol-gel into the bulk material by filling open pores. Moreover, KKarb composite has a significantly lower modulus than Sigri material and consequently the influence of the surface SiC coating on this material is marked. The incorporation of SiC by the sol-gel technique in the KKarb and Sigri CFRC composites tends to induce a more brittle failure mode during fracture. The stress-deflection curve for SiC coated KKarb composite shows, Figure 3.11, a more stepped reduction in stress after the peak stress. For SiC coated Sigri composite the failure mode is more catastrophic. Considering flexural failure modes, Figure 6.3, SiC coating of the KKarb composite at a span/depth ratio = 19:1 substantially increases the extent of ply delamination, Figure 6.3A and 6.3B. In the case of the Sigri material the extent of ply delamination is increased about the neutral axis and the shear cracking in the compressive field is reduced, Figure 6.3C and 6.3D. The changes in failure mode are less marked at span/depth ratio = 35:1.

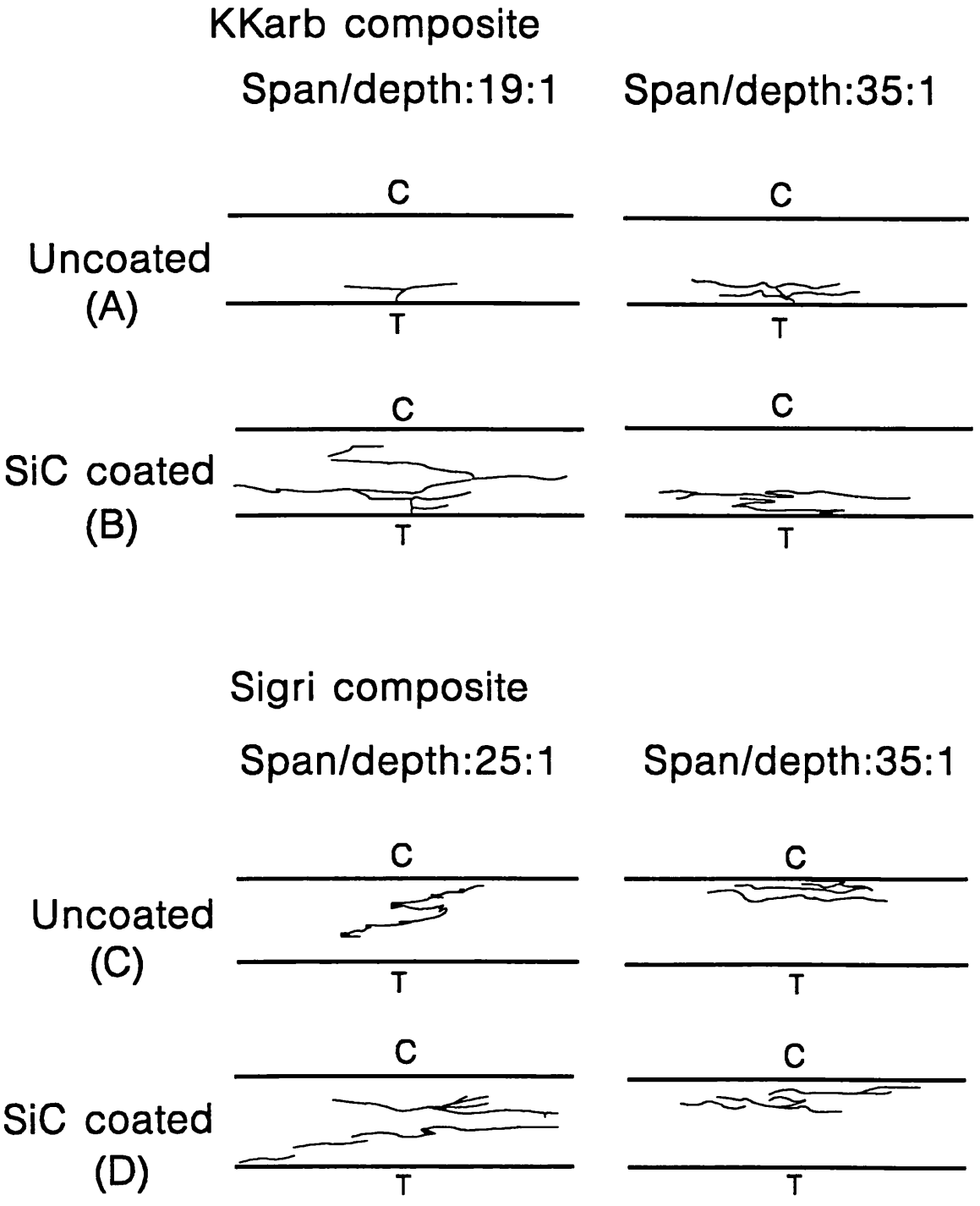

Figure 6.3 - Summary of the failure modes for uncoated and SiC coated KKarb and Sigri composites, at different span/depth ratios.

Naislain and his group (1981) have studied the mechanical properties of CFRC composites modified by chemical vapour infiltration (CVI) of SiC. They found that for CFRC preforms where the volume fraction of open pores is less than 0.35, the compressive strength and compressive modulus increase linearly with the volume fraction of SiC (V_{SiC}) in the range $0.15 < V_{SiC} < 0.35$, but almost no increase in compressive strength or rigidity was observed when the $V_{SiC} < 0.15$. For example, they showed that for $V_{SiC} = 0.25$ the compressive strength of woven CFRC composites parallel to fibre laminae increases by a factor of from 1.5 to 3 and the compressive modulus increases by a factor of from 2 to 5.

Although it is not possible to compare quantitatively the compressive properties measured by Naislain with the flexural properties measured in this work, it is instructive to make qualitative comparisons. The ash determinations reported in the Section 6.11 indicate that the weight fraction of SiC, W_{SiC}, are very low, $W_{SiC} = 0.0135$ and 0.0063 for Sigri and KKarb composites, respectively. Nevertheless the effects of these small amounts of SiC on flexural properties are surprisingly significant. Tables 3.2 and 3.3 show that brush coating KKarb composites with SiC precursor results in increases of flexural modulus of 25% and for Sigri composite brush coating results and increase in flexural strength of 25%.

The SiC sol-gel method was originally developed as a coating (Castro - 1991) rather than for the purpose of infiltration, although this work has shown that the sol-gel alkoxide formulation is suitable for this purpose. One of the advantages of the sol-gel system for infiltration is the ability to control rheological properties which may permit more controlled processing conditions. For example, adjustments in the gel formulation, may improve the extent of SiC for infiltration.

The comparison between effects of CVD and sol-gel impregnation suggests for CFRC composites with a suitable connected open porosity that there may benefits from using a combination of the two methods. One of the disadvantages of CVI technique pointed out by Naislain (1981) is that pores are easily blocked. This can be overcome, or at least minimised, by carrying out a first stage sol-gel impregnation using vacuum/pressurisation techniques described in Chapter Three. The system can be left to gel in an oven, adjusting the rheological properties to reduce gel time. Then the impregnated material can be placed in a CVD/CVI vessel where the initial heating schedule to obtain the SiC sol-gel, Section 2.1.4.1 of Chapter Two, is carried out before the CVD/CVI process is commenced.

6.1.3 - Acoustic Emission on woven CFRC composites

6.1.3.1 - Uncoated Materials

This thesis has presented new work on acoustic emission, AE, under flexural loading from two woven CFRC composites both in the uncoated condition and after SiC coating by the sol-gel method. This work has shown that acoustic emission can provide valuable information relating to fracture behaviour and microstructure of these CFRC composites and it is a complementary technique to the analysis of stress-deflection curves.

The generation of AE for the uncoated KKarb material, Figure 3.15, starts at the onset of stress and there is a progressive increase in the AE, resulting from a substantial amount of sub-critical activity, and giving rise to a large number of AE counts, ≈44000. The AE generation for the uncoated Sigri composite, Figure 3.15, is quite different from KKarb material; with the Sigri composite there is a steady increase of AE until the onset of ply

delamination which is clearly revealed by the deviation of the stress-deflection curve from elastic behaviour.

6.1.3.2 - SiC coated materials

A much higher proportion of AE events, 104000 counts, was detected from the SiC coated KKarb composite, Figure 3.19A, possibly due to a generalised microcracking of the SiC coating present in the compressive and tensile faces of the material. In this case it is also possible that some AE results from cracking under load points as a result of Hertzian contact stresses. The generation of AE for the SiC coated Sigri composite, Figure 3.19B, is in sharp contrast to those obtained from the equivalent KKarb composite. There is a superposition of the AE curves from the uncoated and SiC coated Sigri composites at low stress levels, reflecting similar flexural moduli for both materials, but the onset of ply delamination is shifted to a higher stress level, ≈230 MPa, and this event is accompanied by a sharp increase in the rate of AE.

6.1.4 - Oxidation Resistance of woven CFRC composites

6.1.4.1 - Uncoated composites

The oxidation resistance of carbon materials is a function of the microstructure and the active surface area. The temperatures of onset of oxidation for uncoated KKarb and Sigri composites are between 530 - 570°C, Figure 3.21. Sigri material oxidises faster than KKarb material, due to the larger amount of open porosity, and consequently higher surface area. Zone I oxidation, where the overall reaction rate is controlled solely by the chemical reactivity of the solid, is identified for both materials between 550 - 800°C.

As pointed out by Crocker (1991), as oxidation progresses on KKarb and Sigri composites, the fibre bundles are weakened by selective attack at the fibre/matrix interfaces where there are stressed regions within fibre bundles, while bundle/bundle interfaces and interfaces between plies were relatively unaffected by oxidation

6.1.4.2 - SiC coated composites

An improvement of oxidation resistance was exhibited by the KKarb and Sigri composites when coated with SiC by sol-gel method, Figure 3.22. A modest improvement in the oxidation onset temperature for SiC coated KKarb composite was found due to a thicker SiC coating. A reduction in the transient of Zone I oxidation is observed in all SiC coated samples, because coated surfaces, either internal or external, are not available for reaction. Also a significant reduction was found in the steady state oxidation rate at 1200°C with an average reduction of ≈25% for SiC coated KKarb and Sigri composites in relation to the uncoated specimens. Pressure impregnation of alkoxide *sol* in Sigri composite reduces the oxidation rate by ≈35%, Figure 3.23, indicating that this is a better method for impregnating the sol-gel formulation. As with mechanical properties it has been shown that a small percentage of SiC obtained by sol-gel method is capable of significantly enhancing the oxidation resistance of CFRC composites. Also using vacuum impregnation followed by pressurisation of the alkoxide *sol* can enhance the oxidation resistance of CFRC composites, provided that a suitable controlled porosity is present in these materials, permitting deep filling of pores.

6.1.4.3 - Multilayer coatings on CFRC composites

Multilayer refractory/glassy coatings were made on the KKarb and Sigri composites. The multilayer SiC/B_20_3 coating gave an enhanced benefit in delaying the oxidation onset temperature to 850°C for KKarb composite and to 950°C for Sigri material, Figure 3.25, practically suppressing the Zone I oxidation. These differences in the oxidation onset temperature for KKarb and Sigri composites are explained by the fact that the borate glass has filled remaining open pores of the Sigri composite. In this way the borate glass acts as an internal modifier in addition to acting as an external coating, since the method to apply the borate coating was the same in both materials. A benefit over 40% in the reduction of weight loss at 1200°C was found for this multilayer coating, in spite of the high susceptibility of the B_2O_3 glass to absorb moisture. The benefit of the borate glass in reducing the oxidation of CFRC composites and carbon fibres is well known and it has been shown also by McKee (1986) and Ehrburger (1986). The benefit on coating carbon fibres and CFRC composites demonstrated by McKee (1986) is shown in Figure 6.5. In his work the carbon fibre and the CFRC composite were impregnated with tri-tert-butyl borate followed by addition of ammonium borate, and heat treated up to 500°C to ensure conversion to a glassy borate coating. Borate coated carbon fibres showed weight losses of less than 1% at 1000°C, whereas the borate coated CFRC composite lost less than 0.2%wt at 1000°C. Results obtained in the present work, Figure 3.25, confirm the negligible weight loss on borate coated CFRC composites at 1000°C.

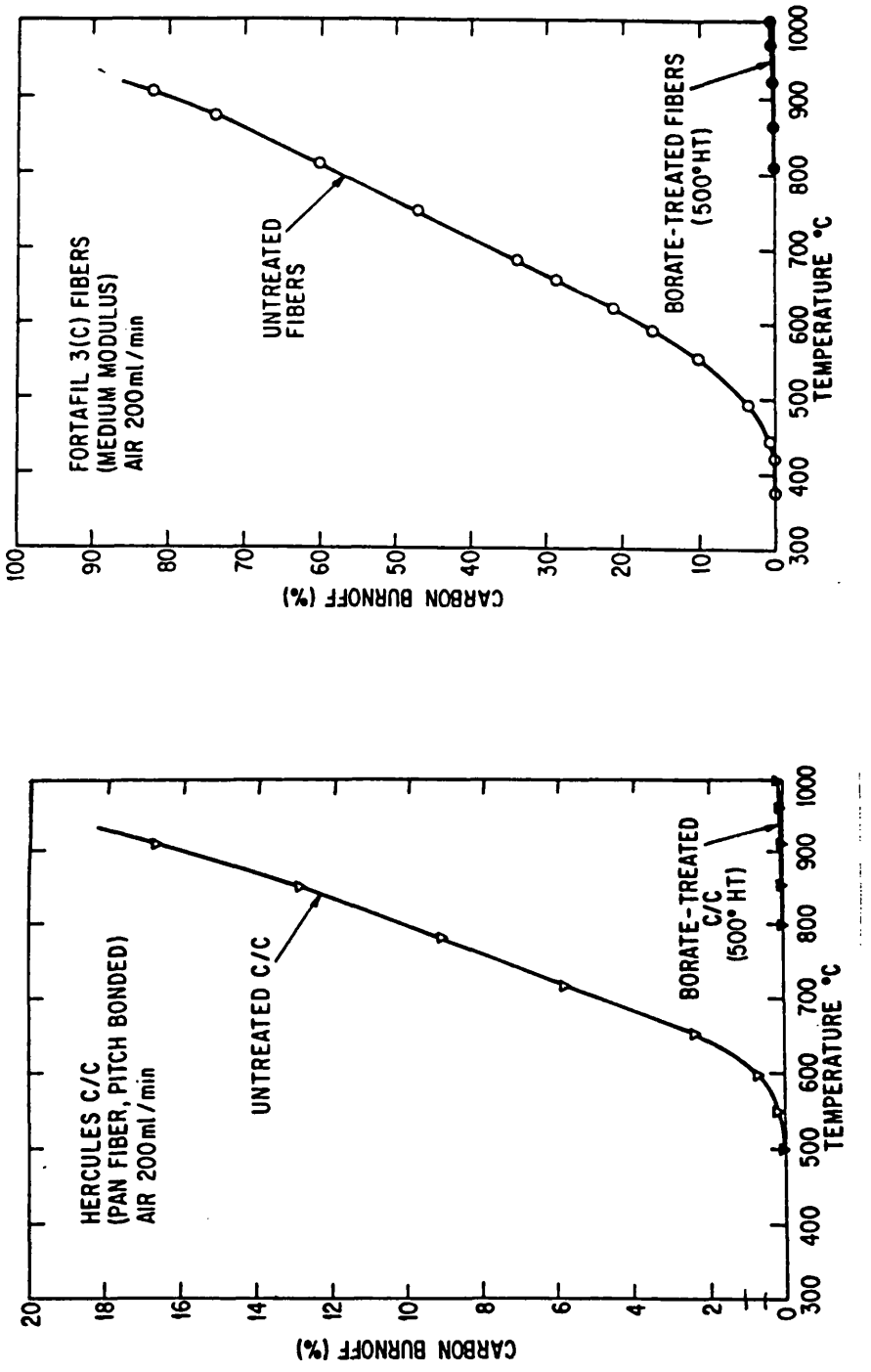

Figure 6.4 - TGA analysis of (A) carbon fibre Fortafil, medium modulus, coated with borate glassy coating, and (B) CFRC composite made with ex-PAN carbon fibres in a pitch matrix. Heating rate : 10°C/min. (McKee - 1986).

The benefit conferred by the SiC/SiO_2-TiO_2/SiC multilayer coating on KKarb and Sigri composites, Figure 3.26, was only slightly greater that provided by than their brush coated SiC counterparts. This suggests that at 1200°C the SiO_2-TiO_2 layer is not an effective coating. SiO_2-TiO_2 layers were devised for higher operating temperatures (≈1600°C) (Castro - 1991).

6.2 - Unidirectional CFRC composites

6.2.1 - Microstructure of unidirectional CFRC composites

The microstructure of the unidirectional CFRC composites is characterised by the presence of large open pores. These pores have an average dimension of approximately ≈500 μm, Figure 4.7. These pores are more numerous than the ones found for Sigri composite, Figure 3.2, which have pore dimensions in the range of 100-600 μm. Pores in CFRC composites having pyrocarbon matrices occur mainly in regions blocked off by deposition of carbon at constrictions in the pore network, and they can be ≈100 μm long, although large numbers of smaller pores (<50 μm) are common (Ehburger - 1981). Thus, the nature of pores in CFRC composites and their distribution in the microstructure depend upon the method of fabrication. The pores in the unidirectional CFRC composites manufactured in this work are mainly formed during the prepreg stacking where air is trapped in between layers. In order to reduce the amount of pores during fabrication it is convenient to perform vacuum moulding simultaneously with hot pressing. Pores that are formed during moulding of the composite laminate can be filled after the first carbonisation schedule by re-impregnation with thermosetting resins or pitch; this is a routine procedure during the fabrication of CFRC composites. If there is not enough connectivity between pores to provide pathways to

subsequent impregnation of pitch and/or resin, it can possibly be achieved by an intermediate graphitisation process in between carbonisation cycles (Weisshaus - 1990a). A pore free structure is not always desired because pores may provide sites for crack deflection or multiplication under load, which results in enhanced fracture toughness (Rief - 1990). It remains to be demonstrated whether or not, either in principle or in practice, one can control the size and spacing of microcracks sufficiently to produce a higher strength in a composite than could be achieved in a pore free structure.

Tows with large numbers of fibres can also trap air in between fibres during the prepreg stage. One of the options to avoid air trapped in between fibre bundles is to use a filament tow with less than 12000 fibres, as was used in this work, *e.g.* tows with 3000 fibres are commercially available. The cross section micrographs for the CFRC composites suggest that the packing array is clustered, as represented by Figure 6.5, rather than as a well separated fibre array. Jortner (1991) pointed out that "well separated" fibre arrays, Figure 6.5A, experience greater cross-sectional shrinkage during carbonization than clustered fibre packing, Figure 6.5B.

Also, the heating schedule and the final heat treatment temperature influence the different microstructures for CFRC composites. Nam (1992) pointed out that high heating rates and thick composites resulted in large gradients of temperature in the matrix within the laminate, which may result in non-uniform carbonisation, creating internal stresses through the laminate. Also, increasing the heating rate and the thickness of composite induce large pressure build-up within the composite, which may result in localized delamination and/or general damage to the char structure of the matrix. In the present study a multistage heating cycle was developed for the carbonisation process, Figure 2.4. A high heating rate was used for heat treatment up to 2500°C (13 - 15°C/min) which was the slowest heating rate

available with the equipment. There is some evidence, Figure 4.9, that this heating rate may be faster than the optimum value, since an extensive pore and crack system was developed for the TS-2500 composite.

Slow heating rates are needed to avoid catastrophic defects from occurring, although it creates economic penalties. Investigations carried out by Naughton (1993) on CFRC composites made from woven ultra high modulus carbon fibre/phenolic laminates showed that varying the linear heating rates in the range 2 - 50°C/h, had little effect on the in-plane or transverse tensile strength after the first carbonization, Table 6.1. In the present work a heating rate of 6°C/h was used in the critical temperature range of 280 - 480°C, and 20 - 30°C/h from 480 - 1100°C. Naughton's results suggest that the mechanical properties of the composites manufactured in this work are not a sensitive function of the heating rates used.

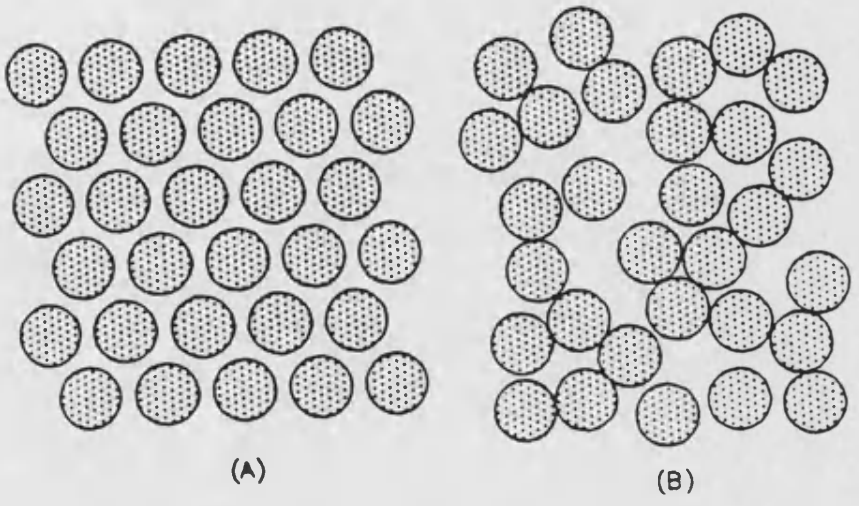

Figure 6.5 - Two packing arrays at 0.60 volume fraction of fibres. (A) well-separated, (B) clustered (Jortner - 1991).

Heating rate(°C/h)	2	5	10	50
In-plane strength (MPa)	137±7	131±7	147±6	155±6
Transverse strength (kPa)	770±64	923±59	851±37	803±38
Density (g/cm^3)	1.41	1.36	1.38	1.40

Table 6.1 - In-plane and transverse tensile strength of a warp aligned (0,90) 8-harness satin CFRC plates (Naughton - 1993)

The surface activity of the carbon fibres plays an important role in the microstructure of the CFRC composites. The nature of the surface treatment in carbon fibres is proprietary, but the most used process is electrochemical oxidation in acid or alkaline aqueous solutions (Donnet - 1990). The objetive of surface treatment is to increase the number of active chemical groups, *e.g.* carboxylic, carboxylic anhydride, ether-type, on the fibre surface and/or roughen the fibre surface to increase the amount of mechanical ``keying'' between fibre and matrix (Savage - 1993). This study confirms that surface treated and sized carbon fibres, *e.g.* Graphil E/XA-S, provide well bonded fibre/matrix interfaces, whereas untreated and unsized carbon fibres, *e.g.* Graphil XA-U, provide composites with limited fibre/matrix interface bonding. As a consequence untreated and unsized fibres are substantially unwetted by resin matrix during processing. A natural consequence of the different microstructures found for the single composites, Figure 4.7, is that the UU-1100 composite has more open porosity (≈40%) than for TS-1100 composite (≈25%), Table 4.1. The present work showed that the microstructures of these CFRC composites keep a *memory* of their previous

green counterparts.

The most substantial modifications in the microstructure of CFRC composites upon heat treatment from 1100 to 2500°C are experienced by the CFRC composite made with treated and sized fibres, where a branched crack network was developed, Figure 4.9. Also many small pores (≈25 μm) are developed in the laminae. Little change was observed for the CFRC composites made with untreated and unsized fibres, except that the crack network is more developed decreasing the fibre volume fraction from 0.60 to 0.58.

Changes in the matrix microstructure and in the carbon fibres were also detected after heat treatment to 2500°C. These changes were observed by X-Ray diffraction. Both carbon fibre and the phenolic resin shifted their d_{002} peak to positions approaching the d_{002} peak of graphite with a narrower shape suggesting that a more ordered structure is present and a reduction in the crystallite size (L_c) occurred, Figures 4.10 and 4.11. Evidences of these changes and of stress graphitisation were also observed by optical microscopy. The phenomenon of stress graphitisation was also observed by Hishiyama (1974), Zimmer (1983), and Zaldivar (1991a, 1991c) in CFRC composites. As pointed out by Rellick (1992) the term *stress graphitization* is somewhat a misnomer, because the process must necessarily involve large strains, but not necessarily large stresses.

6.2.2 - Mechanical Properties of Unidirectional CFRC composites

Many factors contribute to the mechanical properties of CFRC composites, such as type of carbon fibre used, the state of the surface activity of this fibre and the final heat treatment to which the composite is

submitted. The scatter of values found for mechanical properties in this work are between 6-16% for flexural strength and 6-18% for flexural modulus. Crocker (1991) found a similar scatter for a variety of CFRC studied in her work. The scatter in flexural modulus and flexural strength values probably reflects the heterogeneous nature of CFRC composites.

Similar studies addressing the influence of surface activity of the carbon fibres on the mechanical properties of CFRC composites have been published since the late seventies by Fitzer (1980). There is a consensus that CFRC composites made with high strength, surface treated fibres and heat treated between 1100-1400°C fail in a brittle fracture mode with low strain to failure, as found in this work. On the other hand, in CFRC composites made with non surface treated carbon fibres, crack branching and fibre pull-out mechanism can occur resulting in a pseudo plastic failure mechanism.

By using the simplistic approach of the rule of mixtures it is possible to estimate the utilization of carbon fibre mechanical properties. The rule of mixtures is derived for a unidirectional composite, with well bonded fibre/matrix interfaces, with fibres and matrix having similar strains. This model is highly idealised when applied to the CFRC composites studied in the present work, but it can be used for semi-quantitative internal comparisons. The rule of mixtures relates the modulus and strength of the composite, E_c, σ_c, respectively to the same properties of the fibre E_f, σ_f, and the matrix, E_m, σ_m :

$$E_c = E_f.V_f + E_m.V_m$$

$$\sigma_c = \sigma_f.V_f + \sigma_m.V_m$$

where V_f and V_m are the volume fractions of fibre and matrix respectively. In general for practical CFRC composites the volume fraction of pores, V_p

must be considered and so $V_f + V_m + V_p = 1$. Values of E_c and σ_c for TS-1100 and TS-2500 composites calculated from the rule of mixtures are in Table 6.2. Two sets of values of E_c and σ_c are calculated: (1) with $V_p = 0.25$; (2) with $V_p = 0.28$, which were pore volume fractions found in this work for TS-1100 and TS-2500 composites respectively. Values of E_m and σ_m used are those for glassy carbon, Appendix IV, values of E_f, σ_f are those for the high strength carbon fibres used in this work, Appendix IV, and for the high modulus carbon fibres, Appendix VI.

CFRC composite	TS-1100(1)		TS-2500(2)	
	Exp	Calc	Exp	Calc
σ_{CFRC} (MPa)	135±22	2223	297±46	1252
E_{CFRC} (GPa)	115±7	126	120±18	375

Table 6.2 - Experimental, and calculated flexural strength and modulus for TS-1100 and TS-2500 composites according to rule of mixtures. (1) assuming $V_p = 0.25$, $V_f = 0.55$ (2) assuming $Vp = 0.28$, $V_f = 0.50$.

Considering case (1), the rule of mixtures makes a reasonable prediction of the modulus but it indicates a very low utilization of carbon fibre strength, *i.e.* ≈3.5%. This is because the TS-1100 composite undergoes a catastrophic fracture where the crack path runs transverse to the fibre orientation.

For case (2), the prediction of modulus is less good then in case (1) and, as in case (1), there is very poor utilisation of fibre strength, *i.e.* 12%. In this case the fracture mode involves extension of the microcrack network

developed during heat treatment, Figure 4.9, leading to a delamination type of failure, Figure 4.18.

For the composites studied in this work there is a broad correlation between nominal fracture initiation energy and mid-span deflection at failure stress, as shown in Figure 6.6. A high increase in nominal fracture initiation energy and mid-span delfection is exhibited by the CFRC composite made with treated and sized fibres only and heat treated at 2500°C. On the other hand, there is an opposite effect for the CFRC composite made with untreated and unsized fibres. These changes are attributed to the development of a graphitic structure at the fibre/matrix interface in these composites which facilitates microcracking in the TS-2500 composite and fibre bundle sliding in the UU-2500 material.

This work has explored the concept of developing a hybrid composite by combining the characteristics of the two composites described before, *i.e.* CFRC composites made with treated and sized fibres (T) and CFRC composites made with untreated and unsized fibres (U). The characteristic microstructural features of these two single composites are preserved in the *hybrid* composite, Figure 4.7. The original features of the two characteristic laminae made from treated and sized fibres and untreated and unsized fibres can be clearly identified in the hybrid composite. The possibilities to manufacture other forms of hybrid composites using fibres with different surface activities are discussed in the next paragraphs.

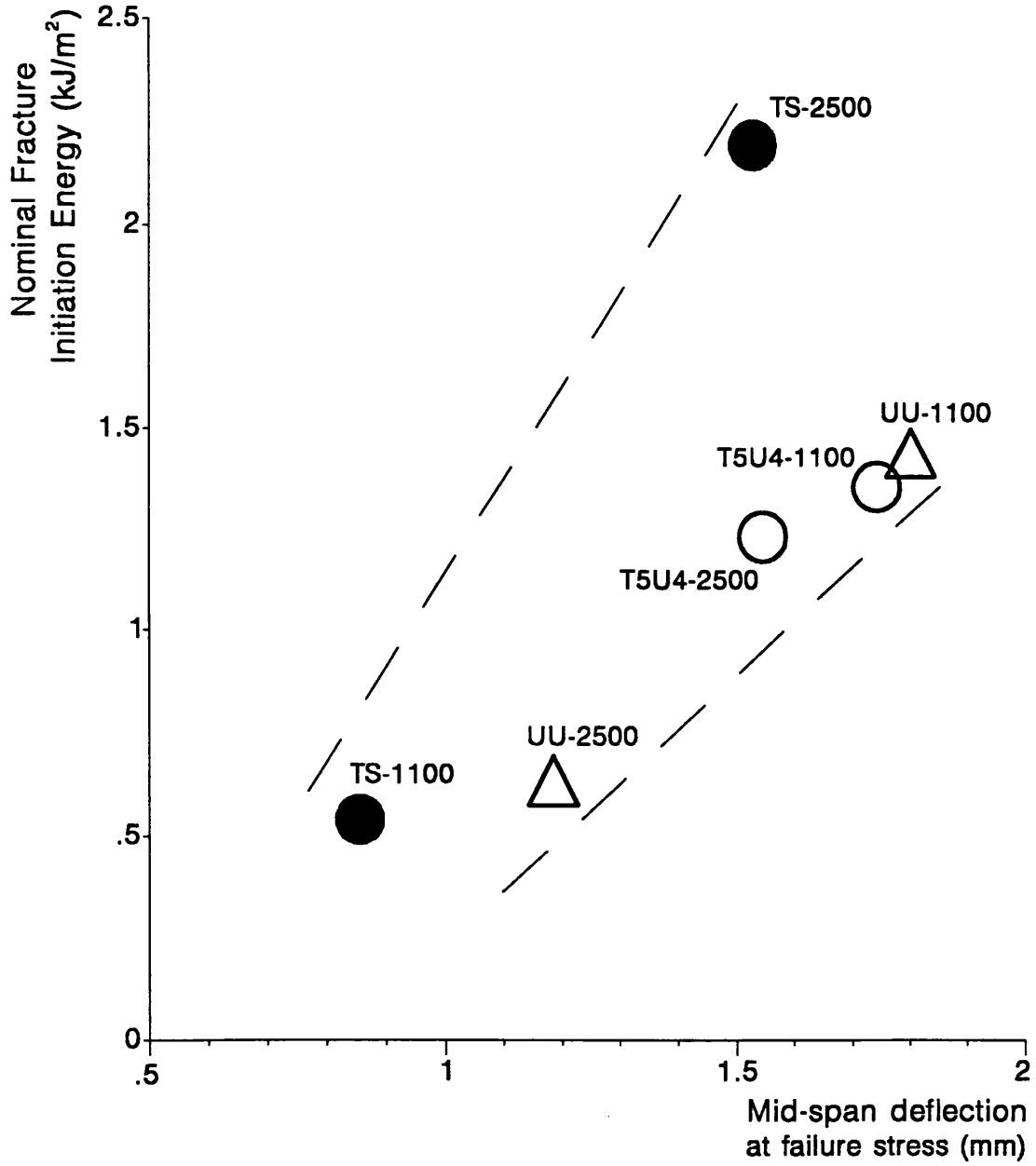

Figure 6.6 - Nominal fracture initiation energy as a function of mid-span deflection at failure stress for CFRC composites.

Considering the mechanical properties of the hybrid composite, a synergistic effect on the flexural strength was found, *i.e.* the flexural strength of the hybrid composite is higher than the flexural strength found for CFRC composites with treated and sized fibres and CFRC composites untreated and unsized fibres individually. Values of mid-span deflection and nominal fracture initiation energy for the T5U4-1100 composite are dominated by the U lamina, and for the T5U4-2500 material these values lie between those of the TS-2500 and UU-2500 composites, Table 4.3 and Figure 6.6.

The concept of using fibres with different surface activities in the same composite offers a new route for controlling mechanical properties of CFRC composites by choosing different fibre types with different lay-ups, different sizing characteristics, carbon fibres from different sources, such as rayon and PAN precursors, and even comingled fibres with different surface activity, as exemplified in Figure 6.6. Figure 6.6A shows a schematic diagram of the composite manufactured in the present work. Figure 6.6B shows a comingled composite, with nearly 0.20 volume fraction of untreated unsized fibres. Figure 6.6C shows a woven fabric made with interwoven bundles of treated and sized fibres and untreated and unsized fibres. Figure 6.6D shows a woven fabric made with interwoven comingled fibre bundles, each bundle has around 0.20 volume fraction of untreated and unsized fibres. It would be interesting to explore the possibilities of developing synergistic effects in the mechanical properties of hybrid CFRC composites with such designs.

The rule of mixtures can also be applied to estimate roughly the properties of hybrid composites with alternating plies of treated and sized fibres, and untreated and unsized fibres, Table 6.3. The contribution of each fibre laminae type is taken from the properties of single composites, *i.e.*

Tables 4.3 and 4.4. A hybrid composite without pores would have 0.56 volume fraction of TS fibres and 0.44 volume fraction of UU fibres. Two set of values of E_c and σ_c are calculated: (1) with $V_p = 0.30$; (2) with $V_p = 0.35$, which are pore volume fractions estimated from the contribution of each laminae based in Tables 4.1 and 4.2. It is interesting to note that, despite the crude assumptions of the rule of mixtures, the rule predits the modulus in case (1) and (2) reasonably well, Table 6.3. Comparing the experimental and calculated values of strength in case (1) it shows clearly the synergistic effect of combining the laminae containing the two fibre types, as dicussed before.

In case (2) the experimental strength is somewhat higher than predicted by the rule of mixtures, but in view of the approximations involved, it cannot be said to indicate a synergistic effect. It should be borne in mind that the failure strain of the two individual laminae are different and this is not taken into account in the rule of mixtures.

CFRC composite	T5U4-1100(1)		T5U4-2500(2)	
	Exp	Calc	Exp	Calc
σ_{CFRC} (MPa)	165±10	97	187±16	140
E_{CFRC} (GPa)	70±4	63	93±10	61

Table 6.3 - Experimental, and calculated flexural strength and modulus for T5U4-1100 and T5U4-2500 composites according to rule of mixtures. (1) assuming V_p=0.30, V_f(TS)=0.385, V_f(UU)=0.315. (2) assuming V_p=0.35, V_f(TS)=0.365, V_f(UU)=0.295.

A different effect is found when CFRC composites made with treated and sized fibres and untreated and unsized fibre are heat treated from 1100°C to 2500°C. The TS-2500 composite has an increase in flexural strength of 120% and an increase in the nominal fracture initiation energy of nearly 300%, Figure 6.6. On the other hand, for the UU-2500 composite the same properties decrease by 20% and 55%, respectively. Fitzer (1980), Thomas (1978) and Manocha (1988, 1991) also found similar increases in mechanical properties for CFRC composites made with treated and sized fibres and heat treated at graphitising temperatures.

As an example, using high modulus treated and sized carbon fibres Manocha (1988) found an increase of 150% in the flexural strength on heat treating a unidirectional CFRC composite from 1000 to 3000°C, and a decrease of 200% when using high modulus untreated and unsized carbon fibres. Manocha (1991) found that graphitisation of a CFRC composite results in more shear deformation, and the stress-deflection curves became more stepped as the orientation of the matrix sheath around the fibre changed and they could slip more easily. Similar results were found in this work, Figure 4.13 and 4.18.

Changes in the microstructure of the CFRC composites heat treated at 2500°C and the development of a graphitic microstructure in the vicinity of the fibre/matrix interface are responsible for changes in the fracture behaviour. The tougher failure mode found for the CFRC composite with treated and sized fibres is mainly a result of the extension of the characteristic crack system of this composite. On the other hand, the graphitic microstructure facilitates the fibre bundle sliding in the CFRC composite with untreated and unsized fibres, thus leading to a reduction in the flexural strength.

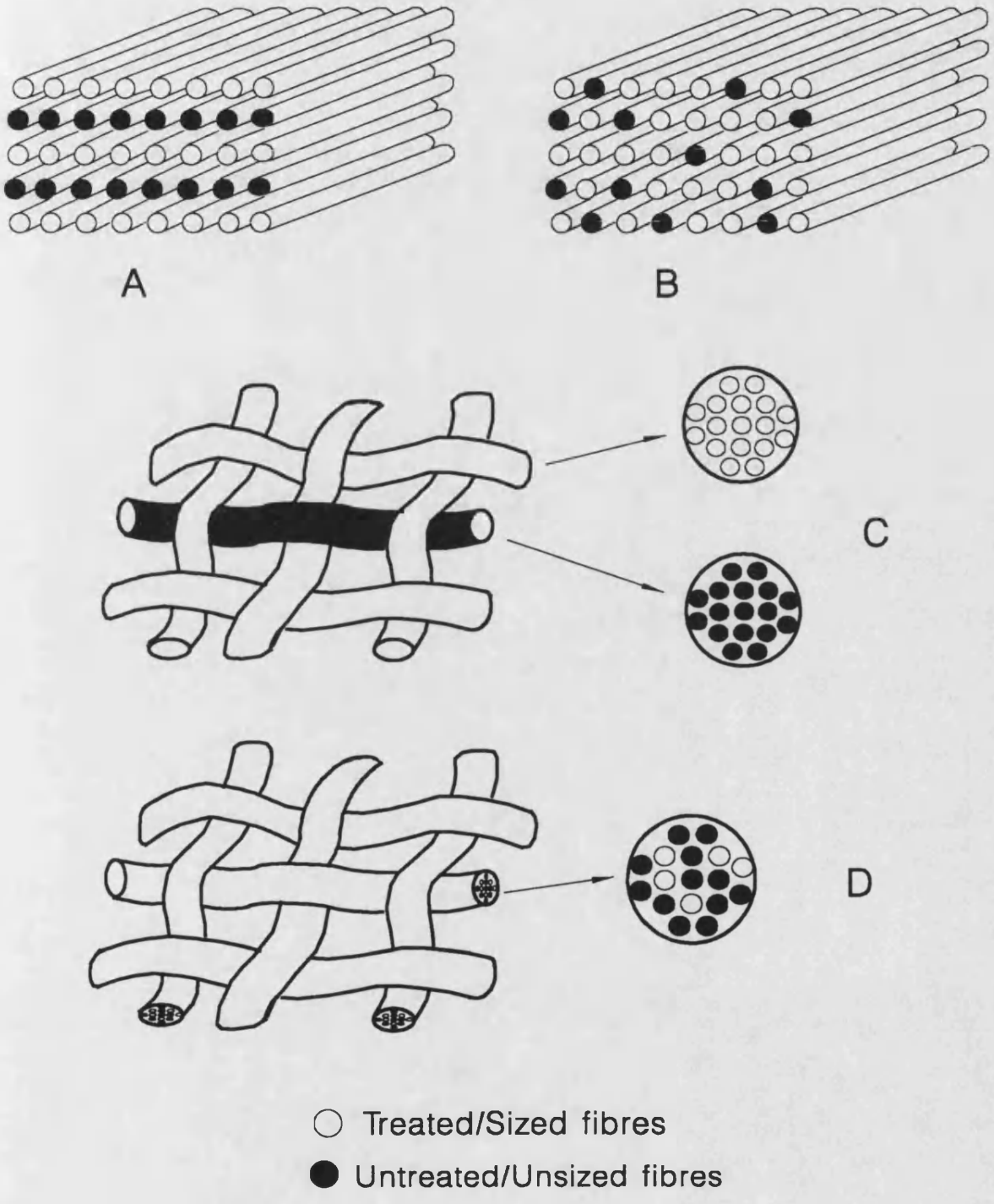

Figure 6.7 - Possible patterns to comingled hybrid fibres. (A) - Unidirectional laminate with intercalated lay-up. (B) Unidirectional laminate with comingled fibre lay-ups. (C) woven comingled fabric. (D) woven comingled fibre bundles.

6.2.3 - Acoustic Emission of Unidirectional CFRC composites

This study has presented new work on AE from single and hybrid unidirectional CFRC composites heat treated at different final temperatures under flexural loading. All the failure modes for the CFRC composites studied involve energy emitting mechanisms, such as fibre breakage, matrix cracking, fibre debonding or pull-out and ply delamination, as schematically show in Figure 1.12. The extent of AE differs for the three composites heat treated at 1100°C, but in each case there is a progressive increase in AE during bend tests, Figure 4.19. Tougher failure modes, such as found for the UU-1100 composite, give rise to many stress waves of low energy and low amplitude. Tougher failure modes tend to generate additional AE counts as a result of shear deformation mechanism, such as fibre bundle sliding and pull-out of fibres. By contrast, brittle failure modes, such as that for the TS-1100 composite, give rise to fewer AE events than those from the UU-1100 composite, but the AE results from stress waves of high energy and amplitude, Figure 4.19.

Thomas (1978a) discussed mechanisms for obtaining useful CFRC composites and by using AE demonstrated the onset of vigorous matrix microcracking well before global failure of the composite. As an example, for a CFRC composite made with high strength carbon fibre and resin carbon matrix the flexural strain at failure in the transverse section is 0.80%, whereas in the longitudinal section is 1.56%. The strain at which AE becomes significant in this composite is 0.6%, and therefore it is very close to the transverse strain to failure which relates to matrix microcracking. No experimental details are given in his study. For all the CFRC composite studied in this work the AE event counts began at the onset of stress. This was also found for graphites (Neighbour - 1993) and it may reflect the increased sensitivity of modern equipment.

Figure 6.8 shows that for all of the composites there is a broad correlation between the number of AE counts at fracture and the nominal failure strain, suggesting that AE is dominated by the applied strain, rather the applied stress for the unidirectional CFRC composites studied in this work.

6.2.4 - Oxidation resistance of unidirectional CFRC composites

For all composites studied in the present work increasing the final heat treatment temperature reduces the reactivity to air and increases the temperature of onset of oxidation. This effect is attributed to the increase in graphitic character of the composite on heat treatment, since it is well know that graphitic carbons are less reactive than non-graphitic ones.

The temperature of initiation of oxidation in the case of carbonised composites lies between 400-460°C which is 150-200°C lower than that of their graphitised counterparts. During the course of the present work, Dhami (1993) reported that the temperature of onset of oxidation for a bidirectional CFRC composites with ex-PAN carbon fibres/resin matrix is 530°C when heat treated at 1000°C, and 710°C when heat treated at 2700°C. The higher oxidation onset temperatures found by Dhami may be attributed, at least in part, to a lower open porosity since reimpregnated composites were used in his work.

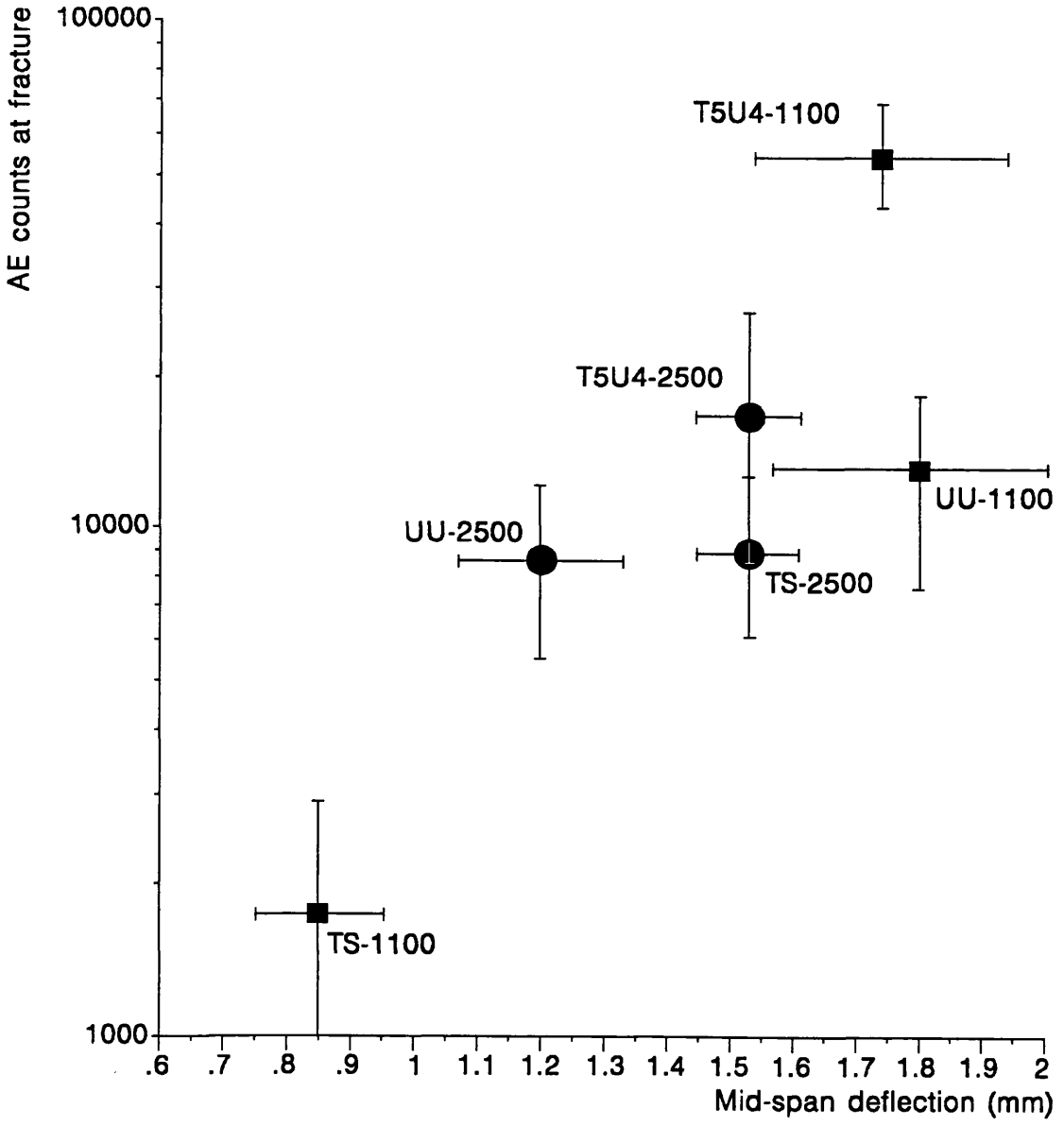

Figure 6.8 - AE counts at fracture as a function of mid-span deflection for unidirectional CFRC composites.

6.3 - Hybrid CFRC composite modified by SiC

6.3.1 - Introduction

Hybrid composites consisting of carbon fibre reinforcement in a C-SiC matrix were obtained using a SiC sol-gel system. Three possible methods of incorporation of SiC sol-gel in the composites were studied, as exemplified in Figure 5.1.

The methods of incorporation of the SiC by the alkoxide sol-gel were carried out by mixing with the phenolic resin at the filament winding stage, brushing between plies of the *green* composite at the lay-up stage, and by brushing the surface of the CFRC composite. The first mentioned method was not satisfactory because a composite with sufficient integrity to be tested was not obtained. The two last mentioned methods showed that it is feasible to process in one heating schedule the CFRC modified by interlayer SiC sol-gel without loss of integrity of the laminate by developing an appropriate heat treatment schedule. As for other ceramic matrix composites currently using sol-gel methods (Russel-Floyd - 1993), the drying of the solvent before moulding for this kind of composites seems to be a critical parameter during processing. The results obtained using these methods are discussed in the next sections.

It is interesting to consider the ultimate working temperature of hybrid C-SiC composites, either as carbon fibres in a SiC (or C-SiC) matrix, as in the present work, or as SiC fibres in a carbon matrix. Two factors will impose an upper limit in the service temperature:

(a) loss of mechanical properties of SiC at ≈1400°C (Srinivasan - 1989), and

(b) the onset of carbothermal reduction of the SiO_2 layer which protects SiC, at ≈1600°C (Buckley - 1988).

It is possible that the hybrid C-SiC materials may be useful at

temperatures in excess of 1400°C, but the extent of improvement (if any) is not known at present.

6.3.2 - Microstructure of Unidirectional CFRC composites modified by interlayer SiC

The micrographs of the *green* unidirectional CFRC composites modified by interlaminar SiC, Figure 5.2 and 5.3, are similar to those of the conventional CFRC composites in the *green* state, discussed in Chapter Four. However in the case of composites with interlaminar alkoxide gel the interface between laminae are more clearly distinguished.

After firing up to 1400°C, the UU-1400-SG composite exhibited a clearly distinguished interlayer of SiC with many cracks, possibly formed during firing. An X-ray map for this composite, Figure 5.6, identifies the SiC in the bulk composite which follows the contours of the laminae. The TS-1400-SG composite has a SiC interlaminar region that appears to be formed as clusters rather than as a continuous layer, as for UU-1400-SG. An X-ray map for Si on this composite, Figure 5.6, showed an interlaminar, discontinuous layer of SiC. Like the conventional CFRC composites, these hybrid C-SiC materials are porous materials. The microcracks and pores generated during the heat treatment schedule are then suitable for subsequent infiltration of the *sol* alkoxide.

6.3.3 - Mechanical properties of CFRC composites modified by interlayer SiC

Modification of CFRC composites by interlayer SiC results in modest changes in properties in relation to their similar conventional CFRC

counterparts heat treated at 1100°C. The mechanical property results obtained on CFRC composites modified by interlayer SiC suggest that the flexural modulus of these CFRC composites is mainly governed by the presence of the interlayer SiC. There is practically no effect of SiC on the flexural strength of the composites, compared with the conventional CFRC composites described in Chapter Four, possibly due to the large scatter of data, Table 5.1.

The TS-1400-SG composite is still a brittle material and failure is followed by a sharp drop in the stress, Figure 5.8. The failure mode of the composite shows that the material does not break in two parts like the TS-1100 composite. Delamination cracking in the TS-1400-SG composite suggests that the interlaminar SiC becomes the weak plane leading to a failure mode that can be defined as catastrophic delamination. The lower flexural modulus, due to the low density, and higher strain to failure of the TS-1400-SG leads to a higher nominal fracture initiation energy, suggesting that the interlayer SiC is beneficial for an increase in toughness, but the fracture pattern is still catastrophic. The UU-1400-SG composite has a significant increase in modulus, possibly due to the stiffening effect of the interlaminar SiC. The stress-deflection curves for both UU-1400-SG and UU-1100 composites are similar, Figure 5.8, suggesting that fibre bundle sliding is still the dominant effect in the failure pattern in the UU-1400-SG.

6.3.4 - Microstruture of Unidirectional CFRC composites modified by brush coated SiC

The main modifications in the microstructure of the CFRC composites SiC brush coated are closely related to the ones discussed for KKarb and Sigri composites. As before, they are concerned with the ability of the SiC

sol-gel to fill pores and cracks and form a surface oxidation resistant coating over the surface of the CFRC composite.

The ability of the SiC sol-gel to fill cracks was clearly demonstrated by the examples showed in Figures 5.9 and 5.11. The SiC sol-gel penetrates deeply inside the the UU-1400-SiC and UU-2500-SiC composites filling many of the microcracks. SiC rich regions linking pores are seen in both composites, suggesting that SiC penetrates via the network of large pores in the composite.

In the composites TS-1400-SiC and TS-2500-SiC the SiC penetrates throughout the thickness of the composite including regions far from the surface, but in a discontinuous and irregular manner, Figures 5.10 and 5.12. Si X-ray mapping also shows that deep penetration of SiC into the composite is facilitated by interconnected pores. In these composites, as for the CFRC composites with untreated and unsized fibres, it is possible that the majority of the brushed of SiC sol-gel applied over the surface of the CFRC composite was consumed in filling cracks and pores rather than in forming a continuous overlayer coating, as observed for the Sigri CFRC composite. This was particularly observed in the TS-1400-SiC coated material, Figure 5.8, where some areas have coating thickness of ≈100 μm and other areas only a thin layer was formed and nearby cracks are filled.

Determinations of the SiC content in the SiC brush coated CFRC composites were made by ASTM-C561 method (Ash, in Graphite). All the brush coated samples revealed a SiC content of 2.0-2.5%wt. After the total burn-off the carbon in the SiC coated unidirectional composites, the residual SiC has a fibrillar nature. Similarly to KKarb and Sigri composites, this small amount of SiC obtained by sol-gel method was sufficient to modify to some extent the mechanical properties, fracture mode and AE patterns, as

will be discussed in the following section.

6.3.5 - Mechanical Properties of Unidirectional CFRC composites SiC brush coated

The failure modes for TS-1400-SiC and TS-1100 composites are similar, Figure 4.14, being dominated by fast fracture characterized by a flat fracture surface with negligible fibre pull-out, Figure 4.17. The incorporation of SiC increase the mid-span deflection of the TS-1400-SiC composite, and as consequence the fracture initiation energy is almost doubled in comparison with TS-1100 material. As for other porous SiC coated composites, *e.g.* Sigri, the SiC brush coating of the TS-1100 composite fills pores and cracks resulting in a TS-1400-SiC composite with increased strength.

Similarly to other CFRC composites made with untreated and unsized fibres, the failure modes for the UU-1400-SiC composite, Figure 5.14, are also dominated by fibre bundle sliding resulting in stress-deflection curves with similar shapes. But the incorporation of SiC in this composites resulted in a lower mid-span deflection, and consequently the fracture initiation energy of the UU-1400-SiC material decreased by ≈35% compared to UU-1100 composite, due the embrittling effect of SiC. Reductions in bulk density, Table 5.2, after the multiple firings for the SiC coated CFRC composites were observed, giving a remarkable increase the nominal fracture initiation energy for the TS-1400-SiC composite and reductions for the other composites, as can be seen in Figure 6.9. Figure 6.9 shows also that, as for the conventional CFRC composites discussed in Section 6.2, there is a broad correlation between the nominal fracture initiation energy and mid-span deflection.

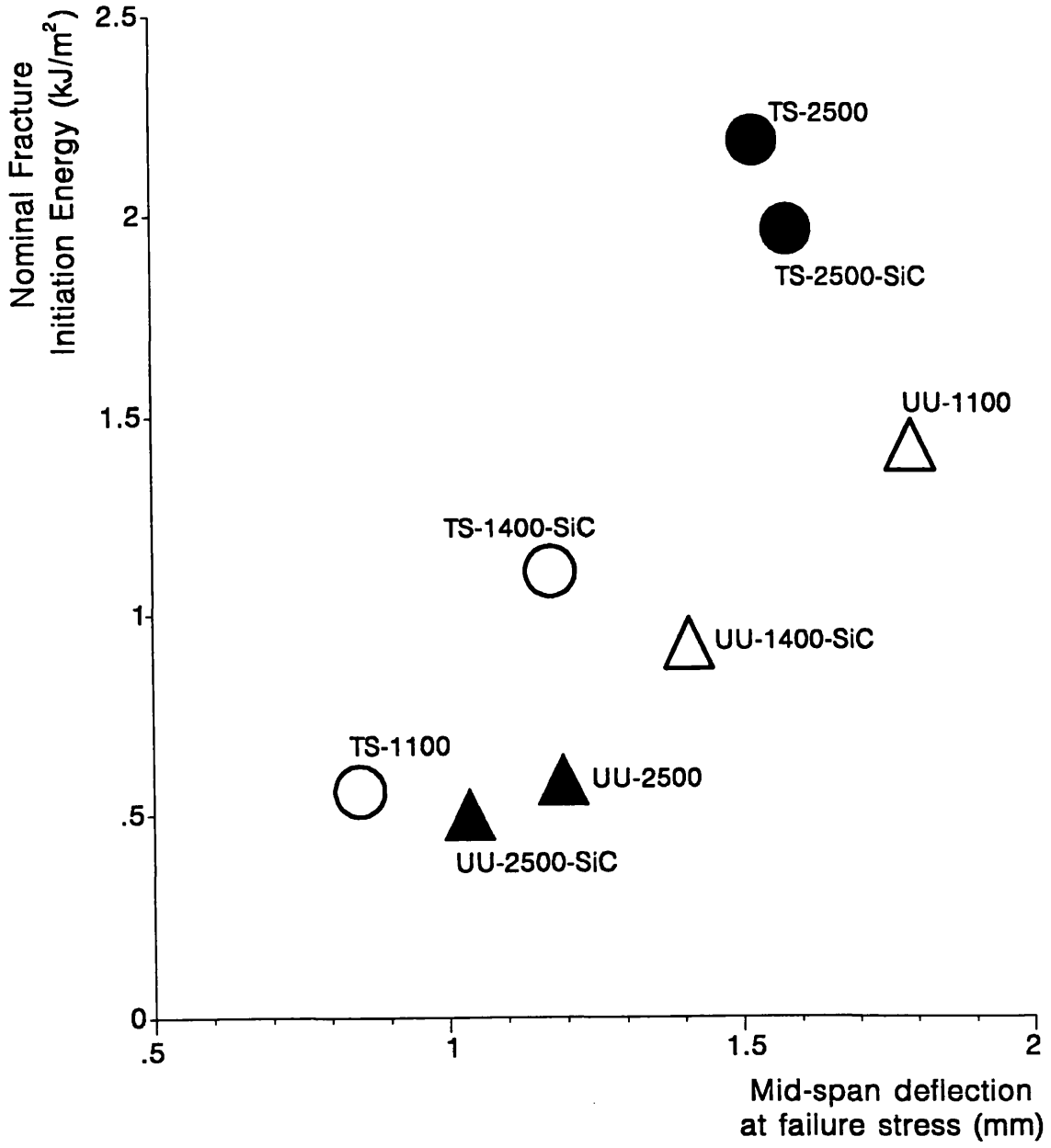

Figure 6.9 - Nominal fracture initiation energy as a function of mid-span deflection at failure stress for CFRC composites coated with SiC.

The SiC brush coating does not affect significantly the deformation and fracture of the TS-2500 material because the coating is not continuous and SiC mainly fills pores and cracks, as can be seen by the optical micrograph of Figure 5.11. As a consequence the TS-2500 and TS-2500-SiC composites have similar stress-deflection curves, flexural strength and flexural modulus, Table 5.3, leading also to a similar failure strain and fracture initiation energy. The failure modes, Figure 5.15, indicate that the presence of SiC in the TS-2500-SiC composite confines the extension of the microcrack network, Figure 4.9A, about the neutral axis, suggesting that most of the SiC is in the outer parts of the TS-2500-SiC composite.

A simple way to consider the effect of SiC on the properties of the unidirectional composites is to apply the rule of mixtures. The micrographs of the SiC coated composites show that there is penetration throughout the porosity by the SiC, Figures 5.10 and 5.13 for example.

Considering the case for the TS-1400-SiC composite, the first assumption which can be made is that the porosity in the composite is completely filled by SiC. The effect on the strength and modulus of the coated composites, σ_{coat} and E_{coat}, can be represented by the rule of mixtures (Hull - 1981):

$$\sigma_{coat} = \sigma_{CFRC} \cdot V_{CFRC} + \sigma_{SiC} \cdot V_{SiC}$$

$$E_{coat} = E_{CFRC} \cdot V_{CFRC} + E_{SiC} \cdot V_{SiC}$$

where σ_{CFRC} and E_{CFRC} are the flexural strength and modulus of the uncoated composites, σ_{SiC} and E_{SiC} are the strength and modulus of SiC and V_{SiC} is the volume fraction of SiC.

The volume of SiC in the TS-1400-SiC can be calculated by the equation:

$$V_{SiC} = \frac{W_{SiC} \cdot \rho_{Coat}}{\rho_{SiC}}$$

where W_{SiC} = weight fraction of SiC in the composite, ρ_{Coat} = density of the coated composite and ρ_{SiC}= density of SiC (≈3.2 g/cm^3) revealed a volume fraction of 0.001 of SiC. The flexural strength of SiC varies between 280 - 930 MPa and the elastic modulus varies between 350 - 550 GPa (Srinivasan - 1989). Assuming that the SiC fills some of the pores from the original TS-1100 composite and forms an interconnected porous SiC network the values of strength and modulus will be assumed as σ_{SiC}=700 MPa and E_{SiC}=415 GPa, respectively. Thus, the calculated strength and modulus for the TS-1400-SiC composite with V_{SiC}=0.001 are in Table 6.4.

CFRC composite	TS-1100(1) exp	TS-1400-SiC(1) exp	TS-1400-SiC(2) calc
σ_{CFRC} (MPa)	135±22	198±28	102
E_{CFRC} (GPa)	115±7	106±7	87

Table 6.4 - Measured flexural properties (1) for TS-1100 and TS-1400-SiC composites, and calculated values (2) of the TS-1400-SiC using the rule of mixtures (assuming V_{SiC} = 0.001 and V_p = 0.25)

A reasonably agreement was found for the experimental and calculated flexural modulus for the TS-1400-SiC, but a lower value for the flexural strength was found. This suggests that the simplistic approach of the rule of mixtures is less sensitive when calculating the flexural modulus as opposed

to the flexural strength. Moreover the density of the TS-1400-SiC composite, Table 5.2, is much lower than the density of the TS-1100 composite, which was used in the calculations.

It is interesting to compare the relative influence of incorporation of SiC in CFRC composites. For example, considering the tensile strength in the X-direction for unidirectional, bidirectional and orthogonal weave composites in Table 1.1. If a tensile strength of a porous SiC is ≈300 MPa (Srinivasan - 1989) then it will make a negligible contribution to the unidirectional composite since this composite has the most effective carbon fibre utilization. On the other hand the tensile strength of SiC would make a significant contribution to the strength of the orthogonal weave composite. The extent to which these contributions are realistic has still to be determined.

6.3.6 - Acoustic Emission of SiC coated CFRC composites

The development of the AE events for the unidirectional CFRC composites and SiC coated CFRC composites, Chapters Four and Five respectively, are mainly dominated by the microcracking of SiC. Although there are increases in AE event counts, these do not appear to influence significantly the shape of the stress-deflection curves, Figures 5.14 and 5.15. These increases in the AE counts at failure stress due to microcracking of SiC have resulted in a shift in the amplitude distribution to higher values for all the composites studied, Figures 5.18 and 5.21.

On heat treatment of the unidirectional CFRC composites made with treated and sized fibres there is an increase in the total number of AE counts at failure from ≈1740 to ≈8900, Tables 4.3 and 5.3 respectively. This increase was attributed to the development of cracks at the fibre/matrix

interface and extension of the microcrack network developed in the composite on heat treatment to 2500°C, Figure 4.9A. Figure 6.10 shows that addition of SiC to the 2500°C composite, TS-2500-SiC, also produces an increase in AE counts at failure, Table 5.3. Comparing the AE counts for the TS-1100 and the TS-2500-SiC composite shows an increase of more than 10 times, Figure 6.10.

On the other hand the AE counts at failure for the UU-1100, UU-2500 and UU-2500-SiC are ≈13100, ≈8570, and ≈16500 respectively, Tables 4.3 and 5.3. The decrease in AE on heat treatment of the uncoated composite was attributed to enhancement of fibre bundle sliding and, as before, the high value of AE counts for the SiC coated composite was due to SiC microcracking. Thus, in the case of the CFRC composites made with treated and sized fibres, AE appears to be additive, whereas for the CFRC composites made with untreated and unsized fibres the AE counts appear to be subtractive.

Figure 6.10 shows also that the correlation between AE counts and failure strain, represented by mid-span deflection for SiC coated CFRC composites. The correlation is weaker than that found for the uncoated composites because in some cases sudden bursts in the AE counts are observed, *e.g.* Figure 5.18, that may weaken the correlation.

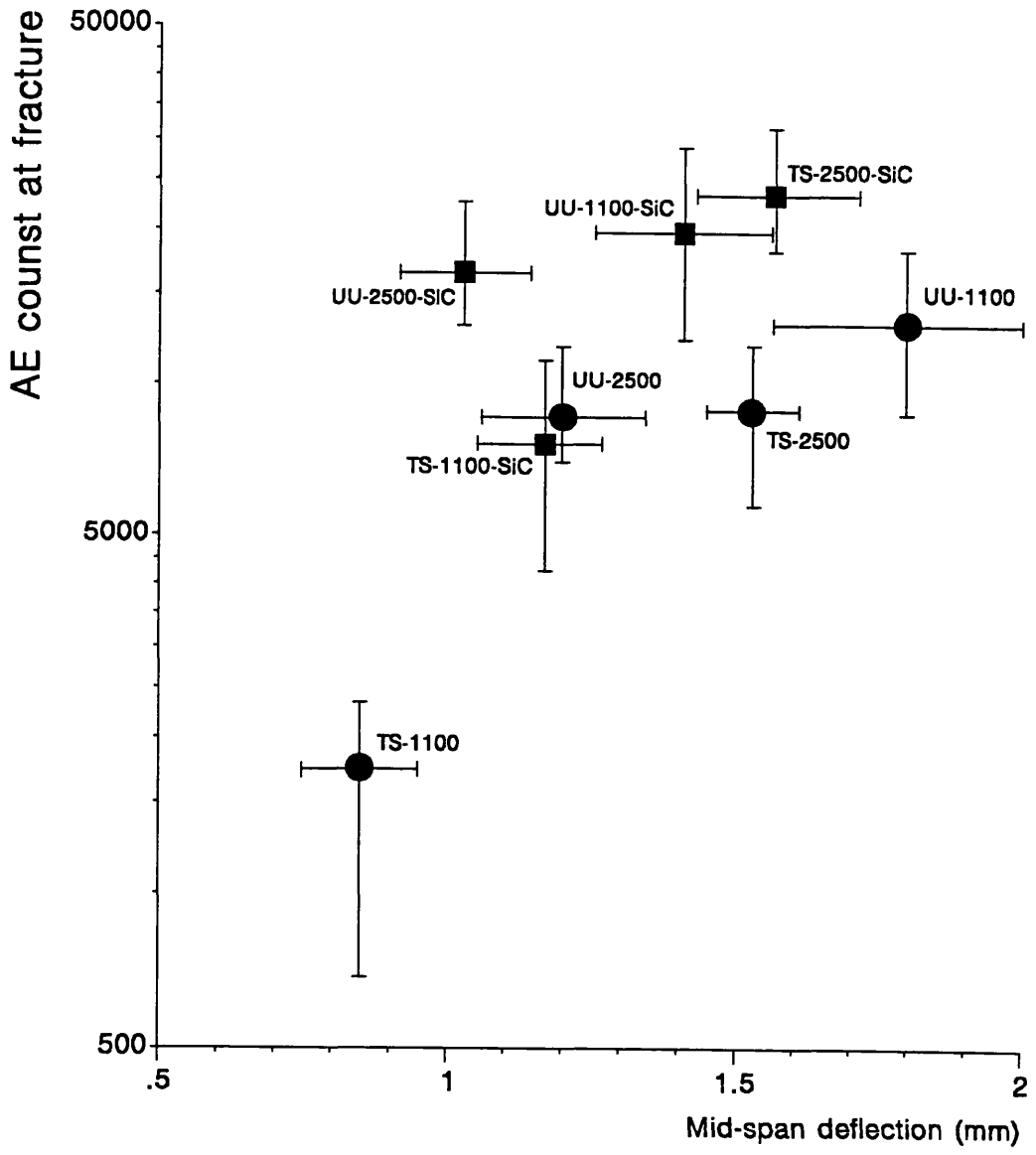

Figure 6.10 - Acoustic emission counts at peak stress as a function of mid-span deflection at peak stress for uncoated and SiC coated CFRC composite.

Amplitude distribution of AE events generated during failure of materials contains the potential information about the fracture mechanism. Common types of amplitude distributions for unidirectional, bidirectional, and SiC coated CFRC composites studied in this work are shown in Figure 6.11. For most of the amplitude distributions a poor fit of the Pollock power law is found.

Figure 6.11A describes a situation where the amplitude distribution is linear in the entire range of amplitude levels, having similar proportions of low and high amplitude events. This type of amplitude distribution conforms the Pollock law in the entire range of amplitude levels, giving a value of $b \approx 1$. Pollock (1973) found values of $b \approx 1$ for most of the materials that he studied and he suggested that $b \approx 1$ may be regarded as describing a normal or standard Pollock law distribution.

Figure 6.11B shows an example of a "bowed" distribution, where there are no AE events above a certain amplitude level. This type of distribution does not conform the Pollock law except possibly in a narrow range of small amplitudes. All the CFRC composites made with untreated and unsized fibres show this type of distribution, probably because failure in these materials is characterized by low energy events associated mainly with fibre bundle sliding.

Figure 6.11C illustrates amplitude distributions where there is a higher proportion of high amplitude events than would be expected from the Pollock plot, and Figure 6.11D illustrates the inverse of Figure 6.11C, *i.e.* a amplitude distribution where there is a lower proportion of high amplitude events than would be expected from the Pollock plot. These amplitude distributions conform to the Pollock law in the low and medium amplitudes, and the exponent b for both situations, Figures 6.11C and 6.11D, can be

calculated in these amplitude ranges. Due to the logarithmic scale care must be taken when calculating the exponent of the Pollock law, and it is always necessary to specify the range in which the Pollock law is found. As a minimum the linear range of the Pollock plot is expected to extend at least for one decade in AE counts, N(a), in the range where the number of AE counts is substantial, *e.g.* for $100 < N(a) < 1000$.

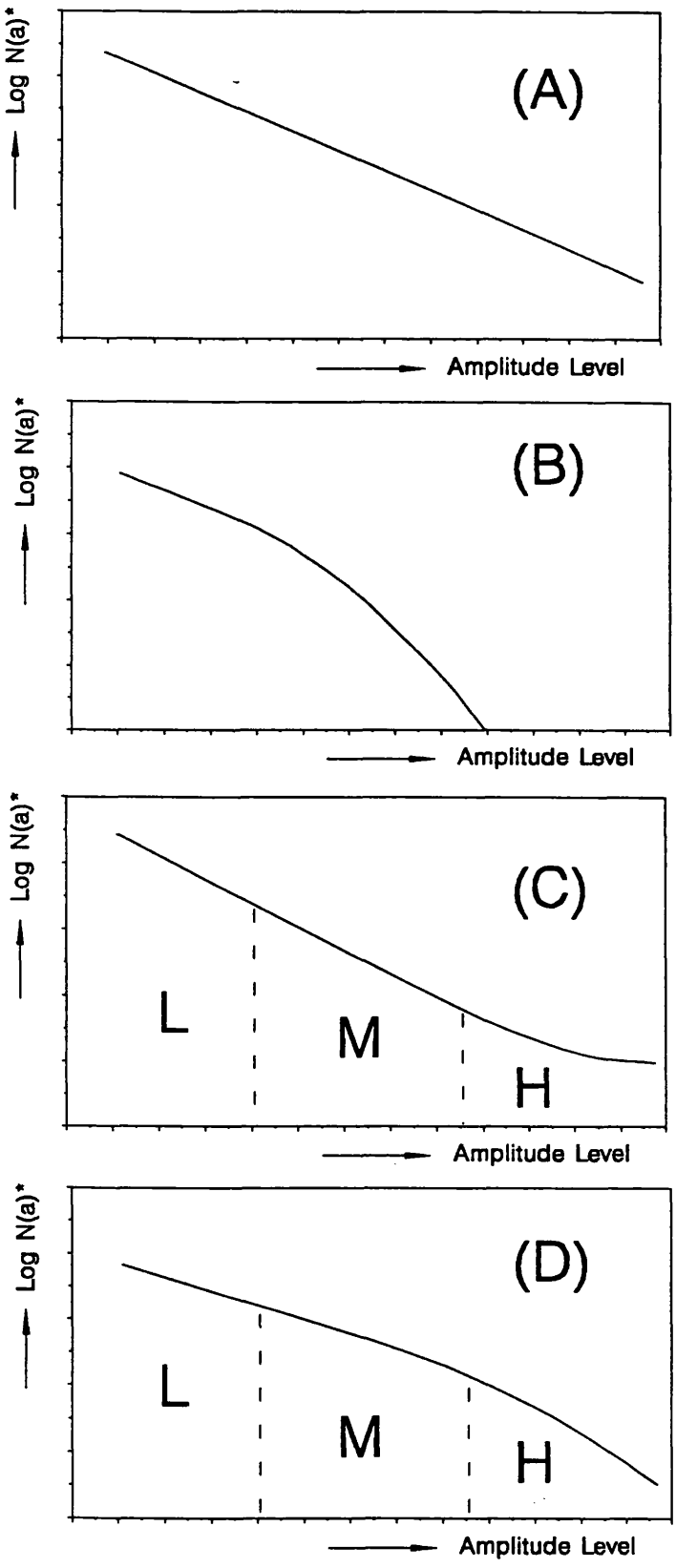

Figure 6.11 - Types of Acoustic Emission amplitude distributions at failure stress found in this work. The composites, and respective Pollock exponent b values, for which these distributions were found are shown in relation to each plot. L, M, H are low, medium and high energy events, respectively. Log N(a)* in arbitrary units.

6.4 - Conclusions

6.4.1 - Commercial woven CFRC composites

The flexural modulus of the Sigri CFRC composite (≈53 GPa) was higher than for KKarb material (≈13 GPa); this is attributed to the greater elastic modulus of the PAN fibres used in the Sigri composite. The flexural strength of the Sigri (≈215 MPa) and KKarb (≈160 MPa) CFRC composites in the warp direction were similar. KKarb material in general fails by ply delamination, whereas the Sigri material fails by a mixture of delamination, cross-bundle and shear cracking, which reflects the different starting materials, composite construction and processing conditions.

Incorporation of SiC obtained by a sol-gel method has been demonstrated for the first time to be useful to enhance mechanical properties of CFRC composites. Using this principle, the flexibility of the formulation can be modified to adjust it for impregnation with a controlled rheology as well as for surface oxidation protection coating.

The relative open porosity between KKarb and Sigri CFRC composites is an important factor to determine the extent of internal penetration of the SiC sol-gel, as revealed by the X-ray maps for Si. A lower open porosity, as in KKarb composite ($V_{pore} \approx 0.05$), gives rise to a thicker layer of SiC and a ≈25% increase in flexural modulus, due to composite beam effect, with no significant change in flexural strength. In composites with higher open porosity, as in Sigri composite ($V_{pore} \approx 0.14$), the SiC sol-gel is mainly consumed by filling cracks and pores, and a 25% increase in strength with no significant change in flexural modulus was found. More studies of other CFRC composites with different extents of porosity will give valuable information about the efficiency of the SiC sol-gel to fill remaining pores and

increase mechanical properties. In that particular, a first step of vacuum impregnation followed by pressurisation and subsequent gelation is a promising procedure to follow, as revealed by this work.

The incorporation of SiC in the CFRC composites, either by brush coating, vacuum impregnation, or pressure impregnation gives rise to a more brittle failure mode in KKarb or Sigri composites. In relation to the uncoated KKarb composite, the SiC coated samples have a mid-span deflection and a lower nominal fracture initiation energy. On the other hand, the SiC coated Sigri has a higher mid-span deflection and a higher fracture initiation energy than the uncoated Sigri.

SiC coating obtained by the sol-gel method mainly reduces the oxidation rate of CFRC composites in air. Reductions in the oxidation rate for Sigri and KKarb composites at 1200°C are over 25%. Thicker surface coatings may improve the temperature of onset of oxidation. In this particular only the borate glassy layer has been satisfactory, with delays in the temperature of onset of oxidation over 300°C. The susceptibility to moisture absorption of borate glasses can be studied by additions of alkali oxides, such as LiO_2, with minimum change in the wetting and viscosity characteristics of the glass-ceramic coating.

6.4.2 - Unidirectional CFRC composites

A systematic study of processing and characterisation of CFRC composites is presented. It has been shown that the surface activity of the carbon fibres affects the microstructure, mechanical properties, failure mechanism, oxidation behaviour and the pattern of the AE events generated during loading. The CFRC composites obtained in this work are highly

heterogeneous so that there is a large amount of scatter in the results of mechanical tests that appears to be an inherent feature of mechanical testing of CFRC composites which must be accepted when working with these materials. Stress graphitisation was identified in CFRC composites made with treated and sized and untreated and unsized carbon fibres, when heat treating these composites at 2500°C. It would be interesting to investigate the mechanical properties of CFRC composites with carbon fibres with different degrees of fibres surface treatment.

Due to weight loss mainly during carbonisation in the temperature range of 200-1000°C the CFRC composites suffer cross sectional shrinkage. After heat treatment and cool down in that temperature range the cross sectional shrinkage of a UU-1100 composite is ≈1/3 of the shrinkage of a TS-1100 composite. Dilatometry could be a valuable tool to investigate more accurately the shrinkage profile of *green* composites.

This work has introduced the concept of making hybrid CFRC composites with carbon fibres of different surface activities in order to control mechanical properties. Different lay-up designs can be investigated in the future. This concept can be extended in the future to use commingled fibres not only for controlling properties but for a reduction in costs.

For CFRC composites heat treated at 1100°C, the T5U4-1100 hybrid composite has the highest flexural strength (≈165 MPa) and the TS-1100 composite has the highest flexural modulus (≈114 GPa). The UU-1100 composite has the highest mid-span deflection, the highest toughness due to fibre pull-out and fibre bundle sliding mechanisms, and it has a flexural strength similar to the TS-1100 composite.

For CFRC composites heat treated at 2500°C, the TS-2500 composite has the highest flexural strength (≈297 MPa) and modulus (≈120 GPa) and the

UU-2500 composite has the lowest flexural strength (≈116 MPa) and modulus (≈61 GPa) at the lowest mid-span deflection. The hybrid T5U4-2500 composite has an intermediate flexural strength and modulus and the mid-span deflection is mainly controlled by the presence of laminae containing treated and sized fibres.

6.4.3 - Unidirectional CFRC composites modified by SiC sol-gel

For the first time a study of carbon fibre reinforced composites with a hybrid C-SiC matrix where the SiC is introduced using a sol-gel method is presented. Prepregging a mixture of the alkoxide sol-gel with a phenolic matrix was shown not be a successful method to obtain unidirectional composites with sufficient integrity. Other reinforcements such as woven preforms can be tested in future work. Brushing SiC sol-gel in between layers of the prepregs during stacking was shown to be successful in obtaining a C-SiC hybrid composite using a heating schedule that matches the carbonisation of the phenolic resin and the firing of SiC. Flexural modulus in these composites is mainly governed by the interlayer SiC, although no significant changes were found in the flexural strength in relation to conventional CFRC composites. Brush coating SiC on unidirectional CFRC composites, as was also shown for woven KKarb and Sigri composites, was shown to be a successful method for modifying mechanical properties. It may be possible to infiltrate the SiC sol-gel by vacuum impregnation followed by pressurisation. This procedure can be used in the early stages of the fabrication of CFRC composites with successive re-impregnation cycles to enhance mechanical properties and oxidation protection. It should be interesting also to investigate the effect of the incorporation of SiC at the early stages of the fabrication process heat

treating the hybrid C-SiC composite at graphitizing temperatures.

For the first time a study of acoustic emission, AE, from unidirectional CFRC composites as a function of applied flexural stress is presented. It was shown that the presence of SiC in the composites generally increased AE due to microcracking of the SiC. AE amplitude distributions proved also to be quite useful in helping to interpret the processes occurring during deformation and failure of the composites. The empirical Pollock law for AE amplitude distribution, which has been used widely for other materials was found to be of limited use when applied to these composites. Overall, this work has demonstrated that AE is a valuable tool to study and correlate the microstructure, mechanical behaviour and failure modes of unidirectional and bidirectional CFRC composites, uncoated and SiC coated.

APPENDIX I

Physical Properties of KKarb Type A and Sigri CC1501G CFRC composites (Manufacture's data)

KKarb Type A

Axis	X (warp)	Y (fill)	Z (out-of-plane)
Compressive Strength(MPa)	70	42	104
Thermal Conductivity W/(m.K) @120°C	14	12	7
Tensile Strength, MPa	70	42	
Tensile Modulus, GPa	15.2	11	
Tensile Strain to Failure(%)	0.6	0.6	
Flexural Strength, MPa	86.2		
Izod Impact Value, N.m	3.4		
Interlaminar Shear strength, MPa	10.4		
Specific Gravity (g/cm^3)	1.36		
Volume of fibres (%)	45		
Bundle size (fibres/tow)	1000		

Sigri CC1501G (HTT = 2000°C)

Flexural Strength (MPa)	210 - 250
Dynamic Modulus (GPa)	60 - 65
Tensile Strength (MPa)	260 - 330
Interlaminar Shear Strength (MPa)	9 - 12
Bulk density (g/cm^3)	1.40 - 1.45
Volume of fibres (%)	38
Bundle size (fibres/tow)	3000

APPENDIX II

Properties of the phenolic resins
(Manufacture's data)

CASCOPHEN SC1008P*

Solids content (3h at 135°C)	58 - 64%
Viscosity at 25°C (cP)	180 - 360
pH	7.9 - 8.5
Specific gravity	1.07 - 1.10

* Typical cure cycle : 24h 70°C, 24h 80°C, 24h 90°C, 24h 100°C, raising temperature 20°C every 12h up to 180°C.

CELLOBOND J2027L

Brownish-red liquid. Unmodified phenol/formaldehyde resol resin.

Viscosity at 25°C	220-320 cP
Relative Density at 25°C	1.22 - 1.23
pH	7.3 - 7.8
Free phenol	11% maximum
Free formaldehyde	2.5% maximum
Flash Point	> 100°C

APPENDIX IIIA : FTIR Spectra of Borden SC1008P Phenolic Resin

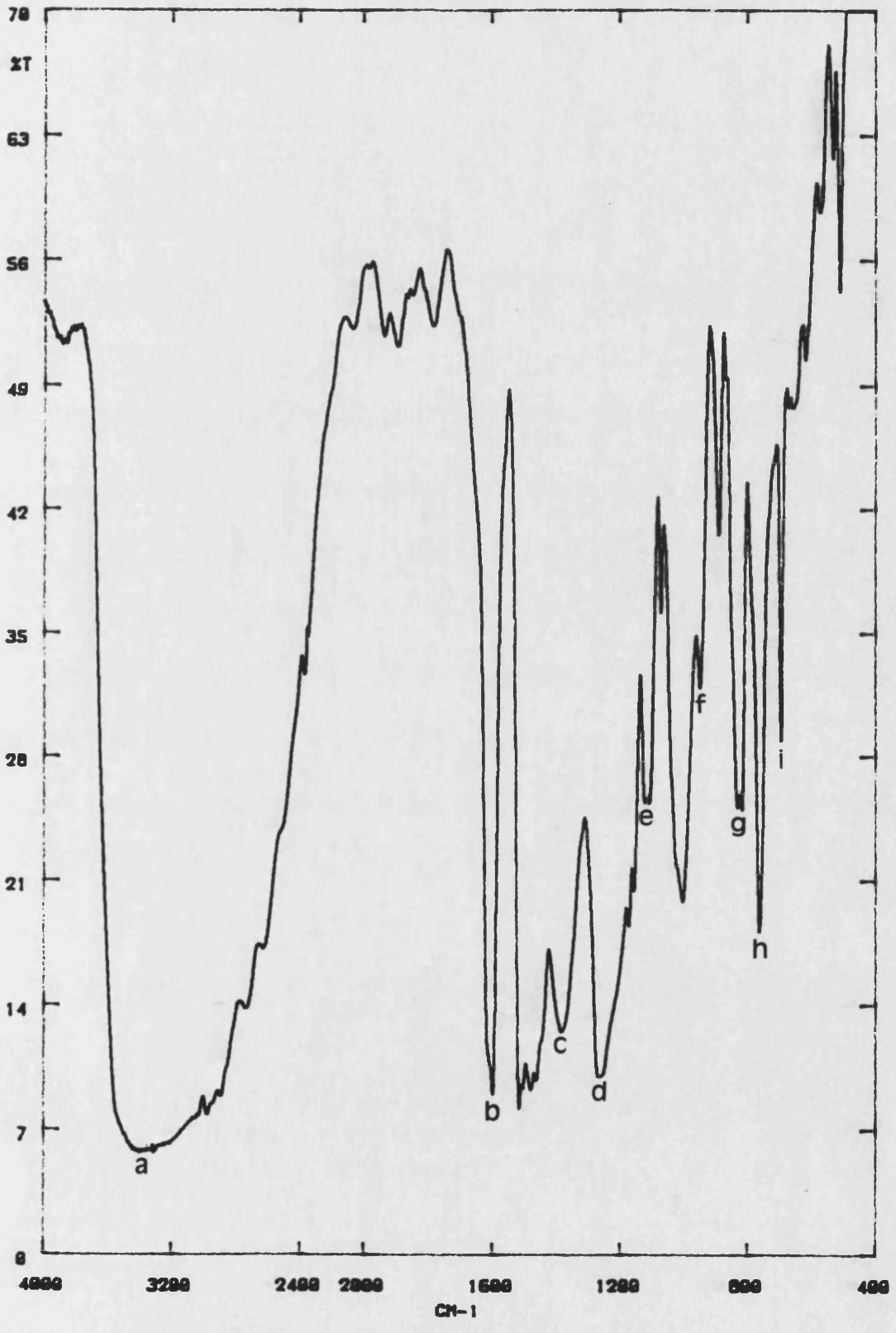

APPENDIX IIIB

Assignment of the main peaks observed in the FT-IR spectrum for the Borden SC1008P Phenolic Resin (Appendix IIIA)

Peak	Wave number (cm^{-1})	assignment
a	3305	-OH stretch
b	1596	C=C conjugated (ring)
c	1381	aromatic alcohol
d	1260	aryl ether
e	1100	-CH deformation (in plane)
f	1071	aromatic ether group
g	947	isopropyl
h/i	761/693	-CH bending (out of plane)

APPENDIX IV

Carbon Fibre Properties
(Manufacture's data)

1) Grafil E/XA-S 12000 Carbon Fibres per tow

Strength (GPa)	4.33
Modulus (GPa)	225
Mass/Unit Length	790 mg/m
Fibre Density	1.80 g/cm^3
Size Content	1.64%/Mass

2) Grafil XA-U/Unsized 12000 Carbon Fibres per tow

Strength (GPa)	4.09
Modulus (GPa)	225
Mass/Unit Length	793 mg/m
Fibre Density	1.79 g/cm^3

APPENDIX V

Formula for Flexural Strength and Flexural Modulus calculations

$$\sigma_{max} = 1.5Ls/(wd^2)$$

$$\tau_{max} = 0.75\ L/\ (bd)$$

$$E = (Ls^3)/(4Dwd^3)$$

where :

σ_{max} = Flexural Strength (Pa)

L = Ultimate breaking Load (N)

s = span (m)

w = width (m)

d = depth (m)

τ_{max} = Shear Strength (Pa)

E = Flexural Modulus (Pa)

D = mid-span deflection at the ultimate breaking load (m)

APPENDIX VI

Bulk densities of some common carbon materials
(Jenkins - 1976, Donnet - 1990)

Material	Bulk Density (g/cm^3)
Fine grained isotropic graphite ($\sigma_f \cong 25$ MPa, $E_f \cong 12$ GPa)	1.90 - 2.00
Typical glassy carbon ($\sigma_f \cong 150$ MPa, $E_f \cong 25$ GPa)	1.45 - 1.50
HM ex-PAN carbon fibre ($\sigma_t \cong 2.50$ GPa, $E_t \cong 500$ GPa)	1.85 - 1.95
HS ex-PAN carbon fibre ($\sigma_t \cong 2.80$ GPa, $E_t \cong 250$ GPa)	1.75 - 1.80
Mesophase Pitch carbon fibre ($\sigma_t \cong 2.00$ GPa, $E_t \cong 650$ GPa)	2.00 - 2.10
Rayon carbon fibre ($\sigma_t \cong 1.80$ GPa, $E_t \cong 30$ GPa)	1.30 - 1.90
Graphite whisker ($\sigma_t \cong 20$ GPa, $E \cong 1000$ GPa)	2.26

where:

σ_f = Flexural Strength

E_f = Flexural Modulus

σ_t = Tensile Strength

E_t = Tensile Modulus

APPENDIX VII : Pore Volume Distribution

(d=pore entrance diameter (nm))

Sigri CC1501G

Distribuition	Volume (cm^3/g)
$d < 10$	0.013
$10 < d < 10^2$	0.042
$10^2 < d < 10^3$	0.019
$10^3 < d < 10^4$	0.026
Total	0.100

KKarb Type A

Distribuition	Volume (cm^3/g)
$d < 10$	0.013
$10 < d < 10^2$	0.029
$10^2 < d < 10^3$	0.007
$2.10^3 < d < 6.10^3$	0.006
Total	0.055

APPENDIX VIII

Acoustic Emission Amplitude Distributions

The Pollock Law

Pollock (1973) suggested that AE amplitude distributions can often to be fitted to an empirical power law of the form

$$n(a) = (a/a_0)^{-b} \qquad \text{(VIII.1)}$$

where n(a) defines the fraction of the emission population whose peak amplitude exceeds a, a_0 is the lowest detectable amplitude and the exponent "b" is used to characterise the amplitude distribution (Pollock, 1973). The minimum detectable AE threshold (a_0) on the Marandy MR1004 AE Analyser is 10 mV and each amplitude distribution level is 2.4 dB wide. The Marandy Analyser has 25 amplitude distribution levels and therefore the threshold of amplitude level, x, is given by 2.4x dB, thus the relationship between the amplitude of an AE event (mV), and the threshold of the amplitude level is

$$2.4x = 20 \log (a/a_0) \qquad \text{(VIII.2)}$$

Equating equations VIII.1 and VIII.2 gives

$$\log n(x) [=\log n(a)] = -0.12bx \qquad \text{(VIII.3)}$$

where n(x) is the fraction of the emission population whose peak amplitude exceeds the minimum threshold of amplitude level x. The fraction of all AE events with amplitudes exceeding the minimum threshold in x, n(x) is

$$n(x) = N(x)/N(x_0) \qquad \text{(VIII.4)}$$

where N(x) is the number of events with amplitudes exceeding the minimum threshold in x, and $N(x_0)$ is the total number of AE events above the minimum detectable threshold a_0. Taking logs on both sides of equation

VIII.4 gives

$$\log n(x) = \log N(x) - \log N(x_0) \qquad \text{(VIII.5)}$$

Substituting equation VIII.3 in equation VIII.5 gives

$$\log N(x) = -0.12bx + \log N(x_0) \qquad \text{(VIII.6)}$$

Therefore, to obtain a Pollock distribution from AE amplitudes from the Marandy system, we must plot the total number of AE events above amplitude level x (inclusive of those AE events in x), log N(x), versus the amplitude level number, x. The gradient of line will equal -0.12b and the intercept on the log N(x) axis will equal log $N(x_0)$. The value of "b" can than be compared to results from other systems.

BIBLIOGRAPHY

Aveston - 1971, J. - "Strength and toughness in fibre-reinforced ceramics", in *The properties of fibre composites - Conference Proceedings*, IPC Science & Technology Pres Ltd, pp. 63-74, 1971.

Bashford - 1992, D. P. - "CVD for high temperature applications" - *Metals and Materials*, pp. 79-84.

Bradshaw - 1978, W. G.; Vidoz, A. E. - "Fiber-Matrix Interations in Unidirectional Carbon-Carbon Composites", *American Ceramic Society Bulletin*, Vol. 57, No. 2, pp. 193-198.

Buckley - 1988, J. D. - "Carbon-Carbon, An Overview", *American Ceramic Society Bulletin*, Vol. 67, No. 2, pp. 364-368.

Burger - 1975, A.; Fitzer, E.; Heym, M.; Terwiesch, B. - Polyimides as precursors for artificial carbon", *Carbon*, Vol. 13, pp. 149-157.

Burns - 1976, R. L.; Cook, J. L. - "Pressure Carbonization of Petroleum Pitches", in *Petroleum Derived Carbons*, ACS Symposium Series 21, Ed. by Deviney, M. L; O'Grady, T. M., Part 13, pp. 139-154.

Castro - 1990, L. D.; McEnaney, B. - Surface Modification of Carbon Materials to Inhibit Oxidation - A Review - *International Symposium on Carbon*, pp. 366-369.

Castro - 1991, L. D. - "*Inhibition of oxidation of Carbon Materials*", PhD Thesis, University of Bath.

Castro - 1992, L. D.; McEnaney, B. - "The Control of High Temperature Corrosion of Engineering Carbons and Graphites", *Corrosion Science*, Vol. 33, No. 4, pp. 527-543.

Chang - 1978, H. W.; Rhee, S. K. - "Oxidation of carbon derived from phenolic resin", *Carbon*, Vol. 16, pp. 17-20.

Chang - 1979, H. W.; Rusnak, R. M. - "Oxidation behavior of Carbon-Carbon Composites", *Carbon*, Vol. 17, pp. 407-410.

Chard - 1976, W.; Conaway, M.; Niesz, D. - "Advanced High Pressure Graphite Processing", in *Petroleum Derived Carbons*, ACS Symposium Series 21, Ed. by Deviney, M. L. O'Grady, T. M., Part 14, pp. 155-171.

Chlopek - 1991, J.; Blzewicz, S. - "Effect of processing variables on the properties of Carbon-Carbon composites", *Carbon*, Vol. 29, No.2, pp. 127-131.

Christin - 1980, F.; Heraud, L.; Choury, J. J.; Naslain, R.; Hagenmuller, P. - "In-depth Chemical Vapour Deposition of SiC within porous Carbon-Carbon Materials", *Proc. 3rd European Conf. on Chemical Vapour Deposition*, pp. 154-161.

Crocker - 1991, McEnaney, B. - "Flexural Strength and Fracture Mechanisms of Oxidised 2D-Carbon/Carbon Composites", *Carbon 91.*

Dacic - 1981, B.; Marinkovic, S. - "Carbon fibre/Carbon Composites form propylene by Chemical Vapour deposition", *High Temperatures-High Pressures*, Vol. 13, pp. 185-192.

Davis - 1976, H. - "Material and Process Effects on Carbon/Carbon Composite Shear Strength", *Journal of Spacecraft*, Vol. 13, No. 8, pp. 456-460.

Dhami - 1993, T. L.. Bahl, O. P. Manocha, L. M. - "Influence of matrix precursor on the oxidation behaviour of carbon-carbon composites" - *Carbon*, vol. 31, No. 5, pp. 751-756, 1993.

Diefendorf - 1987, R. J. - "Continuous Carbon Fiber Reinforced Carbon Matrix Composites", *Engineered Materials Handbook. Vol. 1:Composites*, pp. 911-914, ASM International.

Dillon - 1990, F.; Marsh, H., Thomas, K. M. - "The Influence of Microstructure on the Oxidation Behaviour of Carbon Matrix Material in C/C Composites", *Carbonne 90*.

Donnet - 1990, J. B.; Bansal, R. C. - *Carbon Fibres*, 2nd Edition, Marcel Dekker, Inc.

Downs - 1991, W. B. ; Baker, R. T. K. - "Novel Carbon fiber-carbon filament structures", *Carbon*, Vol. 29, no. 8, pp. 1173-1179.

Duret - 1983, C. ; Pichoir, R. - Protective Coatings for High Temperature Materials: Chemical Vapour Deposition and Pack Cementation Processes, in *Coatings for High Temperature Applications*, E. Lang, Applied Science Publishers.

Economy - 1992, J.; Jung. H.; Gogeva, T. - A one-step process for fabrication of carbon-carbon composites. - *Carbon*, Vol. 30, No. 1, pp. 81-85.

Ehburger - 1981, P.; Lahaye, J.; Bourgeois, C. - "Characterization of Carbon-Carbon Composites - II : Oxidation Behaviour", *Carbon*, Vol. 19, pp. 7-10.

Ehburger - 1986, P.; Baranne, P.; Lahaye, J. - "Inhibition of the Oxidation of Carbon-Carbon Composite by Boron Oxide", *Carbon*, Vol. 24, No. 4, pp. 495-499.

Eitman - 1974, D. A.; Greszczuk, L. B.; Jortner, J. - "Fiber-matrix interactions in Carbon-Carbon Composites", *SAMPE Symp.*, Vol. 19, pp. 346-358.

Fitzer - 1980, E.; Geigl, K. H., Huttner, W. - "The influence of Carbon Fibre surface treatment on the mechanical properties of Carbon/Carbon Composites", *Carbon*, Vol. 18, pp. 265-270.

Fitzer - 1981, E.; Hütner, W. - "Structure and strength of carbon/carbon composites", *J. Phys. D:Appl. Phys.*, Vol.14, pp. 347-371.

Fitzer - 1986, E.; Gkogkidis, A. - "Carbon-Fiber-Reinforced Carbon Composites Fabricated by Liquid Impregnation", in *Petroleum Derived Carbons*, Part 24, pp. 346-379, ACS Symposium Series 303, Ed. Bacha, J. D.; Newman, J. W.; White, J. L.

Fitzer - 1987, E. - "The Future of Carbon-Carbon Composites", *Carbon*, Vol. 25, No. 2, pp. 163-190.

Forrest - 1983, M. A.; Marsh, H. - "The carbonization of blends of pitches and resins to produce anisotropic carbon and the effects of pressure", *Journal of Materials Science*, Vol. 18, pp. 991-997.

Gebhardt - 1976, J. J.; Stover, E. R.; Mueller, W.; Yodsnukis, J. - "Formation of Carbon-Carbon composite materials by pyrolytic infiltration", Part 17, pp. 212-227, *Petroleum Derived Carbons* - ACS Symposium Series 21, Ed. Deviney, M. L.; O'Grady, T. M.

Gee - 1991, S. M.; Little, J. A. - "Oxidation behaviour and protection of Carbon/Carbon Composites", *Journal of Materials Science*, Vol.26, pp. 1093-1100,.

Gibson - 1988, L. J.; Ashby, M. F. - "*Cellular Solids - Structure & Properties*", Pergamon Press.

Gorman - 1991, M. R. - "Acoustic Emission in 2-D Carbon-Carbon Coupons in Tension", *Journal of Composite Materials*, Vol. 25, pp. 703-714.

Goto - 1986, S.; Han, K. H.; Pierre, G. R. - "A Review on Oxidation Kinetics of Carbon Fiber/Carbon Matrix Composites at High Temperature", *Trans. Iron Steel Inst. Jpn*, 26(7), pp. 597-603.

Granoff - 1973, B.; Pierson, H. O.; Schuster, D. M. - "Carbon-Felt, Carbon-Matrix Composites: Dependence of Thermal and Mechanical Properties on Fiber Volume Percent", *J. Composite Materials*, Vol. 7, pp. 36-52,.

Gray - 1990, G.; Payne, R. S.; Savage, G. M. - "Production and densification of carbon-carbon composites using HIP techniques", *Metal Powder Report*, Vol. 45, No. 4, pp. 290-294,.

Guajioty - 1990, E.; Ginoux, J. L.; Tahon, B.; Bonnetain, L. - "Exudation during rebaking pitch impregnated carbon materials", *Carbonne 90*, pp. 234-235.

Hishiyama - 1974, Y.; Inagaki, M.; Kimura, S.; Yamada, S. - "Graphitization of carbon fibre/glassy carbons composites", *Carbon*, Vol. 12, No. 2, pp. 249- 258.

Hull - 1981, D. "*An introduction to composite materials*". Cambridge. Cambridge University Press.

Huettner - 1990, W. - "Potential of Carbon/Carbon Composites as Structural Materials", *NATO ASI Series, Series E: Applied Science*, Vol. 177, pp. 275-300, in Carbon Fibers Filaments and Composites, Ed. by J. L. Figueiredo et. al.

Inagaki - 1990, M. ; Ibuki, T.; Kobayashi, K.; Sakai, M. - "Interaction Between Pitch and Phenol Resin During Pressure Carbonization", *Carbon*, Vol. 28, No. 4, pp. 559-564.

Jenkins - 1976, G. M.; Kawamura, K. - *Polymeric carbons - carbon fibre, glass and char*, Cambridge University Press.

Jones - 1986, L. E.; Thrower, P. A. ; Walker Jr., P. L. - "Reactivity and Related Microstructure of 3D Carbon/Carbon Composites"; *Carbon*, Vol. 24, No. 1, pp. 51-59.

Jortner - 1986, J. - "Macroporosity and Interface Cracking in Multi-Directional Carbon-Carbons"; *Carbon*, Vol. 24, No. 5, pp. 603-613.

Jortner - 1991, J. - "Shrinkage of fibre bundles during carbonization", *21st Carbon Conference*, pp. 402-403.

Kawamura - 1992, K.; Ono, M.; Okazaki, K. - "Silicon Carbide/Carbon Composite sheets derived from PCS/Coal-Tar pitch mixtures"; *Carbon*, Vol. 30, No. 3, pp. 429-434.

Kimura - 1981, S.; Yasuda, E.; Takase, N.; Kasuya, S. - "Fracture behaviour of carbon fibre/CVD carbon composites" - *High Temperature-High Pressures*, Vol. 13, pp. 193-199.

Klein - 1984, L. C. - "Oxide Coatings from the Sol-Gel Process"; *Ceramic Eng. and Sci. Proc.*, Vol. 5, No. 5-6, pp. 379-384.

Knop - 1985, A.; Pilato, L. A. - *Phenolic Resins-Chemistry, Applications and Performance*, Springer-Verlag.

Ko - 1989, Frank. K. - "Preform Fiber Architecture for Ceramic-Matrix Composites", *Ceramic Bulletin*, Vol. 68, No. 2.

Kotlensky - 1973, W. V. - "Deposition of Pyrolitic Carbon in Porous Solids", in *Chemistry and Physics of Carbon*, Vol. 9, pp. 173-262, Ed. by P. L. Walker, Jr. and Peter A. Thrower.

Kowbel - 1990, W.; Shan, C. H. - "The Mechanism of Fiber-matrix Interactions in Carbon-Carbon Composites", *Carbon*, Vol. 28, No. 2/3, pp. 287-299.

Kowbel - 1989, W.; Shan, C. H. - "Fiber-matrix interactions during a densification of Carbon-Carbon Composites", *19th Carbon Conference*, pp. 348-349.

Lachman - 1978, W. L.; Crawfor, J. A., McAllister, L. E. - "Multidirectionally reinforced Carbon/Carbon Composites", *1978 International Conference on Composite Materials*, Ed. B. Noton, R. Signorelli, K. Street, L. Phillips.

Lausevic - 1986, Z.; Marinkovic, S. - "Mechanical Properties and Chemistry of Carbonization of Phenol Formaldehyde Resin", *Carbon*, Vol. 24, No. 5, pp. 575-580.

Lewis - 1966, J. B. - *Thermal Gas Reactions of Graphite*, Chapter IV, pp. 129-199.

Lewis - 1989, C. - "The unique capabilities of Carbon-Carbon composites", *Materiais Engineering*, pp. 27-31.

Lurie - 1970, R. M. - "3-Dimensional Reinforcements", *Applied Polymer Symposium*, No. 15, pp. 103-111.

Luthra - 1988, K. L.; "Oxidation of Carbon-Carbon Composites - A Theoretical Analysis", *Carbon*, Vol. 26, No. 2, pp. 217-224.

Manocha - 1988a, L. M.; Bahl, O. P. - "Influence of Carbon Fiber type and weave pattern on the development of 2D Carbon-Carbon Composites", *Carbon*, Vol. 26, No. 1, pp. 13-21.

Manocha - 1988b, L. M.; Yasuda, E.; Tanabe, Y.; Kimura, S. - "Effect of Carbon Fiber surface-treatment on mechanical properties of C/C composites", *Carbon*, Vol. 26, No. 3, pp. 333-337.

Manocha - 1988c, L. M. - Changes in physical and mechanical properties of carbon fibre-reinforced polyfurfuryl alcohol composites during their pyrolysis to carbon/carbon composites", *Composites*, Vol. 19, No. 4, pp. 311-319.

Manocha - 1991, L. M.; Bahl, O. P.; and Singh, Y. K. Abnormal behaviour during graphitisation of carbon/carbon composite made with pitch based carbon fibres , *Carbon*, 29(3), pp. 351-360.

Marsh - 1989, H. - *Introduction to Carbon Science*, Butherworths Pub., 1989.

Marinkovic - 1985, S.; Dimitrijevic, S. - "Carbon/Carbon Composites prepared by Chemical Vapour Deposition", *Carbon*, Vol. 23, No. 6, pp. 691-699.

Markovic - 1980, V.; Marinkovic, S. - "A study of pyrolysis of phenolic resin reinforced with carbon fibres and oxidized pan fibres", *Carbon*, Vol. 18, pp. 329-335.

McAllister - 1972, L. E.; Taverna, A. R. - "Development and Evaluation of Mod-3 Carbon/Carbon Composites", *Proc. of 17th Nat. SAMPE Symp.*, Paper III-A-3, pp. 1-7.

McAllister - 1983, L. E.; Lachman, W. L. - "Multidirectional Carbon-Carbon Composites"; *Handbook of Composites, Vol. 4 - Fabrication of Composites* - Ed. A. Kelly and S. T. Mileiko.

McAllister - 1987, L. E. - "Multidirectionally Reinforced Carbon/Graphite Matrix Composites", *Engineered Materials Handbook, Vol 1:Composites*, pp. 915-919, ASM International.

McKee - 1986, D. W. - "Borate Treatment of Carbon Fibers and Carbon/Carbon Composites for Improved Oxidation Resistance", *Carbon*, Vol. 24, No. 6, pp. 737-741.

McKee - 1987, D. W. - "Oxidation behavior and protection of Carbon/Carbon composites", *Carbon*, Vol. 25, No. 4, pp. 551-557.

McKee - 1988, D. W. - "Oxidation Behaviour of Matrix-inhibited Carbon/Carbon Composites", *Carbon*, Vol. 26, No. 5, pp. 659-665.

McKee - 1991, D. W. - "Oxidation Protection of Carbon Materials", in *Physics and Chemisrtry of Carbon*, Vol. 23, Part 3, pp. 173-232.

Meetham - 1991, G. W. - "High-temperature materials - a general review", Journal of Materials Science, No. 26, pp. 853-860.

Mevrel - 1986, R.; Duret, C.; Pichoir, R.. - "Pack cementation processes", *Materials Science and Technology*, Vol. 2, pp. 201-206.

Meyer - 1986, R. A.; Gyetvay, S. R. - "Carbon-Carbon Composites - Matrix microstructure and its possible influence on physical properties", in *Petroleum Derived Carbons, ACS Symposium Series 303*, Part 25, pp. 380-394, Ed. Bacha, J. D.; Newman, J. W.; White, J. L.

Mullin - 1973, J. V. ; Mehan, R. L. - "Evaluation of Composite failure through Fracture Signal Analysis", *Journal of Testing and Evaluation*, Vol. 1, No. 3, pp. 215-219.

Nam - 1992, J. ; Seferis, J. C. - "Initial Polymer Degradation as a process in the manufacture of Carbon-Carbon Composites", *Carbon*, Vol. 30, No. 5, pp. 751-761.

Naslain - 1981, R.; Rossignol, J. Y.; Hagenmuller, P.; Christin, F.; Heraud, L.; Choury, J. J. - "Synthesis and properties of new composite materials for high temperature applications based on carbon fibres", *Revue de Chimie minerale*, t. 18, pp. 544-564.

Naslain - 1980, R.; Hagenmuller, P.; Christin, F.; Heraud, L.; Choury, J. J.- "The Carbon Fiber/Carbon and Silicon Carbide Binary matrix composites a new class of materials for high temperature applications", in *Advances in Composite Materials, ICCM-3*, Vol. 2, pp. 1084-1097, Ed. by A. R. Bunsell et al, 1980.

Naughton - 1993, T. D.; Roy, A. K. - "Effect of carbonization heating rates on mechanical properties of C-C", *Extended Abstracts of International Carbon Conference - Carbon 93*, Buffalo, NY.

Neighbour - 1993, G.; "*Microstructural Processes leading to Fracture in Nuclear Graphites*", PhD Thesis, University of Bath.

Niihara - 1983, K.; Suda, A.; Hirai, T. - "Preparation and Mechanical Properties of CVD-SiC", *Proc. of International Symposium on Ceramic Components for Engine*, Japan, pp. 480-489.

Oberlain - 1984, A. - "Carbonization and Graphitization", *Carbon*, Vol. 22, No. 6, pp. 521-541.

Oh - 1989, S.; Lee, J. - "Fracture Behaviour of two-dimensional Carbon/Carbon Composites", *Carbon*, Vol. 27, No. 3, pp. 423-430.

Oh - 1988, S.; Lee, J. - "Effect of microstructure on the mechanical properties of Carbon/Carbon Composites", *Carbon*, Vol. 26, No. 2, pp. 769-776.

Otani - 1991, S.; Oya, A. - "Glass-Like Carbons", *Materials Science and Technology - A Comprehensive Treatment*, Ed. by R. W. Cahn, P. Haasen; Vol. 9 - Glasses and Amorphous Materials, Edl. by Jerzy Zarsyoki, pp. 550-572.

Peebles - 1988, Jr., L. H.; Meyer, R. A.; Jortner, J. - "Interfaces in Carbon-Carbon Composites", in *Interfaces in Polymer Ceramic, and Metal Matrix Composites*, Ed. H. Ishida, Proceedings of the Second International Conference on Composites Interfaces, 1988.

Perry - 1974, J. L.; Adams, D. F. - "An experimental study of Carbon/Carbon Composite Materials", *Journal of Materials Science*, Vol. 9, pp. 1764-1774.

Perry - 1976, J. L.; Adams, D. F. - "Mechanical Tests of a Three-dimensionally-reinforced Carbon-Carbon Composites material", *Carbon*, Vol. 14, pp. 61-70.

Pollock - 1990, P. B. - "Tensile Failure in 2-D Carbon/Carbon Composites", *Carbon*, Vol. 28, No. 5, pp. 717-732.

Pollock - 1973, A. A.; "Acoustic emisson-2/Acoustic emission amplitudes", pp. 264-269, *Non Destructive Testing*.

Ragan - 1991, S.; Emmerson, G. T. - "Oxidation inhibited Carbon-Carbon:Mechanical Properties", *20th Biennial Conference on Carbon*, pp 428-429.

Rahhal - 1991, W. F.; Kotlensky, W. V. - "Modified Short Beam Shear Test", *Carbon 91*, pp. 354-355.

Rellick - 1990, G. - "Densification efficiency of Carbon/Carbon Composites", *Carbon*, Vol. 28, No. 4, pp. 589-594.

Rellick - 1992, G.; Chang, D. J.; Zaldivar, R. J. - "Mechanisms of orientation and graphitization of hard-carbon matrices in Carbon/Carbon composites", *Journal of Materials Research*, Vol. 7, No. 10, pp. 2798-2809.

Rief - 1990, C.; Lindner, M.; Kromp, K. - "Experimental Investigations and a Model Proposal on Damage Mechanisms in a Reinforced Carbon-Carbon Composite", *ASTM STP 1059*, S.P. Garbo, Ed., ASTM, pp. 564-579.

Rolincik - 1987, P. G. - "Autoweave™ - A Unique Automated 3D Weaving Technology", *SAMPE Journal*, Sept/Oct, pp. 40-47.

Rogers - 1975, D. C.; Shuford, D. M.; Mueller, J. I. - Formation mechanism of a silicon carbide coating for a reinforced carbon-carbon composite, *Proc. of 7th National SAMPE Technical Conference*, 7, pp. 319-336.

Rossignol - 1987, J. Y.; Quenisset, J. M.; Naslain, R. - Mechanical behaviour of 2D-C-C/TiC composites made from a 2D-C-C preform densified with TiC by CVI, *Composites*, Vol. 18, No. 2.

Roy - 1989, R.; Agrawal, D. K.; McKinstry, H. A. - "Very Low Thermal Expansion Coefficient Materials", in *Ann. Rev. Materials Science*, Vol. 19, pp. 59-81.

Rummler - 1983, D. R. - "Recent Advances in Carbon-Carbon Materials Systems", *NASA Report 83-N12162*, pp. 293-312.

Russel-Floyd - 1990, R. S. - "Using the Marandy MR1004 Acoustic Emission System", Report for School of Materials Science, University of Bath.

Russel-Floyd - 1993, R. S.; Harris, B.; Jones, R. W.; Cooke, R. G.; Wang, T. H.; Laurie, J.; Hammett, F. W. - "Sol-gel Processing of Fibre reinforced Ceramic Shapes", *British Ceramic Transation*, Vol. 92, No. 1, pp. 8-12.

Sandor - 1990, R. B. - "Polybendimidazole (PBI) as a matrix resin precursor for Carbon/Carbon Composites", *22nd International SAMPE Technical Conference*, pp. 647-657.

Sato - 1989, S.; Kurumada, A.; Iwaki, H.; Komatsu, Y. - "Tensile properties and fracture toughness of carbon-fiber felt reinforced carbon composites at high temperature", *Carbon*, Vol. 27, No. 6, pp. 791-801.

Savage - 1988, G - "Carbon-carbon composite materials", *Metals and Materials*, pp. 544-550.

Savage - 1993, G. - *Carbon-Carbon Composites*, 1st ed., Chapman & Hall.

Schmidt - 1962, D. L.; Jones, W. C. - "Carbon-base fiber reinforced plastics", *Chemical Engineering Progress*, Vol. 58, No. 10, pp.42-50.

Schmidt - 1972, D. L. - "Carbon/Carbon Composites", *SAMPE Journal*, No. 8, pp. 9-19.

Schmidt - 1989, H. - "Chemical Processing up to Gelation", in *Sol-Gel Science and Technology*, Ed. Aegerter, M. A.; Jafelicci Jr., M.; Souza, D. F.; Zanotto, E. D., pp. 61-75, World Scientific Publishing.

Scott - 1991, I. G. - "Basic Acoustic Emission", Nondestructive Testing Monographs and Tracks, Vol. 6, Ed. W. J. McGonnagle. Gordon and Breach Science Publishers.

Sheehan - 1989, J. E. - "Oxidation Protection for Carbon Fiber Composites", *Carbon*, Vol. 27, No. 5, pp. 709-715.

Sheehan - 1987, J. E. - "Oxidation-Resistant Carbon-Carbon Composites", *Engineered Materials Handbook. Vol. 1:Composites*, pp. 911-914, ASM International.

Sim - 1986, S. M.; Krabill, R. H.; Dalzell, W. J.; Chu, P. Y.; Clark, D. E. - "Sol-gel coatings on Carbon/Carbon Composites", in Better Ceramics through Chemistry II, *Materials Res. Society Symp. Proceedings*, Vol. 73, Eds. C. J. Brinker, D. E. Clark and D. R. Ulrich, pp. 647-652.

Srinivasan - 1989, M. - "The Silicon Carbide family of Structural Ceramics", in *Treatise on Materials Science and Technology*, Vol. 29, pp. 99-159.

Stone - 1977, D. E. W.; Dingwall, P. F.; "Acoustic emission parameters and their interpretation", pp. 51-62, *NDT International*.

Strife - 1988, J. R.; Sheehan, J. E. - "Ceramic Coatings for Carbon-Carbon Composites", *Ceramic Bulletin*, Vol. 67, No. 2.

Stoller - 1969, H. M.; Frye, E. R. - "Carbon-Carbon materials for aerospace applications", *Proc. of AIAA/AIME 10th Structures, Struct. Dynamics Conf.*, pp. 193-212.

Tanamura - 1990, T.; Tatsumi, K.; Narisawa, M.; Shioyama, H.; Ikeda, S.; Adachi, M.; Souma, I. - "Fracture behaviour of 3D-C/C by the three point bending test with various rations of span length to thickness (L/T)", *Carbone 90*, pp. 510-511.

Thomas - 1978a, C. R.; Walker, E. J. - "Carbon-Carbon Composites as High-strength Refractories", *High Temperatures-High Pressures*, Vol 10, pp. 79-86.

Thomas - 1978b, C. R.; Walker, E.J. - *Proc. 5th International Conference on Carbon and Graphite*, Vol. 1, pp.520-531.

Thomas - 1986, C. R. ; Walker, E. J. - *Proc. of First International Conference on Materials in Aerospace*, pp. 138-167.

Ulrich - 1988, D. R. - "Prospects of Sol-Gel Processes", *Journal of Non-Crystalline Solids*, No. 100, pp. 174-193.

Vix-Guterl - 1993, C.; Lahaye, J.; Ehrburger, P. - "Reactivity of Silicon Carbide and carbon with oxygen in thermostructural composites", *Carbon*, Vol. 31, No. 4, pp. 629-635.

Walker - 1959, Jr., P. L.; Rusinko, Jr., Frank; Austin, L. G. - "Gas Reactions of Carbon", *Adv. Catalysis*, Vol. 11, pp. 133.

Walker - 1983, Jr. B. E.; Rice, R. W.; Becher, P. F.; Bender, B. A.; Coblenz, W. S. - "Preparation and Properties of Monolithic and Composite Ceramics Produced by Polymer Pyrolysis", Vol. 62, No. 8, pp. 916-923.

Walker - 1993, E. J. - "The importance of fibre type and fibre surface in controlling composite properties", in *Essentials of Carbon-Carbon Composites*, Ed. by C. R. Thomas, The Royal Society of Chemistry.

Warren - 1972, J. W.; Williams, R. M. - "Isothermal CVD processing", *4th National SAMPE Technical Conference*, pp. 623-633.

Weiss - 1973, J. R.; Diefendorf. R. J. - "Relationship of structure to properties in chemically vapor deposited silicon carbide", *Proceedings of IV International Conference on CVD-The Electrochemical Society*, Eds. Wakefield G., Blocher, J., pp. 488-498.

Weisshaus - 1990a, H. ; Kenig, S. - "Carbon/Carbon Composites : Processing-Microstructure-Property relationships", *Carbonne 90*, pp. 490-491.

Weisshaus - 1990b, H.; Kenig, S.; Kastner, E.; Siegmann, A. - "Morphology development during processing of carbon-carbon composites", *Carbon*, Vol. 28, No. 1, pp. 125-135.

Weisshaus - 1991, H; Kenig, S; Siegmann, A - "Effect of Materials and processing on the mechanical properties of C/C Composites", *Carbon*, vol. 29. no. 8, pp. 1203-1220.

White - 1987, D. A.; Oleff, S. M.; Fox, J. R. - "Preparation of Silicon Carbide from Organosilicon Gels: II, Gel Pyrolysis and SiC Characterization", *Advanced Ceramic Materials*, Vol. 2, Part 1, pp. 53-59.

White - 1989, J. L.; Sheaffer, P. M. - "Pitch-based Processing of Carbon-Carbon Composites", *Carbon*, Vol. 27, No. 5, pp. 697-707.

Williams - 1978, J. H.; Lee, S. S. - "Acoustic Emission Monitoring of Fiber Composite Materials and Structures", *J. Composite Materials*, Vol. 12, pp. 348-370.

Wong - 1986, F. W. K.; Doswell, S. J.; Malherbe, M. C. - "A Study of the application and fabrication of advanced ceramics", *Reihe 5: Grund-und Werkstoffe*, Nr.109.

Wu - 1991, Tsung-Ming; Wei,Wen-Cheng; Hsu, Shu-En - "On the oxidation kinetics and mechanisms of vaious SiC-Coated Carbon-Carbon Composites", *Carbon*, Vol. 29. no. 8, pp. 1257-1265.

Wynne - 1984, K. J.; Rice, R. W. - "Ceramics via Polymer Pyrolysis", in *Ann. Rev. Mater. Sci.*, Vol. 14, pp. 297-334.

Yasuda - 1988, E.; Tanabe, Y.; Manocha, L. M.; Kimura, S. - "Matrix modification by graphite powder additives in carbon fiber/carbon composite with thermosetting resin precursor as a matrix", *Carbon*, Vol. 26. No. 2, pp. 225-227.

Yin - 1991, Y; Cooke, R.G.; McEnaney, B. - " Radial variations in fracture and acoustic emission of a thermic graphite electrode", *Carbon*, Vol. 29, No. 8, pp. 1221-1225.

Yoon - 1990, H. S.; Taya, M. Fischbach, D. - Refractory rare metal coatings on Carbon Materials - *International Symposium on Carbon*, pp. 924-927.

Zaldivar - 1991a, R. J.; Kobayashi, R. W.; Rellick, G. S. and Yang, J. M. - "Catalytic Graphitization of Thermoset-derived Carbon-Carbon Composites", *Carbon 91*, pp. 388-389.

Zaldivar - 1991b, Kobayashi, R. W. ; Rellick, G. S. - "Carborane-catalyzed graphitization in polyarylacetylene-derived carbon-carbon composites", *Carbon*, vol. 29, no. 8, pp. 1145-1153.

Zaldivar -1991c, R. J.; Rellick, G. S. - "Some observations on stress graphitization in carbon-carbon composites" - *Carbon*, vol. 29. no. 8, pp. 1155-1163.

Zimmer - 1983, J. E.; White, J. L. - "Mesophase alignment within carbon-fibre bundles", *Carbon*, Vol. 21, No. 3, pp. 323-324, 1983.